THE FUSION BEHAVIOUR OF UNPLASTICISED POLYVINYL CHLORIDE:

EFFECTS OF PROCESSING AND FORMULATION

BY

OGABA PHILIP OBANDE

A Doctoral Thesis submitted in
partial fulfillment of the requirements
for the award of Doctor of Philosophy
of Loughborough University
of Technology

September, 1984

Supervisors : M. Gilbert, Ph.D., FPRI, MRSC, C Chem.
Institute of Polymer Technology
D.E. Marshall, Ph.D., MIP.
Institute of Polymer Technology

© **O.P. Obande (1984)**

ACKNOWLEDGEMENTS

The author gratefully acknowledges the invaluable guidance and encouragement from Dr M. Gilbert and Dr D.E. Marshall throughout the course of this study, including time freely given for sessions of very helpful discussion.

It gives the author an opportunity to thank Professor A.W. Birley, formerly Director of Institute of Polymer Technology (IPT), whose tireless effort attracted the author to the institute, and also to Dr D.E. Marshall, Acting Director of IPT for providing the facilities for the studies.

Thanks are also due to the following: the entire technical staff at IPT, including in particular, Mr M. Mulla, former technical staff, and Dr R.P. Higgs, former research assistant, for the help rendered. Dr J.M. Hutchinson of the Department of Metallurgy, University of Nottingham, for the interest shown and assistance given in the development of the distribution model. BP Chemicals, ICI, Akzo Chemie, Cornelius Company, Cookson Group, all in the U.K., for generously providing samples and equipment without obligation.

Special thanks are due to Toyin, my wife, for making the sacrifice demanded by our disposition over the years.

The author is grateful to Ahmadu Bello University, Zaria, for an award of a study fellowship, and to the Federal Government of Nigeria for providing the grant to undertake this study.

Finally, by no means the least, the devotion and interest shown by John Whitehead in typing the manuscript is gratefully acknowledged.

This is to certify that this thesis is a record of research work carried out by me.

Neither this thesis nor the original work contained therein has been submitted to this or any other Institution for an award of a degree.

O.P. Obande

(Sept., 1984)

Dedicated

to the memory of

Chief Obande Ominyi

(a man of exceptional foresight)

ABSTRACT

The fusion behaviour of commercial grade PVC has been studied by capillary rheometry and thermal analysis for twin-screw extruded rigid formulations. The role of shear in fusion was also investigated by extrusion at different rates and by compression moulding.

Aspects discussed include thermodynamic fusion (melting) and gelation (network formation). The former is measured by thermal analysis and the latter by rheometry. Fusion is dictated primarily by the level of heat generated during processing while gelation depends both on the equipment shear regime and on formulation.

In the molecular weight range studied, M_W = 6.0 - 10.0 x 10^4 g/mol, fusion level is inversely related to M_W at a specific processing temperature, but the maximum fusion level attainable within temperature limits is largely independent of molecular weight.

At a given processing temperature below 200°C impact strength (IS) of notched Izod samples is linearly related to the extrusion (shear) rate; above 200°C, however, little change is observed. The IS of samples processed at different temperatures, keeping extrusion rate constant, goes through a maximum, but this depends on the temperature range,the shear level, and the formulation.

From the results of solvent sorption, density, and wide angle x-ray diffraction, an overall decrease is observed in the level of order left in the processed material with increasing processing temperature.

From a mathematical model proposed for the fusion behaviour percentage fusion is shown to be equivalent to the degree of crystallinity. The maximum % fusion observed, about 8%, corresponds to the crystalline level of the unprocessed powder. Based on this model activation energies of 1.0 kJ/mol and 2.2 kJ/mol are obtained for the fusion of the relevant morphological units.

TABLE OF CONTENTS

		Page
List of Figures		(i)
List of Tables		(v)
List of Symbols		(viii)
CHAPTER 1	**INTRODUCTION**	
1.1	**Processing Related Properties of PVC**	1
1.1.1	Powder Morphology	1
1.1.2	Crystallinity	5
1.1.3	Thermal Stability	10
1.2	**PVC Melt Processing**	11
1.2.1	Principles of Formulation	11
1.2.2	Mixing and Compounding	13
1.2.3	Principles of Twin-Screw Extrusion	14
1.3	**The Melting Behaviour of PVC**	16
1.3.1	Melting of Crystalline Structure	16
1.3.2	Melting at the Level of Morphological Units – Fusion Mechanisms	17
1.4	**Assessment of Fusion Level**	23
1.4.1	Capillary Rheometry	23
1.4.2	Solvent Testing	26
1.4.3	Thermal Analysis	26
1.5	**Evaluation of Structural Order in PVC**	30
1.5.1	X-ray Analysis	30
1.5.2	Density Measurements	34
1.5.3	Solvent Sorption	36
1.5.4	Thermal Analysis	42
1.6	**Mechanical Properties of PVC: the Impact Resistance**	43
1.6.1	Impact Test Methods	47
1.7	**Aim of Study**	50

CHAPTER 2 EXPERIMENTAL TECHNIQUES

2.1	**Materials**	51
2.1.1	Poly(vinyl chloride)	51
2.1.2	Additives	52
2.2	**Sample Preparations**	54
2.2.1	Formulation	54
2.2.2	Dry Blending	55
2.2.3	Compression Moulding	57
2.2.4	Extrusion Details	57
2.3	**Density Measurements**	61
2.4(a)	**Sorption Measurements**	62
2.4(b)	**Methylene Chloride Tests**	62
2.5	**Capillary Rheometry**	63
2.6	**Thermal Analysis**	63
2.7	**X-ray Analysis**	66
2.8	**Impact Tests**	69

CHAPTER 3 RESULTS AND DISCUSSION

I. GELATION STUDIES

3.1	**A Summary of Extrusion and Compression Moulding**	71
3.1.1	Extrusion	71
3.1.1.1	Output Rate	71
3.1.1.2	Power/Torque Variations	72
3.1.2	Compression Moulding	75
3.2	**Capillary Rheometry**	78
3.2.1	Effect of Processing Temperature	78
3.2.2	Percent Gelation (CR)	81
3.2.3	Effect of Extrusion Rate	85
3.2.4	Effect of Molecular Weight	85
3.3	**Thermal Analysis**	90
3.3.1	The B-onset Temperature, T_B	90
3.3.2	Effect of Processing Temperature	93

3.3.3	Effect of Extrusion Rate	97
3.3.4	Effect of Molecular Weight	99
3.3.5	Percent Gelation	99
3.4	**Methylene Chloride Tests**	101
3.5	**Comparisons of the Gelation Tests**	104
3.5.1	A General Observation on Thermal Analysis	110
3.6	**Characterization of Fusion by Thermal Analysis: A Model for Simulating the Heats of Fusion**	112
3.6.1	Introduction	112
3.6.2	Testing the Model	116
3.6.3	Comparison of the Theoretical and Experimental Heats of Fusion	118
3.6.4	Application of the Distribution Model to Quantitative PVC Fusion Analysis	128
3.6.4.1	Activation Energy of Particle Breakdown	128
3.6.4.2	Evaluation of Fusion Level using the Distribution Model	137
3.6.5	Heats of Fusion of the Perfect PVC Crystal	139
3.7	**Conclusions**	144

CHAPTER 4 RESULTS AND DISCUSSION

II. EFFECTS OF PROCESSING ON CRYSTALLINITY

4.1	**Acetone Absorption**	146
4.1.1	Sorption Kinetics	146
4.1.2	Estimation of Relative Crystallinity from Sorption Kinetics	156
4.1.3	**Dependence of Equilibrium Sorption on Gelation Level**	156
4.2	**Densities of Processed Samples**	162
4.3	**X-ray Analysis**	169
4.3.1	Advantages of the H-W Method in X-ray Analysis of Processed Samples	169
4.3.2	X-ray Crystallinity Index of the Processed and Unprocessed PVC	172
4.3.3	The Minimum Crystallinity at 200°C Melt Temperature	176

4.4 **A Comparison of the Crystallinity Index Measured by Different Methods** 179

4.4.1 Values of X_r for the Unprocessed Powder and Q_r for the Most Fused Processed Sample 179

4.4.2 Effects of Processing Temperature 181

4.5 **Conclusions** 184

CHAPTER 5 **RESULTS AND DISCUSSION**

III. IMPACT PERFORMANCE OF PROCESSED PVC

5.1 **Variation of the Force-Displacement Trace with Fracture Toughness** 186

5.2 **Fracture Surface Macromorphology** 188

5.3 **Effects of Material and Processing on Impact Strength** 189

5.3.1 Effect of Formulation 189

5.3.2 Effect of Extrusion Rate 189

5.3.3 Effect of Extrusion Temperature 190

5.3.4 Effect of Molecular Weight 192

5.4 **Dependence of Failure Mechanism on Fusion** 193

5.4.1 Formulation with Solid Additives 193

5.4.2 Formulation with Liquid Additives 197

5.5 **Conclusions** 198

General Conclusions 207

Suggestions for Further Study 210

References 211

Appendix 225

LIST OF FIGURES

Figure		Page
1.1	Schematic representation of the mechanism of VCM Polymerization	2
1.2	Schematic representation of the internal structure of PVC resin particle	5
1.3(a)	Proposed model for PVC crystallinity	9
1.3(b)	The microdomain structure of PVC	9
1.3(c)	Average crystal size of PVC	9
1.4	Schematic illustration of intermeshing twin screws	15
1.5(a)	A Schematic illustration of the three patterns of fusion	19
1.5(b)	A generalized picture of the fusion process	19
1.6(a)	Mechanism of gelation during processing	21
1.6(b)	A classification of processing machinery in terms of the communition/densification mechanism of gelation	21
1.7	Schematic illustration of the molecular diffusion fusion mechanism	22
1.8	Schematic DSC trace of PVC over the temperature range 20-600°C showing major areas of thermal activity	27
1.9	DSC thermograms of processed and annealed PVC	28
1.10(a)	Variation of T_g and T_{sub} with annealing temperature	29
1.10(b)	'B' onset temperature vs. extrusion temperature	29
1.11(a)	Plot of M_t/M_∞ vs. $t^{\frac{1}{2}}$	41
1.11(b)	Sorption curves showing Fickean (A) and non-Fickean (B) behaviour	41
1.12	Variation of stress-intensity factor at failure as a function of specimen thickness	45
1.13	Geometry of testing and specimen support arrangement for (a) Charpy; and (b) Izod tests	49

Figure		Page
2.1	A schematic representation of the T.K. Fielder	56
2.2	Schematic representation of the Leistritz LS.30.34 twin-screw extruder	58
2.3	Schematic representation of the Krauss Maffei KMD L-25 twin-screw extruder	59
2.4	Schematic diagram of the Davenport Capillary Rheometer: Front view	64
2.5	Calorimetry cell of the Du Pont 990 thermal analyser	65
2.6	Schematic reflection diffraction geometry	68
2.7	Dimensions of Izod test specimen	70
3.1	Variation of output rate with extrusion rate for sample A using the Leistritz at 200°C	73
3.2	Variation of power required for extrusion of samples A and B with extrusion rate using the Leistritz at 200°C	74
3.3	Dependence of capillary rheometer pressure on processing temperature for samples A and B using the Leistritz	82
3.4	Variation of gelation level (based on rheometer pressure) with processing temperature for samples A and B	83
3.5	Dependence of rheometer pressure on processing temperature for extruded and compression moulded samples	84
3.6	Variation of rheometer pressure with extrusion rate for samples A and B extruded on the Leistritz at various temperatures	86
3.7	Dependence of rheometer pressure on processing temperature for different molecular weight samples extruded on the Krauss Maffei	88
3.8	DSC thermograms for (a) powder, (b) extrudate at 160°C, and (c) extrudate at 190°C	92
3.9	Heat of fusion as a function of processing temperature for extruded (L-) samples	95
3.10	Heat of fusion as a function of processing temperature for compression moulded (CM-) samples	96
3.11	Heat of fusion as a function of processing temperature for extruded (KM-) samples	100

Figure		Page
3.12	Variation of rheometer pressure with heat of fusion for extruded (KM-) samples	105
3.13	Dependence of fusion level (based on thermal analysis) on processing temperature for extruded (KM-) samples	108
3.14	Sampling regions for cross-sectional differences in melt temperatures and heats of fusion	109
3.15	Comparison of eqn. 3.5 with experimental results using the results shown in Figure 3.9	117
3.16	Comparison of eqn. 3.14 with experimental results using the results shown in Figure 3.9	125
3.17	Comparison of eqn. 3.14 with experimental results using the results of compression moulded samples	126
3.18	Comparison of eqn. 3.14 with experimental results using different molecular weight samples	127
3.19	Variation of ln Q_t with inverse temperature, $1/T_B$, for L-samples	131
3.20	Variation of ln Q_t with inverse temperature, $1/T_B$, for CM-samples	132
3.21	Variation of ln Q_t with inverse temperature, $1/T_B$, for KM-samples	133
3.22	Dependence of activation energy of particle fusion on additive concentration for CM-samples	134
3.23	Dependence of fusion level (based on reduced increment in Q_r) on processing temperature for L-samples	140
3.24	Dependence of fusion level (based on Q_r) on processing temperature for CM-samples	141
3.25	Dependence of fusion level (based on Q_r) on processing temperature for KM-samples	142
4.1	Sorption curves for sample A processed over a range of temperatures using the Leistritz	148
4.2	Results of Figure 4.1 replotted as % weight gain vs. reduced time	149
4.3	Plot of M_t vs. t for the diffusion of acetone in PVC processed at different melt temperatures	152
4.4	Plot of M_t/M_∞ from data of Figure 4.1	154

Figure		Page
4.5	Equilibrium % sorption curves for samples extruded on the Leistritz over a range of temperatures	158
4.6	Equilibrium % sorption curves for samples compression moulded over a range of temperatures	160
4.7	Equilibrium % sorption curves for samples extruded on the Krauss Maffei at different temperatures	161
4.8	Dependence of density on melt temperature in extrusion	164
4.9	A typical diffraction pattern of PVC powder sample with fitted amorphous template	170
4.10	Normalized values of crystalline vs. amorphous areas using x-ray diffraction curves for samples listed in Table 4.4A	171
5.1	Force-displacement plots from the Ceast Fractoscope for different failure modes	200
5.2	Fracture surface SEM micrographs of sample A	201
5.3	Fracture surface SEM micrographs of sample S68	202
5.4	Notched Izod impact strength vs. melt temperature for Leistritz extrudates	203
5.5	Notched Izod impact strength vs. melt temperature for Krauss Maffei extrudates	204

LIST OF TABLES

Table		Page
1.1	List of PVC nomenclature	3
1.2	Order of magnitude characteristic of various impact tests	49
2.1	Technical data for PVC samples	51
2.2	Molecular weight of PVC samples	52
2.3	Technical data of additives	53
2.4	PVC formulations	54
2.5	Blending conditons on the T.K. Fielder mixer	55
2.6	Extrusion conditions on the Leistritz	60
2.7	Extrusion conditions on the Krauss Maffei	61
3.1	Output and power requirement for samples extruded at different temperatures using the Leistritz at 20rpm	76
3.2	Output and torque for samples extruded on the Krauss Maffei at 20rpm	77
3.3	Capillary rheometer pressure and percentage gelation for samples extruded at different temperatures using the Krauss Maffei	89
3.4	Heats of fusion for samples extruded at different rates and temperatures using the Leistritz	98
3.5	Time taken for methylene chloride attack on processed samples	103
3.6	Variations in melt temperature and heat of fusion over sample cross-section for Leistritz and Krauss Maffei extrudates	109
3.7	Relative shear levels for samples processed on different machines measured by the ratio of observed to calculated heat of fusion at 210°C	124
3.8	Thermal analysis results for extruded formulations	135
3.9	Percentage fusion for compression moulded samples based on reduced increment in Q_r	136

Table		Page
3.10	Variation of activation energy for particle breakdown for KM samples	137
3.11	Reported heats of fusion of the fully syndiotactic crystalline PVC	143
4.1	Kinetic parameters for acetone absorption at 23°C	153
4.2	Comparison of observed and calculated sorption half time	155
4.3	Densities of samples extruded at different temperatures using the Leistritz	165
4.4	Densities of samples extruded at different speeds using the Leistritz	166
4.5	Densities of samples extruded at different temperatures using the Krauss Maffei	167
4.6	Crystallinity indices of processed samples calculated from sample densities	168
4.7	The crystallinity index, X_r, measured by x-ray analysis of processed PVC samples	175
4.8	Values of the crystallinity index of the unprocessed polymer measured by thermal analysis and by x-ray diffraction	181
4.9	Effect of processing temperature on the crystallinity index measured by thermal analysis, x-ray diffraction, and density	183
5.1	Notched Izod impact strength of samples A and B extruded at different rates and temperatures	205
5.2	Dependence of impact strength on the crystallinity index measured by thermal analysis, x-ray diffraction, and sample density	206

Appendix Tables

3.1A	Output and power requirement for samples extruded at different rates using the Leistritz	226
3.2A	Capillary rheometer pressure and percent gelation for samples extruded at different temperatures using the Leistritz	227
3.3A	Capillary rheometer pressure at different rates of extrusion for Leistritz extrudates	228

Table		Page
3.4A	Capillary rheometer pressure for compression moulded samples	228
3.5A	Heats of fusion and 'B' endotherm temperatures for samples extruded on the Leistritz	229
3.6A	Observed heats of fusion for samples compression moulded at different melt temperatures	230
3.7A	Heats of fusion for Krauss Maffei extrudates	231
4.1A	Acetone absorption with time for sample A extruded at different temperatures	232
4.2A	Equilibrium % weight gain in acetone absorption for compression moulded samples	233
4.3A	Equilibrium % weight gain in acetone absorption for KM samples	234
4.4A	Experimental and normalized crystalline and amorphous areas of some x-ray diffraction patterns	235

LIST OF SYMBOLS

A	pre-exponential factor, also used to represent value of the x-ray diffraction intensity (area) of a 100% amorphous sample
A_o	total initial sample surface area in diffusion tests
α	amorphous weight fraction
β	chain mobilization factor
C	value of x-ray diffraction intensity (area) of a 100% crystalline sample, also used as penetration concentration in diffusion tests
C_p, C_{pa} and C_x	heat capacity, values for the amorphous and crystalline polymer respectively
D, D*	diffusion coefficient, coefficient in the completely amorphous polymer
d	diameter of sorbing particles
d_c	sample density
δ	total thickness of a surface swollen with penetrant
E_D	activation energy of diffusion
g_o and g_t	initial sample weight and weight at time t after immersion in a penetrant
g_i	intensity factor
ΔH^*, ΔH_f, and $\Delta H(T)$	measured heat of fusion
h	Boltzman's constant
I	x-ray diffraction intensity
K	correction factor in x-ray analysis
k	Planck's constant
l	sample thickness in diffusion test
L/D	length to diameter ratio of a die
$\bar{M}_n$ and $\bar{M}_w$	number and weight average molecular weights respectively

M_t and M_∞	weight gain at time t and at equilibrium respectively in diffusion tests
N	sum of n_i parts of chain molecules melted
n	viscous term in capillary rheometry, also represents chain configuration constant in diffusion tests
P	extrusion pressure
ΔP	entrance pressure drop in capillary rheometry
P_i	additive concentration in PVC in phr
ϕ_a and ϕ_c	amorphous and crystalline areas of x-ray diffraction trace
ψ	geometric impedance factor in diffusion tests
Q	quantity of molecular units melted
Q_r	relative reduced value of Q (fusion level)
R	gas constant
S_R	recoverable strain
T	temperature (°C of K)
T_g	glass-transition temperature
T_m	melting temperature
t	time
τ	wall shear stress
U	energy term in impact tests
v	velocity of penetrant
W	sample weight
X	Crystallinity index
X_r and X_d	x-ray and density crystallinity indices respectively

" . . . many shall run to and fro,
and knowledge shall be increased"

The Book of Daniel

Knowledge, however, mocks itself in philosophy.

OPO

Chapter 1

INTRODUCTION

1.1 Processing Related Properties of PVC

1.1.1 Powder Morphology

Electron microscopy (EM) has long been used to reveal structural features of processed polymers. The technique was pioneered by Rochow[1] in a series of studies of EM fractographs of poly(methyl methacrylate), PMMA, polyacrylonitrile, PA, and polystyrene, PS. In these studies Rochow[1,2] demonstrated the existence of supermolecular structures in the bulk phase of the processed samples.

One of the first studies of polyvinyl chloride, PVC, morphology involved the direct observation of particle growth in suspension polymerisation of the resin, using an electron microscope, by Bort et al.[3] Approximately 0.1μm particles were observed which grew with conversion.

Although Rochow[1,2] had produced substantial evidence in favour of the existence of submicro particles in extruded and moulded plastics the significance of this finding to PVC processing was not recognised until the works of Berens and Folt[4-6] which provided the first evidence for the particulate nature of PVC melt flow. Since these reports the morphology of PVC particle has been extensively studied.

It is now well established[12-16] that PVC has a particulate structure ranging in size from about 100μm down to 10nm. The suspension polymerized resin (S-PVC) consists of grains 100μm in size which are composed of agglomerates of 1-μm primary particles.[8] In Table 1.1 by Allsopp[16] the various particles are listed and described using the accepted

nomenclature suggested by Geil.[10] Similarly in Figure 1.1 the morphogenesis during polymerization is shown schematically.

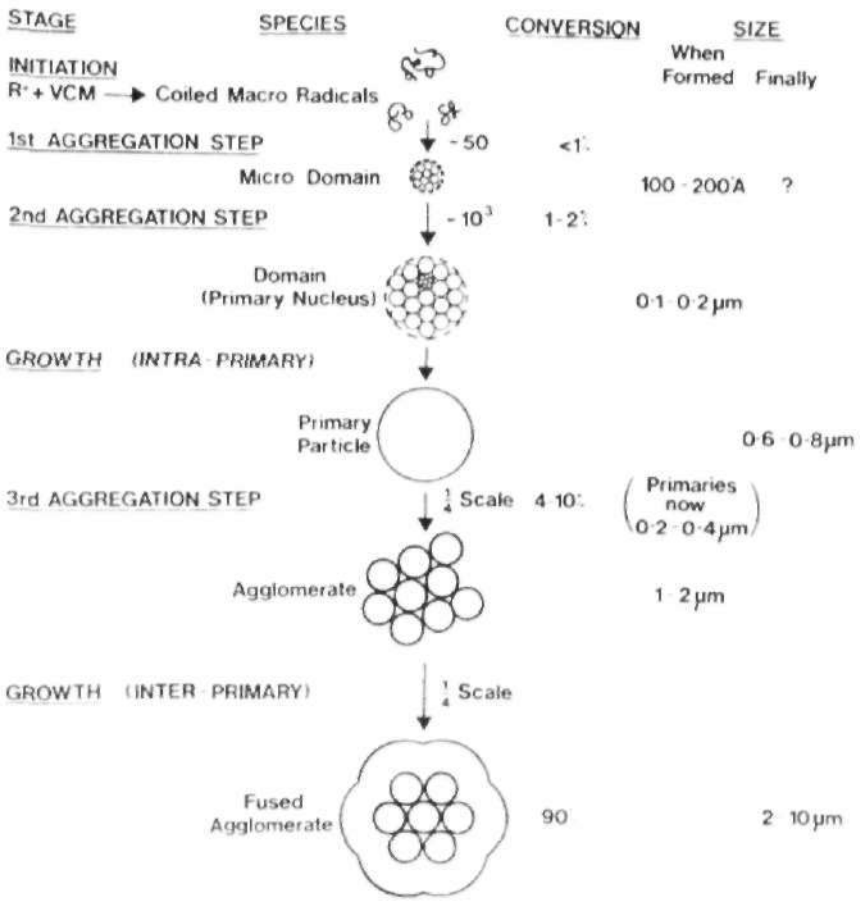


Fig. 1.1

Schematic representation of the mechanism of VCM polymerisation

As shown in Table 1.1 the primary particles are said to be made up of smaller structures at the 0.01µm microdomain levels.[15] However, the existence of these levels of (nodular) structure in the bulk polymer is presently an open debate since some authorities consider it to conflict with Flory's[17] random-flight model of the amorphous polymer chain upon which a number of major theories are based. In a series of works Uhlmann and his collaborators dispute the existence of nodular structures in PMMA,[18] PC[19] and PVC;[20,21] they attribute reported observations of these structures in

Table 1.1

List of PVC nomenclature[16]

Term	Approximate Size		Origin or Description	Previous Terminology (with References)
	Range μm	Average μm		
Grain	50-250	130	Visible constituent of free flowing powders, made up of more than 1 monomer droplet.	Granule (2) Cellular grain (3)
Sub-grain	10-150	40	Polymerised monomer droplet.	Sub granule (2) Unicell (3)
Agglomerate	1-10	5	Formed during early stage of polymerisation by coalescence of primary particles (1-2 μm). Grows with conversion to size shown.	Aggregate (2) Cluster (3) Macro globule (4)
Primary particle	0.6-0.8	0.7	Grows from domain. Formed at low conversion (less than 2%) by coalescence of micro-domains: grows with conversion to size shown.	Microgranule primary particle (2) granule (3) micro-globule (4)
Domain	0.1-0.2	0.2 (200nm) (2000 Å)	Primary particle nucleus. Contains about 10^2 micro-domains. Only observed at low conversion (less than 2%) or after mechanical working. Term only used to describe 0.1 μ species; becomes primary particle as soon as growth starts.	Primary nucleus (2) Granule (3)
Micro-domain	0.01-0.02	0.02	Smallest species so far identified. Aggregate of polymer chains - probably about 50 in number.	Basic particle (2) Particle (3)

Notes on Table 1

1 The domain is not a feature of PVC morphology in high conversion polymer samples since a growth of this species with conversion obliterates all memory of it. It may only be "regenerated" and observed after subsequent processing.

2 As soon as formation of the domain is complete and growth is registered it is preferable to call it a primary particle. Therefore, the term domain is often ignored in favour of primary particle even at the point of morphogenesis of the 0.2μm primaries at low conversion.

3 The reason for a separate identity for the domain is that it may be shown in future to contain an atypical morphological or molecular feature, eg higher level of crystallinity.

fractographs of processed polymers to the effect of either under-focusing or over-focusing the electron microscope.[21] It is noted that the random-flight model per se does not rule out the existence of microstructures in the bulk phase of amorphous polymers since in practice most of these polymers are found to deviate markedly from the ideal elastomeric state for which the model applies.

In PVC, observations of the microdomain have been widely reported by a number of investigators using a range of techniques: Hattori et al.[22] used electron microscopy on extruded S-PVC, embedded in methyl methacrylate. They observed that the 1µm particles are broken down to fibrils 10-30nm in thickness during powder extrusion. Neilson and Jabarin[23] and Wenig[24] showed the existence of microdomains in unplasticized PVC (UPVC) using small-angle x-ray scattering (SAXS). The same structure has been found in plasticized PVC (PPVC) by Gezovich and Geil[25] using SAXS; Tsou and Geil[26] using EM, and Singleton et al.[27] using SAXS, and more recently by Soni et al.[15]

Using plasticized samples Soni et al.[15] showed that the SAXS technique reveals an increase in the size of the microdomain with increased plasticizer content. This is perfectly in line with a model proposed by Summers[28] which identifies the microdomain structure with the crystalline entity.

It should be noted that Allsopp[16] has suggested (Table 1.1) that the domain structure is not a feature of PVC morphology in high conversion samples. This suggestion is supported by the findings of the IUPAC Commission[14] and those of Bort et al.;[3] indeed it is readily observed from the literature that whereas observation of the microdomain is widely reported, this is not the case for the domain structure. The aggregation of these particles in the final resin particle is shown in Figure 1.2.

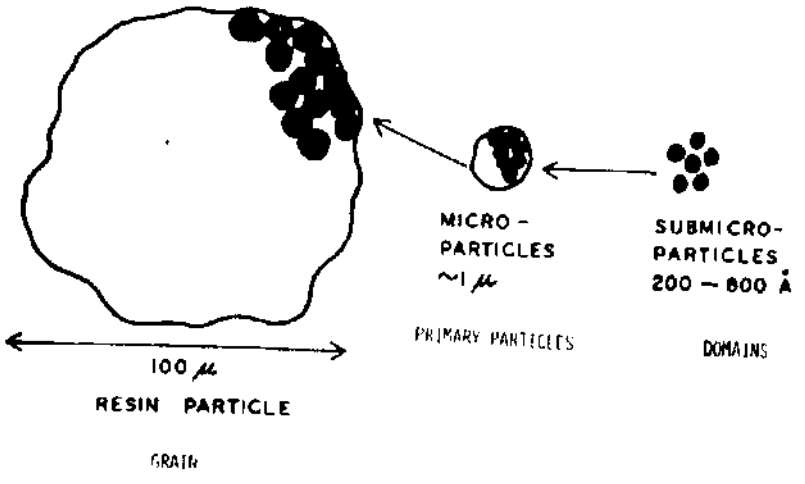


Figure 1.2

Internal structure of PVC resin particles[15]

1.1.2 Crystallinity

First indications of crystallinity in PVC stemmed from the creep resistance of plasticized samples. The creep resistance was explained on the basis of permanent network junctions formed by crystals too small to be clearly apparent by conventional techniques in the normal technological material.[29,30] Natta and Corradini[31] provided the first proof of the existence of crystallinity in PVC based on wide-angle x-ray diffraction (WAXD) studies of the crystal structure of oriented fibres of commercial PVC. They found an orthorhombic crystal structure with unit cell dimensions a = 1.06nm, b = 0.54nm, and c = 0.51nm. Single crystals of PVC were first reported by Smith and Wilkes;[32] and in a later study using single crystals Wilkes et al.[33] confirmed the orthorhombic crystal lattice but determined a more compact unit cell with dimensions a = 1.027nm, b = 0.524nm, and c = 0.508nm. These authors also noted that the order along

the chain axis (c-axis) is relatively poor. More recent determinations of the unit cell dimensions by Keller and Lemstra[34] provide values intermediate between the values reported by the above authors.

The crystallinity of commercial grade PVC has been extensively studied by several other investigators. It is found that the syndiotactic sequence is the crystallizable unit and the syndiotactic fraction decreases with increasing polymerisation temperature.[35,36] Commercial PVC has been assigned none[20,37] or low levels of crystallinity. Based on density measurements Nakajima et al.[35] found 5-7% crystallinity for commercial PVC; Rehage and Halboth,[38] and D'Amato and Strella[39] estimated 5-10% from WAXD; Ohta et al.[40] found 5% using heats of fusion calculated from differential scanning calorimetry (DSC) thermograms. A range of 5 to 10% crystallinity is generally found for the commercial polymer.[24] Higher crystallinity may be obtained by employing special preparative techniques using butyraldehyde[39,41] or the urea clathrate method.[42]

The various reflections giving rise to the peaks in the region 10°-50° 2Θ have been assigned.[38,41] Baker et al.[42] have suggested that the reflections giving rise to the peaks in the region 16°-18° 2Θ are mainly a measure of two-dimensional order perpendicular to the chain direction, while those responsible for the region 24°-26° 2Θ are a measure of three-dimensional order. This is substantiated by the works of Gilbert and Vyvoda[43] which showed that for highly oriented 'skins' and uniaxially stretched core of injection moulded samples an enhancement of the peak at 17° 2Θ is observed.

In x-ray diagrams of PVC (particularly the commercial polymer) a reflection is sometimes found which cannot be ascribed to the

orthorhombic crystal form. This reflection has been assigned[44-48] to a structure intermediate in order between the completely ordered and the completely disordered phase — a mesomorphic or nematic phase. This structure is found to be present to an extent determined by the thermal history of the material.[48]

A number of textures have been proposed for the PVC bulk crystal. Juijn et al.,[48-50] Ceccoruli et al.,[36] and Keller and co-workers[34,51,52] propose two crystal forms consisting of a relatively well developed, presumably, chain folded lamella crystals and less well developed, presumably, fringed micelle crystals. Keller et al.[34,51,52] regard both the former and the latter forms of crystallinity (termed A- and B- crystals respectively) as features of the as-polymerized PVC. They suggest that during melt processing melting of the less ordered B-crystals is involved, the melting point of the A-crystals being too high[36] and, therefore, inaccessible as a result of degradation at much lower temperatures. Juijn et al.,[48-50] however, propose that the better developed crystal structure (primary crystallinity) forms the main feature of the as-polymerized sample. It is converted to the less ordered structure (secondary crystallinity) during melt processing. Both groups of workers, however, agree that the secondary crystallinity (B-crystals) cannot be converted to the primary crystallinity (A-crystals) in melt processing. Fringed micelle crystallites have been proposed previously[53] for PVC gel network junctions which supports the findings of Keller et al.[51,52] More recently, however, Mandelkern[54] has cautioned that the widespread concept of fringed micelles accompanying gelation is not universal to all gelation-crystallization processes.

In order to account for the broad melting range and effect of annealing on conventional PVC, Illers[55,56] has proposed a distribution of crystal sizes and perfection for the polymer. Thus all the forms of ordered structures discussed above can be considered as belonging to a broad structural distribution.

The location of the crystallites within the morphological structures has been widely investigated but results are inconclusive.[7,14,27] Manson et al.[57] and Summers[28] have presented models for the PVC crystallite. In the model of the former workers, Figure 1.3(a), the crystallites are regarded as thin lamellar about 5-10nm long and wide and 1-1.5nm thick connected by longer disordered segments. An important feature of this model is that attempts are made to relate crystallite dimensions to overall degree of crystallinity of the material. Chain folding is regarded as generally unlikely, being made unfavourable by the presence of long atactic sequences attached to very short regular ones. Summers[28] identifies the microdomain structure with the crystallites, Figure 1.3(b) and (c), the average crystallite size is given at about 4.1 X 4.1 X 0.7nm. These crystallites are joined together by tie molecules with inter-crystallite spacing of about 10nm. Munstedt[58] has found that even after destruction of the primary particles PVC still shows abnormal melt flow properties. This unusual rheological behaviour is explained by the assumption of a network structure formed by crystallites in the melt which are shown by EM to be of the same size as the microdomain.

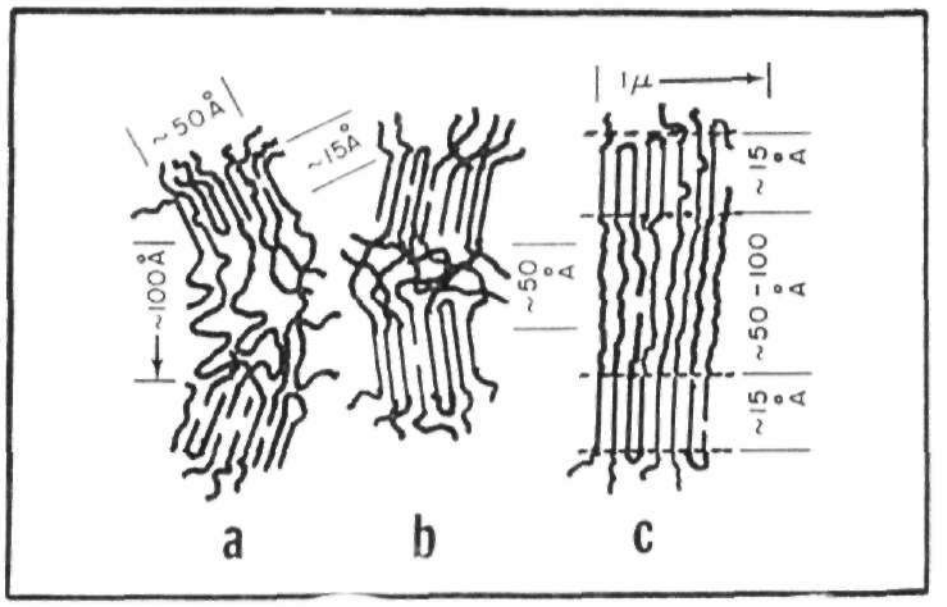


Fig. 1.3(a)

Proposed model (not to scale) for PVC:

(a) 10% crystallinity (b) 30% crystallinity; (c) low-molecular-weight polymer (10% crystallinity) in lamellar form. Note kinks and chains in crystal lattice. Crystallites in (a) and (b) extend laterally about 50A: in (c), 1μ or more in single crystals.[57]

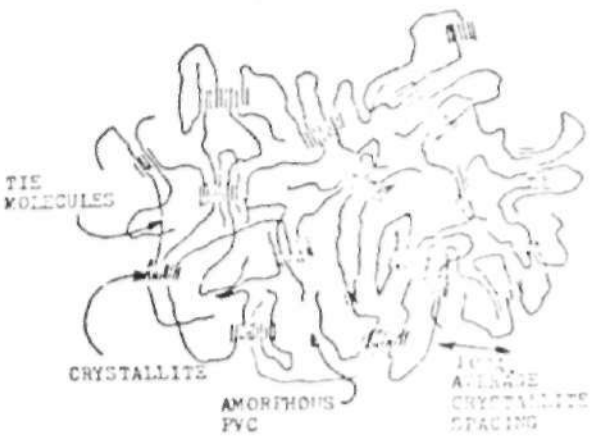


Fig. 1.3(b)

The microdomain structure of PVC[28]

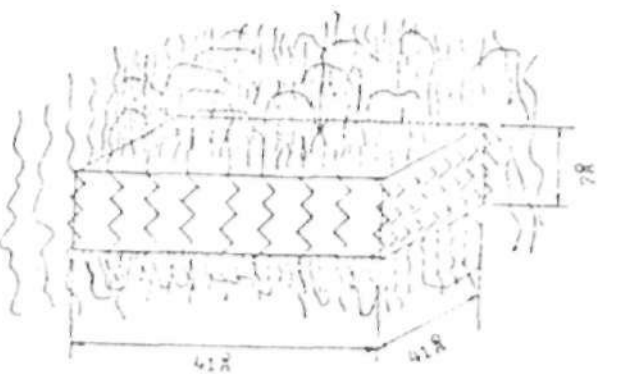


Fig. 1.3(c)

Average crystal size of PVC.

Real crystals are probably not so uniformly structured.[28]

1.1.3 Thermal Stability

With the exception of poly(vinyl acetate), PVAC, PVC has the lowest activation energy for decomposition of all known plastics.[61] Difficulties encountered with its processing can often be related to its degradation threshold temperature which is much lower[62] than the crystalline melting temperature. In addition to the low degradation temperature, its melt viscosity is unusually high.[63-65] On heating to above 180°C the polymer begins to decompose with the evolution of HCl and discolouration.[67,68] The colour changes from white through yellow to brown then black.[68] The low decomposition temperature has been attributed[69] to the arrangement of the chlorine atoms along the chain rather than chain branching. Tertiary chlorine, estimated[70] at 0.1 to 0.2 mole% are also said to be among possible sites of instability.

While decomposition can be induced by other forms of energy, in practice thermal decomposition is by far the most important.[67] Using mass spectrometry, Bersch et al.[71] have shown that the only volatile product of decomposition below 200°C is HCl; above this temperature small amounts of aliphatic, unsaturated, and aromatic hydrocarbons are formed — free chlorine or HCl is not detected.[72]

In general the heat stability increases with increasing molecular weight,[67] with mass-polymerized PVC having marginally better heat stability than suspension polymers most of which are in turn more heat stable than emulsion PVC.

1.2 PVC Melt Processing

Practically every kind of plastics processing can be applied to PVC in one form or another, and some PVC processing, e.g. paste processing, are not generally applicable to other polymers.[67] The various processing techniques have been described[67,73-76] fairly fully in several monographs.

All PVC processing techniques involve three basic stages – mixing, compounding, and shaping. All three stages are vital and no one stage may be mutually exclusive of the others. To overcome the problems of thermal degradation and high melt viscosity (discussed in the preceding section) while enhancing the overall property of the processed material, PVC is often loaded with a number of additives. In plasticised formulations these additives can account for as much as half or more of the total resin content by weight. It is essential that these ingredients are very thoroughly mixed to ensure homogeneity of the processed material.

1.2.1 Principles of Formulation

In unplasticized compositions possible additives to the resin can include a stabilizer system, lubricants, impact modifiers, processing aids, pigments, fillers, and antistatic agents. In order to reduce the effect of additives on the parameters of interest to this study only stabilizer and lubricant are added to the resin; the discussion is, therefore, confined to these two additives only.

A stabilizer system must be sufficiently effective to minimise decomposition to an acceptable level during processing. Choice of the stabilizer depends, among other factors, on end-use requirements, toxicity,

local control regulations, cost, and ease of handling. Stabilizers in wide use include lead salts, tin compounds (organo tin, and thio-organo tin), barium/cadmium/zinc systems, epoxy compounds, and organic phosphites. Combinations of these stabilizers are commonly used in practice.

Three types of lubricant actions are generally known:[77] they can prevent the resin from permanently adhering to the surface of the processing equipment, reduce the internal friction of the polymer molecules, and improve the external appearance of the extrudates. On the basis of their chemical structure, they can be classified into several groups: straight chain hydrocarbons, such as paraffin waxes, straight chain hydrocarbons with polar end groups, such as monoglycerin esters and steric acids, and molecules having a polar centre with long carbon chains on each side, such as metal stearates. On the basis of their action, they are traditionally classified as being either external or internal, or intermediate depending on their compatibility with the resin. External lubricants have little compatibility with the resin and thus act on the interface between resin and equipment surface reducing adhesion. They may also coat aggregates of the polymer molecules and reduce internal friction between the aggregates. Internal lubricants have substantial compatibility with the resin and can diffuse into the polymer aggregates acting somewhat as a plasticizer. In practice this sharp division of lubricant activity is, however, meaningless; a given lubricant usually performs both external and internal lubricating functions to varying degrees depending on the concentration and processing conditions.

The additives in PVC formulation have profound effects on the processing behaviour and on product properties; much work has been done to understand the basis of these effects. Tin stabilizers, being liquid,

diffuse into the resin particles and thus increase both the rate of fusion[78] and the crystallinity of the product.[24,40,79,80] The effect of lubricants on fusion,[77,81] and on the melt rheology[82] has also been studied; external lubricants are found to retard fusion but in general the effect of the lubricant system depends on the compound composition and the processing conditions.[82]

1.2.2 Mixing and Compounding

The terms mixing and compounding are used interchangably by different authors and strictly speaking the distinction is more in principle than in practice. The object is to attain an acceptable degree of homogeneity or uniformity of composition[77] and to some extent of morphological structure.

The principles of mixing and compounding are well treated in several works.[67,73-76,83] A number of theories have been proposed for quantitative evaluation of the expected degree of mixing given a combination of equipment and mixing conditions. As a result of the number of parameters that should be taken into account most of these theories can at best only give indications of the expected degree of mixing.

Several types of machines, mostly adopted from older disciplines, are used. High speed internal mixers have been found to give satisfactory performance in PVC powder blending. The essential feature is that the movement of the components to be mixed is achieved by a rotor, at the base of the mixing chamber, rotating on a vertical axis at speeds ranging from a few hundred to a few thousand revolutions a minute. Under these conditions the components are thrown out by the centrifugal action of the rotor and up the walls of the mixing chamber, return down the central

zone, thus exhibiting a fluid-like movement with a vortex. Depending on the precise design of the rotor and its speed, more or less intensive frictional heat is developed and the temperature rises continuously within the mixing mass. The resin powder may be broken down and/or agglomerated depending on the speed, temperature, and duration of the process. The intensity of the mixing action results in excellent dispersion of the additives.

1.2.3 Principles of Twin-Screw Extrusion[76]

The shaping stage in processing (section 1.2) may be further subdivided into softening (plasticating), shaping, and setting the shape. These three processes are achieved in every melt processing equipment. Although a significant degree of mixing is achieved with the high speed mixers it is not sufficient to meet the demands of melt processing and end-use requirements of the product.

The efficiency of a specific additive component depends on its physico-chemical properties as well as on the level of its dispersion and distribution[84] in the polymer matrix. For this reason it is not sufficient that the extruder plasticates and conveys the PVC compound to the die, it must also provide as much compounding action as possible within an acceptable shear regime. In practice this apparently simple requirement can hardly be said to have been satisfactorily met by existing equipment. A recent advancement in melt compounding is afforded by the Cavity Transfer Mixer (CTM) developed at RAPRA.[85] Results of its pilot tests are particularly promising.

Although twin-screw extruders have higher capital costs per unit output compared with single-screw extruders they offer a number of

advantages and so are being increasingly preferred for rigid PVC processing. Several types of twin-screws are available; they include co-and contra-rotating screws with interrupted flights, changes in the number of flights, tapered screws, and other variations. Figure 1.4, by Tester,[86] is a schematic illustration of single-stage intermeshing contra-rotating twin screws. An important functional difference between co- and contra-rotating intermeshing screws is the shear developed on the polymer in the region in which the screw flights overlap (the nip, Figure 1.4). In co-rotating screws the shear can be quite high in the overlap region because the flanks of the flights move in opposite directions. Modern co-rotating screws have wider tolerances in this region but for equivalent clearances, they pass a smaller percentage of total material through the nip than do contra-rotating screws. Contra-rotating screws generate less shear in the nip since the flights travel in the same direction (Figure 1.4). Of greater significance is that a greater percentage of the total product can pass per revolution through the overlap region, in effect contra-rotating screws have more efficient compounding characteristics.

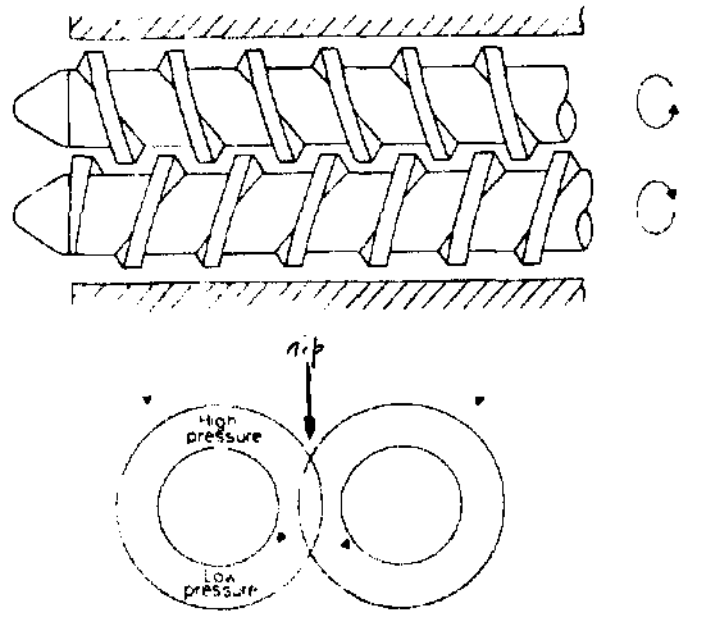


Fig. 1.4

Schematic illustration of intermeshing twin screws

1.3 The Melting Behaviour of PVC

It is evident from sections 1.1.1 and 1.1.2 that PVC melting must involve a complex process. Three aspects of the melting process can be considered: melting of the ordered structures, melting at the level of the particulate units, and the relative roles of temperature and shear on the melting process.

An equilibrium static melting temperature[87] and a shear dependent dynamic melting temperature[88,89] may be defined for a polymer crystal. Both as-polymerised and processed PVC melt over an unusually wide range of temperatures.[36,48,55,90]

1.3.1 Melting of the Crystalline Structure

Although polymers in general do not have sharp melting temperatures and in some cases[48,91] multiple melting found, the breadth of PVC melting range seems to be particularly unique. Wunderlich[87] explains that in polymer melt processes diffuse melting temperature is only true in the case of metastable crystals; equilibrium polymer crystals melt as sharply as small molecules. Mandelkern[92] has also shown that the thermal history of the polymer has a strong influence on the diffuseness of the melting temperature. A sample that is annealed above the T_g for a sufficient length of time (which is often inaccessibly long in practice[92]) would show the same sharp first-order thermodynamic transition as does the crystal of a small molecule. In a number of papers[93-95] Sheldon and his co-workers have shown that discrete ordering of chains as a unique interpretation of endothermal peaks is not necessary. In their studies of factors which give rise to endothermal peaks in thermal

analysis they were able to show that the broad peaks are characteristic of amorphous polymers in keeping with a concept of 'free-volume entrapment' on the one hand and local chain ordering on the other. This concept is in line with the approach used recently by Lyngaae-Jorgensen and Singh[96] to show that the decrease in T_g observed[36] in successive DSC traces of PVC powder is not due to a drop in crystallinity (the crystallinity was actually shown to increase) but to the relaxation of internal stresses.

The mechanism of melting of chain folded crystals has been widely studied. Evidence has been found[97,98] in favour of a 'surface-melting' mechanism whereby fusion occurs by the progressive transfer of chain segments from the folded surfaces of the crystalline lamella to the amorphous or melt phase. The process involves progressive thinning[97] or lateral shrinkage[98] of the folded chain towards the centre of the crystal. Conte et al.[99] have shown that highly syndiotactic PVC crystal structure is chain folded lamella; for commercial PVC, however, the crystal structure is not[7,27,100] chain folded lamella but fringed micellar.[40,50,52,53,55] The melting of crystals with varying perfection has been theoretically considered by Zachman and co-workers.[100] A broad melting range is postulated for the case of (amorphous) loops of random length. This specific case is analogous to a distribution of crystallite sizes as found for processed PVC.

1.3.2 Melting at the Level of the Morphological Units — Fusion Mechanisms

The terms 'fusion' and 'gelation' are widely used in reference to the disappearance of PVC particle boundaries resulting from the combined effects of temperature and shear during processing. A process of

molecular interdiffusion across particle boundaries is thought to be involved,[28] however, as observed by Uitenham and Geil,[101] the unique and complex behaviour of PVC in the 'melt' makes it difficult to define 'PVC fusion' in terms of known processing and physical property parameters.

Following the works of Berens and Folt[4-6] which demonstrated the particulate nature of PVC melt flow, the fusion process has been extensively studied. Attempts have been made to understand the mechanism and thus quantify the measured parameters.[63,78,82,102-105] Quite clearly the final state of the melt is strongly dependent on its thermomechanical history, but the path leading to this state is still largely ill-defined.

Two main mechanisms are presently recognised: depending on the temperature and shear history, fusion progress may involve particle elongation or particle breakdown. In a third and closely related mechanism more emphasis is placed on the molecular interdiffusion process in fusion.

(a) The Particle Breakdown Mechanism

Fusion has often been associated with particle breakdown during powder extrusion.[22,101] Most workers have proposed[63,82,89,102-106] that the 100μm grains are first broken down to 1μm particles; these are then compacted, followed by sintering and interdiffusion of the primary particles and the microdomain particles. Sieglaff[63] and Krzewki and Collins[82,106] have, however, observed that fusion can take several different paths. These authors have produced an overall picture of three possible routes to the fused state as reproduced in Figures 1.5(a) and (b). In the first route there is breakdown of the resin grains to submicron (microdomain) particles, then compaction of the microdomains and

interdiffusion to form the fused material. The second route involves breakdown of the resin into primary (micro-) particles. These are compacted and internally fused or the particles themselves form a fused material. In the third mechanism there is no breakdown, but through compaction, heating, and long residence time, internal fusion of the resin particles and interdiffusion to the fused state is achieved.

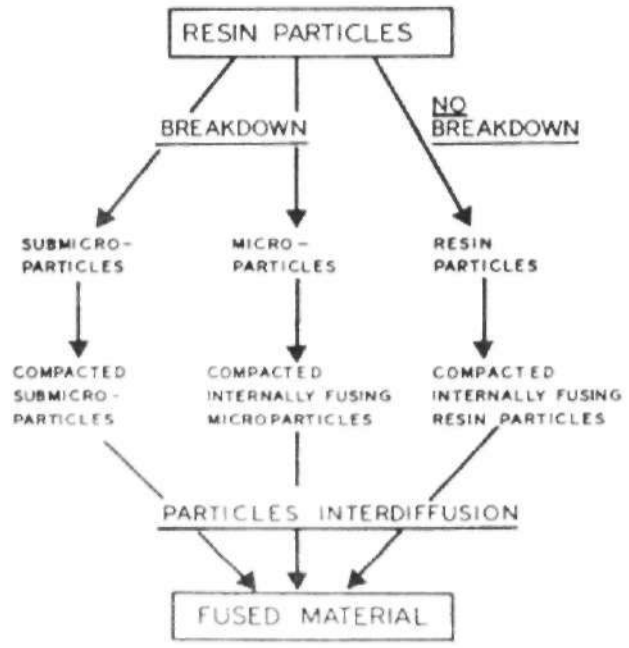


Fig. 1.5(a)

A schematic illustration of the three patterns of fusion

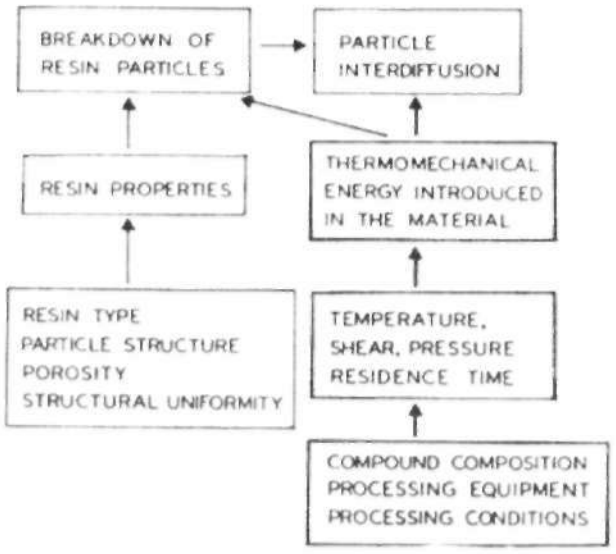


Fig. 1.5(b)

A generalized picture of the fusion process

(b) Particle Elongation Mechanism

It is apparent that shear would be an important factor in the breakdown of the powder grain.[63] Kulas and Thorshaug[89] observe that frictional heat appears to be dissipated inside loosely agglomerated resin particles, possibly as a result of the relatively large surface area of these particles. This additional heat, which depends on the shear rate, is said to influence the melting behaviour considerably. Lyngaae-Jorgensen[88] has derived a semi-empirical relation which yields the 'dynamic' melting temperature at a specific shear level. A generalised fusion model by Allsopp[107] is based primarily on the relative shear intensity of the processing equipment, Figure 1.6(a) and (b). At a given processing temperature the path to the fused state depends on the shear rate. If the shear rate is sufficiently high the grains are broken down into primary particles and the fusion process is described by the particle breakdown mechanisms described above. If the shear rate is sufficiently low as obtains for instance in twin-screw machines, Figure 1.6(b), the fusion process involves compaction, densification, fusion and elongation of the grains – the CDFE mechanism. It is important to note that the fused state is not precisely defined, intermolecular diffusion is of course implied, and this is said to occur simultaneously with, or even before, elongation of the grains.

It is necessary to note that with the exception of the works of Hattori et al.,[22] Kulas and Thorshaug[89] and Uitenham and Geil[101] most of the authors who propose particle breakdown as the sole fusion mechanism based their conclusions on studies involving the use of Brabender Plasticorder which is a high shear equipment; these conclusions are, therefore, understandable in the context of Figure 1.6(b). Results of

microscopy studies on extrudates and compression moulded samples at this Institute are in support of Allsopp's model. Highly elongated grains have been observed[84] in extracts from screw channels in the metering zone of the Leistritz LS 30:34 twin-screw extruder.

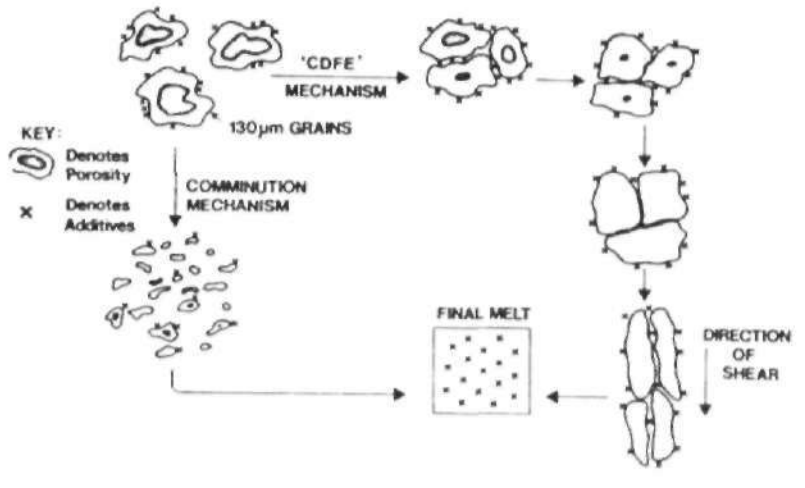


Fig. 1.6(a)

Mechanism of gelation during processing

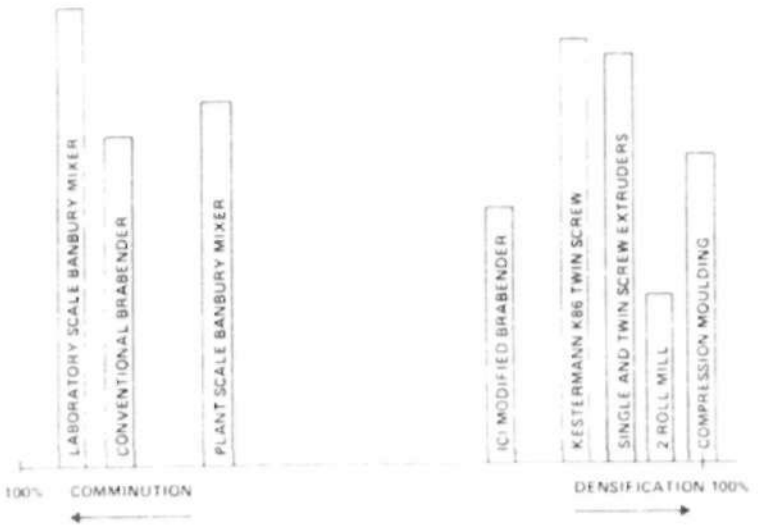


Fig. 1.6(b)

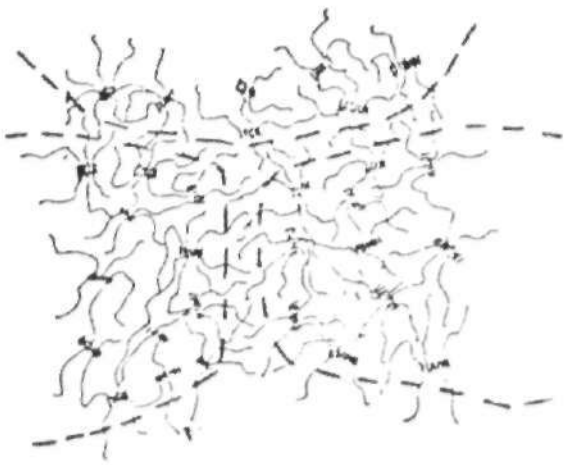
A classification of processing machinery in terms of the comminution/densification mechanism of gelation

(c) Molecular Diffusion Mechanism

Clearly the loss of particle boundaries in the final melt accompanying fusion must involve molecular interdiffusion across boundaries;[63,106] Summers[28] has proposed a fusion model based primarily on molecular interdiffusion. This model, reproduced in Fig. 1.7(a) to (d), considers the 100μm grains to be broken down to primary particles which form the flow units;[4-6] for a given combination of processing temperature and shear rate, the level of fusion is determined by the state of interdiffusion of molecules across primary particle boundaries.



(a) The microdomain structure of PVC



(c) Primary particles, partially melted and interacting in a 177°C melt (not to scale)



(b) Primary particles in a low temperature melt (162°C)(not to scale)



(d) Primary particles after cooling and recrystallization from 177°C melt (not to scale)

Fig. 1.7 Schematic illustration of the molecular diffusion fusion mechanism

As observed by Sieglaff,[63] in practice it is possible that all the mechanisms discussed above or their combinations are involved in the fusion process. Observations[84,107] of highly elongated particles and the well known fact that particle memory is preserved[103,108] lend strong support for the CDFE mechanism in powder extrusion.

1.4 Assessment of Fusion Level

Several tests have been developed for quantitative evaluation of fusion level. These tests fall into two main categories,[108] those that depend upon the evaluation of the retention or otherwise of particulate structure and those that depend upon measurement of the presence or otherwise of molecular network. An example of the former category is microscopy and examples of the latter include rheometry (capillary and torque rheometry), dynamic oscillatory testing, elongational flow, solvent testing, and, more recently, a proposal for thermal analysis. Only those tests that are relevant to this study are reviewed, for more detailed treatment a number of literatures, as cited, may be consulted.

1.4.1 Capillary Rheometry

The pressure necessary to extrude a PVC compound through a capillary die is dependent on both the mechanical parameters (e.g. barrel/die temperatures), and on the resistance offered by the compound to melt deformation.[106,108] For a capillary with diameter D and length L the entrance pressure loss, ΔP, can be expressed as:[108]

$$\Delta P = \tau [4L/D + (2n + S_R)] \qquad 1.1$$

where τ is the wall shear stress, n, a viscous term, and S_R is the recoverable strain. The term (4L/D) represents the viscous behaviour and the term $(2n + S_R)$ is the energy loss due to entrance effects, [109,110] which includes both the viscous loss and the elastic term, S_R, – also called the recoverable strain.[106] It is clear from eqn. 1.1 that if a die with a high L/D is used the viscous behaviour predominates; however, if a die with low L/D is used the loss due to entrance effects predominates. The entrance pressure loss, ΔP_{ent}, is the sum of two parts[106] comprising the viscous entrance pressure drop, ΔP_{vis}, and the elastic entrance pressure drop, ΔP_{ela}:

$$\Delta P_{ent} = \Delta P_{vis} + \Delta P_{ela} \qquad 1.2$$

Han[111,112] has shown that in several polymer melts the viscous entrance pressure drop is only 10% of the total pressure drop, so that

$$\Delta P_{ent} \simeq \Delta P_{ela} \qquad 1.3$$

Thus the variation in entrance pressure loss can be attributed primarily to changes in the elasticity of the material under test.[111]

Eqn. 1.3 was developed from studies on polymers which attain a true molten state. For the method to be applicable to PVC melt a further assumption is made that changes in the morphology of the material can be related directly to changes in the elastic development. Since the elastic development is dependent on the fusion level, the assumption implies a direct dependence of the entrance pressure loss on the fusion level.

There are two methods commonly used to determine the entrance pressure loss.[106]

1. Bagley plots

With decreasing L/D ratio, the contribution of the capillary pressure loss to the total pressure loss decreases and becomes zero for a zero-length capillary. Plots of L/D at a constant shear rate give straight lines and extrapolation to zero L/D provides the pressure loss at the capillary.

2. 'Zero-length' capillary method

With a very short capillary (small L/D ratio), the pressure drop is nearly identical to the entrance pressure drop and can be obtained from a single measurement.

The capillary rheometry fusion test is very widely used[102-106] with most investigators showing a preference for the quicker 'zero-length' method. Ways of maximizing the discriminating power of the test have been investigated.[108] Testing below T_g will obviously be ineffective since the rigidity of the structure will not permit separate investigations of the network which is of interest. The higher the test temperature above T_g the lower will be the value of the entrance pressure losses and the lower will be the discriminating power of the test. Gonze[102] observed large differences between the extrusion pressure for materials extruded at 130°C and lesser differences at higher temperatures. Also the higher the shear rate the greater the entrance pressure losses and the better the discriminating power of the test. However, the mechanical limitations of the equipment determine the maximum shear rate available. An apparent shear rate of 100 sec^{-1} has been found suitable.[108]

The pressure loss is not an absolute value of fusion, therefore, several methods of quantifying fusion by this technique have been

proposed.[102,105,106] A widely used practice is to establish a standard gelation (fusion) curve (s.g.c.) using the relationship:

$$\% \text{ fusion} = \frac{P - P_{min}}{P_{max} - P_{min}} \times 100 \qquad 1.4$$

where P is the pressure required to extrude the sample of unknown fusion level and P_{min} and P_{max} the minimum and maximum pressure corresponding to the least fused and the most fused samples respectively.

1.4.2 Solvent Testing

This is a qualitative standard fusion level technique decribed by BS 3505:1968/82 and ASTM D2152:1967/72.

Swelling the fused PVC sample in a suitable solvent has little or no mechanical effect on the cohesion of the sample because of the restraining effect of the network.[108] But where particles which are not part of the molecular network and are held together at best by sintering exist, it is reasonable to expect that sufficient swelling could dislodge them from their neighbours and cause some disintegration of the sample. On this basis the test is carried out by simply immersing sections of the processed sample in a suitable solvent (acetone or methylene chloride is widely used). The samples are left for some time (maximum, 2 hrs) at room temperature after which they are visually examined for solvent attack on the surface.

1.4.3 Thermal Analysis

Differential thermal analysis (DTA) or differential scanning calorimetry (DSC) of PVC shows a number of characteristic peaks. These

peaks were first assigned by Matlack and Metzger[113] and since then have been investigated by several authors.[40,49,55,114] As shown in Fig. 1.8 the first observed response is a sub-T_g endotherm, R, which for annealed samples increases in magnitude and shifts to higher temperatures with increased time and temperature of annealing. Berens and Hodge[115] have shown that as the annealing temperature, T_e, approaches the glass transition temperature, T_g, the sub-T_g endotherm is superposed on the T_g base-line shift thus appearing as the well-known T_g overshoot. They propose that a non-exponential, non-linear, relaxation function is essential for the development of this peak.

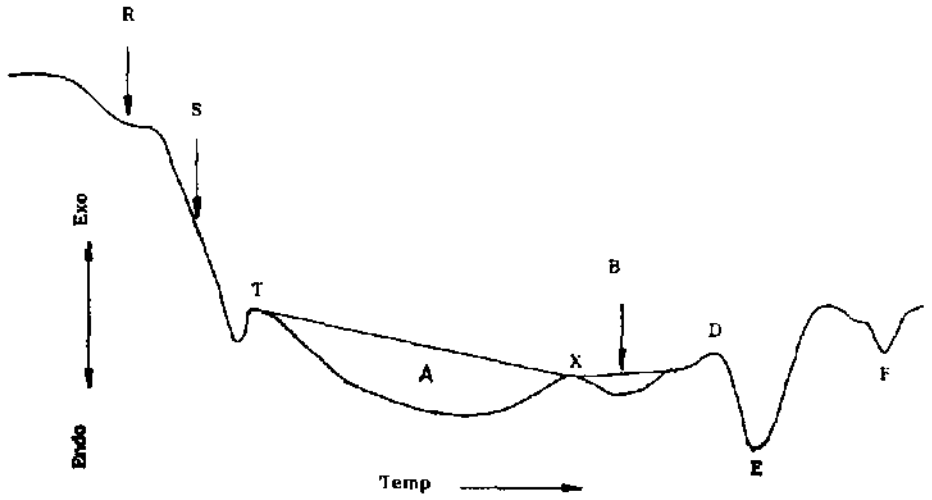


Fig. 1.8

Schematic DSC trace of PVC over the temperature range 20-600°C showing major areas of thermal activity

The sub-T_g endotherm, R, is followed by a T_g baseline shift, S, in the region 70-80°C, and between 100-230°C, a first-order endothermic response occurs which is regarded as the practical fusion or 'melting' range for the conventional resin. The breadth of this endotherm, TX, depends on the heat history of the sample. The onset of thermal degradation, D, depends on the stabilizer system used, 250°C has been claimed[113] for a tin stabilized formulation. Decomposition and evolution of HCl is said to occur in the region 270-310°C, E, it is influenced by the type and quantity of the lubricant.[113] At about 450°C, point F, another first-order transition, characteristic of all PVC compounds, occurs which is attributed to depolymerization.

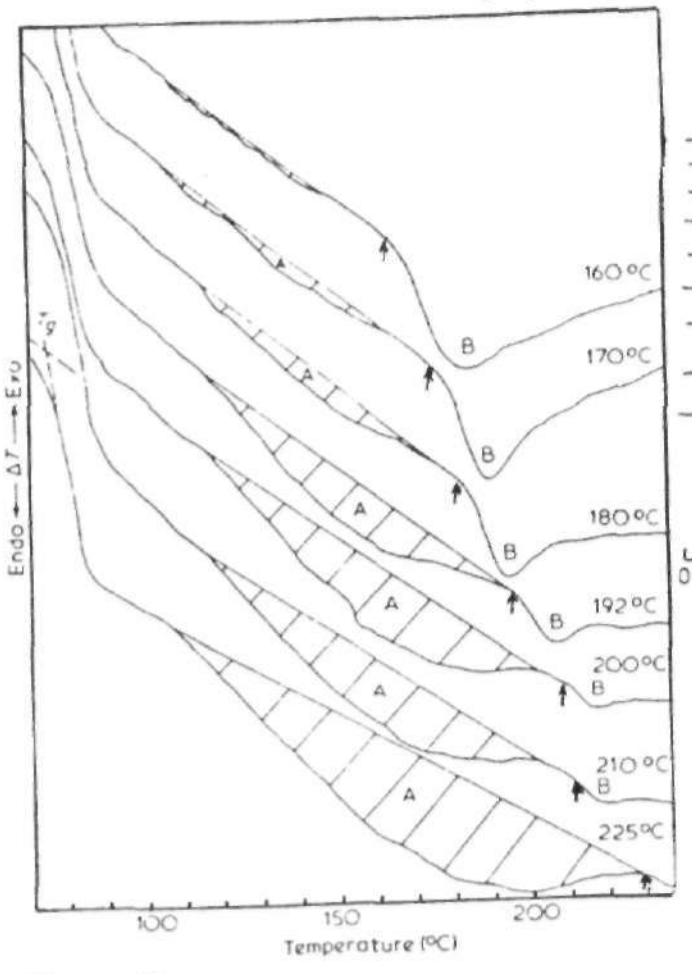


Fig. 1.9(a)

D.s.c. thermograms of PVC compression moulded at various temperatures[114]

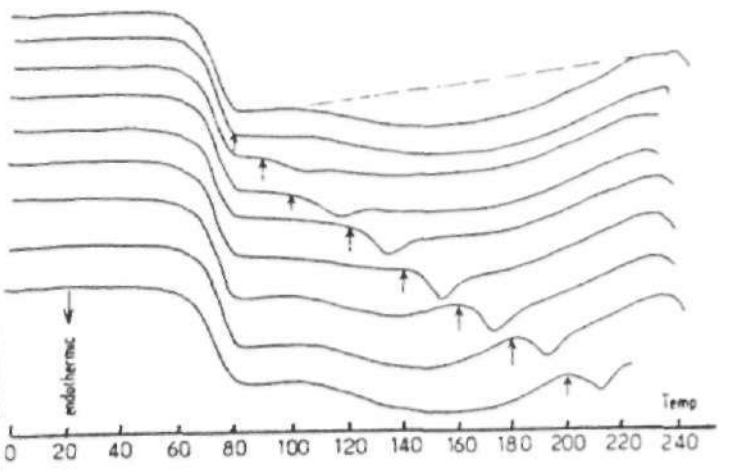


Fig. 1.9(b)

Differential scanning calorimetry of a suspension PVC sample cooled at 20°C/min from 240°C and annealed 5 min at the indicated temperature

Note: T_B *is indicated by the arrow* in both Figures 1.9(a) and 1.9(b).[56]

Most studies have been confined to the effect of annealing below[55,115] or above the T_g.[36,40,56,96] However, Gilbert and Vyvoda[114] investigated the effect of various processing techniques, including samples prepared on a Brabender Plasticorder, extruded on a twin-screw, and compression moulded. Results of thermal analysis on these samples (Figure 1.9(a)) are remarkably similar to the results of annealing above T_g reported by Ohta[40] and Illers[56](Figure 1.9(b)). Gilbert and Vyvoda[114] identified two melting (A- and B-) endotherms (Figure 1.9(a)), corresponding to the melting of lower and higher ordered crystal structures; which is reminiscent of the two crystal populations discussed in section 1.1.2. These authors also showed that the onset of the 'B'-endotherm, designated 'B-' onset temperature T_B, gives an accurate measure of the processing temperature as shown in Figure 1.10(b). Exactly the same obsrvations were made by Illers[56] and by Ohta et al.,[40] when an annealed sample is scanned, the latter authors found that an endotherm peak temperature, "T_{sub}", always corresponded with the annealing temperature as shown in Figure 1.10(a).

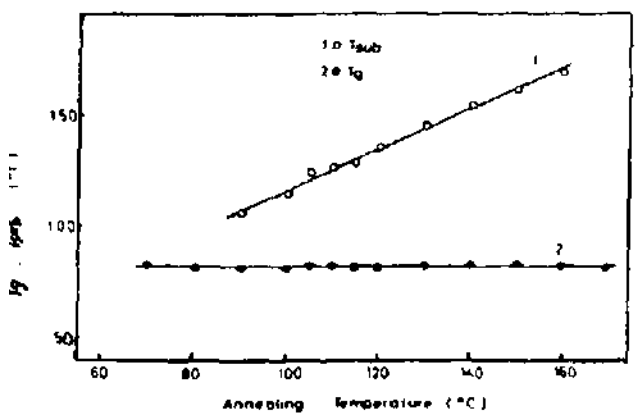


Fig. 1.10(a)

The variations of T_g and T_{sub} with annealing temperature[40]

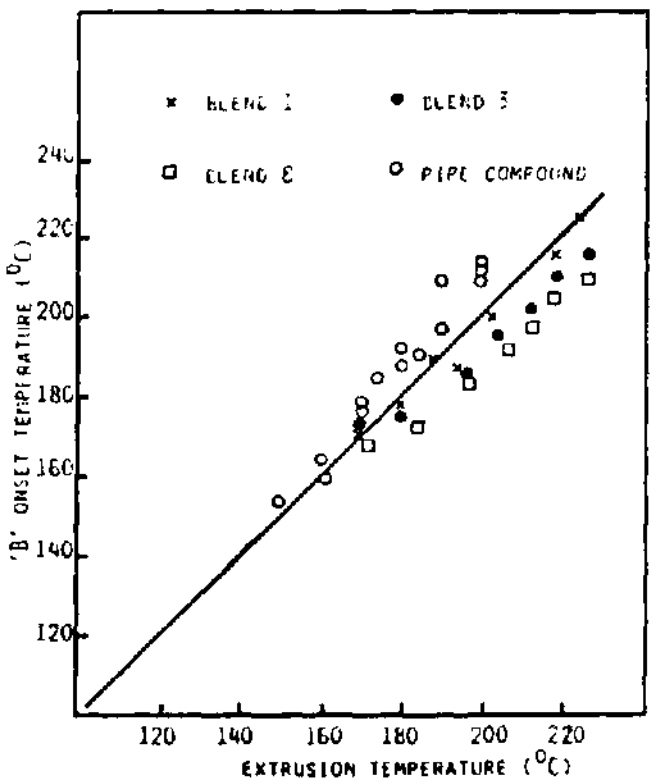


Fig. 1.10(b)

'B' onset temperature vs. extrusion temperature[114]

The obvious conclusion from the above is that processing PVC on a high shear equipment such as the Brabender Plasticorder or on a low shear equipment such as compression moulding produces a thermal effect on the ordered molecules identical to the effect of simple annealing at the same temperature. This fact has been noted by Illers[56] and Gilbert and Vyvoda.[114] The latter authors also showed that the endothermal energy corresponding to the A-endotherm varies with processing temperature in the same fashion as the entrance pressure loss in capillary rheometry of the same sample. Based on these findings they suggested thermal analysis as a potential method of PVC fusion level evaluation. As will be shown in section 1.5.4, if the absolute value of the heat of fusion of the perfectly syndiotactic PVC crystal is known, absolute values of fusion level may be obtained that will depend only on the processing temperature.[116]

1.5 Evaluation of Structural Order in PVC

1.5.1 X-ray Analysis

The theoretical basis of x-ray diffraction by polymers is well covered in the litarature.[117-120] Three types of studies[121] are performed on PVC by x-ray techniques, wide-angle x-ray diffraction (WAXD), covering Bragg angle 2Θ 10° to 50°; small-angle x-ray diffraction (SAXD), 2Θ 0.2° to 2.0°; and small-angle x-ray scattering (SAXS), 2Θ 0.06° to 1.0°. This study is restricted to the WAXD technique.

Observation of the x-ray pattern of PVC is difficult[129] owing to the very low diffraction intensity. This can be attributed to a number of factors: the crystallizable syndiotactic fraction is low for the commercial (atactic) polymer[49,50] so that a significant contribution to the amorphous

background by the non-crystalline isotactic and atactic fractions may be expected. Order along the chain direction is poor[31,33] which reduces the number of effective reflection planes contributing to the measured intensity, and lastly, the crystallites are of small sizes (Figures 1.3(a) to (c)), this results in line broadening and poor resolution of the peaks even at optimum instrument setting. The technique is nontheless a very useful one.

Quantitative analysis of x-ray diffraction by polymers is based on the existence of two phases, a crystalline phase of ordered-chain segments forming linkages between an amorphous phase of disordered chains (Figure 1.3(b)). Since the intensity of the x-rays scattered over all angles by a given assemblage of atoms is independent of their state of order or disorder,[119] it should follow that if the crystalline scattering, I_c, and the amorphous scattering, I_a, can be separated from each other, the crystalline fraction, X, is equal to the ratio of the integrated crystalline scattering to the total scattering.

$$X = I_c/(I_a + I_c) \qquad 1.5$$

In determinations of absolute crystallinities, the measured intensities must be corrected for a number of experimental factors;[119] however, for the purpose of ranking sample crystallinities, such corrections may not be necessary[129] since they are expected to be common to all samples. Moreover, in conventional PVC x-ray studies the inherent error involved in separating I_c and I_a, particularly in very diffuse patterns, may not justify rigorous correction.

Several methods are available for quantitative analysis of the diffraction trace, a simplified method developed by Ruland[120] gives the crystalline fraction as:

$$X = I_c/(I_c + KI_a) \qquad 1.6$$

where K as a correction factor, taking into account among other effects that the scattering intensity of the chosen crystalline reflections occurs at a different angular distribution than the amorphous.[118] Mammi and Nardi[44] and Lebedev et al.[122] have obtained the value K = 1 for PVC in the region 2Θ 10°-46°, thus for PVC eqns. 1.5 and 1.6 are identical.

A major problem with x-ray analysis of PVC is finding a reliable means of separating the crystalline peaks from the amorphous background.[123] Although claims have been made of quenching from high temperatures to obtain[36,39,41,45] an amorphous sample, there is sufficient evidence to doubt the amorphous character of quenched samples.[2,47,123-127] It is known that order at the microdomain level is very stable and persists well into the degradation temperature,[36,58,90,113] and indeed in some instances, as observed in this study, the peak intensities of quenched samples may be better defined than those of normal samples at high temperatures. Roldan[123] and his co-workers have developed a technique for obtaining an amorphous trace without the need for a completely amorphous sample. It is claimed[123] that a disoriented scan can be obtained by rotating the sample, with the aid of a rotating specimen holder, at a specific speed. Hermans and Weidinger[128] have developed an analytic procedure which can be used in case a completely amorphous standard is not available comprising the following steps.

(1) The diffraction patterns of a number of specimens of the polymer with various degrees of crystallinity are normalized to equal x-ray optical density and equal intensity of the direct beam.

(2) A reasonable demarkation line is drawn between the crystalline and amorphous scattering.

(3) Suitable peak or integral intensities proportional to the crystalline, I_c, and amorphous, I_a, fractions are selected and measured.

(4) Linearity of the I_c vs I_a curves to within experimental error provides confirmation that the method of measuring these quantities is in harmony with theory.

The crystalline, ϕ_c, and amorphous, ϕ_a, areas are then assumed to be proportional to the weight fraction of the crystalline polymer, X, and the weight fraction of the amorphous polymer, 1-X, so that

$$\phi_c = XC \qquad 1.7$$

and

$$\phi_a = (1-X)A \qquad 1.8$$

where C and A are the respective values of ϕ_c and ϕ_a for 100% crystalline and 100% amorphous samples respectively. Eliminating X and rearranging leads to

$$\phi_c = -\frac{C}{A}\phi_a + C \qquad 1.9$$

By plotting ϕ_c vs ϕ_a a linear curve results from which values of C and A may be obtained which can be used in conjunction with eqn. 1.7 or 1.8 to calculate the crystallinity index

$$X = \frac{1}{(C/A)(\phi_a/\phi_c) + 1} \qquad 1.10$$

Normalization, which takes account of non-angular dependent intensity differences, is carried out by dividing ϕ_c and ϕ_a by the total area under the

curve between 2Θ 10° to 46°. As a result of this normalization the Hermans-Weidinger method has a further advantage of not requiring correction of the diffraction intensities. This method has, therefore, been used in this study.

1.5.2 Density Measurements

Density is the most basic macroscopic quantity of the crystal, being linked directly to the unit cell parameters. Thus the density of the sample if carefully determined should give the most reliable value of the crystallinity.

Densities of a series of polymer samples may differ by only very small amounts, therefore special techniques are required for accurate measurements. Three techniques are widely used,[118] density gradient column, dilatometry, and pycnometry. The gradient method is a further development of the floatation technique[130] in which the density is determined by matching the bouyancy of the unknown solid and the surrounding liquid so that the solid floats freely for an extended length of time. The column is set up by mixing various proportions of a heavy and a light solvent so that the density in a glass column increases linearly from the top to the bottom. The gradient is determined with calibrated floats which are accurate to $\pm 0.0002 g/cm^3$ at a fixed temperature. Since heights of floatation can be measured to $\pm 0.05 cm$, four-digit accuracy can be achieved routinely.

Density determinations on melt crystallized polymers show clearly that experimental values do not reach the unit cell densities. The data obtained lie somewhere between the crystalline and amorphous density. Based on these observations, a fractional crystallinity is usually

calculated based on the assumption that the sample consists of relatively perfect crystals and an unaffected amorphous region (basically the same two-phase system used for x-ray analysis) the weight fraction crystallinity, X, *is then evaluated as:*[118]

$$\text{total volume} = \frac{W}{\rho} = \frac{W_a}{\rho_a} + \frac{W_c}{\rho_c} \qquad 1.11$$

where W and ρ are the total sample weight and density respectively and the W_a, ρ_a, W_c, ρ_c are the respective values for the amorphous and crystalline sample respectively. By definition, the weight fraction crystallinity, X, is

$$X = \frac{W_c}{W} \qquad 1.12$$

substituting for X in eqn. 1.11 gives

$$\frac{1}{\rho} = \frac{1 - X}{\rho_a} + \frac{X}{\rho_c} \qquad 1.13$$

eqn. 1.13 can be rearranged to give the crystalline fraction,

$$X = \frac{(\frac{\rho_c}{\rho})(\rho - \rho_a)}{(\rho_c - \rho_a)} \qquad 1.14$$

Similarly the volume fraction crystallinity can be obtained as

$$X_v = \frac{(\rho - \rho_a)}{(\rho_c - \rho_a)} \qquad 1.15$$

1.5.3 Solvent Sorption

A readily accessible property of the dense phase is the resistance offered to the diffusion of small molecules. A study of the kinetics of diffusion was reported long ago by Fick,[131,132] however, the diffusion of solvent molecules in a glassy polymer is often accompanied by 'anomalous' effects not easily understood in terms of Fick's law. The non-Fickean behaviour is characterized, according to Alfrey et al.,[133] by several features: (1) As the solvent molecules penetrate into the polymer, a sharp advancing boundary separates the inner glassy region from the swollen outer shell. (2) At temperatures well below T_g of the unswollen polymer, the distance of penetration, or the weight gain, increases linearly with time, i.e., the boundary between the glassy core and the swollen shell advances at a constant velocity.

Diffusion occurs only in the amorphous regions, therefore appropriate analysis of the diffusion kinetics could provide useful information about the crystallite structure and the bulk phase morphology. According to Micheals and Parker,[134] the reduction in diffusion constants[131] due to the presence of crystallites could be expressed as

$$D = D^*/\psi\beta \qquad 1.16$$

where D^* is the diffusion constant in the completely amorphous polymer and ψ is a geometric impedance factor accounting for the necessity of molecules to bypass crystallites and move through amorphous regions of non-uniform cross-sectional area. β is a chain mobilization factor reflecting decreased chain segment mobility in the amorphous phase due to proximity of crystallites. The impedance factor, ψ, has been related by Micheals and Bixler,[135] to the amorphous fraction, α, using the expression

$$\psi = \alpha^n \qquad 1.17$$

where n is a constant characterized by the chemical nature of the molecules and the configuration of the chains.

In general, however, two models of diffusion, Fickean (Case I)[131] and Fickean-Relaxation (Case II),[133] have been employed in interpreting organic vapour transport in glassy polymers. Using Crank's model[132] of discontinuous changes of the diffusion constant, D, with concentration, generalized diffusion models have been developed.[136-143]

The diffusion of acetone in unplasticized, PVC, UPVC, was shown by Kwei et al.[139] to be well described by the combination of both Case I and Case II mechanisms. Lapcik et al.[140] derived the expression

$$\delta = (2Dt)^{1/2} \qquad 1.18$$

for the rate of penetration of a number of organic solvents in UPVC, where δ is the total thickness of the swollen surface at time t. They found the dependence of the diffusion constant, D, to be described by the usual Arrhenius relation

$$D = D^* \exp(-E_D/RT) \qquad 1.19$$

where D* is defined in eqn. 1.16, E_D the activation energy of diffusion, R the gas constant, and T the temperature.

Berens[141] has carried out an extensive study of the conditions where Case I or Case II sorption predominates in the sorption of vinyl chloride monomer (VCM) by PVC powder grains. He demonstrated that pseudo non-Fickean behaviour can be observed where powdered PVC is the solid phase, even under known Fickean conditions. His work has been

extended by Daniels and Longeway[142] to VCM desorption from PVC, and by Quy[143] to plasticizer absorption by suspension PVC powder. In the ensuing paragraphs the theoretical basis is presented in the framework of the generalized models developed previously[132,136-143] to describe the combination of Fickean and Case II mechanisms.

The expression for diffusion in one dimension is

$$\frac{dc}{dt} = \frac{d}{dx}\left[\left(D\frac{dc}{dx} - vc\right)\right] \qquad 1.20$$

where c is the concentration at time t and distance x from the surface. The second term in the square brackets describes the contribution of internal stress arising from swelling of polymers and the quantity v represents the velocity of solvent penetration as a direct consequence of the internal stress effect. Both D and v are assumed to be constant in eqn. 1.20. For diffusion in a semi-infinite polymer with a constant penetrant concentration C_o at the surface, the concentration profile of the penetrant in the swollen polymer is given by

$$C(x,t) = \frac{C_o}{2}\left[e^{xv/D}\ erfc\ \left(\frac{x + vt}{2\ Dt}\right) + erfc\ \left(\frac{x - vt}{2\ Dt}\right)\right] \qquad 1.21$$

(The error function complement, erfc(x), is defined in ref. 132 and in standard mathematics texts)

The total amount of the penetrant per unit area entering the polymer is given by

$$M_t = C_o\left\{\frac{D}{v}\ erf\left[\frac{v}{2}\left(\frac{t}{D}\right)^{\frac{1}{2}}\right] + \frac{vt}{2}\ erfc\left[-\frac{v}{2}\left(\frac{t}{D}\right)^{\frac{1}{2}}\right] + \left(\frac{Dt}{\pi}\right)^{\frac{1}{2}}\ \exp\left(-\frac{v^2t}{4D}\right)\right\} \qquad 1.22$$

At large times eqn. 1.22 reduces to

$$M_t = C_o (D/V + vt) \qquad 1.23$$

In developing eqn. 1.23 Crank's[132] model has been adopted, i.e., the sharp advancing front of the penetrant is a consequence of the discontinuity in the diffusion coefficient as concentration changes. The advancing solvent front is located at C_x, and it is assumed that $D = D_t$ at $C > C_x$ and $D = D_2 \approx 0$ at $C < C_x$. The value of C_x can be calculated from plots of depth of penetration , l, vs t by use of eqn. 1.21. The three parameters V, D and C_x define the concentration profile of diffusion. Eqn. 1.23 is a linear dependence of weight gain with time, the slope gives the velocity of the solvent front and the intercept gives the diffusion constant, D.

The above model has been modified by Tshudy et al.[138] to incorporate a parameter for irreversible immobilization which considers sorption to occur by two distinct mechanisms: ordinary diffusion-controlled sorption and sorption resulting from the immobilization of diffusing gas molecules by pre-existing sites in the polymer. Meares is reported[144] to have demonstrated the existence of structural defects or 'holes' in the glassy state of poly(vinyl acetate), PVAc, which disappeared above the T_g. While these 'holes' have a profound effect on the sorption behaviour of glassy PVAc, causing abnormally high solubilities and negative enthalpies of sorption, the diffusion process of gaseous molecules appears to be normal and Fickean.[144] The advantage of Tshudy's model is its demonstrated ability to reveal the independent effects of normal diffusion-controlled sorption and sorption by immobilization caused by the presence of 'holes'. However, his conclusion that Case II behaviour is accounted for

solely by immobilization-controlled sorption is questionable if Meares' results for PVAc are generally true for semi-crystalline glassy polymers.

The average particle size of the sorbing units can be evaluated from the generalized model of Berens.[141] Using Crank's[132] solution for the non-steady-state diffusion in a sphere of uniform particles, Berens showed that at constant concentration at the surface, and constant D, the reduced weight gain with time is

$$\frac{M_t}{M_\infty} = 1 - \frac{6}{\pi^2} \sum_{n=1}^{\infty} \frac{1}{n^2} \exp\left(-4Dn^2 \pi^2 t/d^2\right) \qquad 1.24$$

where d is the diameter of the sorbing particles. For a distribution of particle sizes, Berens found that the particle diameter, d, can be replaced by an average value $\bar{d}$ with equal validity. This procedure was adopted by Daniels and Longeway[142] and Quy,[143] eqn. 1.24 may then be rewritten as

$$\frac{M_t - M_\infty}{M_o - M_\infty} = \frac{6}{\pi^2} \sum_{n=1}^{\infty} \frac{1}{n^2} \exp\left(-4n^2 \pi^2 Dt/\bar{d}^2\right) \qquad 1.25$$

The average particle diameter $\bar{d}$ is obtained from a plot of M_t/M_∞ vs $t^{\frac{1}{2}}$ using eqn. 1.24, and for rigid PVC film, Berens[141] found from this plot (Figure 1.11(a)) that

$$t_{0.5} = 0.049 \frac{l^2}{D} \qquad 1.26$$

where l is the thickness of the film. It may be noted that eqn. 1.26 predicts inconveniently long times for experiments on films of any reasonable thickness.

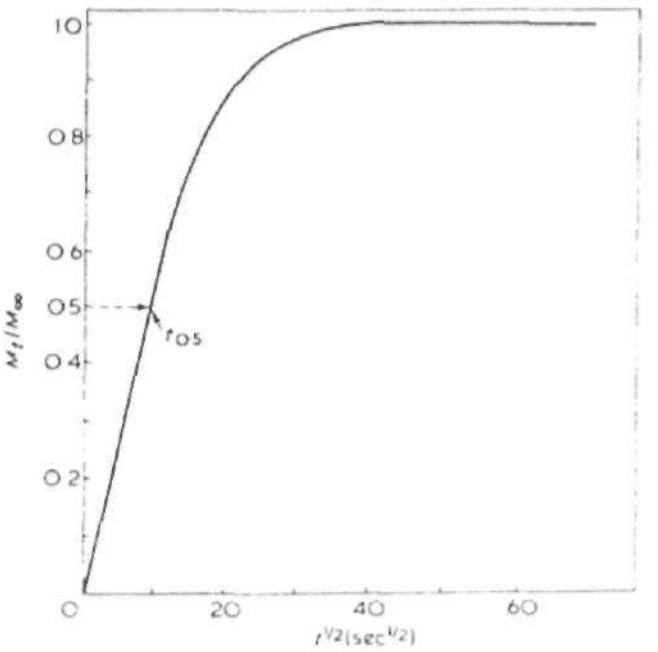


Fig. 1.11(a)

Plot of M_t/M_∞ vs. $t^{\frac{1}{2}}$

calculated from $\bar{d}^2/D = 10^4$sec

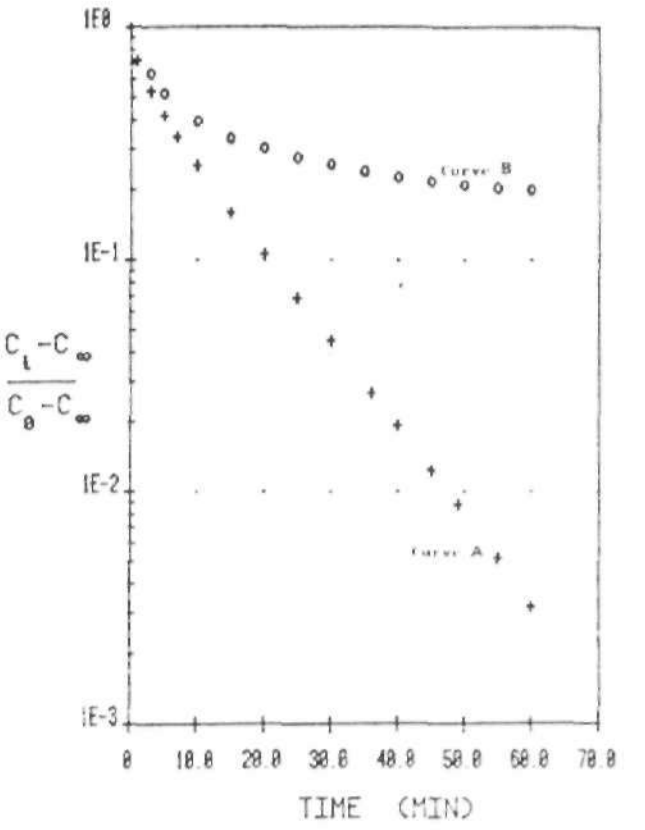


Fig. 1.11(b)

Sorption curves showing Fickean (A)

and non-Fickean (B) behaviour

Alternatively $\bar{d}$ can be obtained using eqn 1.25 from the slope of $\log (M_t - M_\infty) / (M_0 - M_\infty)$ vs t (Figure 1.11(b)) and

$$\text{slope} = -\frac{4\pi^2 D}{2.303\bar{d}^2} \qquad 1.27$$

The various effects of particle size non-uniformity and Case II mechanisms on the observed deviation from Fickean sorption have been described by Berens.[141]

1.5.4 Thermal Analysis

Thermal analysis as a tool for studying the fusion process has been described in section 1.4.3. The technique can be used to determine the degree of crystallinity since an imperfect crystalline polymer shows an increased enthalpy compared with that of the perfect crystal. Adiabatic calorimetry as well as differential thermal analysis have been used.[145-147]

The general equation relating the weight fraction crystallinity, X, to a thermal measurement is:[118]

$$C_p = XC_{pc} + (1-X)C_{pa} + (dX/dT)\,\Delta H_u \qquad 1.28$$

where C_p is the measured heat capacity which is composed of the proper fractions of the heat capacity of the crystalline polymer, C_{pc}, and the heat capacity of the amorphous polymer, C_{pa}. ΔH_u is the heat of fusion of the perfect chain folded crystal. With data obtained on polyethylene, Wunderlich[148] has shown that the first deviation due to $dX/dT \neq 0$ occurs above T_g but remains a relatively small percentage of the total heat of fusion as T_m is approached. As a result, in the usual method of crystallinity determination, one tries to eliminate the heat capacity contribution by an approximate choice of baseline. The heat of fusion evaluated therefrom, ΔH^*, is compared to the heat of fusion of the completely crystalline polymer, ΔH_u, to obtain the weight fraction crystallinity:[40,118]

$$X = \frac{\Delta H^*}{\Delta H_u} \qquad 1.29$$

Problems arising from the use of eqn. 1.29 in PVC studies involve determination of ΔH_u.[55,56,116]

Use of Flory's[17] theory of melting of copolymers may be considered in the case of commercial PVC, here the copolymer comprises of crystallizable syndiotactic sequences and non-crystallizable atactic sequences. The melting point depression is related to the crystalline fraction, X, as:

$$\ln X = \frac{\Delta H_f^*}{R} \left(\frac{1}{T_m} - \frac{1}{T_m^\circ} \right) \qquad 1.30$$

where R is the gas constant, T_m° the melting temperature of the completely crystalline sample, and T_m the melting temperature of the copolymer with crystalline fraction, X, having a heat of fusion ΔH^*.

1.6 Mechanical Properties of PVC:

The Impact Resistance

The mechanical properties of a plastic material depend on the basic properties of the polymer chain molecule as well as on other factors such as processing and environmental conditions.[149] Two modes of failure may be broadly defined, ductile and brittle fracture. In ductile fracture failure is preceded by substantial deformation of the failure zone, while in brittle fracture failure does not involve deformation but results from crack propagation.[150] A third important failure mechanism is crazing, this is considered to be the formation of microcracks bridged by fibrillar structures.[151]

Three modes of failure have been identified for pressurized PVC pipes,[152] brittle fracture when circumferential stress level is high, partially ductile fracture only after prolonged times at medium stresses, and thermal crack growth (creep crazing) after very long times at low

stress levels. In general, however, a ductile/brittle transition can be observed. This transition is accompanied by an abrupt drop in impact strength,[153] thus impact testing is vital to an understanding of the factors controlling the fracture process. The transition from ductile to brittle fracture can be induced by several modifications to the testing conditions[153] such as:

(1) Reducing the testing temperature

(2) Changing the testing rate

(3) Notching with sharp cracks

(4) Having surface rather than edge cracks, and

(5) Increasing the specimen thickness.

The first two variables modify the physical properties of the polymer through the normal time- and temperature-dependence. The other three geometric factors have the effect of producing plane-strain (biaxial stress field) conditions at the crack tip, Figure 1.12. The thickness effect, for instance, arises because the state of stress near the crack tip varies from plane stress (triaxial stress field) in the surface regions of a relatively thin plate, or throughout the thickness of a thin plate, to plane strain in the centre of a thick plate. If the testing conditions are kept constant, a ductile/brittle transition may also be induced by making modifications to the material[153] such as

(6) annealing (or processing)

(7) reducing the molar mass

(8) reducing the plasticizer content, and

(9) cross-linking (network formation).

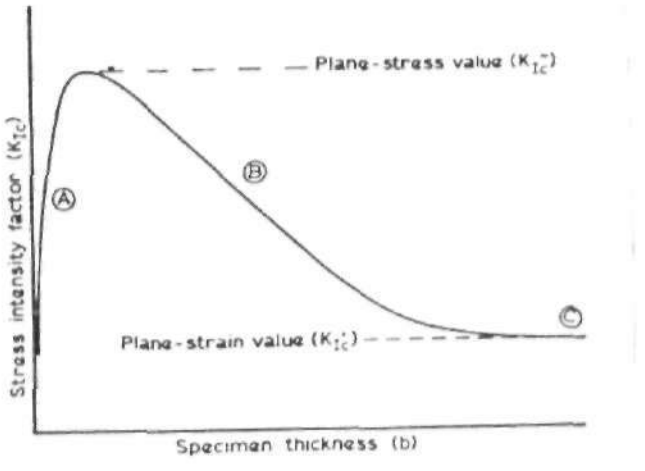


Fig. 1.12

Variation of the measured stress-intensity factor, K_{1c}, at failure as a function of specimen thickness, b.[153]

The effect of processing on the impact strength of PVC has been extensively studied; however, results differ markedly between different research groups.

An increase in both notched and unnotched impact strength (NIS and UNIS) with increased processing temperature has been found by some authors, notably Berens and Folt[6] and Gonze[102] for tensile impact tests (TIS); Menges and Berndsten[154] for Charpy-UNIS; Lamberty,[103] for falling weight impact strength (FWIS), and Summers.[155] These workers performed the tests on samples extruded at different temperatures. For compression moulded and roll-milled samples, however, Malac[156] and Gross et al.[157] found a decreasing NIS with increased temperature.

Considering the factors affecting the ductile-brittle transition a maximum impact strength with increased processing temperature should be expected due to the annealing effect of the processing temperature on the unmelted crystallites. Such a maximum is demonstrated by the works of

Bystedt[158] using FWIS, Benjamin[159] using TIS, and Terselius[160,161] using FWIS and Charpy-NIS and UNIS.

Pezzin et al.[162] have shown that for commercial PVC, room temperature tensile modulus and yield properties are little affected by processing history and crystallinity while elongation at break and fracture energy increase, at fixed strain rate, with milling temperature. The dynamic spectrum below T_g (T_α) was unaffected by thermal history and crystallinity.

Results obtained by a working party of IUPAC[163] on dynamic mechanical and impact properties of PVC have shown that two transition zones might be involved in impact and tensile tests. The first one, in the low strain-rate range, corresponds to a tough-tough mechanism and is caused or strongly influenced by adiabatic heating of the specimens; it was attributed by Oberst and Retting[164] to the glass transition of PVC. The second one, at much higher strain rates, gives rise to a tough-brittle mechanism. The tough-brittle transition was attributed to the β-transition measured in dynamic mechanical tests and the fracture in usual impact tests is said to take place in the time-temperature range of the β-transition. It seems, therefore, that contrary to Pezzin's[162] findings the results of the IUPAC Commission,[163] and results obtained by several research groups, suggest that the dynamic spectrum below the T_g should be affected by the thermal history as is the case with the impact strength. Randon,[165] for instance, found a close association between the β-transition and the maximum observed in fracture toughness measured both at high and at low rates of loading.

1.6.1 Impact Test Methods

The importance of impact testing is that such tests frequently indicate that many polymers which appear to exhibit tough, ductile failure when tested by tensile loading at a low or moderate strain-rate may suffer brittle fracture under impact loading when the strain rate is relatively high. A large number of tests have been devised to measure impact resistance, however, the impact strength is not a fundamental material property,[153] it depends both on the specimen geometry as well as on the specific test method. Thus, it is difficult to correlate the results obtained from different test techniques, and equally difficult to correlate the results of tests on specimens of the material to the impact performance of the manufactured article. Nonetheless results of tests on specimens will continue to serve as useful indications of the performance of articles in service. Some attempts[166-168] have been made which enable the correlation of results of the Charpy and Izod test methods by the use of fracture mechanics approach.

The difficulties of interpretation and correlation of impact strength measurements arise from the fact that the energy measured is a composite term. In the case of flexed-beam pendulum tests (Charpy and Izod), Ireland[169] has identified five causes of energy loss:

$$U_H = U_{SD} + U_I + U_B + U_{MV} + U_{ME} \qquad 1.31$$

where U_H = loss in pendulum energy when the hammer strikes the specimen

U_{SD} = total energy consumed by specimen deformation and fracture, e.g. in bending, crack initiation and propagation,

U_I = increment of energy required to accelerate the specimen fvom rest to the velocity of the hammer,

U_B = energy absorbed by the impact machine through vibrations after initial contact with the specimen, and

U_{ME} = elastic energy stored by the machine.

Turner[170] has pointed out that the term 'impact strength' is a loose misnomer since the usual practice is to record the energy absorbed by the specimen before it breaks. Thus the impact energy is actually determined which may then be expressed as:

(1) the energy per unit area of the broken cross-section

(2) the energy per unit length of the notch

(3) the energy per unit width of the specimen, or

(4) the energy per unit volume of the specimen.

It is generally agreed that expressing the impact strength as the energy absorbed per unit area of the broken cross-section is the most satisfactory of the various definitions.

Three basic categories of test methods are used for impact strength measurement:[170]

(1) Flexed-beam impact

(2) Falling-weight impact, and

(3) High-speed tensile impact.

Two flexed-beam impact tests, the Charpy and the Izod methods, are most commonly used, and a standard test procedure is described for both in BS 2782 and ASTM D256.

Table 1.2

Order of Magnitude Characteristics of Various Impact Tests

Test method	Order of magnitude of strain rate (s^{-1})	Impact velocity (ms^{-1})
Flexed beam		
Charpy	10	3
Izod	60	2
Falling weight	10^{-1}-10	1-4
Conventional tensile	10^{-3}-10^{-1}	10^{-5}-10^{-1}
Pneumatic gun	10^{2}-10^{4}	20-240
Hydraulically operated	1-10^{2}	0.008-4

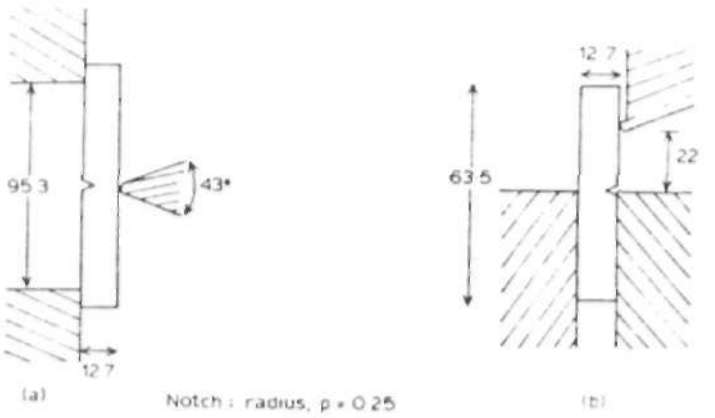


Fig. 1.13

Geometry of testing and specimen support arangement for (a) Charpy; and (b) Izod tests specified in ASTM D256 (All dimensions in mm)

While impact tests are generally considered to cover the high-strain-rate end of the strain-rate spectrum, the data tabulated by Reed[171] (Table 1.2) indicate that flexed-beam and falling weight impact tests do not necessarily provide particularly high strain rates. In the notched beam tests, however, the strain-rate at the notch tip is considerably higher and has been estimated[153] to be of the order of $5 \times 10^3 s^{-1}$. The basic difference between the Charpy and the Izod tests is the manner in which the specimen is supported as shown in Figure 1.13. It is held horizontally but not clamped in the Charpy test, and clamped in a vertical position at its lower end in the Izod.

1.7 Aim of Study

This study is basically an investigation of fusion (or gelation) at molecular level as it relates to processing variables; the methods used in fusion measurement are also critically re-examined. The aim is to get a better understanding of the fusion process and of the factors that affect the reliability of its measurement.

The impact behaviour of processed samples was also studied to obtain a possible correlation between gelation levels, as measured by the various methods, and impact strength. It is hoped to get a better understanding of the effect of variations of material and processing on impact performance.

Chapter 2

EXPERIMENTAL TECHNIQUES

2.1 Materials

2.1.1 Poly(vinyl chloride)

Five commercial grade suspension PVC homopolymers, covering a range of molecular weights, were used. These include a 'Breon' sample, S110/11, of medium molecular weight supplied by BP Chemicals, UK, and four 'Corvic' samples having a range of K-values supplied by ICI Ltd., UK. The technical data for these materials are presented in Table 2.1, and in Table 2.2 their molecular weights and weight distributions are given. The latter were determined by gel permeation chromatography at the Rubber and Plastics Research Association, Shawbury, UK.

Table 2.1

Technical data for PVC samples[172,173]

Property/Units	- Corvic -				Breon
	S57/116	S62/109	S68/173	S71/102	S110/11
K-value	57	62	67	71	66
Viscosity number	80	95	116	128	111
Packing density g/ml	0.62	0.64	0.65	0.54	0.55
Apparent density g/ml	0.55	0.59	0.57	0.50	-
Passing 250μm wt%	99.9	99.9	99.9	99.5	99.5
Passing 75μm wt%	5.0	5.0	5.0	2.0	2.0
Volatile content wt%	0.2	0.2	0.2	-	0.5

Table 2.2

Molecular weights of PVC samples

Sample	$10^{-4}\bar{M}_n$		$10^{-4}\bar{M}_w$	$\bar{M}_w/\bar{M}_n$
S57/116	3.00	6.13	7.00*	2.04
S62/109	3.42	7.24	-	2.12
S110/11	4.44	10.00	12.00*	2.25
S71/102	4.38	10.26	20.00*	2.35
S68/173	4.75	10.43	14.00*	2.20

The choice of molecular weight range is limited by the processibility of the polymer with regard to bulk density, particle size distribution, ease of gelation, powder mixing properties and heat stability.

2.1.2 Additives

The additives used include lead, and thio-organo tin stabilizers, dibasic lead stearate (DBLS), and dibutyl tin mercaptide (stanclere T135) respectively, with a combination of lubricants having external or internal lubricating properties. These include normal lead stearate (external), calcium stearate (internal lubricant and stabilizer), and Georg Schultz 2411P wax, a grade of the so-called hard wax with external lubricating property. All additives were supplied by Akzo Chemicals, UK, with the exception of Georg Schultz 2411P wax which was supplied by Cornelius Company, UK. The technical data for these additives is provided in Table 2.3.

* Values of $\bar{M}_w$ provided by ICI Ltd, Runcorn, UK. These values were found to be in excellent agreement with the results of the various studies in this work.

Table 2.3

Technical data of additives[174,175]

Additive	Form/ colour	Specific gravity 20°c	Melting point 1°C	Viscosity poise 20°C	Refractive index n_D^{20}	Lead content %
Dibasic lead stearate $2PbO.Pb(C_{17}H_{35}CO_2)_2$	Powder white	1.9	7200	-	1.60	51
Normal lead stearate $Pb(C_{17}H_{35}CO_2)_2$	Powder white	1.4	112	-	1.59	27.7
Stanclere T135	Liquid Gardner	1.11	-	0.5	1.506	-
Calcium stearate $Ca(C_{17}H_{35}CO_2)_2$	Powder white	1.03	120-196	-	-	-
G.S. Wax 2411P	Powder white	-	84-101	-	-	-

It was observed that whereas DBLS could not effectively stabilize the polymer in compression moulding, and was therefore not used, the organo tin stabilizer provided excellent stabilization giving products with good clarity. The tin stabilizer was therefore used in both compression moulding and in extrusion using the Krauss-Maffei. Use of DBLS was thus restricted to extrusion using the Leistritz. This point is further discussed in Chapter 5.

2.2 Sample Preparation

2.2.1 Formulation

In order to reduce the effect of the additive system on the measured variables, a very simple formulation has been used based on PVC-stabilizer-lubricant system. Details of the composition are provided in Table 2.4.

Table 2.4 PVC Formulations

Sample Code	Breon S110/11	Dibasic lead Stearate*	Stanclere T135* (phr)	Normal lead Stearate*	Calcium Stearate*	Wax+ GS2311P
A	100	2.5	-	-	0.8	0.3
B	100	1.5	-	1.5	0.4	0.3
S0	100	-	3.0	-	-	-
SCa	100	-	3.0	-	3.0	-
L02	100	-	3.0	-	3.0	0.25
L05	100	-	3.0	-	3.0	0.50
L10	100	-	3.0	-	3.0	1.0
L15	100	-	3.0	-	3.0	1.50
L30	100	-	3.0	-	3.0	3.0
L45	100	-	3.0	-	3.0	4.5

* Supplied by Akzo Chemical (UK) Ltd.

\+ Supplied by Cornelius Co., London.

To prepare the formulation the required amount of additive is weighed into 2kg portions of PVC powder and manually mixed with the resin with the aid of a spatula. This process helps to prevent flocculation of the additives during high-speed blending. Material so formulated is then transferred into the preheated high-speed mixer for dry blending.

2.2.2 Dry Blending

A 8l T.K. Fielder laboratory high-speed mixer was used at conditions previously determined [176,177] to give optimum blend properties.

A schematic diagram of the Fielder is shown in Figure 2.1; it consists of a combination of a mixing and a cooling unit. The mixer is a 8l steam heated jacket incorporating a set of rotors and an adjustable baffle. The rotor blades provide the high impact energy necessary for particle breakdown while the baffle optimizes the mixing action by changing the flow pattern. The conditions used are shown in Table 2.5.

Table 2.5

Blending conditions on the T.K. Fielder mixer

Conditions	Stage	
	mixing	cooling
Jacket temp (°C)	75 ± 2	ambient
Dwell time (min)	15 ± 3	5 ± 2
Rotor speed (rpm)	3600	1000
Discharge temp (°C)	120	50

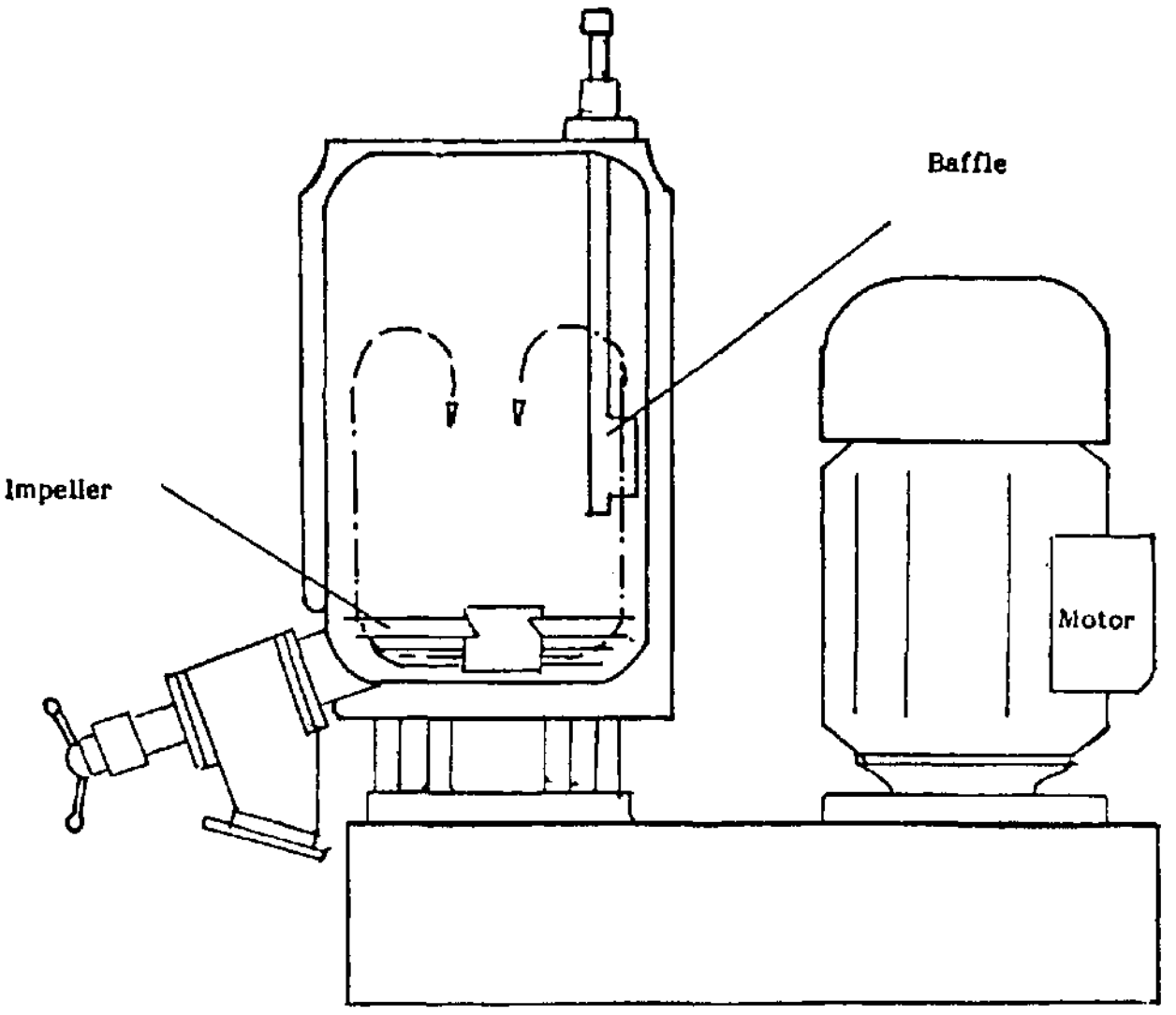


Fig. 2.1 A schematic representation of the T.K. Fielder

2.2.3 Compression Moulding

Flat sheets, 200mm x 200mm x 4mm were compression moulded from the powder blend at temperatures ranging from 160-220°c using an electrically heated press.

It is stated in BS 2782 pt 9, method 901A for PVC, that the mould charge should preferably be in the form of milled sheet rather than powder, but this has to be modified here in order to avoid the well known effect of heat history on the moulded product.

To obtain samples free from defects, the following conditions were used:

charge weight	250g
moulding temp.	(160-220) $\pm$ 10°C
heating duration	15 $\pm$ 3 min
cooling time	10 $\pm$ 2 min
cooling temp.	55 + 5°C
pressure	70 bar

2.2.4 Extrusion Details

The extrusion programme was carried out on Leistritz LS30:34 and Krauss-Maffei KMDL-25 contra-rotating twin screw extruders fitted with strip dies, 3mm x 20mm and 4mm x 30mm respectively. Tables 2.6 and 2.7 show the temperature and extrusion rate conditions used, and Figures 2.2 and 2.3 depict the screw configurations along with temperature/pressure zones and monitoring positions for the Leistritz and Krauss-Maffei respectively.

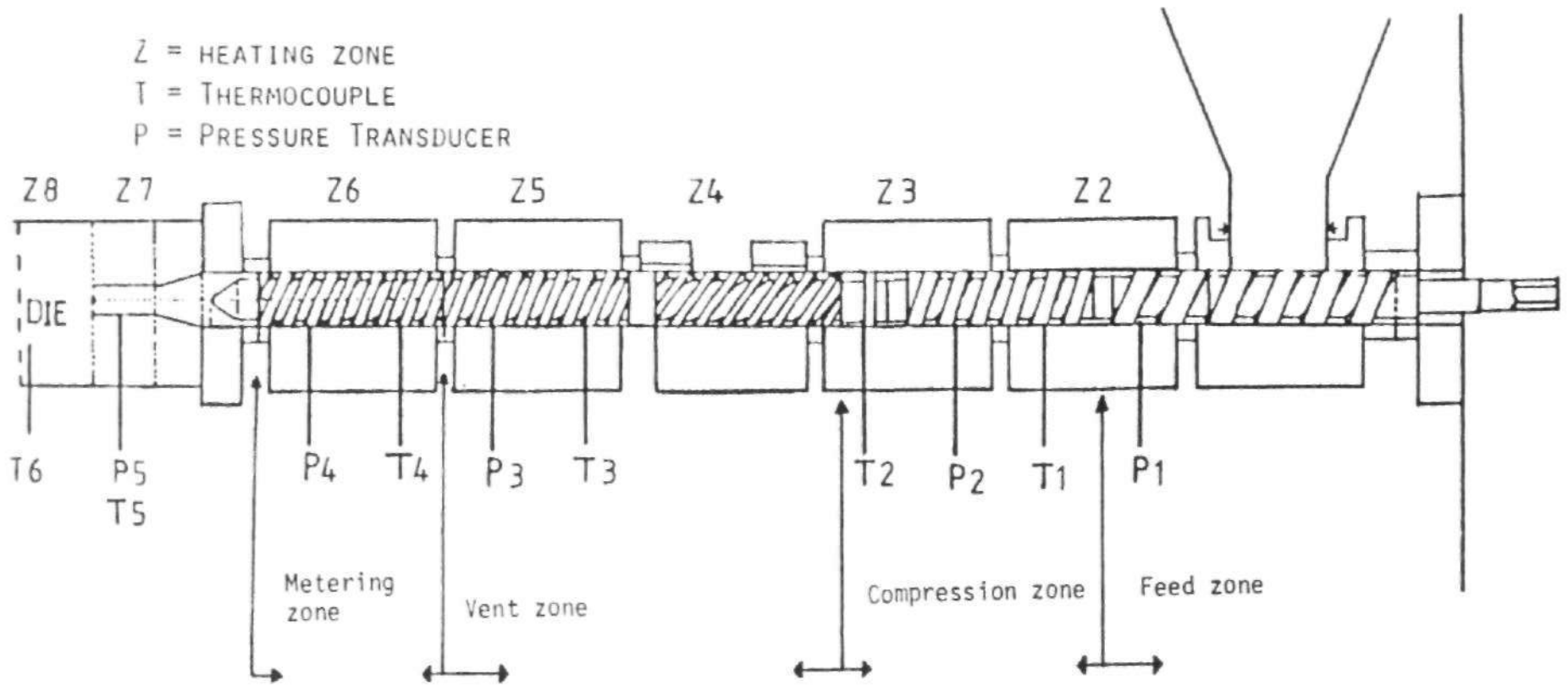


Fig. 2.2 Schematic representation of the Leistritz LS.30.34 twin-screw extruder

Z = Heating Zone

T = Thermocouple

P = Pressure Transducer

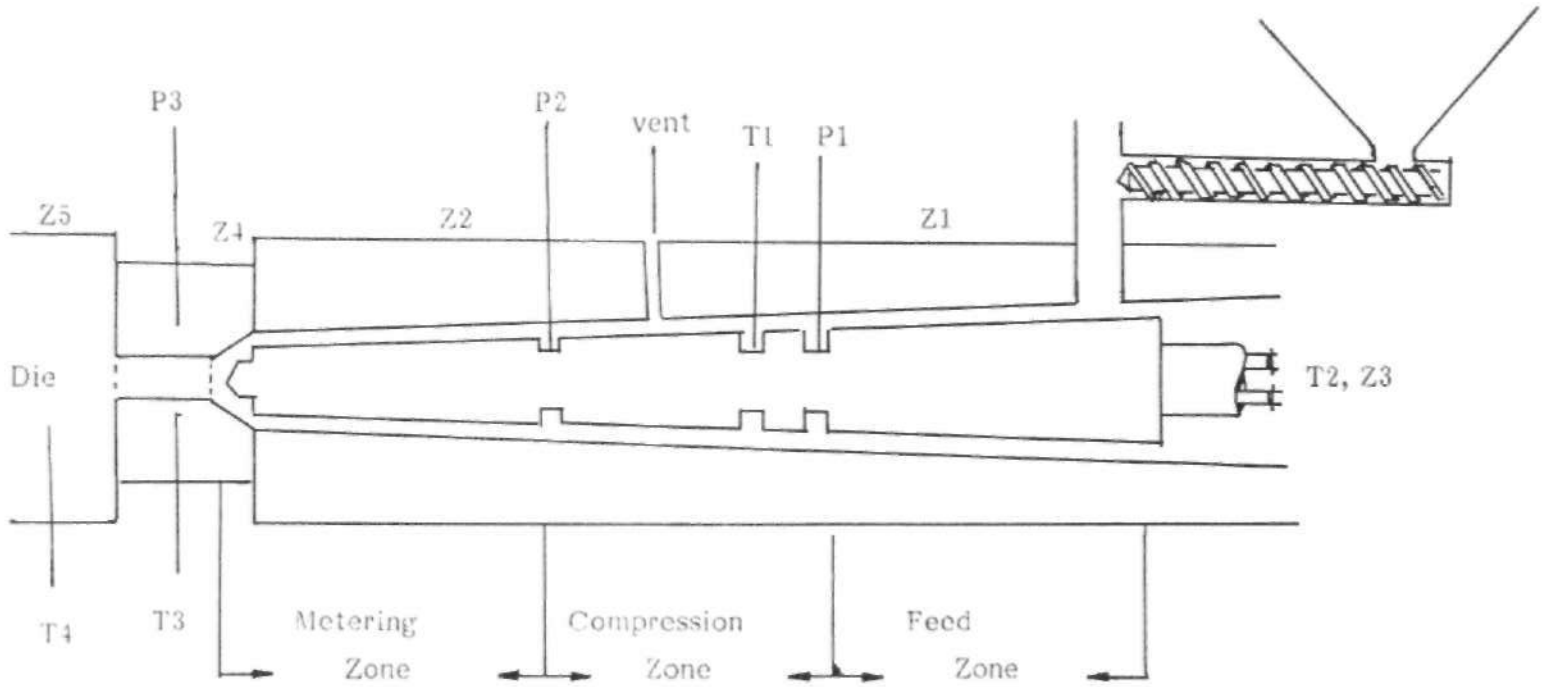


Fig. 2.3 Schematic representation of the Krauss-Maffei KMDL-25 twin-screw extruder

Attached to the Leistritz is a Hewlett Packard 1000 computer which recorded temperature and pressure data at 0.05 second intervals in each run. Such data were available only from the control panel of the Krauss-Maffei.

The extruded strip was sized and cooled in a water trough then hauled-off at a rate dependent on the extrusion conditions. The extrudate was sampled at equilibrium conditions. Samples taken at accurate time intervals (1.0 min or 30 sec depending on extrusion rate) were weighed to obtain the output rate.

Table 2.6

Extrusion conditions on the Leistritz

Extruder zone temperature/°C							Temperature
Z2	Z3	Z4	Z5	Z6	Z7	Z8*	profile
161	160	161	157	155	161	170	A
167	165	165	160	161	168	180	B
169	173	171	171	171	177	190	C
177	180	180	169	169	183	197	D
168	190	190	184	184	193	205	E
168	208	208	202	202	207	213	F
173	217	216	212	211	215	220	G
173	215	214	212	210	214	227	H

Extruder screw speeds/rpm							
10	15	20	25	30	35	40	50

* Die temperature

Table 2.7

Extrusion conditions on the Krauss-Maffei

Extruder zone temperature/°C				Temperature
Z2	Z3*	Z4	Z5+	profile
160	130	168	170	A
170	130	178	180	B
180	135	188	190	C
190	140	198	200	D
200	150	208	210	E
210	160	218	220	F
220	160	228	230	G

Dosing = 40/min; extrusion rate = 20rpm

* Screw temperature

\+ Die temperature

2.3 Density Measurements

The densities of processed samples were measured using a Davenport density gradient column at 23.0 ± 0.1°C. The column was filled with aqueous calcium nitrate and calibrated with glass floats of accurately known densities. Carefully prepared samples were cleaned in ethanol and dipped in a solution of calcium nitrate before placing in the column. Polishing the surface and dipping in a solution prevent air bubbles from adhering to the sample surface. The average of three measurements was used for each extrusion condition and samples were allowed 4 hours to attain equilibrium positions before each measurement.

To obtain the density of processed PVC alone, measured values were corrected for the densities of additives using the relationship[67]

$$d_c = \frac{100 + \Sigma P_i}{(100/d'_c) + \Sigma P_i/d_i} \qquad 2.1$$

where d_c is the measured density, P_i's are the concentrations in phr of the additives, d_i's their relative densities, and d'_c the actual density of the processed PVC.

2.4(a) Sorption Measurements

Specimens of the processed material, about 28mm x 14mm x 4mm, were prepared and weighed. These were then immersed in excess reagent grade acetone contained in 30cm^3 stoppered glass bottles. The acetone uptake was followed gravimetrically with time over a 30-hr period at 23°C. The percentage weight gain was calculated and presented as reduced sorption curves. Averages of five measurements were used although from the consistency of the results averages of three measurements would have been sufficient.

2.4(b) Methylene Chloride Swelling Tests

This test, very basic in its procedure, is one of the widely used tests for gelation level of processed PVC. It has been carried out to ASTM D2152 specifications.

Specimens of the processed sample, about 100mm x 10mm, were immersed to a depth of 40mm in reagent grade methylene chloride contained in sample bottles.

The samples were continuously inspected (visually) for attack on the surface, i.e. the lifting, raising or removal of any material from the specimen. The time taken to the initiation of attack was assumed to be

representative of the degree of fusion. Solvent attack was monitored for 2 hrs after which the sample was passed as "unattacked".

2.5 Capillary Rheometry

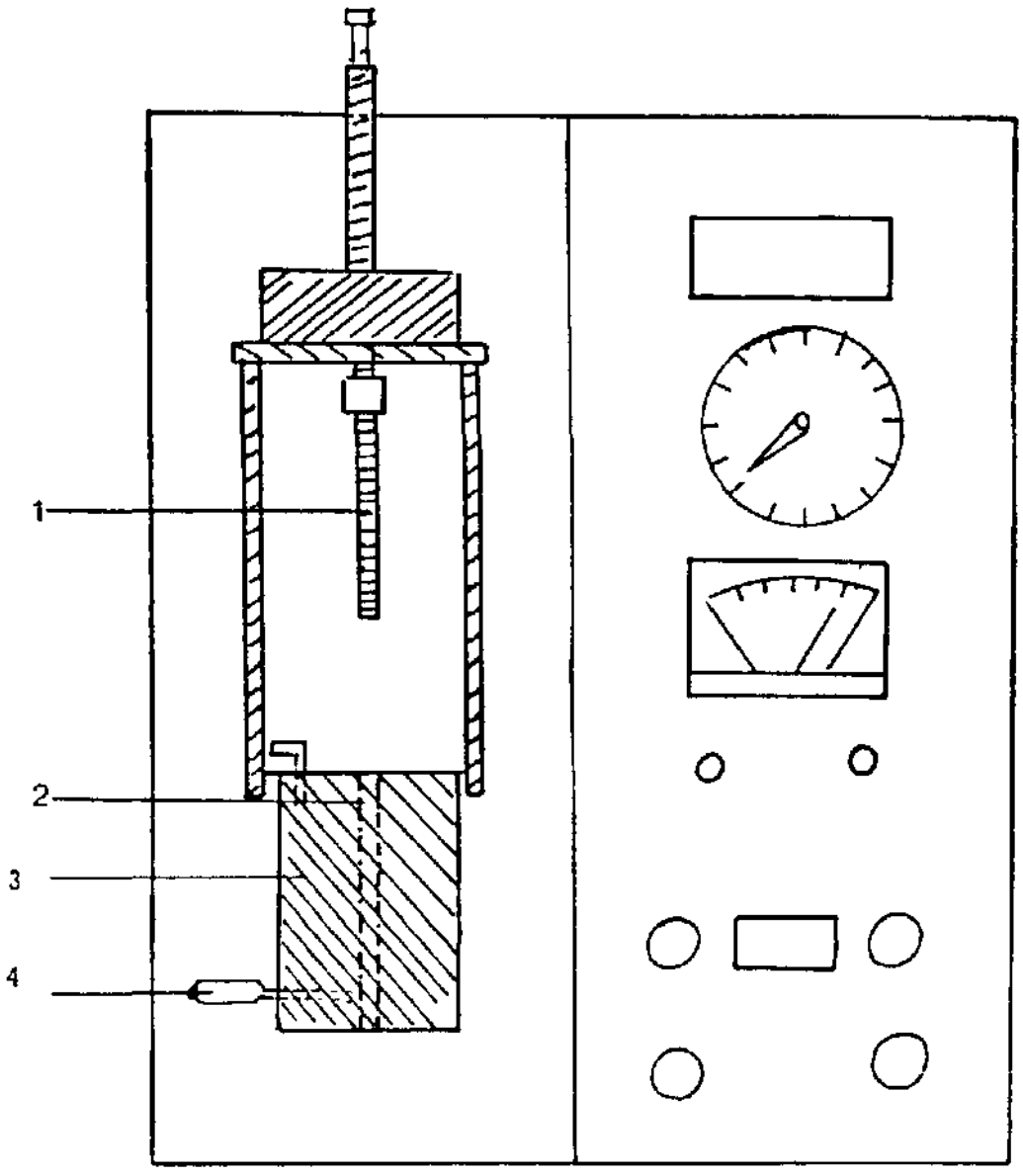
The gelation level was estimated with a Davenport capillary rheometer equipped with an effectively zero-length die (L/D = 0.38).

The rheometer consists of a 22mm diameter piston capable of being driven in or out of a controlled heated barrel. The die is fitted into the base of the barrel so that the polymer is extruded vertically downwards. A pressure transducer fitted into the barrel which flushes with its sides and with the top end of the die measures the extrusion pressure which is recorded on a calibrated chart recorder as mV. This is converted to pressure using a calibration curve.

About 30g of processed PVC were packed into the barrel and compressed by lowering the piston. It was left to thermally equilibrate at 130°C for 10 min then extruded using a piston speed of 20mm/min. The average of three measurements was used. A schematic diagram of the front view of the rheometer is shown in Figure 2.4.

2.6 Thermal Analysis

The heats of fusion of the processed polymer were determined using a Du Pont 990 Thermal Analyser equipped with a DSC cell. A diagram of the calorimetry cell is shown in Figure 2.5. A sample pan and a reference pan were positioned on the two raised platforms of the constantan disc as shown. The cell operates at a constant heating rate using a single heating block as the heat supply for both sample and



1 - Piston

2 - Capillary

3 - Barrel

4 - Transducer

Fig. 2.4 Schematic diagram of the Davenport Capillary Rheometer: Front view

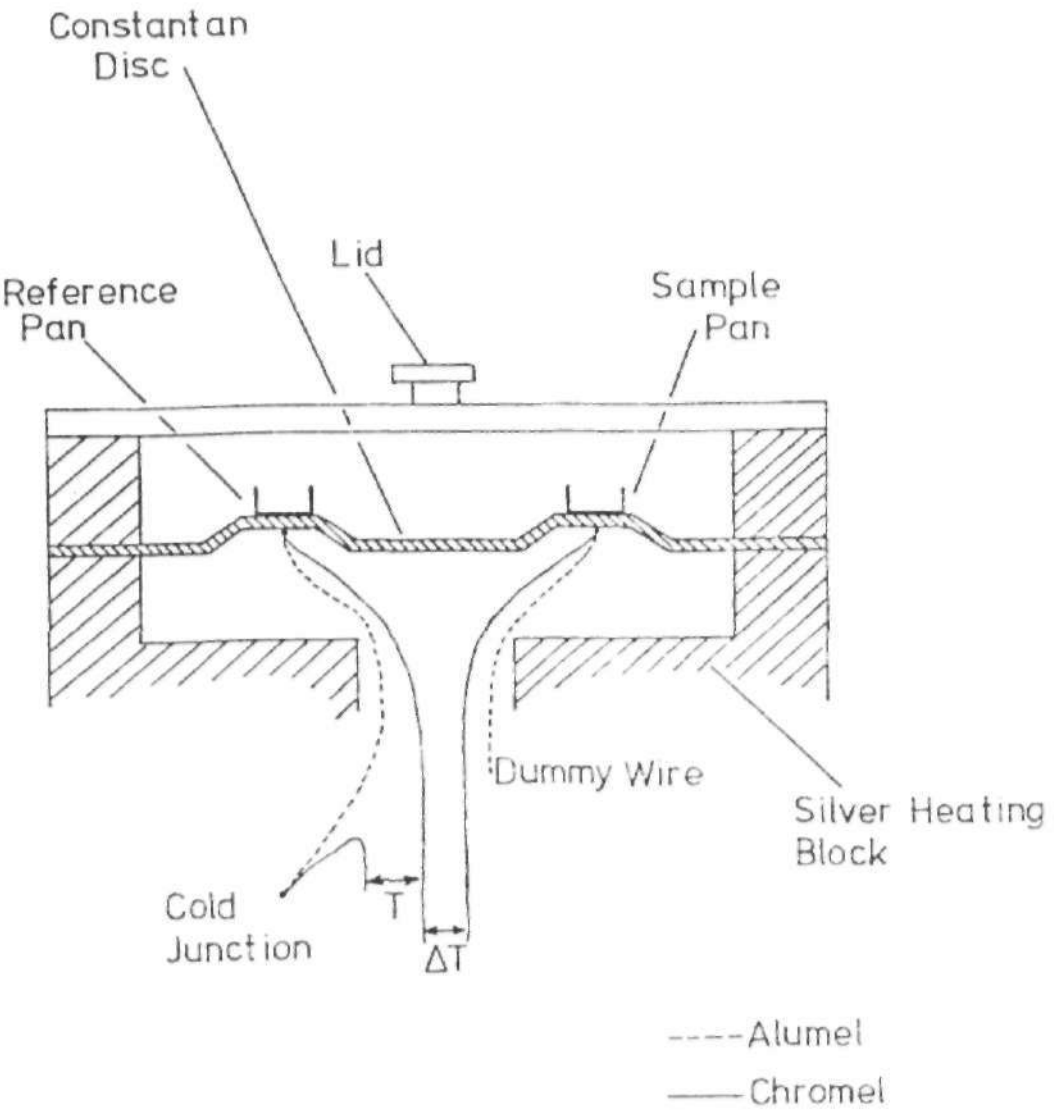


Fig. 2.5 Calorimetry cell of Du Pont 990 Thermal Analyser

reference pans. The instrument was used in the calorimetric mode such that the temperature difference ($_{\Delta}T$) between the sample and the reference junction was plotted against the reference temperature.

The temperature axis of the instrument was calibrated using pure samples of indium and tin metals having melting points of 156.6°C and 231.9°C and heats of fusion of 6.79cal/g and 14.14cal/g respectively.

About 10mg of the processed polymer were scanned from room temperature to 240°C at a heating rate of 20°C/min. and y-axis (Δ T-axis) sensitivity of 2mV/cm.

Areas of the thermograms were measured with the aid of a planimeter and the heat of fusion evaluated using the expression:

$$\Delta H_f = \frac{A}{m} (60\ B\ E\ {}_{\Delta}qs) \qquad 2.2$$

where ΔH_f = heat of fusion (J/g)
A = endothermic area (cm^2)
m = sample mass (mg)
B = Time Base setting = 0.5 min/cm
Δ_{qs} = y-axis sensitivity (mV/cm.sec)
and E = cell calibration constant characteristic of the calorimeter cell used. It is evaluated from endotherm areas of standard (tin or indium) samples of accurately known ΔH_f.

2.7 X-ray Analysis

Wide angle x-ray data were obtained for a series of processed PVC samples with Jeol DX-GE-2S generator equipped with a DX-GO-S vertical goniometer using Ni-filtered Cu Kα radiation in an air atmosphere. Symmetric reflectance mode (Figure 2.6) measurements were made using

rectangular samples, 40 x 15 x 3mm. The following instrument settings were used:

tube voltage = 40kV

tube current = 30A

Slits : divergent, D = 2°; receiving, R = 0.1°;
and scattering, S = 2°

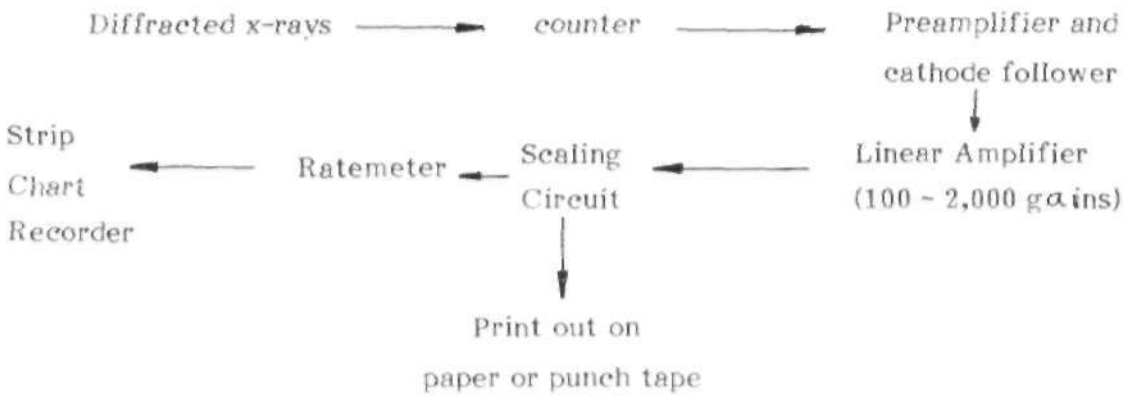
sensitivity = 1×10^3 cps

scan rate = 1°/min

Chart speed = 10mm/min

Angular range = 10° - 46° 2Θ

Trace of intensity against scattering angle was provided by a chart recorder equipped with two pens. One of the pens provided the trace while the second marked the chart at ½°2Θ intervals thus enabling calibration of the angular position. A schematic representation of the components of a diffractometer is shown below.



Detection of the scattered radiation by a counter technique offers the advantages of shorter exposure time and a more accurate determination of the intensities. Conversion of photographic film blackening to intensity cannot be done with the highest possible accuracy.

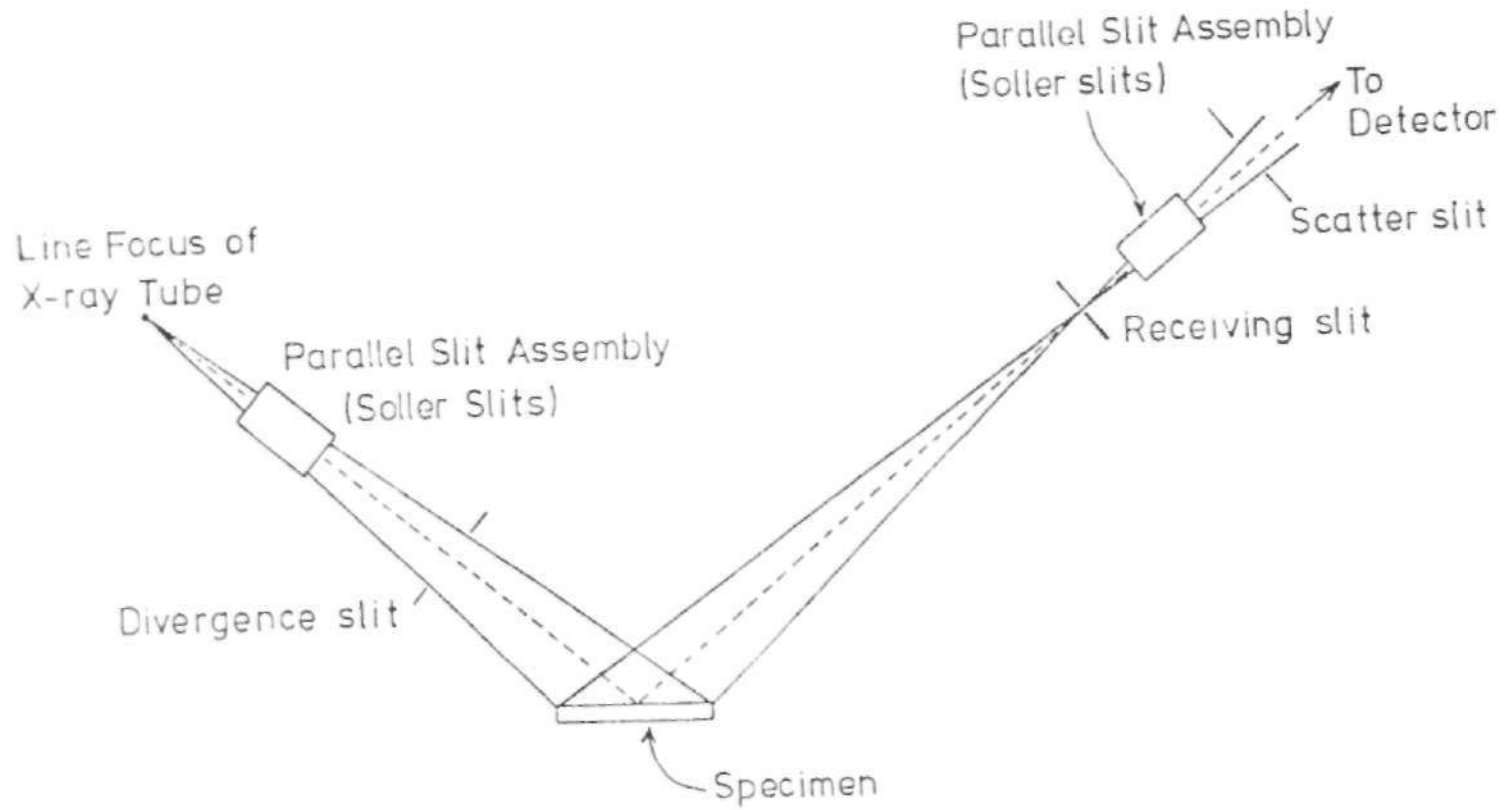


Fig. 2.6 Symmetric reflection diffractometer geometry

2.8 Impact Test

In order to obtain reproducible impact energy values, careful sample preparation is required.

The sample, cut along the extrusion direction, was polished using a conventional metallic tool polisher, the samples being firmly held in position with the aid of a double-sided tape. Polishing effectively eliminates die swell and surface roughness. Polished samples were trimmed to the standard length and width set by ASTM D256, the thickness was variable. Details of the dimensions are provided in Figure 2.7

Impact strength was determined with Ceast Analogic Fractoscope model AFS/MK2. The instrument consists essentially of two semi-independent units made up of the pendulum unit and the memory unit. The pendulum unit provides a direct measure of the impact energy when corrected for a 'friction factor' which is displayed in a free-fall, while the memory unit measures and stores the impulse at impact and the resistance (force) offered by the material to failure.

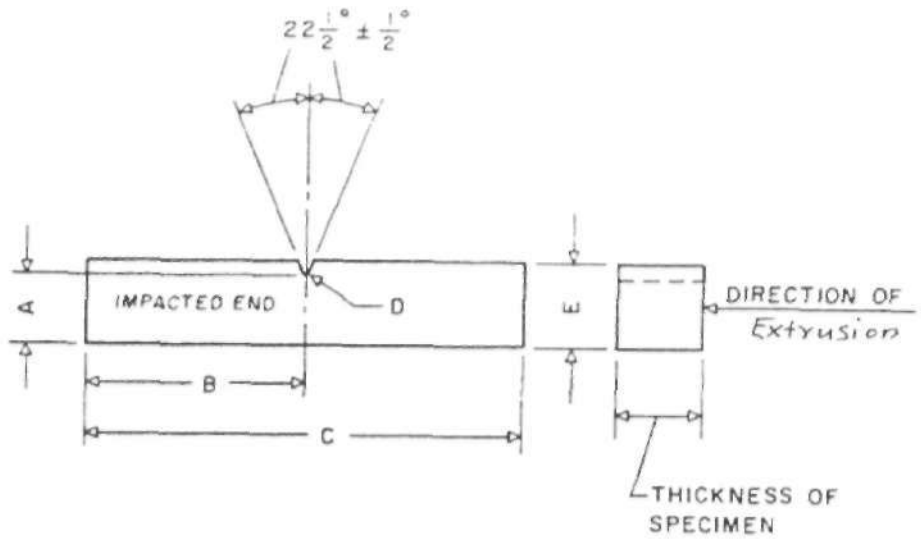
The traditional impact tester measures impact energy by measuring the rise-angle in the case of pendulum and statistically in the case of falling weight apparatus. With the AFS/MK2 system such measurement is obtained by processing the force-time values held in the memory. These values can be reproduced, prior to subsequent tests, as maximum load at break; integrated as force-time plots giving the variation of force and energy with the progress of failure; and giving the maximum failure energy when contribution from 'noise' (equipment vibration) is discounted.

The instrument was used in the 'Izod' mode, Figure 1.13, this mode had been previously found to give better discrimination between samples.[178] Tests were carried out at room temperature using the following conditions:

Force range	=	191 daN
Pendulum energy	=	15J
Pendulum mass	=	2.5kg
Impact speed	=	$3.46 ms^{-1}$
Time scale	=	0 - 2ms

The impact strength, , was evaluated as:

$$I.S = \frac{\text{impact energy (J)}}{\text{area behind notch } (m^2)}$$



A	=	10.2mm
B	=	31.8mm
C	=	63.5mm
D	=	0.25°
E	=	12.7mm
Specimen thickness	=	3 ± 1mm (variable)

Fig. 2.7 Dimensions of Izod impact test specimen

Chapter 3

RESULTS AND DISCUSSION

I. GELATION STUDIES

3.1 A Summary of Extrusion and Compression Moulding Results

3.1.1 Extrusion

A Leistritz LS:30:34 laboratory twin-screw extruder was used to prepare samples from 'Breon' PVC formulated as samples A and B (Table 2.4). The samples are described as L-(Leistritz) samples to distinguish them from compression moulded (CM) samples and Krauss Maffei extruded (KM) samples. The individual sample is also coded as shown in Tables 3.1 to 3.3.

At constant extrusion rate of 20rpm processing temperature was varied in steps of about 10°C between 170° to 230°C; and at constant temperature extrusion rate was varied between 10 to 50rpm in stages of about 5rpm over four different temperatures.

A Krauss Maffei KMD-L25 laboratory twin-screw extruder was used to extrude 'Corvic' PVC formulated as sample A (Table 2.4); a range of molecular weights was studied (Table 2.2). Extrusion rate was kept constant at 20rpm except where a higher rate was required, as indicated in Table 3.2, to offset polymer degradation.

3.1.1.1 Output Rate

Output rate varies only slightly with formulation and with molecular weight (Tables 3.1 and 3.2).

For a given molecular weight output rate is substantially constant with processing temperature. A slight increase is observed with increased lubricant loading (formulation B) and with increased molecular weight (KM samples).

The lubricant functions in reducing adhesion of the polymer to the metal surface and in reducing interparticle friction (section 1.2.1). As a consequence the more lubricated the material the faster it is passed through the extruder at constant extrusion rate. Reduced residence time results in increased output with increased lubricant loading.

Lubricant-polymer interaction decreases with increased molecular weight. If polymer flow characteristics do not change with changes in molecular weight, decreased interaction makes the lubricant action more external (section 1.2.1) reducing polymer-metal and interparticle friction. These result in increased output rate at constant extrusion rate as discussed above.

Output rate increases linearly with extrusion rate up to about 40rpm (Figure 3.1, also Table 3.1A in Appendix).

3.1.1.2 Power/Torque Variations

The power (or torque) needed to extrude the resin depends on the melt viscosity of the formulation. The melt viscosity decreases with increased melt (processing) temperature and with increased[77] lubricant loading. The power requirement is shown to follow similar trend (Figure 3.2).

The higher the molecular weight the greater the torque needed to extrude the polymer at constant temperature and for equal formulation (Table 3.2). Melt viscosity increases with increased molecular weight due to increased entanglement.

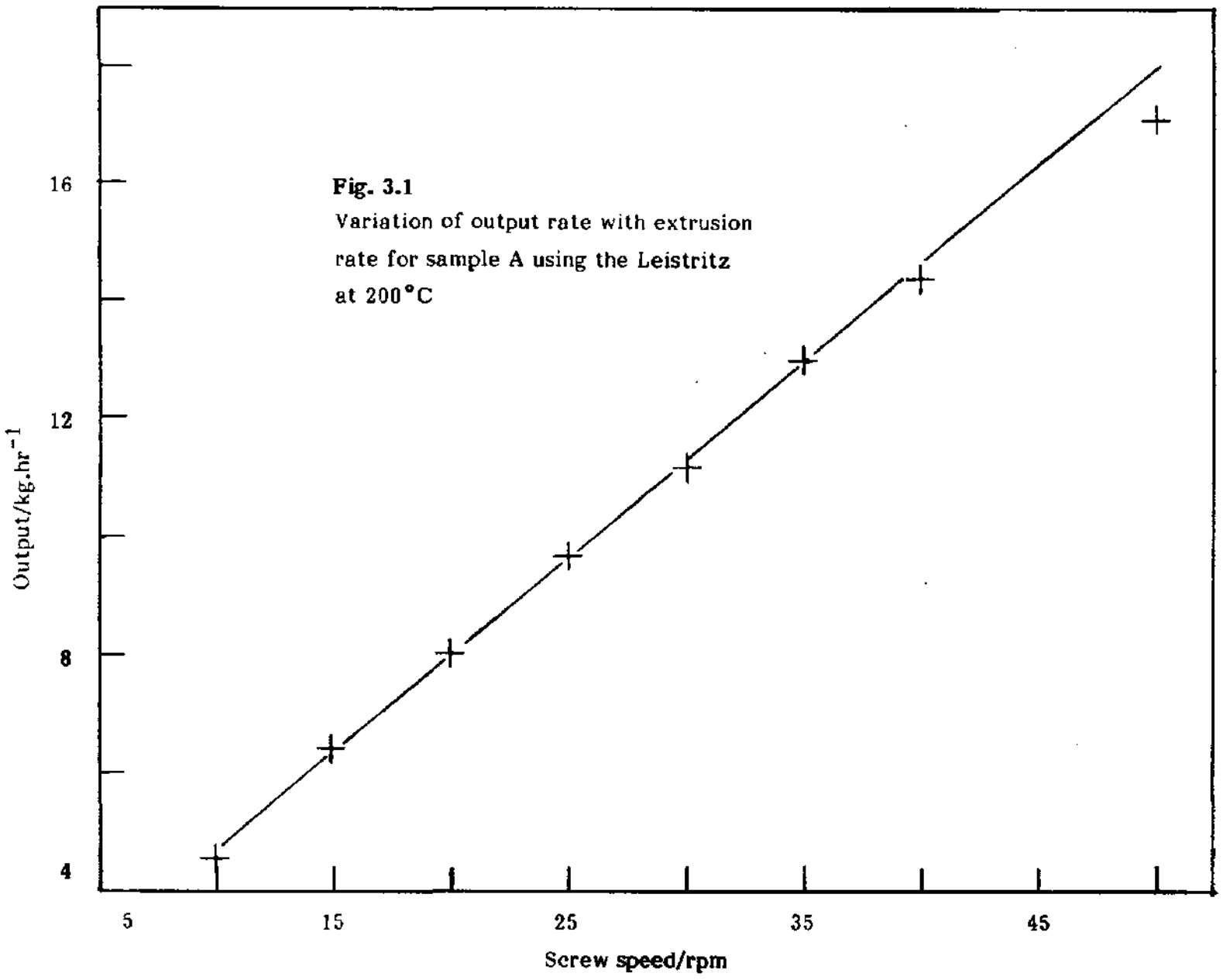


Fig. 3.1
Variation of output rate with extrusion rate for sample A using the Leistritz at 200°C

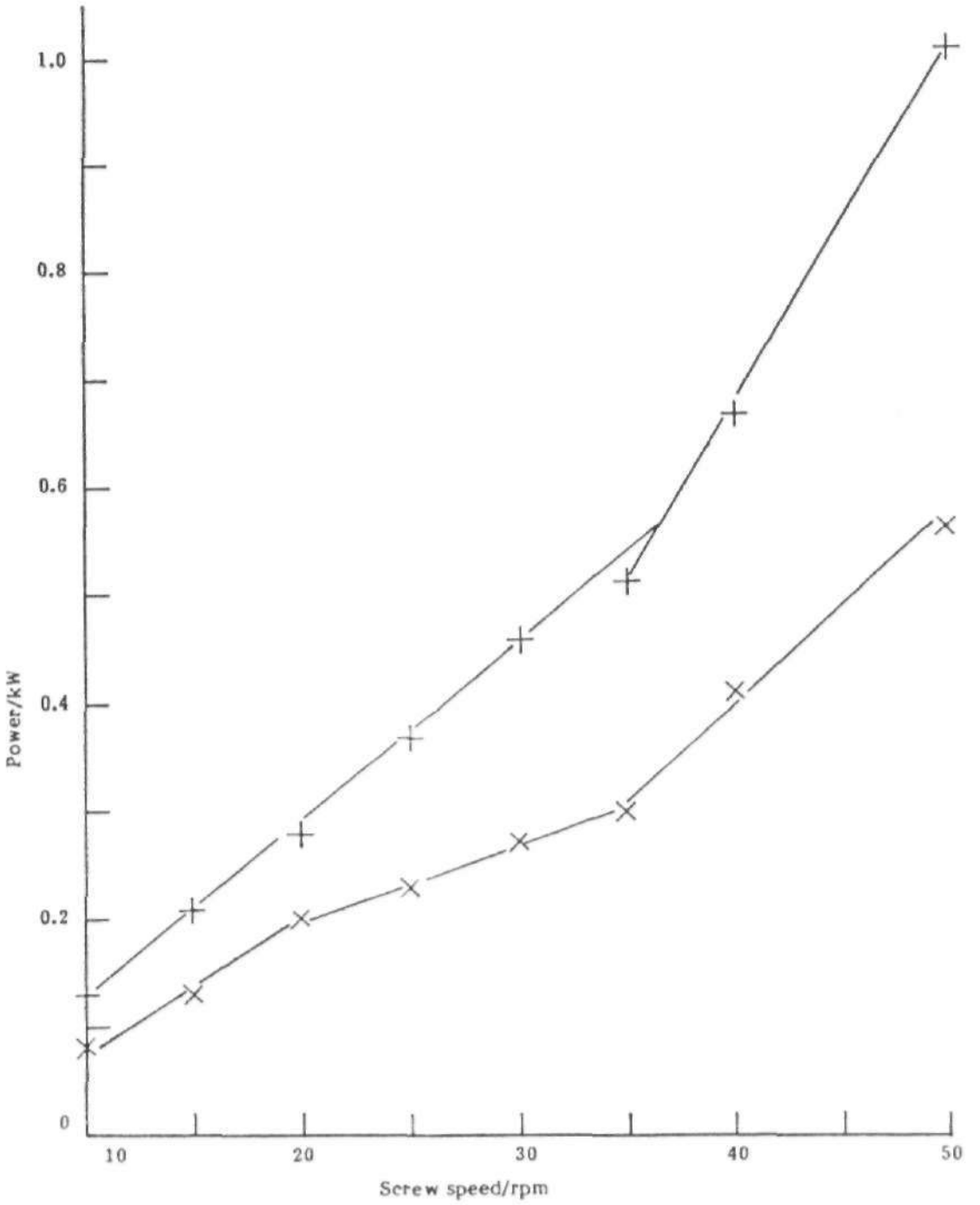


Fig. 3.2
Variation of power required for extrusion of samples A and B with extrusion rate using the Leistritz at 200°C; +, sample A; X, sample B

It is noted that for all properties measured in the KM series, sample S71 (Tables 2.1 and 2.2) is an exception. Thus both its output rate and power requirement are lower than would be expected for its K-value (Table 3.2). Repeated GPC characterizations (Table 2.2) gave lower than expected molecular weight and difficulties were experienced with its flow through the extruder. These differences are shown in Chapter 4 to arise from lower fusion levels for this sample.

Power requirement increases with increased extrusion rate as expected (Figure 3.2). The increase although linear is not uniform. Two or more changes in slope may be observed depending on the formulation. It is observed that (Chapter 5) there is an interesting relationship between the changes in slope and the impact resistance of these samples.

3.1.2 Compression Moulding

Large temperature differences, sometimes as high as $\pm 15^{\circ}C$, were observed between the opposite ends of the moulded sheet. For this reason samples could not be meaningfully tested for impact resistance as the size of the test specimen would include a range rather than a specific moulding temperature. For the same reasons capillary rheometry results are considered with caution. This limitation, however, does not affect the results of thermal analysis and methylene chloride tests since sample sizes are reasonably small.

Samples prepared as described before were tested for gelation (fusion) by capillary rheometry (CR), thermal analysis (TA), and methylene chloride attack (MCT). The results are presented and discussed below.

The terms gelation and fusion are used interchangeably except in section 3.6 where fusion is used in the thermodynamics sense to refer to melting.

Table 3.1

Output and power requirement for samples extruded at different temperatures using the Leistritz at 20rpm

Sample Code	*Die set* temp (°C)	*Die melt* temp, T_B(°C) method I	method II	Output kg/hr	Approx power (kW)
Sample A					
A-1	170	170	188	7.8	0.38
A-2-1	180	176	190	7.7	0.32
A-2-2	185	180	191	7.7	0.32
A-3	197	184	197	8.0	0.30
A-4	205	195	203	7.7	0.20
A-5	213	200	208	7.7	0.26
A-6	220	208	218	7.7	0.21
A-7	227	220	220	7.5	0.20
Sample B					
B-1	171	170	180	8.1	0.27
B-2-1	182	174	185	8.3	0.30
B-3	197	180	192	8.0	0.20
B-4	207	191	200	8.0	0.20
B-5	213	198	210	7.7	0.10
B-6	218	205	215	8.0	0.13
B-7	227	210	220	8.3	0.10

Table 3.2

Output and torque for samples extruded on the Krauss-Maffei at a constant rate, 20rpm

Sample Code		Die set temp (kW)	Die melt temp, T_B(°C) method I	method II	Output kg/hr	Approx torque (kW)
S57:	M11	160	161	176	6.0	24
	M12	172	162	176	6.0	20
	M13	180	174	185	6.1	20
	M14	190	175	184	6.3	18
	M15	201	185	196	6.1	15
	M16	210	190	200	6.0	15
	M17	220	200	214	6.2	15
S62:	M21	160	-	-	6.1	26
	M22	171	165	180	6.2	25
	M23	180	170	185	6.4	24
	M24	190	180	190	6.6	23
	M25	200	186	196	6.3	20
	M26	210	200	208	6.3	22
	M27	220	205	215	6.3	24
S68:	M31	170	165	180	6.9	30
	M32	180	170	185	7.0	28
	M33	190	178	190	7.1	24
	M34	200	185	198	7.1	23
	M35	210	195	205	7.0	20
	M36	220	206	214	7.1	21
	M37	230	218	227	7.3	23 (30rpm)
S71:	M41	170	165	182	5.7	25
	M42	180	174	184	5.8	24
	M43	190	180	192	5.9	23
	M44	200	190	199	6.0	22
	M45	210	197	205	6.0	20
	M46	220	208	219	6.0	20
	M47	230	216	225	5.8	18

3.2 Capillary Rheometry

CR test results are summarized in Figures 3.3 to 3.7. Detailed results for all processed samples are included in the appendix, the first number of the table refers to the relevant chapter, the capital letter 'A' designates 'Appendix'.

These results are discussed with respect to the effects of material and processing variables.

3.2.1 Effect of Processing Temperature

The entrance pressure loss, ΔP, at constant processing temperature, T_B, depends on the level of entanglement (elastic response level) attained during processing (section 1.4.1).

A sigmoid curve is usually observed (Figures 3.3 and 3.7), generally, however, curves can range from linear to sigmoid (Figure 3.5); and it is possible that in the absence of degradation a maximum could be observed for particular formulations. These variations are well illustrated in Figure 3.5 where the results of L- and CM-samples are compared.

The sigmoidal curve, which has been widely reported,[102-106] appears to depend on sample formulation and processing. For a CM sample containing no lubricant (sample SO) ΔP is linearly related to T_B (Figure 3.5). A linear relationship has not been reported in the literature. Linearity in the absence of the lubricant suggests that the sigmoidal nature of the curve arises from the effect of the lubricant. Capillary action has been evoked below to explain this effect.

Another interesting observation from Figure 3.5 is that in the absence of the lubricant (sample SO) highest values of ΔP obtain over the

entire range of T_B, suggesting that these samples are much more fused than even the extrudates. This is supported, surprisingly, by the results of thermal analysis and methylene chloride tests (sections 3.3 and 3.4).

Upon addition of the lubricant, however (Figure 3.5), even at low levels, a significant reduction in ΔP results (see Tables 3.2A to 3.4A for details) and the characteristic sigmoid curve, or its segment, is observed.

The results obtained for the CM series (Figure 3.5) are identical to those obtained by Krzewki and Collins[106] on samples with different lubricant loadings prepared on a Brabender Plasticorder. These authors have discussed their results on the basis of a particle breakdown fusion mechanism. It was shown in section 1.3.2(b) that particle breakdown is not generally applicable to all gelation processes.

The fusion process described by Figure 3.5 is discussed in the context of lubricant capillary action and its effect on interparticulate network formation and elastic development.

Allsopp[107] has shown that when PVC is processed on a low or medium shear equipment such as in twin-screw extrusion and compression moulding (Figure 1.6(b)), the grains are first compacted, densified, fused, and finally elongated — the 'CDFE' fusion mechanism (section 1.3.2(b)). This mechanism is supported by results of microscopy on our extrudates and compression moulded samples.[84] Indeed it is well known that compression moulding does not involve particle breakdown, therefore the sigmoid curves obtained for CM samples arise from effects other than breakdown of particles. In what follows an attempt is made to account for the sigmoid curve on the basis of lubricant action.

At low gelation (g-) levels (T_B below about 180°C), the processed sample contains largely densified and compacted granular particles. The

additives at this stage are located in between these particles in what seems like a two dimensional array of irregular hexagons.[84] Densification and compaction enhances the capillary action of the lubricant. As discussed elsewhere,[180] in capillary extrusion tests a lower ΔP than that of the unprocessed powder is obtained. The grains in the unprocessed powder are not sufficiently densified to enhance lubricant capillary action which permits lower ΔP by relieving applied pressure through particle slippage.

Lubricant lowering of $_{\Delta}P$ by capillary action explains the initial trough at low melt temperatures, absent when no lubricant is present (sample SO). The same effect is responsible for the negative g-levels[106] observed with increased lubricant loading.

With increased processing temperature polymer-lubricant interaction, initially low for the external lubricant, improves. The lubricant action becomes more internal[77] and the onset of molecular network formation across particle boundaries (elastic development) gives rise to increased ΔP creating the trough at T_B below 190°C. The depth and width of this trough are a measure of the lubricant efficiency in capillary action and in delaying elastic development respectively. Both the width and depth can increase with increased lubricant content and with increased shear. This is shown by our results (Figure 3.5) where samples have been prepared by compression moulding and by the results of Krzewki and Collins[106] where they were prepared on the Brabender.

Depending on the lubricant loading and the shear level a sudden rise in ΔP may be observed over a narrow temperature zone (Figure 3.5 and ref. 106). This change in slope corresponds to the well established change in the nature of the flow units in the melt.[181] It has been shown to correspond to the breakdown of the grains and the onset of primary

particle fusion,[28,63,101-107] with consequent increase in the rate of network formation.

The rise in ΔP levels off at high T_B (high g-levels) as a result of another capillary action of the lubricant; this time at molecular level. The levelling off may also be due to a decrease in the rate of elastic development.

The above explains the exceptionally high values of ΔP for unlubricated samples and its linear dependence on T_B. In the absence of the lubricant elastic development increases progressively through the entire fusion process. Many more networks are formed resulting in higher values of g-level (and therefore ΔP) with increased T_B.

3.2.2 Percent Gelation (CR)

An established procedure for quantitative capillary rheometry relates the g-level to the reduced relative pressure loss by eqn. 1.4. This procedure was adopted to obtain Figure 3.4. A negative g-level, shown by sample B, is often observed.[106]

It is evident in Figure 3.5 that the establishment of a standard gelation curve (sgc, section 1.4.1) using eqn. 1.4 is of little value. The maximum pressure loss for a particular formulation can fall below the minimum for another over the same T_B range. This formulation dependence is well recognised and is a major limitation of CR test for g-level.

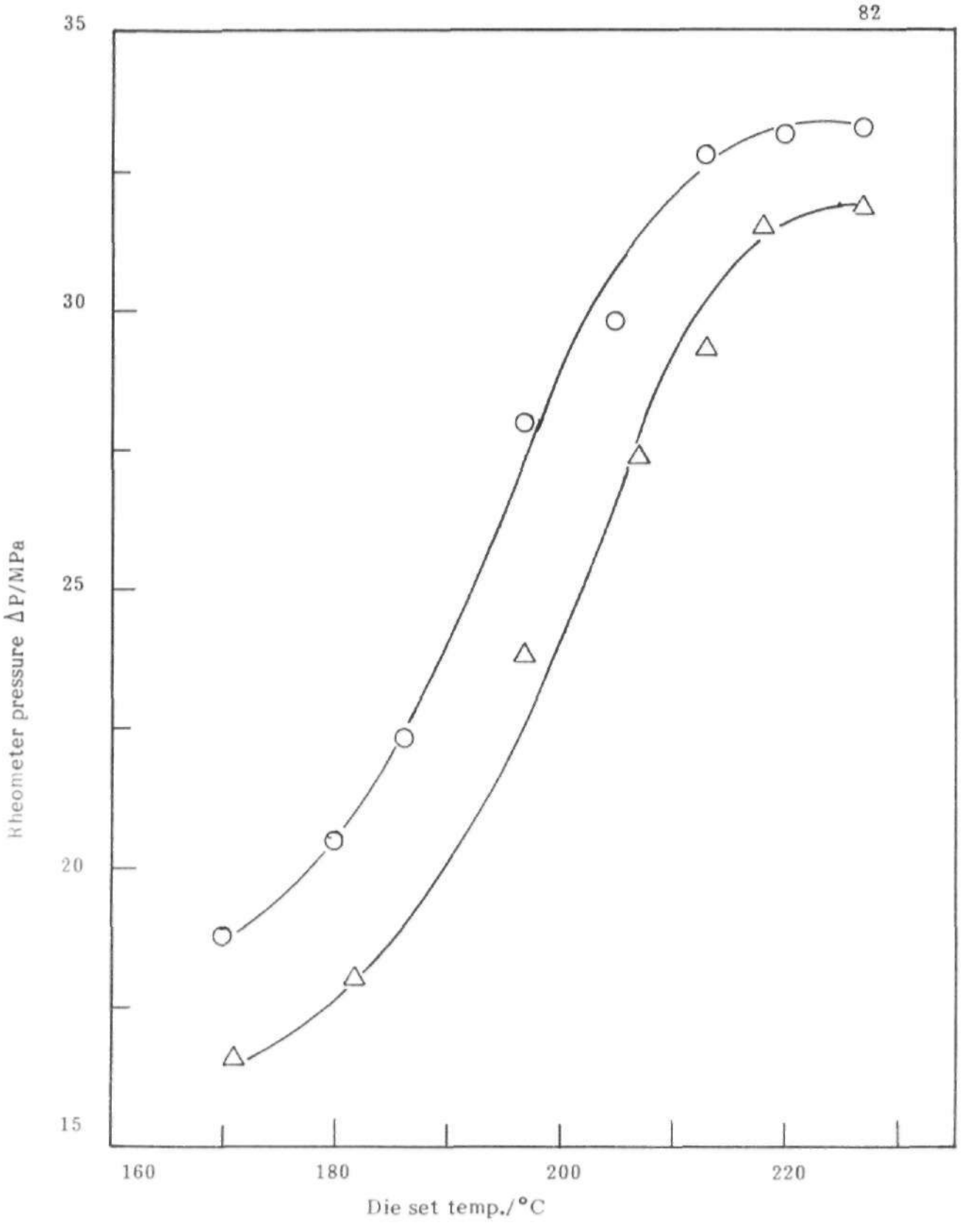


Fig. 3.3

Dependence of capillary rheometer pressure on processing temperature for sample A and B using the Leistritz; O, sample A; △ , sample B

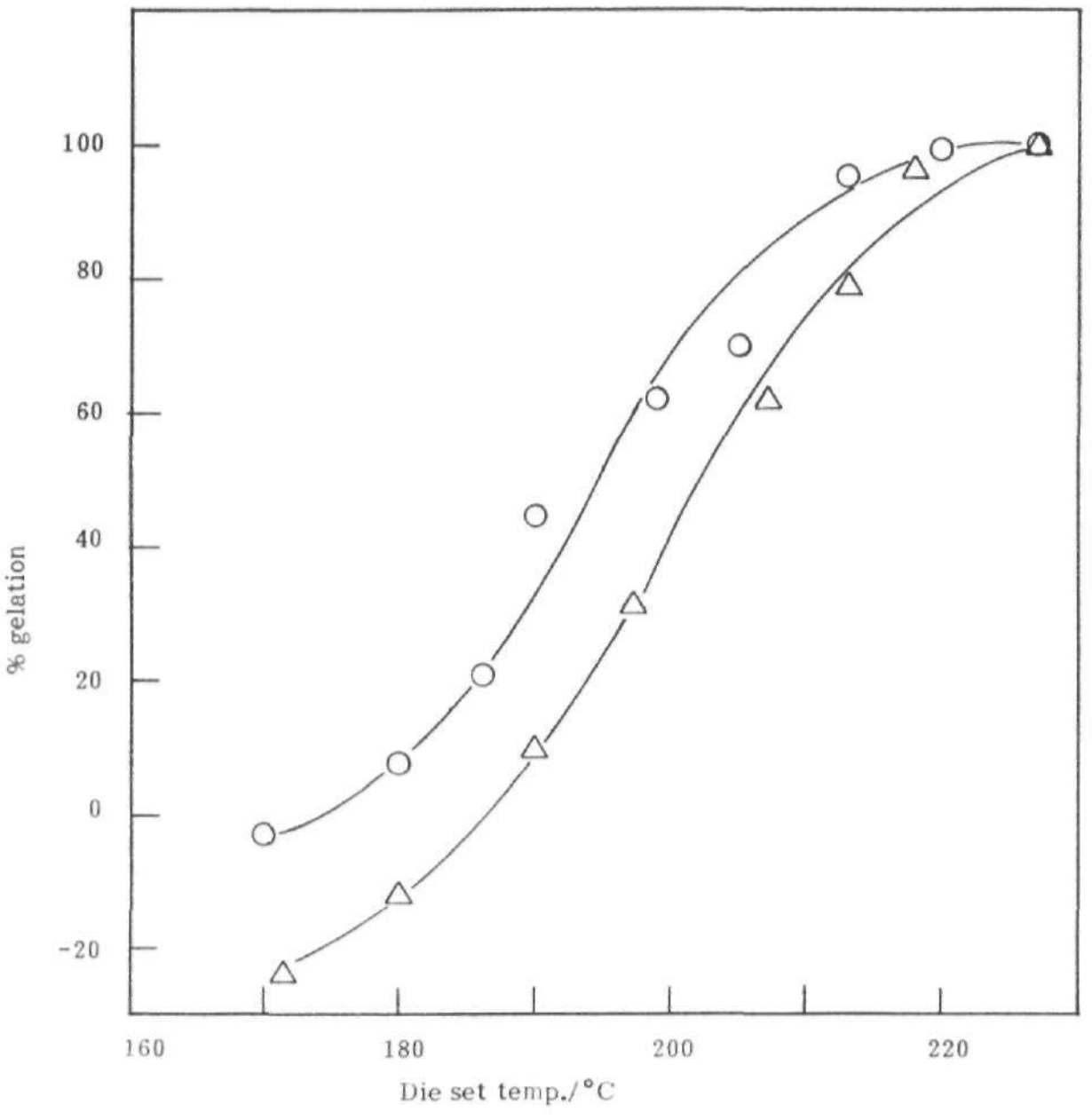


Fig. 3.4
Variation of gelation level (based on rheometer pressure) with processing temperature for samples A and B ; O, sample A;△, sample B

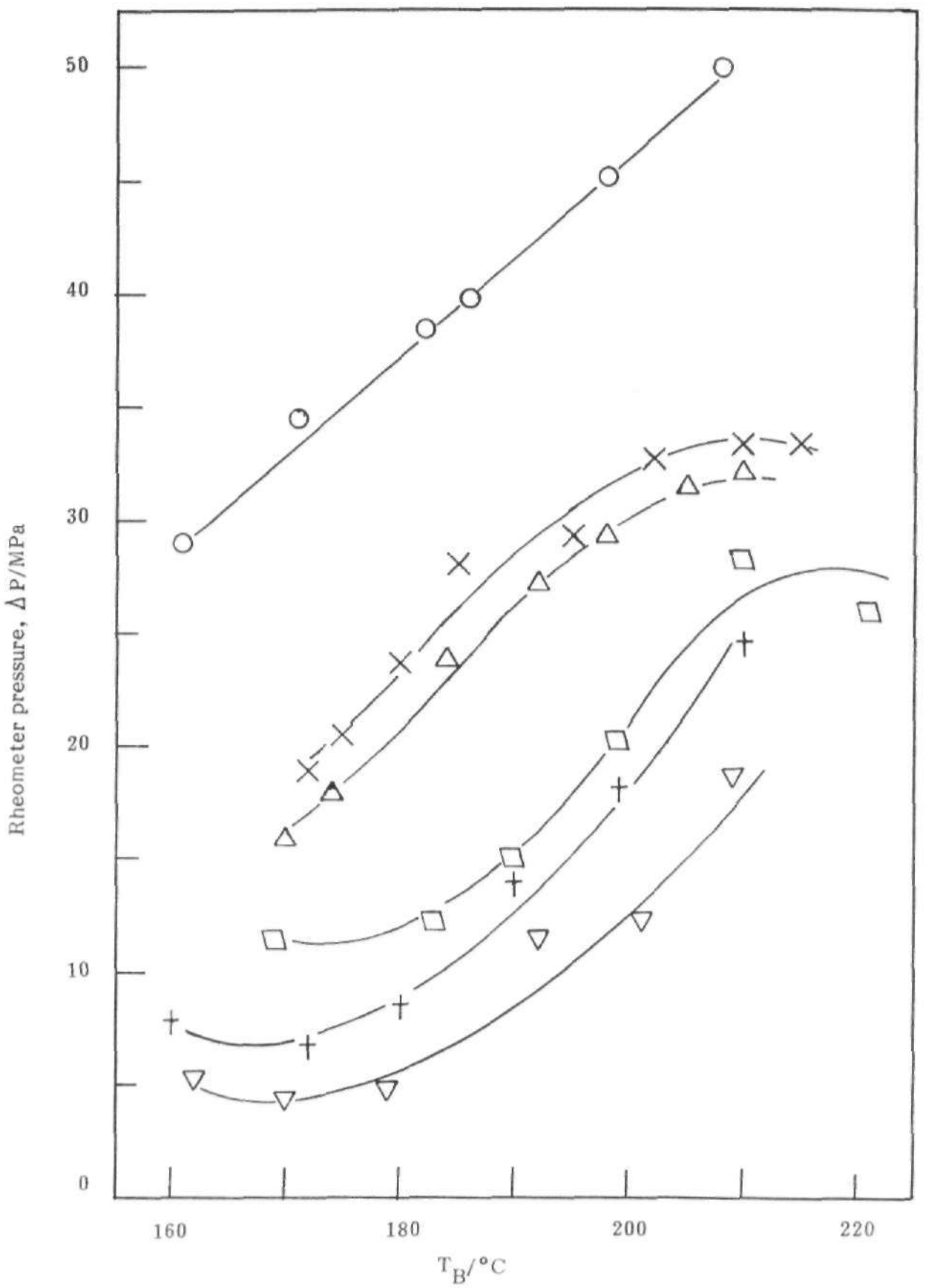


Fig. 3.5

Dependence of rheometer pressure on processing temperature for extruded samples: X, sample A; △, sample B; and for compression moulded samples: O, SO; □, LO5; +, L30; ▽, L45

3.2.3 Effect of Extrusion Rate

The overall effect of extrusion rate is minimal (Figure 3.6); however, a significant difference in ΔP is noticed for the materials processed at lower melt temperatures. For sample A processed at 190°C (die set temperature) an increase in extrusion (shear) rate produces increased ΔP indicating an increase in g-level. This increase is due to a greater contribution to gelation from shear heating for particular combinations of formulation and temperature. The effect is substantially linear in the region 15 to 35rpm. The same trend is not observed for sample B (processed at the same temperature) because its higher lubricant loading reduces shear heating and delays gelation as discussed above.

Although differences between samples A and B are still observed for the 200°C die temperature ranges, they are absent for extrudates prepared at a die temperature of 220°C. These results demonstrate that the effect of temperature on gelation far outweighs that of shear.

3.2.4 Effect of Molecular Weight

It should be noted before the proceeding discussion that the KM samples were formulated as sample A (Table 2.4), however, a tin stabilizer was used in place of lead for better stabilization. The KM samples contain some molecular weights, S68 and S71, comparable to the molecular weight of the L-series. Similar variations in properties should, therefore, be expected between S68 and S71 and sample A (L-series). However, the KM-samples and the L-samples were perpared on different extruders with completely different machine variables. The fusion path in both extruders will, therefore, be expected to vary accordingly, even when extrusion conditions are kept apparently constant.

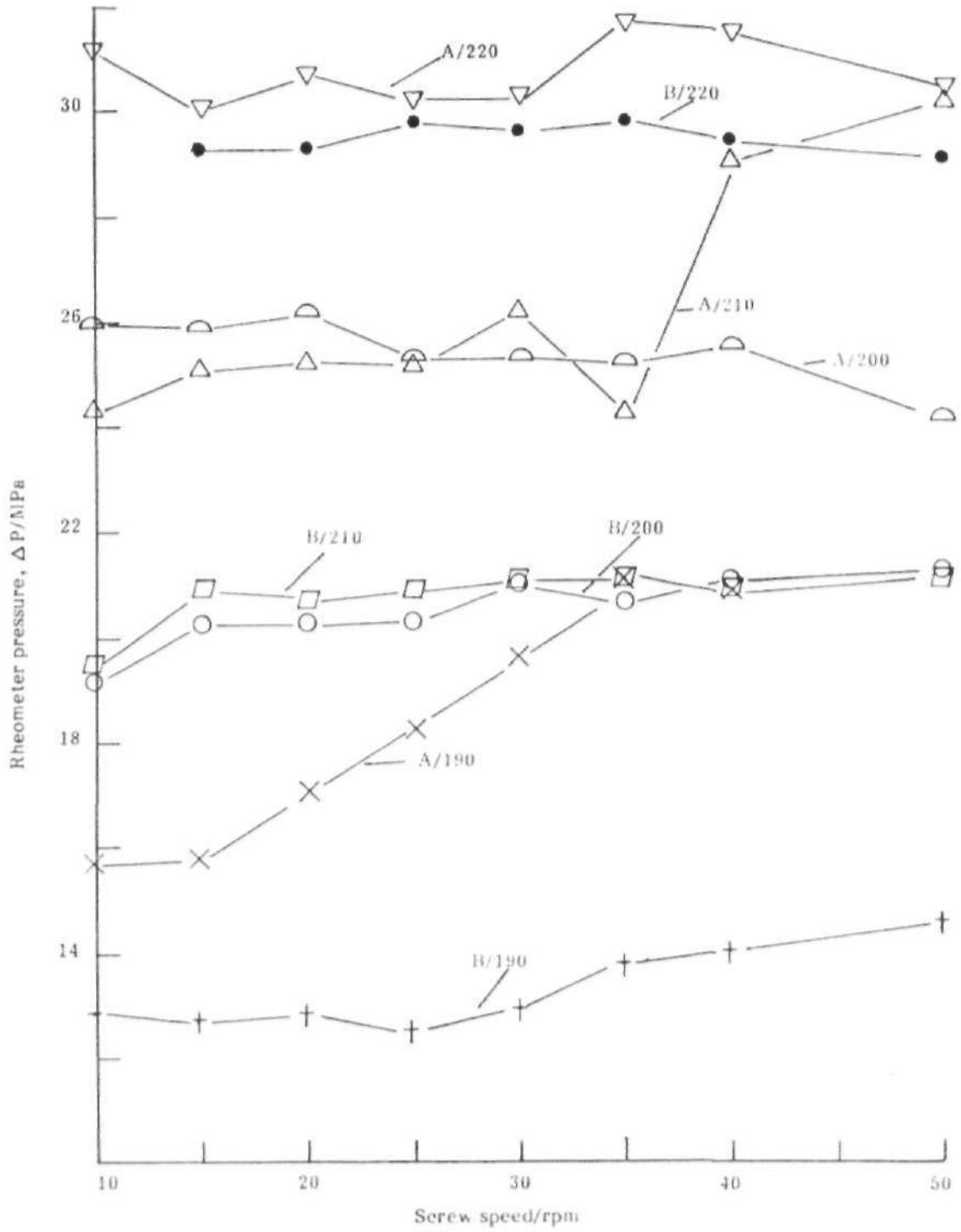


Fig. 3.6
Variation of rheometer pressure with extrusion rate for samples A and B extruded on the Leistritz at various temperatures

It follows that in principle meaningful comparisons in observed properties cannot be made without taking into account equipment differences. These differences were not investigated for practical reasons, related to limited availability of both extruders which were kindly provided by BP Chemicals, Barry, Glamorgan, and Cookson Group, Perivale, Middlesex.

Results of CR tests on KM samples are shown in Figure 3.7 and provided in detail in Table 3.3.

With increased processing temperature ΔP increases and the usual sigmoid curve, discussed in section 3.2.1, is observed.

Values of ΔP are notably low for these samples. These values increase with increased molecular weight, the sigmoid shape being better defined the higher the molecular weight. The behaviour is quite similar to the effect of lubricant observed with compression moulded formulations in Figure 3.5. This similarity suggests that an identical mechanism controls the measured parameters, viz the effect of shear. Figure 3.7 can, therefore, be explained with the aid of Figure 3.5.

Comparison of the two figures (3.5 and 3.7) shows that the gelation of a medium molecular weight sample, containing different levels of an external lubricant, follows the same path as the gelation of a series of molecular weights containing the same amount of the lubricant. Thus sample S57 (Figure 3.7), exhibiting identical form as samples L30 and L45 (Figure 3.5), is 'poorly' fused, being relatively over-lubricated. The results of MCT show this to be the case (section 3.4). If, however, the different molecular weights had been formulated differently, as normally is the case, samples S62 and S57 would have behaved differently.

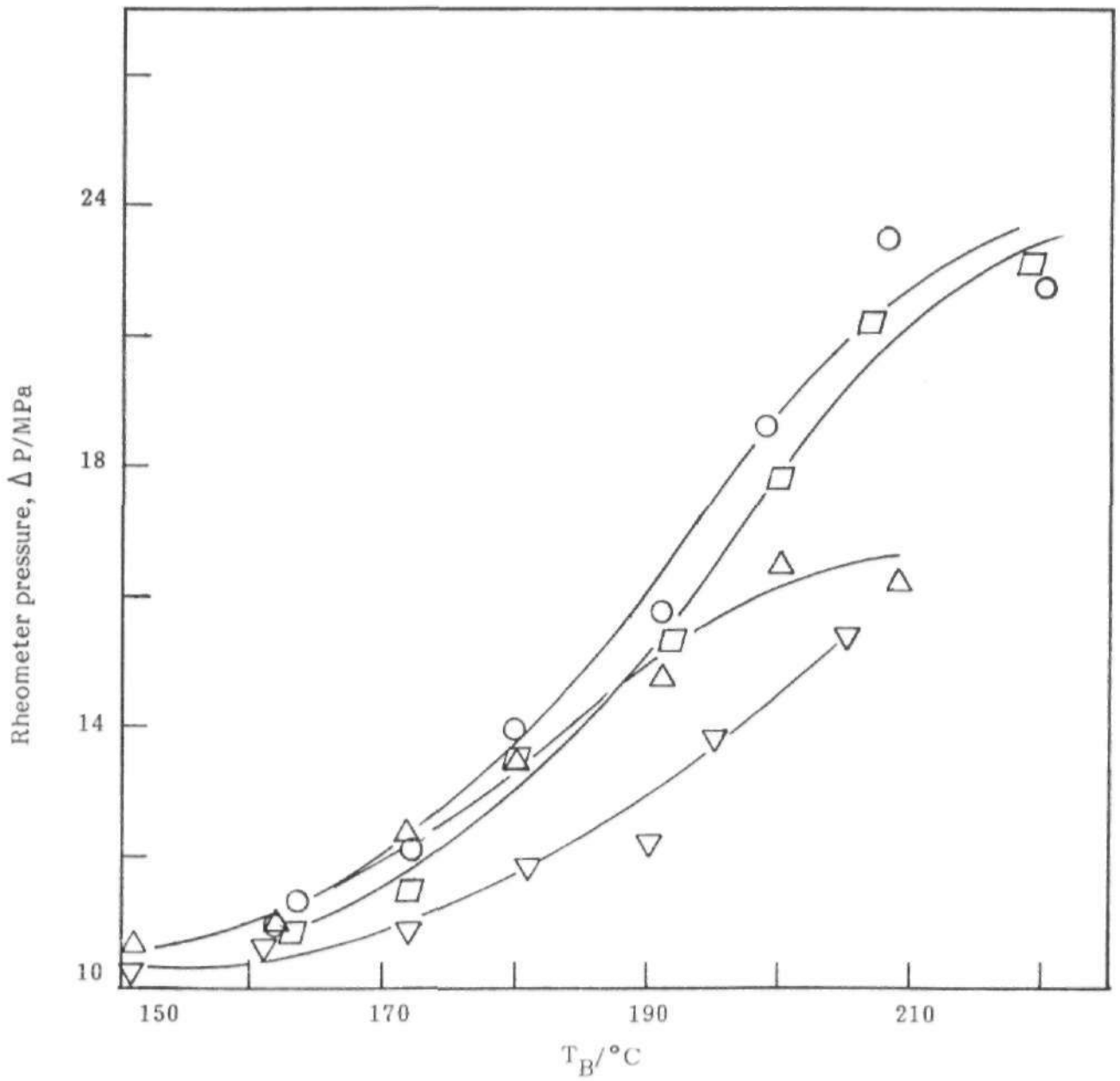


Fig. 3.7
Dependence of rheometer pressure on processing temperature for different molecular weight samples extruded on the Krauss Maffei:
O, S71; □, S68; △, S62; ▽, S57

Table 3.3 Capillary rheometer pressure and percentage gelation for samples extruded at different temperatures using the Krauss-Maffei

			S57 (Powder = 10.1 MPa)				
Temp (°C)	151	161	172	181	190	195	209
Pressure MPa	10.3	10.6	10.8	11.9	12.1	13.9	15.4
% gelation	3.6	10.2	14.2	33.8	38.6	71.6	100
			S62 (Powder = 11.3 MPa)				
Temp (°C)	151	162	172	180	190	200	205
Pressure MPa	10.7	11.0	12.5	13.4	14.8	16.5	16.0
% gelation	-12.8	-7.0	72.6	40.0	67.3	100	90.7
			S68 (Powder = 13.0)				
Temp (°C)	166	172	180	192	200	207	219
Pressure MPa	10.9	11.5	13.5	15.3	17.8	20.2	21.1
% gelation	-25.4	-17.8	6.4	28.9	59.3	88.6	100
			S71 (Powder = 13.1)				
Temp (°C)	167	174	180	191	199	208	220
Pressure MPa	11.3	12.1	14.0	15.8	18.8	21.5	20.7
% gelation	-21.8	-11.4	10.3	32.0	68.0	100	90.3

Figure 3.7 demonstrates that the delayed gelation, caused by the lubricant, is greater the lower the molecular weight. Hence equivalent g-levels are shifted to higher melt temperatures with decreased molecular weight. In this respect sample S71 appears to have the highest molecular weight contrary to GPC results (Tables 2.1 and 2.2). This is also suggested by the results of thermal analysis and MCT. However, it should be noted that sample S71 exhibits peculiar flow properties as demonstrated by decreased output rates (Table 3.2). The peculiar character of sample S71 should be noted when comparing its properties with those of other samples of the KM-series.

Even when comparison is limited to equivalent molecular weights, the KM samples have generally lower ΔP values than the L samples (Figures 3.5 and 3.7). As observed previously this difference cannot be accounted for without reference to unavailable machine variables. For the purpose of this study, however, the results obtained for the KM samples are internally consistent and self-sufficient for meaningful conclusions.

3.3 Thermal Analysis

Results of thermal analysis on processed samples are summarized in Figures 3.9 to 3.13. Details are included in Tables 3.5A to 3.7A for all samples.

3.3.1 The B-onset temperature, T_B

The second and third columns of Tables 3.1 and 3.2 compare the die set temperature with the melt temperature measured by the value of the B-onset temperature, T_B (section 1.4.3, Figures 1.9(a) and 1.9(B)).

As shown in the third columns of Tables 3.1 and 3.2, T_B can be measured in two different ways. It can be measured as the shoulder (method I) of the B-endotherm following the procedure of Gilbert and Vyvoda[114] and of Illers.[56] Or it can be measured as the B-endotherm peak (method II) following the procedure of Ohta et al.[40]

Melt temperatures measured by the two methods differ by about 10°C and this difference is not constant over the range of processing temperatures.

For die set temperatures lower than 190°C T_B by method I aptly describes the extrudate melt temperature, and the peak value of method II clearly overestimates the melt temperature. For die set temperatures 190°C and greater, method I underestimates the final melt temperature (Tables 3.1 and 3.2).

The difference in T_B between the two methods is better understood by comparing the endotherm of the unprocessed powder with endotherms of the same sample prepared at different temperatures (Figure 3.8).

A single broad melting endotherm is observed for the unprocessed powder (Figure 3.8(a)). Its onset temperature starts at about 120°C and it has a peak between 180-190°C. This peak can be regarded as the equilibrium melting temperature, T_m, of the available ordered structures (crystallites) in the unprocessed material.

Processing below the equilibrium T_m has little effect on the crystallites and invariably gives a peak over the same range (180-190°C) in thermal analysis. Hence method II gives much higher T_B value than method I for these samples.

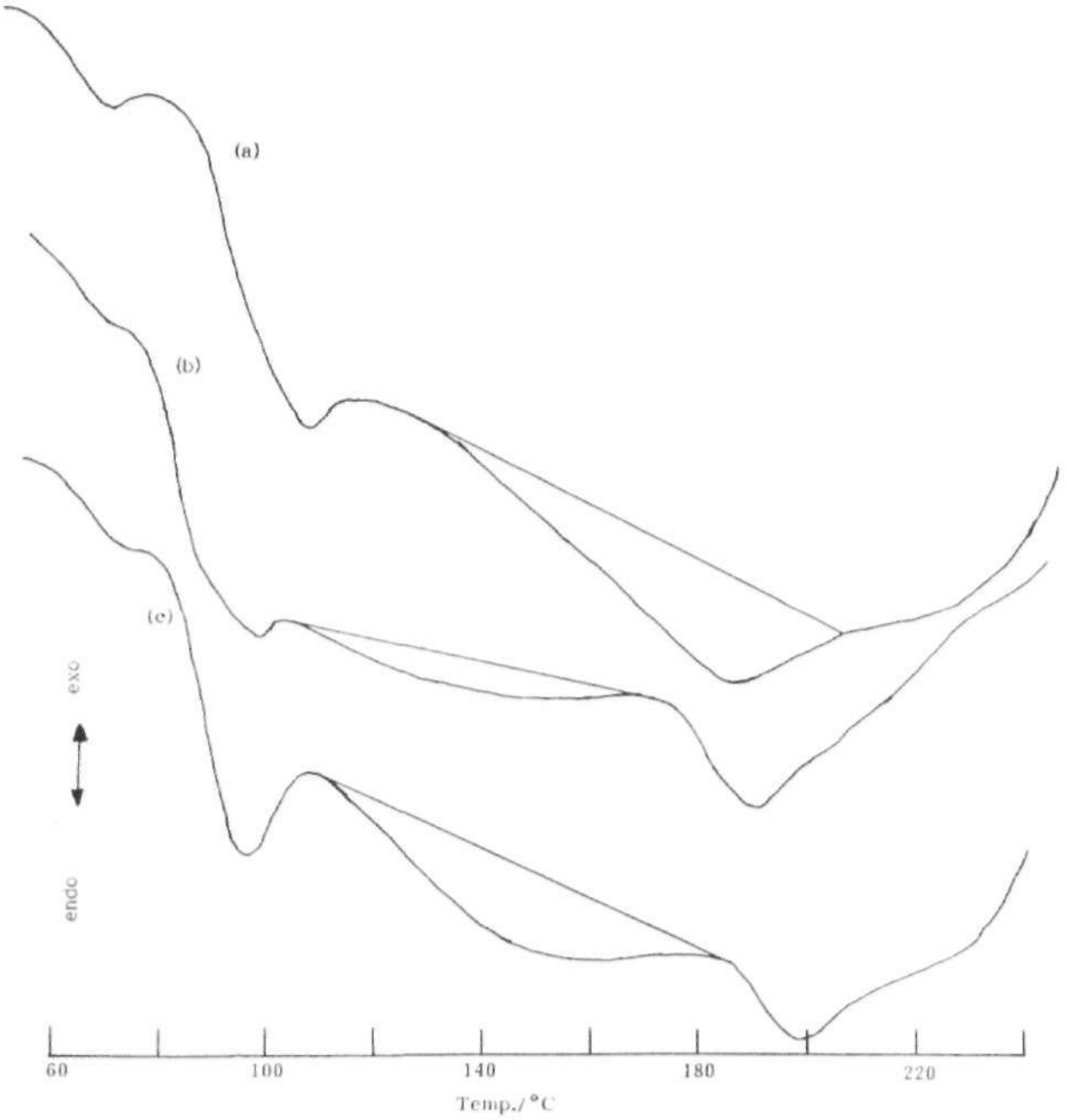


Fig. 3.8

DSC thermograms for (a) powder formulation;
(b) formulation extruded at 160°C; and
(c) formulation extruded at 190°C

Processing above the equilibrium T_m leads to the melting of the crystallites. The melt recrystallizes on cooling[48,49,114] and unmelted crystallites are annealed. The resulting crystallinity of the processed sample is now more strongly dependent on the processing conditions, and method II yields T_B more characteristic of the true melt temperatures than method I (Tables 3.1 and 3.2).

For consistency, values of T_B used in this study represent the onset temperature (method I).

3.3.2 Effect of Processing Temperature

The effect of processing temperature on the measured heat of fusion, $\Delta H(T)$, is demonstrated in Figure 3.9 for extrudates of L-series, Figure 3.10 for some compression mouldings, and in Figure 3.11 for extrudates of KM-series.

Sigmoid curves are observed in all cases. Therefore, unlike in CR tests the sigmoid curve is characteristic of $\Delta H(T)$ vs T_B dependence.

It is helpful to refer to section 1.4.3 for the basis of the ensuing discussion.

Thermal analysis (TA) has been conducted by monitoring the progress of the A-endotherm[114] (Figure 1.9). It has been shown (section 1.4.3) that this endotherm results from the melting of less perfect secondary crystallites formed by recrystallization (during processing) of more perfect primary crystallites.[48,49,114] Increased A-endotherm (and, therefore, $\Delta H(T)$) with increased T_B shows that more secondary crystallites result from higher melt temperatures.

The sigmoid shape (of $\Delta H(T)$ vs T_B) is another indication of a sudden change in the nature or amount of the crystallites being fused. It is

analogous to the change observed in ΔP in capillary rheometry. Illers[55,56] has shown that PVC melting is better described by considering a range of ordered structures. At low melt temperatures (below 190°C) only the least ordered structures are melted and recrystallized. Subsequent thermal analysis of the sample yields low $\Delta H(T)$.

The region 190-200°C is a transition zone. The same transition was observed in CR tests, and indeed it is observable for most changes in PVC properties with increased temperature. This transition is well demonstrated by sharp increases in the slopes of the curves. And again irrespective of material and processing technique the shapes of the curves are significantly the same. Characteristic of a transition zone, small changes in melt temperature produce substantial changes in $\Delta H(T)$ up to about 200°C, depending on the material. Beyond 200°C only moderate changes in $\Delta H(T)$ are observed for relatively large changes in T_B (Figures 3.9 to 3.11). The transition is shifted to higher temperatures with increased lubricant loading for the reasons discussed previously (section 3.2).

If no changes occurred in the rate of increase of ordered structures in the melt (during processing), $\Delta H(T)$ would be linearly related to T_B and no transition would be observed. Therefore, the transition (change of slope of $\Delta H(T)$ with T_B) is a consequence of increased rate of generation of recrystallizable structures in the melt pool.

Collins and Krier[181] were the first to show that the transition in question is due to a change in the nature of the flow units in the melt. This has been confirmed by a number of authors,[7-15] and it is now well established[101-107] that changes in the polymer morphology are responsible.

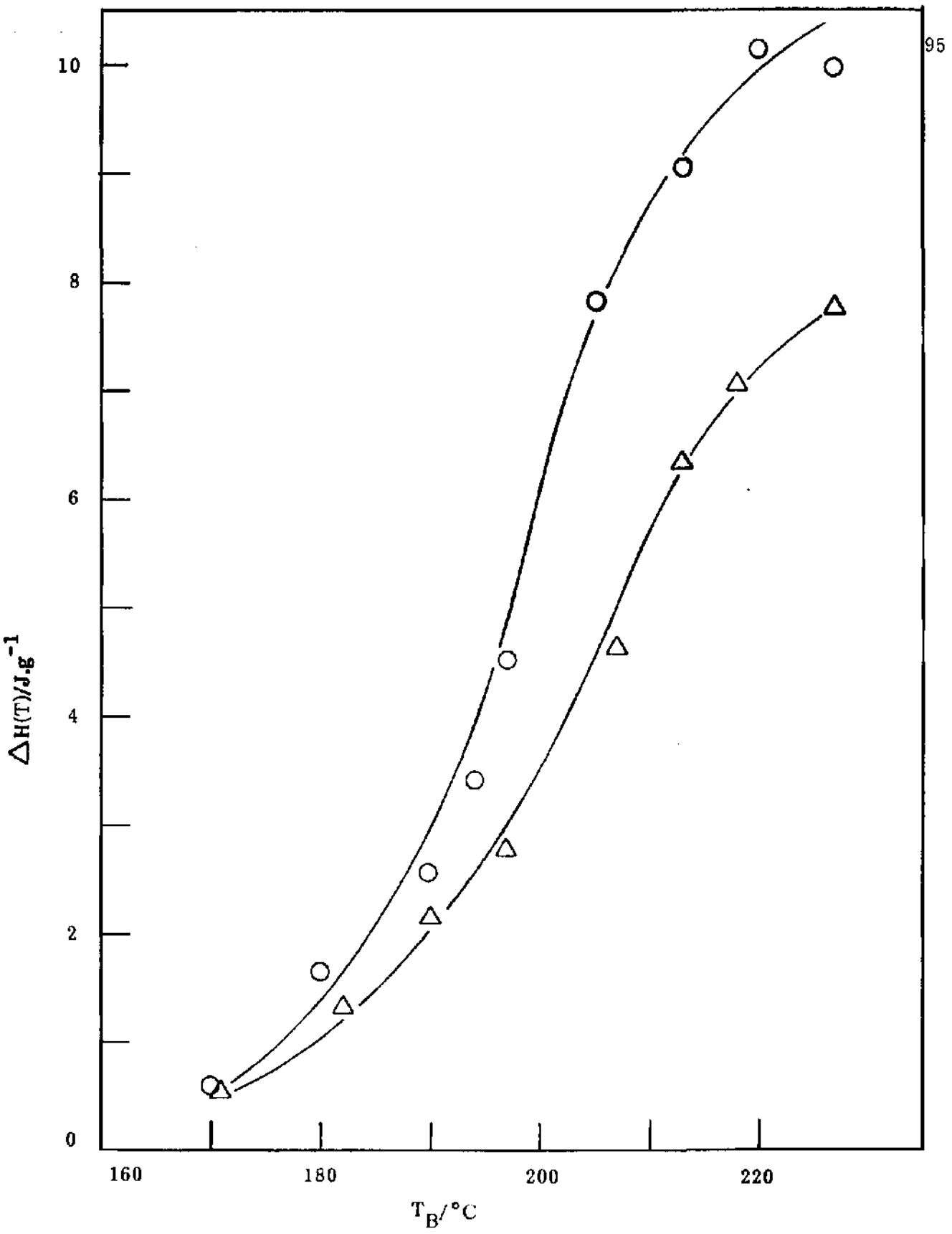


Fig. 3.9
Heat of fusion as a function of processing temperature for extruded (L-) samples: O, A ; and, △, B

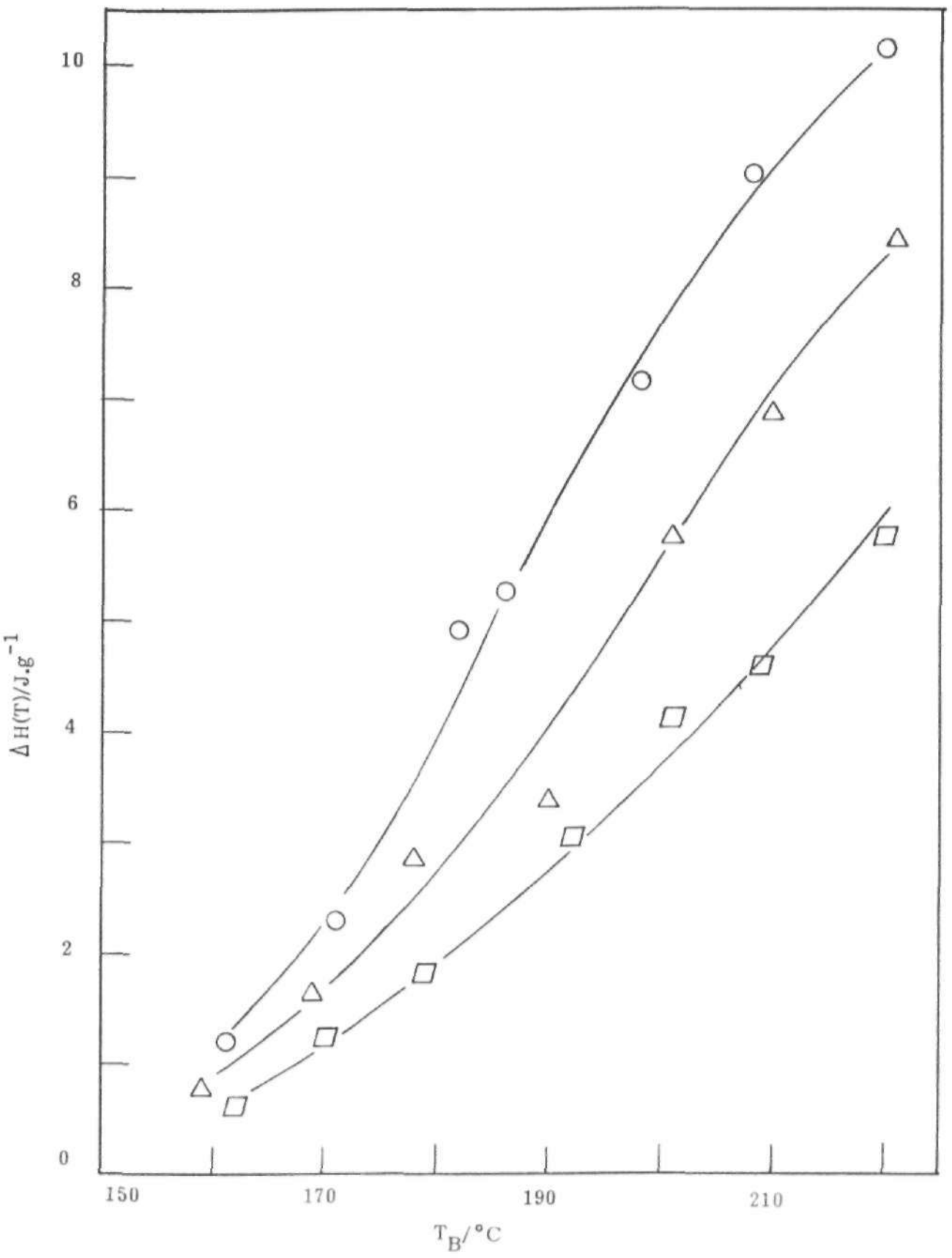


Fig. 3.10
Heat of fusion as a function of processing temperature for compression moulded samples: O, SO; △, L10: □, L45

The ordered structures (presumably microdomain particles) are distributed within the primary particles.[22-28] Changes in order in the processed sample are, therefore, dependent on the destruction or otherwise of the primary particles. These particles are significantly unaffected below 190°C,[28,106] therefore, gradual increases in $\Delta H(T)$ are observed up to this temperature. Between 190 and 200°C the loss of the primary particle structure becomes important.[28,63,84,106,107] Small temperature changes, therefore, produce a relatively large amount of recrystallizable material in the melt. Subsequent thermal analysis of the processed sample yields large increases in $\Delta H(T)$. Above 200°C a significant proportion of the primary particles has been melted, the fraction of recrystallizable structures in the melt decreases and $\Delta H(T)$ levels off.

The net effect of these changes gives rise to the sigmoid curve and the curve is characteristic of the processed sample irrespective of processing history.

3.3.3 Effect of Extrusion Rate

Heats of fusion, $\Delta H(T)$, of samples processed at different rates are provided in Table 3.4.

The results are very similar to the CR test results for the same samples (Figure 3.6). A noticeable difference, however, is a relative decrease in $\Delta H(T)$ at 20rpm. This decrease seems to result from opposing effects of shear, which decreases crystallinity[201], and of shorter residence time, which leads to the survival of greater amount of the secondary crystallinity.

The lower the extrusion rate the longer the residence time and length of heating. Also, the lower the processing temperature, the higher the melt viscosity (for a given formulation) and, therefore, the higher the shear rate at a specific rate of extrusion. Longer heating periods at higher shear rates produce less crystallinity, and lower $\Delta H(T)$ is observed. Although longer heating periods result in increased amount of melted primary crystallites the increase over the duration of residence time is minimal.

At a specific extrusion rate $\Delta H(T)$ increases with processing temperature for reasons discussed previously (section 3.3.2).

At constant processing temperature increased extrusion rate reduces residence time. Although shear rate is higher, the shorter residence time results in the survival of a greater amount of the primary crystallite, and higher $\Delta H(T)$ is observed.

As observed in capillary rheometry, it is shown by thermal analysis (Table 3.4) that temperature has a greater influence on gelation than shear rate.

Table 3.4 Heats of fusion for samples extruded at different rates and temperatures using the Leistritz

Formulation	Extrusion rate rpm							
temp.°C	10	15	20	25	30	35	40	50
Sample A								
190	3.34	3.81	4.40	4.51	6.10	6.84	6.32	-
200	4.91	4.55	3.49	4.84	5.74	7.23	7.13	8.42
210	3.86	6.54	5.51	7.42	7.85	7.33	6.75	7.20
220	8.42	7.71	6.99	8.10	6.25	8.13	8.49	7.66
Sample B								
190	3.15	2.88	3.06	2.93	3.42	3.67	3.01	2.13
200	2.59	3.21	3.15	4.30	4.85	4.45	3.96	4.44
210	5.28	5.66	6.00	6.56	6.21	5.90	6.17	6.51
220	-	4.11	4.02	5.46	6.20	5.88	5.66	5.31

3.3.4 Effect of Molecular Weight

At constant processing temperature $\Delta H(T)$ is higher the lower the molecular weight (Figure 3.11). Which shows, as expected, that at a given processing temperature the greater the amount of material melted and recrystallized the lower the molecular weight. In effect equivalent fusion levels are shifted to higher temperatures with increased molecular weight.

Sample S71 is shown to have the highest molecular weight as was also observed in capillary rheometry (Figure 3.7). These results are contrary to the GPC results (Table 2.2) as discussed previously.

The same trend is observed for $\Delta H(T)$ vs T_B relationship for all samples. This is another demonstration of the characteristic independence of $\Delta H(T)$ with changes in material and processing techniques.

3.3.5 Percent Gelation (TA)

$\Delta H(T)$ can be converted to gelation levels by relating values to the heat of fusion of the perfectly crystalline sample (the procedure is discussed in section 3.6.4)

Gelation levels calculated with the aid of eqn. 1.29 are shown in Figure 3.13. Higher gelation with decreased molecular weight is clearly demonstrated as discussed above. Comparing the respective $\Delta H(T)$ values as molecular weight increases, it appears that the lowest molecular weight (sample S57) is already degraded at 200°C. Visible discolouration of this sample beginning at 200°C supports this observation.

Since gelation levels (better described as order factors[129]) calculated with eqn. 1.29 rely only on one standard, which is the invariable equilibrium melting temperature of the perfect PVC crystal, values are

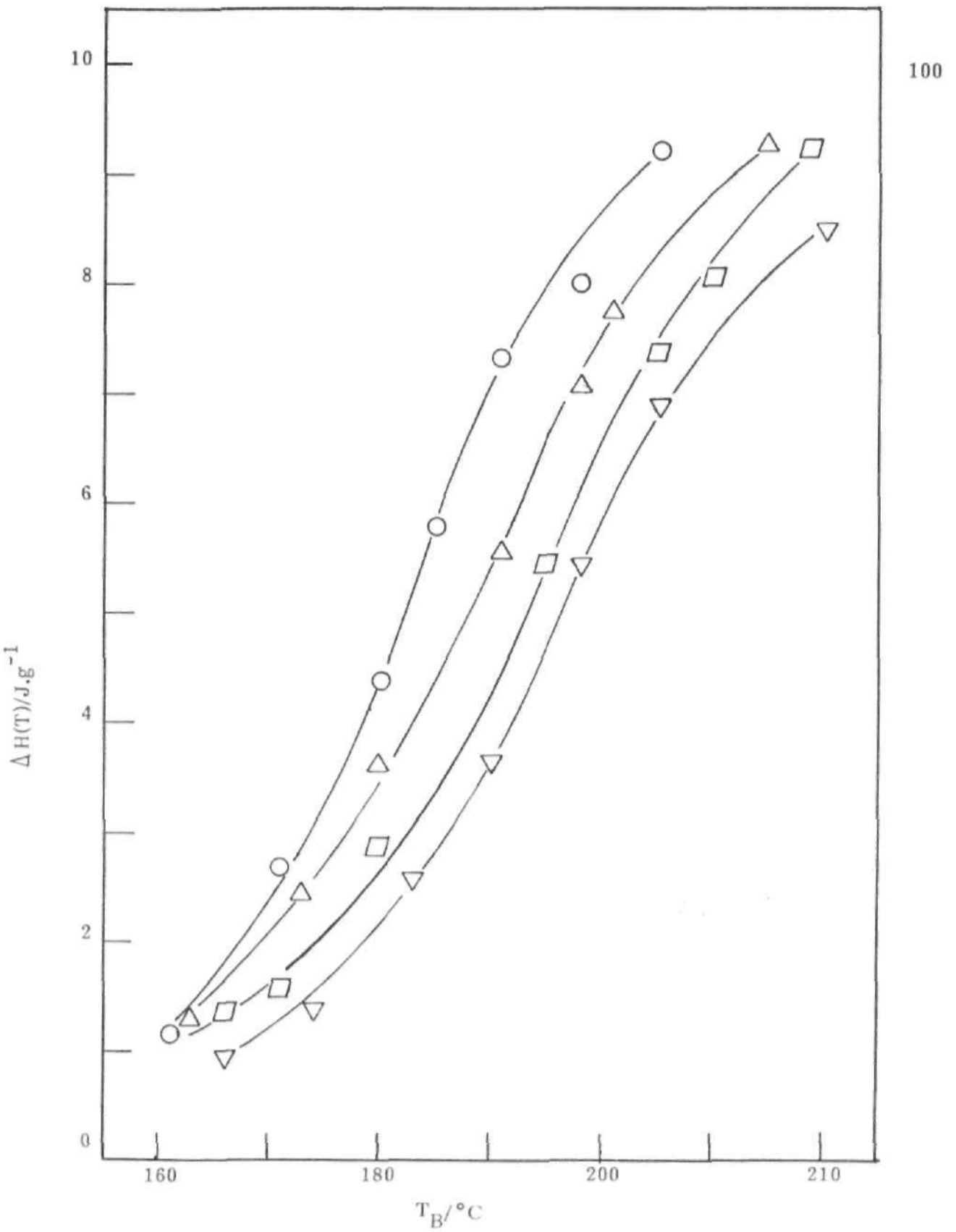


Fig. 3.11

Heat of fusion as a function of processing temperature for extruded (KM-) samples: O, S57; △, S62; □, S68; ▽, S71

characteristic of the sample's thermal history. This feature results in significantly independent g-level even with large differences in processing technique. Hence samples of widely different processing histories can be reasonably compared.

3.4 Methylene Chloride Test

Results of methylene chloride attack on extrudates of L- and KM-samples and on compression mouldings are shown in Table 3.5. Methylene chloride was preferred to acetone (which is recommended in ASTM D2152) because it is more effective.[161]

Only the samples prepared over a range of temperatures have been tested. Differences in the rate of solvent attack are not observable with samples processed at different rates at constant temperature. The same effect has been shown for capillary rheometry and thermal analysis.

The observations are discussed with respect to the processing history.

291942

(i) Leistritz extrudates (L-samples)

A fast rate of attack is observed for melt temperatures, T_Bs, below about 180°C. At equal T_B values the attack is slower the higher the lubricant level (sample B).

All samples processed below T_B of 190°C have been attacked in less than 20 minutes. These samples are, therefore, not sufficiently gelled. With the exception of sample B4 all samples processed above 190°C are not attacked even after long durations in excess of 2 hrs. Up to 24 hrs and longer these samples remain

swollen but intact. They can therefore be considered to be well fused.

(ii) Compression moulded (CM) samples

Only two samples were investigated, sample SO containing no lubricant and sample LO5 containing 3.5phr total lubricant level.

The rate of attack is significantly similar (for both samples) to that observed for the extrudates discussed above.

At 190°C (T_B) and above no attack is observed within the duration of the test and over an extended period (above 24 hrs). Sample LO5 processed at 190°C is an exception. For this sample some attack is discernible after about 2 hrs.

The results indicate once again that the lubricant appears to protect the polymer from solvent attack. Hence the rate of attack does not increase with lubricant level although the samples are less fused. The results also suggest that comparable levels of fusion can be observed for extrusion and compression moulding.

(iii) *Krauss Maffei (KM) extrudates*

The lower the molecular weight the faster the rate of solvent attack at equivalent temperatures. For the lowest molecular weight (sample S57) only the sample prepared above T_B = 200°C (M17, Table 3.2) survive unattacked at 2 hrs and beyond.

The processing temperature above which the samples survive the attack decreases with increased molecular weight. The values are 210°C for S57, 200°C for S62, 195°C for S68 and 190°C for S71.

Table 3.5

Time taken for methylene chloride attack on processed samples

				Sample A				
T_B/°C	170	176	180	184	195	200	208	220
Time/min	0.5	3	15	17	-	-	-	-
				Sample B				
T_B/°C	170	174		180	191	198	205	210
Time/min	0.75	1		7	1.5	-	-	-
				S57				
T_B/°C	161	162	174	175	185	190	200	
Time/min	0.5	1	3	5	6	105	-	
				S62				
T_B/°C	161	165	170	180	186	200	205	
Time/min	0.75	2	6	15	-	-	-	
				S68				
T_B/°C	165	170	178	185	195	206	218	
Time/min	1	2	10	20	-	-	-	
				S71				
T_B/°C	165	174	180	190	197	208	216	
Time/min	1	5	10	-	-	-	-	
				SO				
T_B/°C	161	171	182	186	198	208	220	
Time/min	0.5	1	2	-	-	-	-	
				LO5				
T_B/°C	160	169	183	190	199	210	221	
Time/min	0.5	1	6	120	-	-	-	

These results, like previous results from CR and TA, also show that sample S71 has the highest molecular weight.

It can be concluded from these results that solvent attack is more delayed the higher the lubricant loading. Therefore, absence of attack on a highly lubricated sample is not related solely to enhanced gelation.

Both lubricated and unlubricated CM samples appear to be more gelled at all processing temperatures than expected. It has, however, been demonstrated by capillary rheometry that CM lubricated samples have greatly reduced interparticulate network characterized by low levels of entrance pressure loss.

At equivalent gelation levels the rate of solvent attack is found to depend on sample molecular weight given a constant formulation. Therefore, a low molecular weight sample which fails the test may not necessarily be poorly fused. Indeed, sample S57 which almost failed the test over the entire range of processing temperatures has been shown (TA) to be much more fused than the other samples. Faster rate of attack on low molecular weight samples is related to increased solubility of the polymer with decreasing molecular weight.

3.5 Comparisons of the Gelation Tests

Capillary rheometry entrance pressure loss, ΔP, has been related to the heat of fusion in Figure 3.12 using results from KM-samples. A similar relationship has been reported[116] for the L-samples and a range of other samples.

It is observed that a linear relationship obtains between ΔP and $\Delta H(T)$ over the T_B range studied. This appears to be the case if the

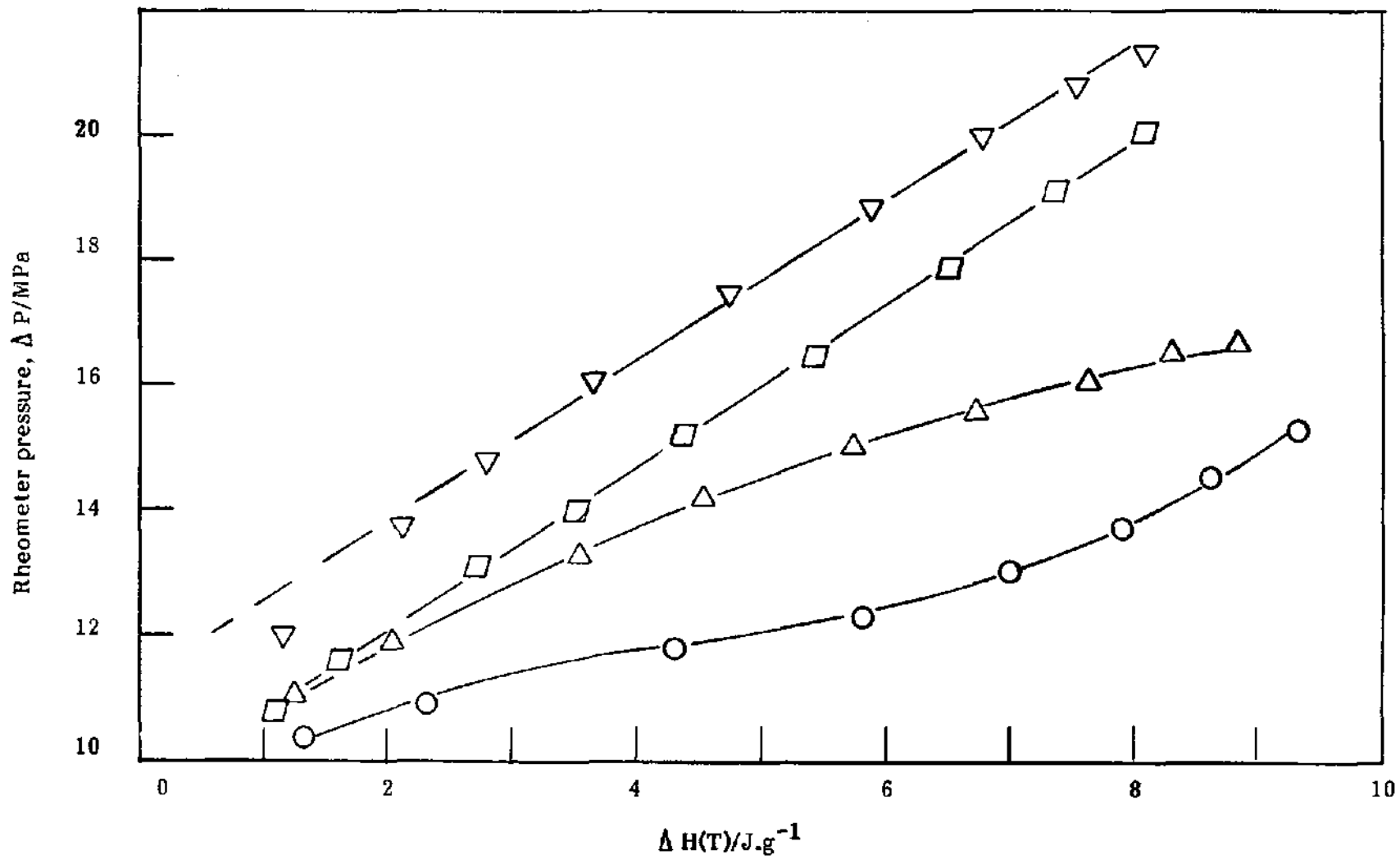


Fig. 3.12
Variation of rheometer pressure with heat of fusion for extruded (KM) samples: ▽, S71; □, S68; △, S62; O, S57

polymer molecular weight is sufficiently high and sufficient elastic development occurred during processing.

In a recent work[182] it was shown that the increase in ΔP reaches a limiting value as $\Delta H(T)$ increased over the same T_B range. This work was limited to plasticized formulations. Figure 3.12 and the previous report[116] demonstrate that for unplasticized formulations the linear relationship cannot be doubted. It is further shown in Figure 3.12 that deviation from linearity can occur with changes in elastic development (network formation). Thus for samples S57 and S62 which show weak elastic responses (see Figure 3.7) deviation from linearity is observed (Figure 3.12).

It can be concluded, therefore, that the dependence of ΔP on $\Delta H(T)$ is specific to the material used.

Despite large differences in the techniques used results of the three fusion tests, CR, TA and MCT, show substantial agreement (Figures 3.3 to 3.13 and Table 3.5).

All three tests show that below a melt temperature, T_B, of 190°C the samples are generally poorly fused and above 200°C they are well fused.

MCT is very basic in its procedure. It is fast, cheap, and does not require technical ability beyond visual aid. However, it is strongly limited by lack of discrimination between narrow ranges of gelation. Within a small but important range of processing temperature in the critical transition zone at 190-200°C this technique is unable to show differences in g-level and only the very worst samples are failed. If, however, the product performance does not require critical control of g-level this test appears sufficient.

CR requires higher technical expertise than MCT; it is also more costly in terms of equipment , sample size, and time. In return CR offers much better sensitivity to small differences in g-levels particularly in the relevant 190-200°C zone. However, it is very limited by a dependence on equipment shear regime and material formulation. Although CR gives useful information on elastic response which is closely related to mechanical properties, dependence on material and machine causes problems when different batches or machines serve the same production line. Relative g-levels of samples with different processing histories cannot be meaningfully compared without the aid of a sgc (section 3.2.1) for each formulation/machine combination. If the sgc is established, however, and as long as no change of machine or formulation is made, CR can be reliably used to measure the 'bulk' g-level. This term refers to a g-level representative of the sample average. It is completely insensitive to local variations in g-levels within a small region of the sample, say across the profile thickness.

TA is a little more expensive than CR particularly in initial investment costs. However, this technique offers in return several cost saving advantages. Only small sample sizes are required and non-destructive tests can be performed on the product. Milligram sample size allows differences across less than 1mm profile thickness to be easily investigated. This procedure was adopted, for example, for selected L- and KM-samples. TA was conducted for samples prepared from different regions of the extrudate cross-section (Figure 3.14, Table 3.6). Table 3.6 shows that T_B and $\Delta H(T)$ vary markedly over the cross-section and the wall thickness.

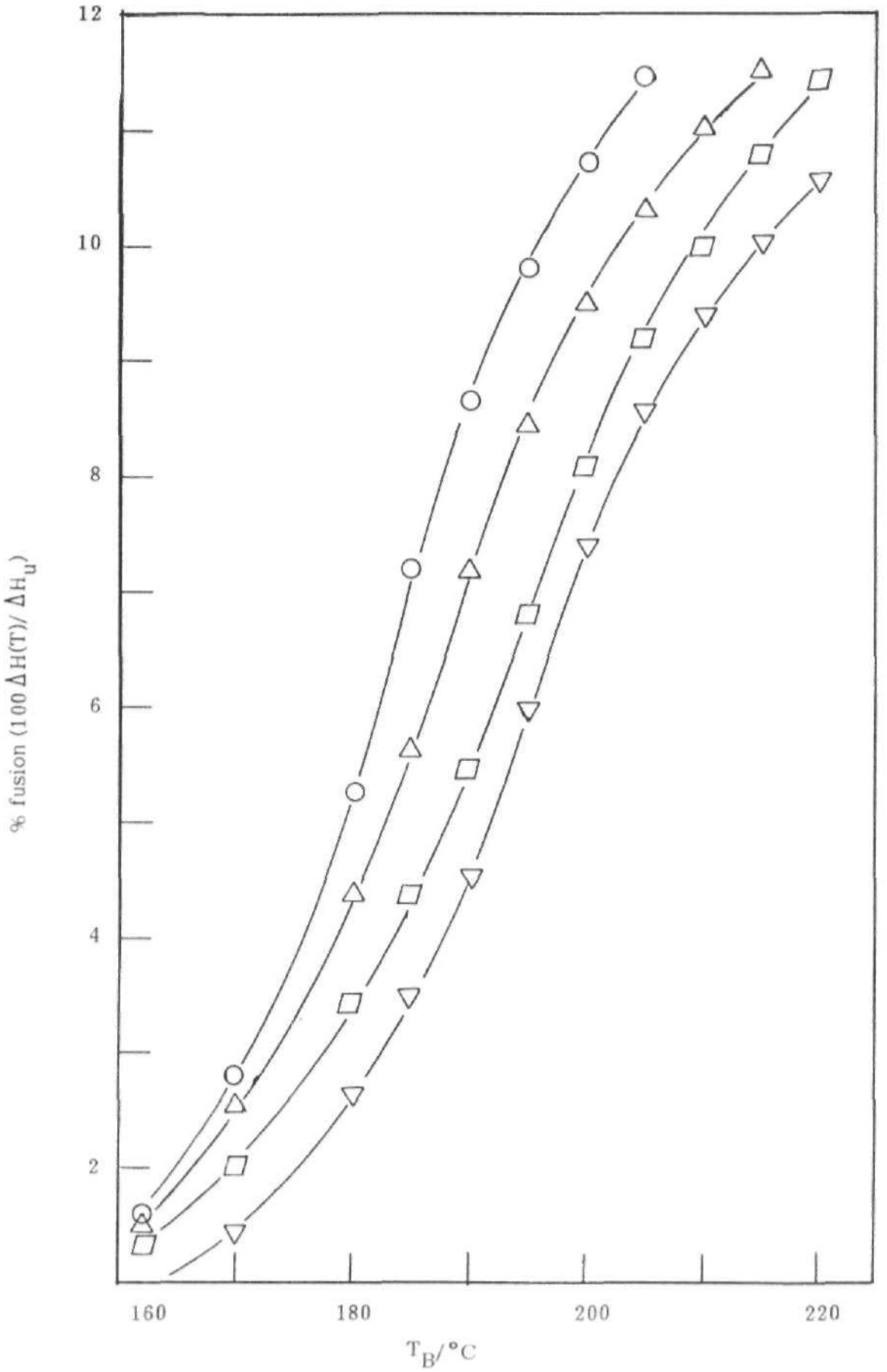


Fig. 3.13

Dependence of fusion level (based on thermal analysis) on processing temperature for extruded (KM) samples: O, S57; △, S62; □, S68; ▽, S71

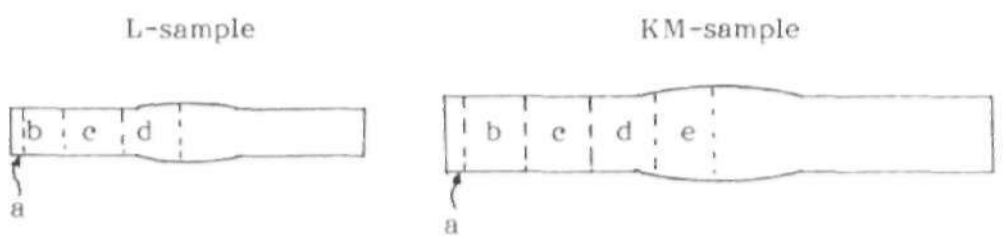
Table 3.6

Variations in melt temperature and heat of fusion over sample cross-section for Leistritz and Krauss-Maffei extrudates

Sampling region	Property	Leistritz Sample A			Krauss-Maffei S68		
		A2-2	A4	A6	M33	M34	M35
	Die set temp./°C	192	205	213	190	200	210
(a)		188	193	210	187	198	207
(b)	Die melt	184	191	204	179	190	197
(c)	temp.	183	192	200	179	185	197
(d)	T_B/°C	184	191	200	177	185	194
(e)		-	-	-	177	188	194
(a)		3.44	10.46	15.84	6.71	6.76	17.16
(b)	Heat of	3.66	4.94	11.18	3.20	7.22	7.58
(c)	fusion	3.56	6.52	8.92	3.29	4.53	8.09
(d)	$\Delta H(T)/J.g^{-1}$	3.02	5.34	9.24	3.05	5.27	5.65
(e)		-	-	-	2.58	5.16	5.02

Fig. 3.14

Sampling regions for cross-sectional differences in melt temperatures and heats of fusion



This ability to detect 'micro' differences within the bulk material makes TA a powerful tool for precise control of g-level. Since failure is often initiated at micro levels (cracks, inhomogeneities, etc) ability to detect differences in g-level at this level is vital to strict quality control.

3.5.1 A General Observation on Thermal Analysis

Since the thermal analysis technique is still under development it may be useful to note the following observations:

It is shown in Table 3.6 that the outer skin of the extrudate exhibits higher T_B and $\Delta H(T)$ values. However, once the 'skin' is transversed little change is observed in these quantities.

Higher T_B at the skin results from close contact of the material to the metal surface, particularly as it passes through the die.

Higher $\Delta H(T)$ at the skin is due to the effects of uniaxial orientation and a higher melt temperature. Orientation at the skin level[43] and higher melt temperature results in higher recrystallizable material in the melt (section 3.3.2).

The results from the KM-samples (Figures 3.11 and 3.13) show that in the context of established gelation-property relationship, TA should be interpreted with caution.

Sample S57 is shown to be the most fused in the series but it by no means has the best mechanical properties (Chapter 5); in fact this sample has the least mechanical properties. It can be considered as over lubricated (with respect to its molecular weight) and over gelled. The same may be true for S62 to a limited extent.

The point is made to emphasize that by its nature TA is insensitive to the mechanical properties of the sample. Although a sample is passed as well fused, such as may be observed with annealed powder samples,[40,55,56] the degree of fusion bears little relationship (per se) with mechanical properties. The latter have to be independently investigated. CR provides the relevant information in this case and it is evident in Figure 3.7 that samples S57 and S62 have poorer elastic properties than the rest of the series.

The point made above is not very relevant to practical processing since a clear understanding of the expected mechanical performance is a prerequisite for processing. In practice, therefore, inability to obtain knowledge of mechanical behaviour from TA is not a significant limitation.

3.6 Characterisation of Fusion by Thermal Analysis: A Model for Simulating the Heats of Fusion

In this section a mathematical model is developed for the fusion behaviour. The predicted heats of fusion are compared with measured values and the theory is applied to quantitative fusion evaluation.

3.6.1 Introduction and Model

It has been shown (section 1.1.1) that as-polymerized PVC consists of a range of particles (Figure 1.1). These particles are formed by a series of aggregations during polymerization.[16] Thus the smallest observable particles, the microdomain structure, about 10nm diameter, is an aggregate of crystallites.[11,15,24-28] The microdomains in turn aggregate to form the primary particles,[16,28] about 1μm, and the primary particles aggregate to form the grains and subgranular particles, about 100μm in diameter.

It may be recalled that Illers[56] has shown that PVC crystallinity is better described by a distribution of crystalline sizes and perfection. In a model proposed by Summers[28] the microdomains are regarded as crystallites, spaced at 10nm, which act as crosslinks in a three-dimensional network comprising the primary particle. Juijn et al.[48,49] have shown that the original crystallinity (the primary crystallinity) is melted during processing. The melt recrystallizes to produce a less perfect secondary crystallinity. These authors further showed that the primary crystallinity cannot be regenerated by melt processing once it is destroyed.

Gilbert and Vyvoda[114] showed that the lower melting endotherm (A-endotherm) observed in thermal analysis of processed PVC (Figure

1.9(a)) is due to the melting of the less ordered secondary crystallites; and the higher melting endotherm (B-endotherm) results from the melting of the better ordered primary crystallites. From this it follows that increased A-endotherm with increased processing temperature is an indication that more secondary crystallites are produced at higher melt temperatures of the primary crystallites.

The fusion model proposed here is basically that proposed by Summers[28] with a slight modification incorporating a distribution of ordered structures as proposed by Illers.[55,56] Thus the primary particle is assumed to consist not of discrete ordered and disordered regions but of a continuum of ordered structures. The order increases progressively from the most random chain segments in the 'amorphous' regions (which comprises of 'tie' molecules[28]) to the core of the most perfect crystallite in the microdomain. Quite clearly the primary and secondary crystallinity concept is a specific case of the distribution model.

At the lowest temperatures the least ordered crystallites are melted while more perfect crystallites are annealed.[48,49,114] It is not unreasonable to expect that the most perfect crystallites are formed by the highest molecular weight species and vice versa. Thus before these crystallites melt, the lower molecular weight species, having been melted at lower temperatures undergo excessive thermal agitation and degrade. It has been shown[41,58,113] that melting extends well into degradation temperatures.

The glass transition process has been widely treated as a process of structural relaxation having a wide distribution of relaxation times.[115,183-185] A close similarity between glass transition and melting processes has long been recognized. Bunn,[186] Beaman,[187] and Boyer,[188]

showed that the molecular motion occurring on melting is similar to motion occurring on heating through T_g. It is explained that the difference between T_m and T_g arises from the long range order involved in the former as opposed to the short range order involved in the latter. The secondary crystallites are not detectable by wide angle x-ray techniques,[28,47] they can thus be regarded as local ordered structures.[93-95] The endothermic effects observed for the melting of these structures is accountable on the basis of Bunn's[186] hypothesis, and the process can be theoretically considered using a distribution model.

The theoretical basis adopted assumes that the melt process is an activated process. The same assumption was made by Kovacs[189] on studies of the melting of poly(ethylene oxide) single crystals in the bulk. For PVC we assume a distribution of activated molecular process.

A unit of the chain is regarded as melted if by gaining enough energy it is able to overcome the attractive forces of neighbouring molecules. The melting process is thus basically one of 'freeing' structural units from restrictions existing in the crystalline solid. Following the usual Arrhenius type relationships the quantity of units freed, N, is given by

$$N = A\exp(-\Delta H/RT) \qquad 3.1$$

where A is the Arrhenius constant, ΔH is the heat of fusion, R is the gas constant, and T is the melting temperature.

Hutchinson[190] has proposed that for discrete processes the distribution is discrete and at a given temperature each molecular process will free a corresponding quantity of repeat units. The total quantity freed up to a temperature T, N(T), is the sum of a number of parts N_i freed at a rate corresponding to their heats of fusion, thus

$$N(T) = N_1 + N_2 + N_3 + \ldots + N_i + \ldots$$
$$= A_1\exp(-\Delta H_1/RT_1) + \ldots + A_i\exp(-\Delta H_i/RT_i) \ldots \quad 3.2$$

The measured heat of fusion, $\Delta H(T)$, is an average value of all the heats of fusion contributing to the total quantity N(T) of freed units. This average is a weighted average, i.e. those processes contributing most to N(T) will contribute most to $\Delta H(T)$, thus one can write

$$\Delta H(T) = g_1 \frac{N_1}{N(T)} \Delta H_1 + \ldots + g_i \frac{N_i}{N(T)} \Delta H_i + \ldots \quad 3.3$$

where g_i is a weighting factor which represents the relative strength of the ith molecular process and the general term $N_i/N(T)$ represents the contribution of the ith process with a heat of fusion ΔH_i, i = 1 to N(T). A_i can be assumed constant over the temperature range used, thus substituting for N_i and N(T) from eqn. 3.2 we have

$$\Delta H(T) = \frac{\Sigma\, g_i\, \Delta H_i \exp(-\Delta H_i/RT_i)}{\Sigma \exp(-\Delta H_i/RT_i)} \quad 3.4$$

It is reasonable to assume initially that all the g_is are equal and $\Sigma g_i = 1$ so that eqn. 3.4 becomes

$$\Delta H(T) = \frac{\Sigma \Delta H_i \exp(-\Delta H_i/RT_i)}{\Sigma \exp(-\Delta H_i/RT_i)} \quad 3.5$$

This equation was tested by comparing predicted $\Delta H(T)$ with values measured on samples prepared at different temperatures.

A simple computer (BASIC) programme was written to evaluate $\Delta H(T)$ as described below (section 3.6.2). This programme is included in the appendix. The parameters of the programme are described as follows:

Let $\Delta H(T) = S$ 3.6

then $S = X/Y$

where $X = B_1 + B_2 + B_3 + \ldots B_i + \ldots$ 3.7

and $Y = C_1 + C_2 + C_3 + \ldots C_i + \ldots$ 3.8

such that:

$B_i = \Delta H_i C_i$ 3.9

$C_i = \exp(-A_i)$ 3.10

and $A_i = \Delta H_i / RT_i$ 3.11

The value of S calculated as described above is the uncorrected 'theoretical' heat of fusion (eqn. 3.5), it is termed S1. When corrected (eqn. 3.14), as described below (section 3.6.2), the new value is termed S2 where S2 is the product of S1 and the correction factor, g_i (denoted as Z_i).

3.6.2 Testing the Model

It should be possible to extract the distribution directly by calculating ΔH_i from measured $\Delta H(T)$ but within the available parameters this procedure is not readily feasible using eqn. 3.5. An indirect method has, therefore, been adopted whereby ΔH_i values are obtained from the $\Delta H(T)$ vs T curves (corrected for scatter) at 1°C intervals, Figures 3.9, 3.10 and 3.11. These values are subtituted in eqn. 3.5 and 'theoretical' values of $\Delta H(T)$ are evaluated. The resulting curve for one of the extruded formulations, sample A, is shown in Figure 3.15.

It is evident in Figure 3.15 that eqn. 3.5 simulates the form of the experimental data but not the magnitude. To account for the difference the assumptions leading to eqn. 3.5 are re-examined. It was assumed that

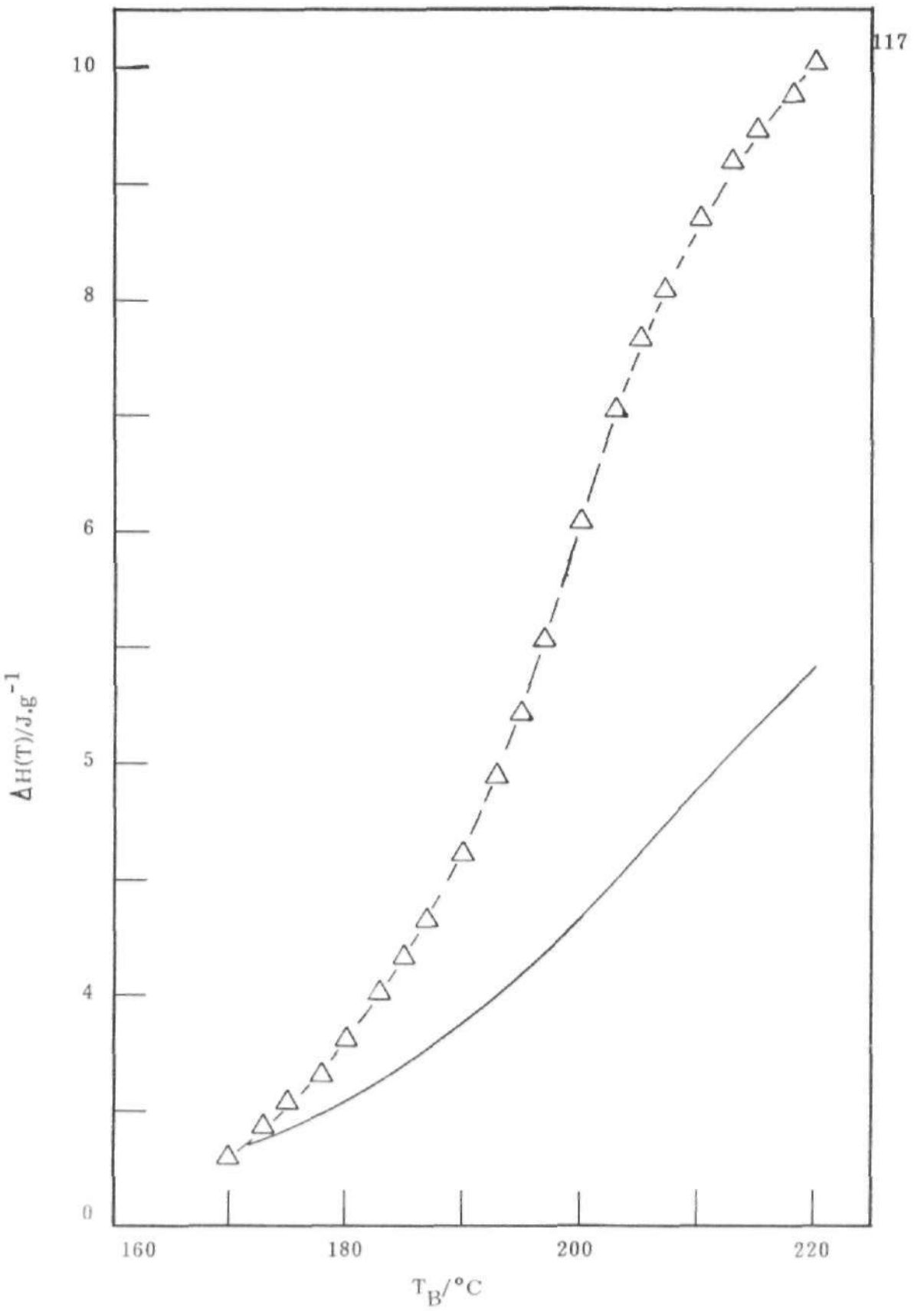


Fig. 3.15

Comparison of eqn. 3.5 with experimental results using the results shown in Figure 3.9 for sample A: △, experimental; ————, theoretical

all the A_is and g_is are equal, since $A_i = kT/h$, k and h being the Planck and Boltzmann constants respectively, no significant variation in this quantity is found over the temperature range covered. The second assumption is clearly an oversimplification since the more perfect the crystallite the greater the entropy change on melting, i.e. the greater the intensity of the melting process, thus g_i increases with crystalline melting temperature.

It may be possible to derive g_i from the basic principles but a simple procedure is adopted here. It is found from Figure 3.15 that the ratio $\Delta H_{obs}/\ ^{\Delta}H_{calc}$ varies from 1.0 to 2.0. This suggests that g_i as expressed in eqn. 3.4 is a function of the form

$$\lim_{i \to \infty} g_i = 2 \qquad 3.12$$

having a lower limit of 1.0. One such function is simply

$$g_i = \frac{2n_i}{n_i + 1} \qquad 3.13$$

This value when substituted for g_i in eqn. 3.4 gives

$$\Delta H(T) = \frac{\Sigma\ 2n_i/(n_i + 1)\ ^{\Delta}H_i \exp(-\Delta H_i/RT_i)}{\Sigma\ \exp(-\Delta H_i/RT_i)} \qquad 3.14$$

where $\Sigma n_i = N$. Values of $\Delta H(T)$ calculated from eqn. 3.14 compare well with values measured for the processed samples as discussed below.

3.6.3 Comparison of the Theoretical and Experimental Heats of Fusion

Application of eqn. 3.14 to the heats of fusion of processed samples (Figures 3.16, 3.17 and 3.18) show good agreement with the experimental values.

Some features of the theoretical and experimental curves can be noted. First, however, it is necessary to consider the significance of eqns. 3.5 and 3.14.

Eqn. 3.5 was developed by assumimg a continuous distribution of the ordered structures. Thus this equation implies a uniform variation of Δ H(T) over the processing temperature range. It has been noted (section 3.3.2) that the rate of production of recrystallizable structures in the melt is not uniform, but increases sharply in the critical region 190-200°C. It was also noted that this sudden change results from a change in the flow units in the melt. A change from grains to primary particles is generally believed.[15,28,101-106] The following reasons can, therefore, be suggested for the marked deviation of eqn. 3.5 from the experimental data (Figure 3.15):

(1) Eqn. 3.5 does not contain a parameter that accounts for the effect of the structural change on the heat of fusion.

(2) More significantly, eqn. 3.5 implies that the intensity of the melting process is independent of the structural perfection by the assumption of equal g_js.

It is not surprising, therefore, that eqn. 3.5 underestimates the changes in Δ H(T) with increased melt temperatures.

Since g_i was evaluated empirically to obtain eqn. 3.14 (which is a modified version of eqn. 3.5) the structural change is automatically taken into account by eqn. 3.13. The modification also implies that irrespective of the processing technique, the intensity of subsequent fusion of the recrystallized material is uniform, being described by eqn. 3.13.

It turns out that all deviations of experimental curves from eqn. 3.14 can be explained on the basis of eqn. 3.13: i.e. on the basis of changes of the intensity of the fusion process with crystalline perfection and with the shear history.

The following observations can be made from the results

(i) Leistritz (L-) samples (Figure 3.16)

(1) An intersection is observed between the theoretical and experimental curves. It shifts to a higher temperature with increased lubricant loading; being 190°C for sample A and 197 for sample B.

(2) Below the intersection the predicted $\Delta H(T)$ is higher than the observed value, and above it the reverse is the case.

The intersection clearly marks the critical temperature at which a change in the flow unit occurs in the melt. The value obtained in this study (190-197°C) is within the range (190-200°C) reported long ago by Collins and Krier.[181] This change shifts to a higher temperature with increased lubricant loading for reasons discussed previously (section 3.3.2).

Lower than expected heats of fusion below the critical temperature implies that the structures being melted at low processing temperatures are less ordered than would obtain in a uniform distribution of ordered structures. This observation is in agreement with the initial assumption that the least ordered structures are first melted.

From Figures 3.17 and 3.18 it is obvious that shear makes some contribution to the intensity of subsequent fusion after processing. Hence higher than expected $\Delta H(T)$ above the critical temperature results from an

enhancement of the order due to the effects of shear. This enhancement may not necessarily involve improved crystallinity (though that cannot be ruled out). Most likely, more recrystallizable structures are 'freed' into the melt pool as a result of shear. This effect would correspond to a 'combing out' of the melted primary crystallites during processing. It is equivalent to the elongation stage in the CDFE fusion mechanism discussed earlier (section 3.2.1).

It is reasonable, therefore, to expect that the maximum ratio, $\Delta H(T)_{obs}/\Delta H(T)_{calc}$ at a temperature above the critical region gives a measure of the shear intensity of the processing equipment for the material and processing conditions. This possibility is explored later.

(ii) Compression moulded (CM-) samples (Figure 3.17)

(1) For the non-lubricated sample (SO) observed $\Delta H(T)$ falls below theoretical values through the entire range of processing temperatures.

(2) With increased lubricant loading observed and theoretical values of $\Delta H(T)$ attain similar values at a temperature which increases with lubricant loading.

(3) At very high lubricant levels (3.0phr calcium stearate + 4.5phr wax) an intersection is observed between observed and calculated $\Delta H(T)$. This intersection is similar to those observed in extrusion (L-samples).

The temperature at which $\Delta H(T)_{obs}$ and $\Delta H(T)_{calc}$ attain similar values in compression moulding corresponds to the structural change discussed widely above. For the unlubricated sample (SO) this temperature is 197°C. Its shift to a higher value relative to the value for the extruded (less lubricated) sample A is due to very low shear levels for SO in

compression. Low shear also accounts for the absence of intersection between the theoretical and experimental curves for most of the CM samples. As lubricant level is increased in CM, flow of the material improves, therefore, $\Delta H(T)_{obs}$ and $\Delta H(T)_{calc}$ attain closer values. Eventually the two curves intersect at a sufficiently high lubricant level where flow becomes significant (sample L45). Under conditions of melt flow, particularly at temperatures where lubricant action becomes more internal,[77] the effect of shear becomes more relevant. Molecules freed as a result of crystalline melting can now be combed out and the presence of more recrystallizable structures in the melt pool results in an intersection similar to that observed in extrusion. The structural change occurs at a lower temperature despite a higher lubricant level because flow is much more enhanced at this temperature.

(iii) Krauss Maffei (KM-) samples (Figure 3.18)

(1) Two intersections between the theoretical and experimental curves are observed.

(2) The first intersection corresponds to the critical temperature discussed before. It occurs below 190°C for the lowest molecular weight sample and shifts to higher temperatures with increased molecular weight. The values being 184°C, 190°C, 196°C, and 193°C for S57, S62, S68, and S71 respectively.

(3) Above the critical temperature $\Delta H(T)_{obs}$ rises slightly above $\Delta H(T)_{calc}$, but except for sample S71, it falls again below $\Delta H(T)_{calc}$ at a higher temperature. For sample S71 this fall is not observed and the resultant curves are similar to the curves for L-samples.

Comparison of Figure 3.18 with Figures 3.16 and 3.17 shows that the shear level obtained for the material formulations and die back pressure used on the Krauss Maffei is intermediate between the low shear level in compression moulding and the medium shear level in the Leistritz. This conclusion was apparent from the low values of the entrance pressure loss in CR tests (section 3.2.1), however, the differences could not be easily quantified. It is interesting that simulation of the heats of fusion makes it possible to obtain quantitative values of differences in the relative shear levels.

$\Delta H(T)_{obs}$ rises above $\Delta H(T)_{calc}$ after the critical temperature because the effect of shear in combing out the melted species is still favoured. However, as the processing temperature is further increased the polymer melt becomes less viscous, and in the absence of sufficient back pressure in the extruder the shear level decreases. Combing out of melted species becomes less favoured, $\Delta H(T)_{obs}$ decreases and falls below the predicted value. The temperature at which this fall occurs increases with molecular weight, being 196°C, 209°C, and 213°C for S57, S62, and S68 respectively. The second intersection is not observed for S71, however, there is an indication of its occurrence at a temperature outside the processing range.

Sample S71 behaves in a manner similar to the L-samples. This suggests that the shear level for this sample was higher than for the other samples in the series. It will be recalled that it had been observed previously that some difficulty was encountered in the flow of S71 in the extruder. The results here serve to explain the source of this difficulty. It can be deduced that once again the results indicate that S71 is of a higher molecular weight than indicated by the GPC results.

It can be concluded from the above that although shear has little if any effect on the melting of the primary crystallites during processing; it, however, plays an important role in the total degree of melting by combing out melted molecules. This combing out helps in overall heat conduction to the crystalline core and also in interparticle network development. The differences in elastic response of the L- and KM-samples are shown to be due to differences in the maximum shear level reached during processing.

The relative contribution of shear to overall fusion can be evaluated from the ratio $\Delta H(T)_{obs} / \Delta H(T)_{calc}$ at a specific temperature above the critical temperature. This ratio calculated at 210°C for all the samples (Table 3.7) shows clearly that the relative shear level decreases as:

$$\text{L-samples} > \text{KM-samples} \simeq \text{CM-samples}$$

The results agree with the existence of low shear level in compression moulding. The increase in the ratio with increased lubricant level shows that above the critical temperature the lubricant acts more internally thus facilitating higher shear.

Table 3.7

Relative shear levels for samples processed on different machines, *measured by the ratio* $\Delta H(T)_{obs} / \Delta H(T)_{calc}$ *at* 210°C

Leistritz extruded samples		Krauss Maffei extruded samples		Compression moulded samples	
Sample A:	1.17	S57:	0.91	SO:	0.95
		S62:	0.99	L10:	0.99
Sample B:	1.21	S68:	1.01	L45:	1.04
		S71:	1.07		

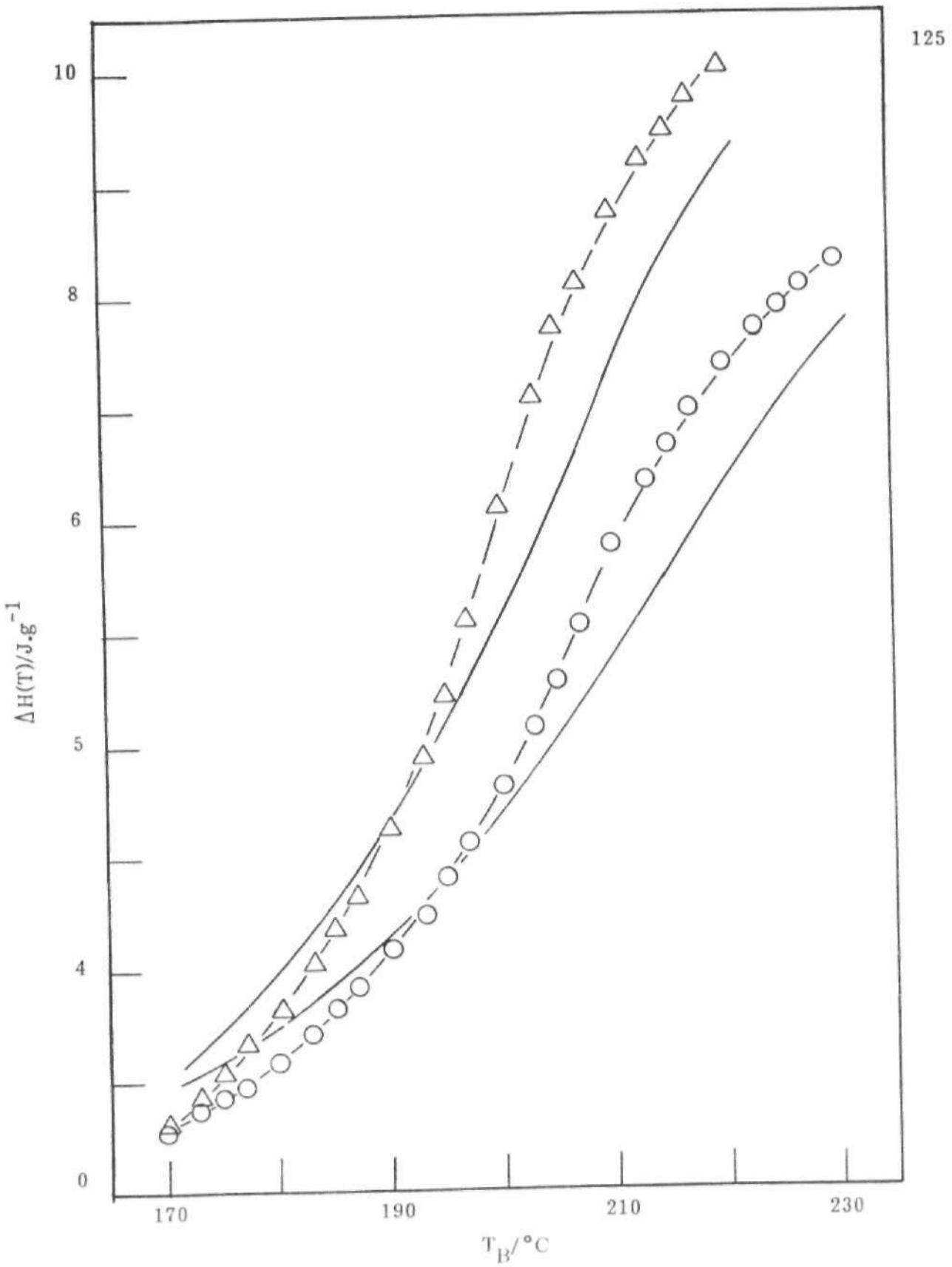


Fig. 3.16

Comparison of eqn. 3.14 with experimental results using the results shown in Figure 3.9: △ , sample A: O, sample B; ————, theoretical

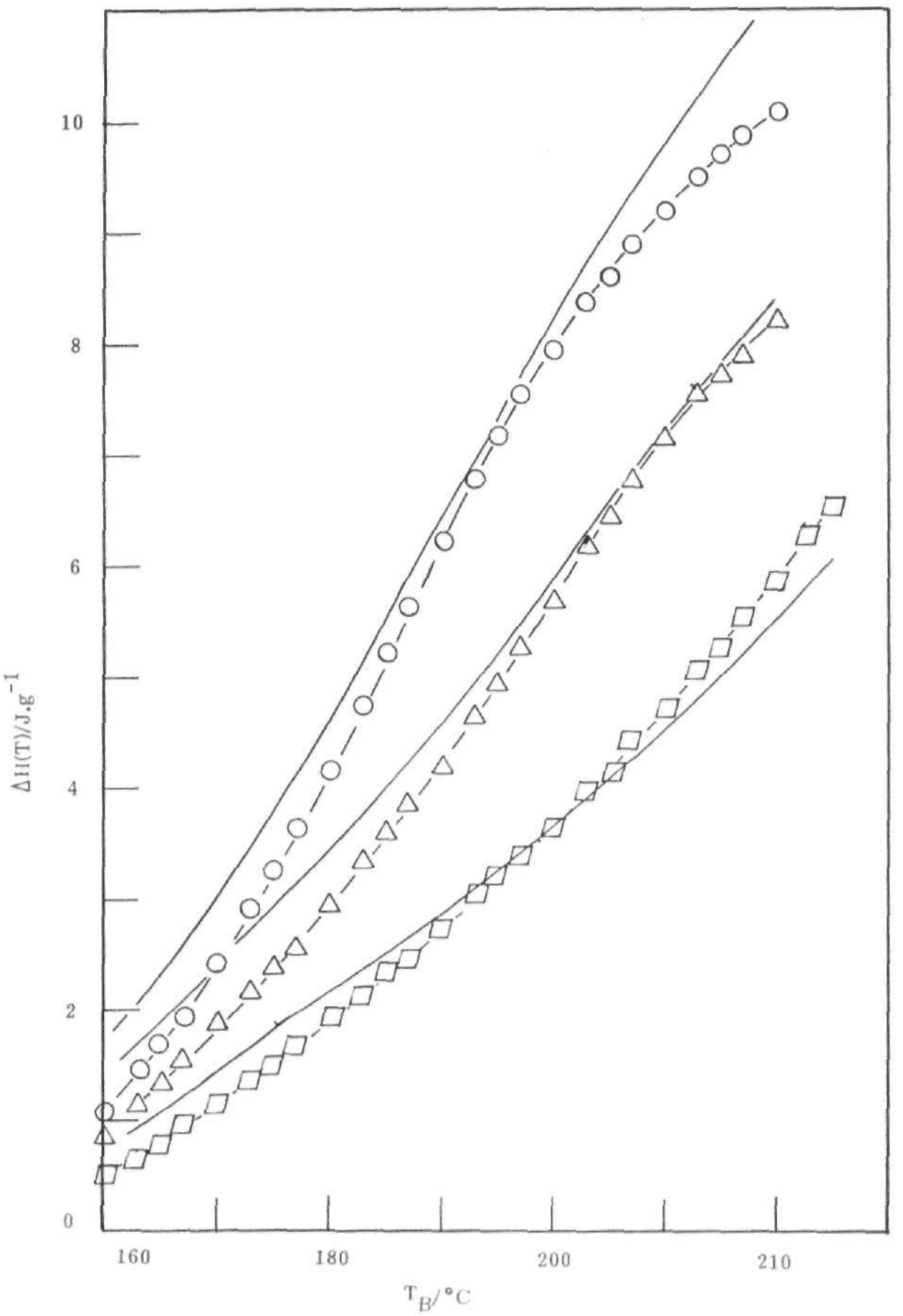


Fig. 3.17

Comparison of eqn. 3.14 with experimental results using the results for compression moulded samples: O, *SO*; △, *L10*; □, *L45*

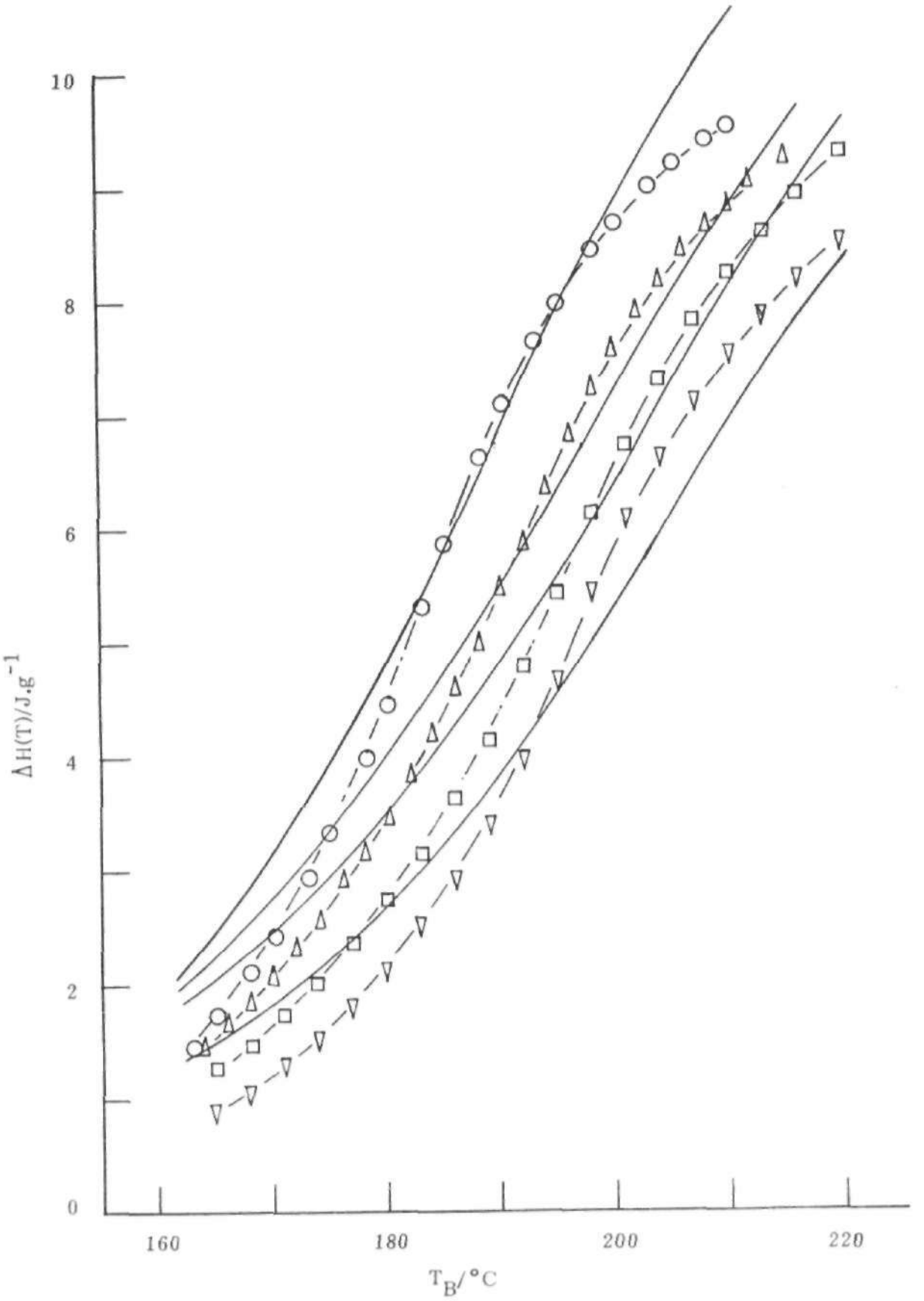


Fig. 3.18

Comparison of eqn. 3.14 with experimental results using different molecular weight samples: O, S57; Δ, S62; □, S68; ∇, S71

3.6.4 Application of the Distribution Model to Quantitative PVC Fusion Analysis

3.6.4.1 Activation Energy of Particle Breakdown

It was shown in section 3.6.1 that the quantity of repeat units, N, melted (freed) at a processing temperature, T, is given by

$$N = A \exp(-\Delta H(T)/RT) \qquad 3.1$$

where A and R are the Arrhenius and gas constants repectively.

Let us assume that at a reference temperature, T_o, a unit quantity, Q_o, of repeat units is freed, then

$$Q_o = A \exp(-\Delta H(T_o)/RT_o) \qquad 3.15$$

where $\Delta H(T_o)$ is the heat of fusion of Q_o units at the reference temperature T_o. With a suitable choice of T_o above the glass transition temperature, T_g, of the compound, but before melting occurs, $\Delta H(T_o) \approx 0$ and, therefore, $Q_o = A$. Thus Q_o is constant at T_o and can be assigned a unit value.

At a higher processing temperature, T, we have

$$Q_T = A \exp(-\Delta H(T)/RT) \qquad 3.16$$

and the relative increase in Q between the reference and a higher temperature is

$$\ln \frac{Q_T}{Q_o} = \frac{\Delta H(T)}{R} \left(\frac{1}{T} - \frac{1}{T_o}\right) \qquad 3.17$$

Eqn. 3.17 suggests a linear relationship for $\ln Q_T$ vs $1/T$ from which the activation energy, E_a for fusion of the morphological unit,

characteristic of the formulation, can be calculated. E_a values for different concentrations can be extrapolated to zero to obtain the true activation energy for breakdown of the particle. A value of $T_o = 100°C$ is chosen based on the literature[56,58] and corresponds to $\Delta H(T_o) = 0$.

Figures 3.19 to 3.21 show the variation of ln Q_T with inverse melt temperature I/T_B. Figure 3.19 is a summary of the data for the L-samples shown in detail in Table 3.8, while Figure 3.20 and Table 3.9 show the data for the compression moulded samples. Data for the KM-samples are included in Figure 3.21 only.

Plots of ln Q_T vs I/T_B produce two distinct linear regions with a clear break at $I/T_B = 2.15 \times 10^{-3} K^{-1}$ in both Figures 3.19 and 3.20, corresponding to $T_B = 195°C$. Equivalent T_B values for the KM-samples (Figure 3.21) are 184°C, 188°C, 192°C, and 192°C for S57, S62, S68, and S71 respectively. These critical temperatures have been discussed at length in the preceding sections. It is, however, demonstrated here that the lower the molecular weight the lower the critical temperature at which the change in the flow unit occurs for a given formulation.

It is also demonstrated that within the limits of usual processing temperatures, the morphological change involves the breakdown of two types of particles. It is not immediately known which particles are involved in the two regions. The temperature at which the lower ordered particles breakdown (releasing the higher ordered structures) occurs at higher temperatures in compression moulding (Figure 3.17). It is shown that for unlubricated formulation in CM this breakdown may not be observed (sample SO). It has been shown[84] that for compression moulding the grains persist to much higher temperatures; this is demonstrated in

Figure 3.17 as the temperature at which $\Delta H(T)_{obs}$ and $\Delta H(T)_{calc}$ attain similar values or intersect. It is, therefore, reasonable to expect that the two regions of breakdown involve loss of particulate structure at the grain and primary particle levels below and above the critical temperature respectively.

Activation energies of particle fusion were evaluated from Figure 3.20 and reproduced in Figure 3.22 as a function of total additive loading. Multiple regression analysis of the data (Figure 3.22) suggests a first order polynomial fit. From the intercepts activation energies of about 1.0 kJ/mol and 2.2 kJ/mol are obtained for the pure polymer. These values correspond to the breakdown of the grains and primary particles respectively.

It appears that the slopes of the curves in Figure 3.22 give a measure of the efficiency with which the additives reduce the activation energy. This efficiency may be related to the specific PVC-lubricant interaction.[77,191] Below the critical temperature this interaction is low and the slope is lower in this region (region I). Above the critical temperature the interaction improves and an increase in the slope is observed (region II).

The activation energies for particle breakdown for the KM-samples are shown in Table 3.10. The values are generally lower which suggests the melting of less perfect crystallites than observed in L-and CM-samples. The decrease observed with increasing molecular weight below the critical temperature (region I) implies that only the very least ordered structures are fused at low melt temperatures with increased molecular weight. Above the critical temperature, however, little variation in E_a is observed with changes in $\bar{M}_w$, which implies the fusion of structures having similar perfection.

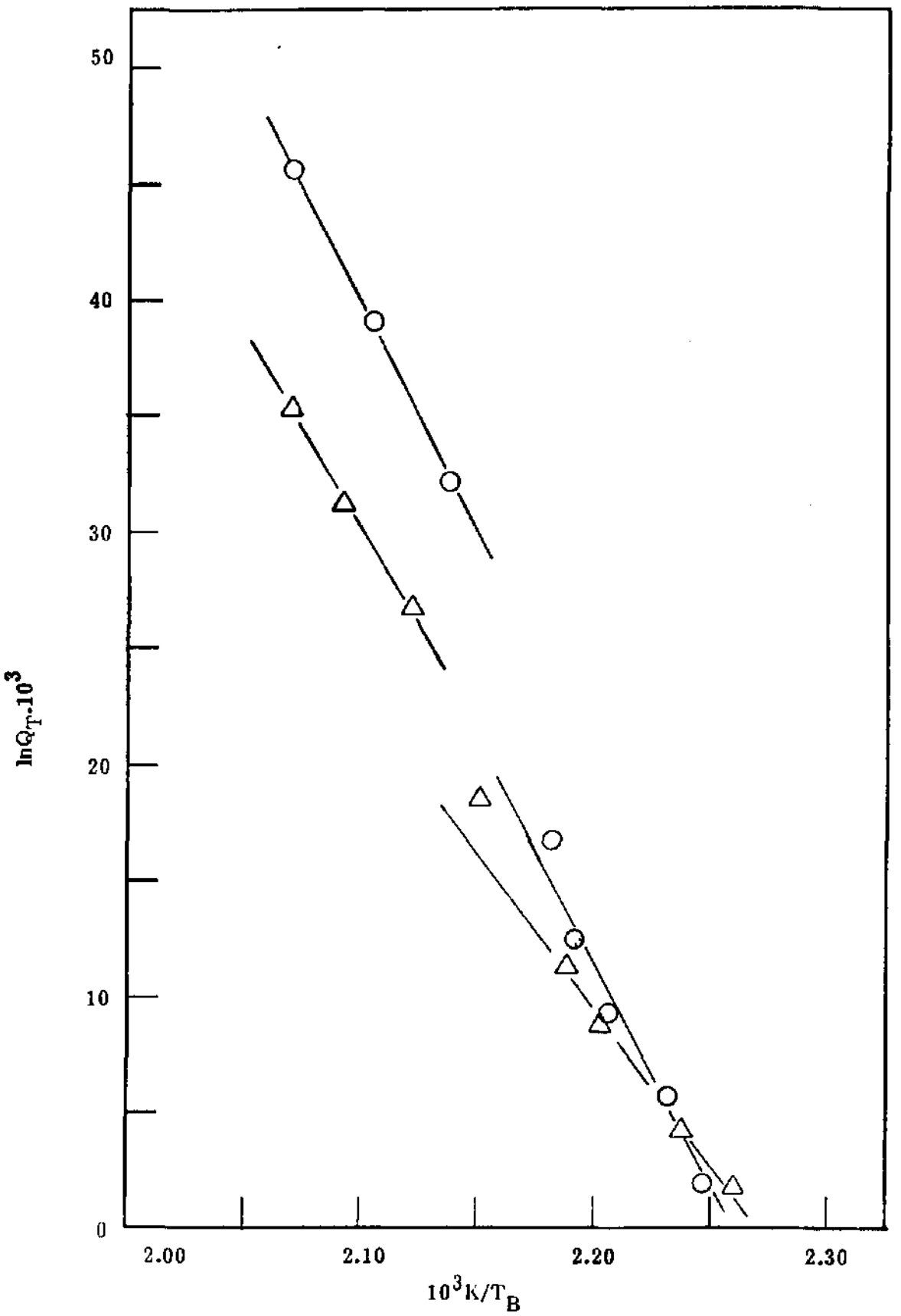


Fig. 3.19

Variation of $\ln Q_T$ with inverse temperature, $1/T_B$ for L-samples: O, A; △, B

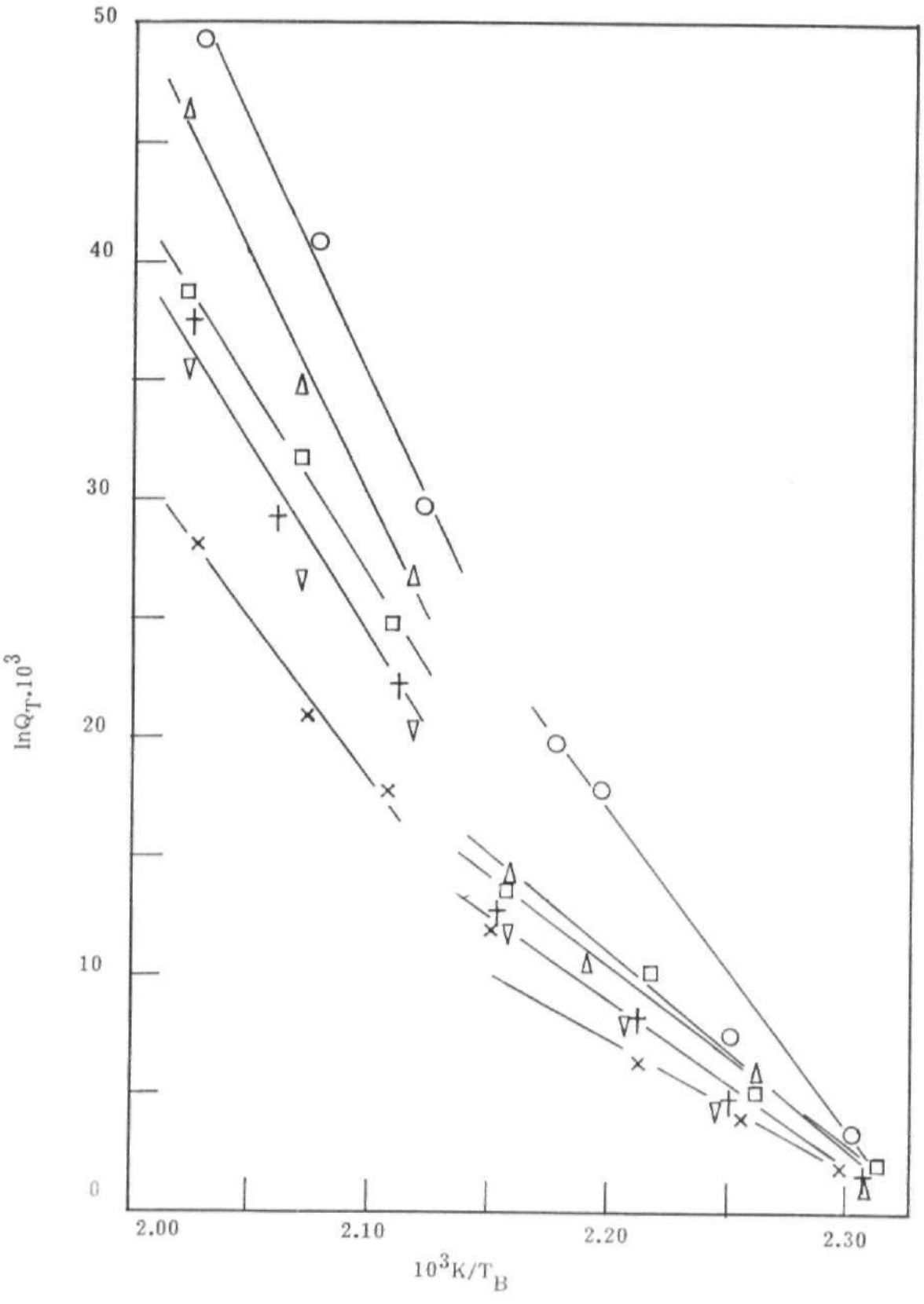


Fig. 3.20

Variation of $\ln Q_T$ with inverse temperature I/T_B for CM-samples: O, SO; Δ, L05; □, L10; +, L15; ×, L30; X, L45

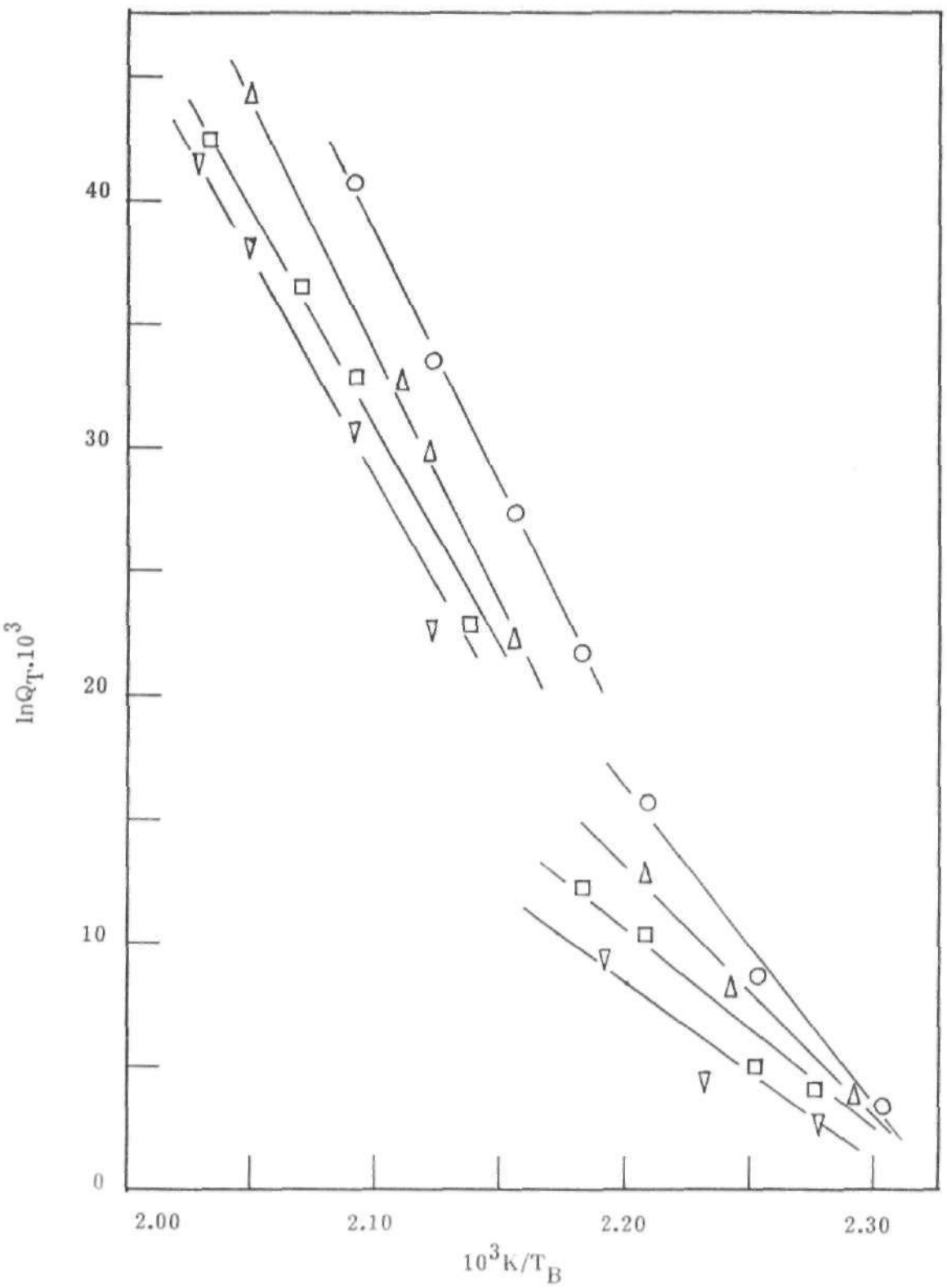


Fig. 3.21

Variation of $\ln Q_T$ with inverse temperature for kM-samples: O, S57; Δ, S62; □, S68; ∇, S71

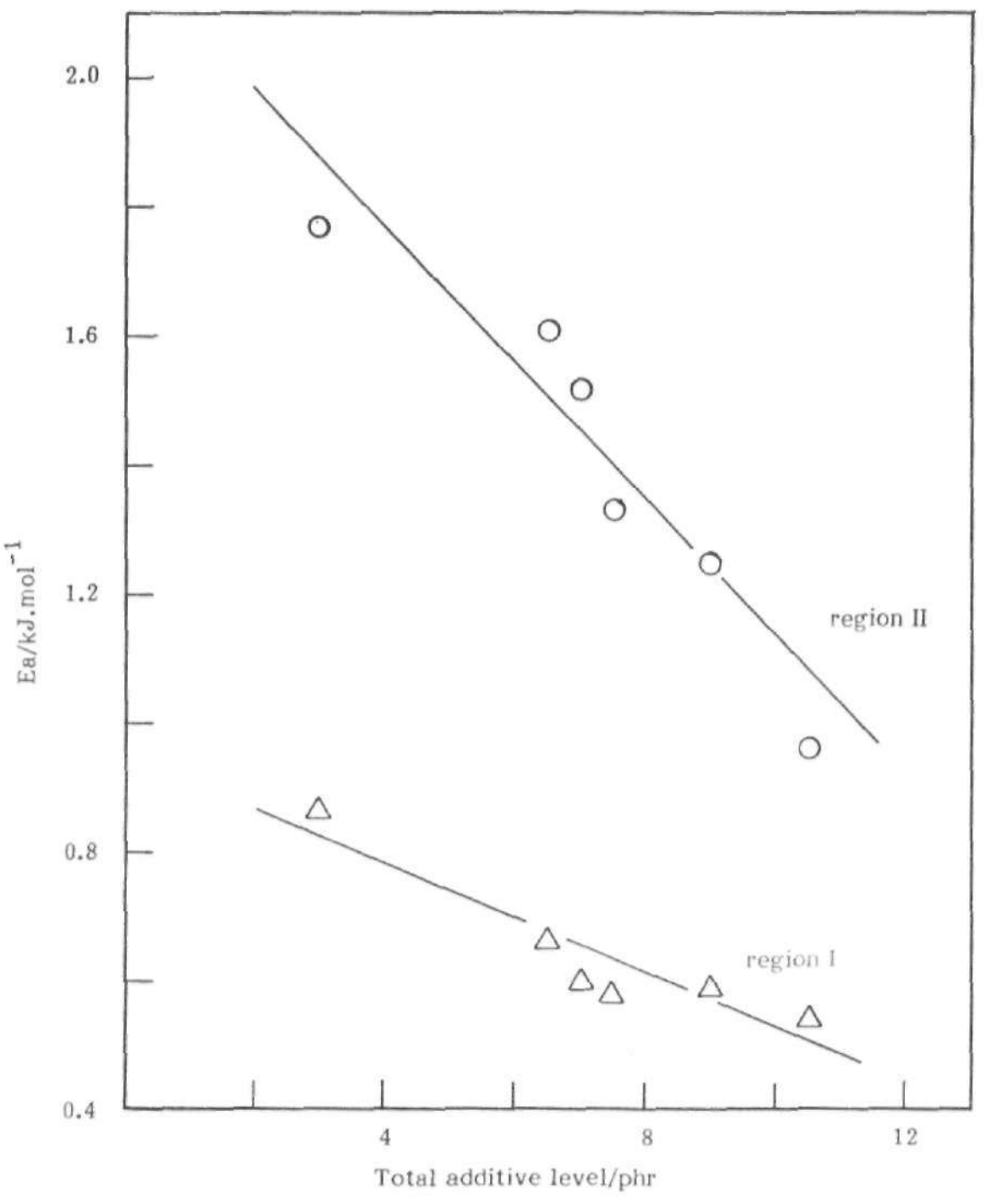


Fig. 3.22

Dependence of activation energy of particle fusion with additive concentration for CM samples at: △, lower temperature region I, T_B 195°C; and O, higher temperature region II, T_B 195°C

Table 3.8

Thermal analysis results for extruded formulations

PVC sample*	Melt temp. T_B/°C	Heat of fusion Δ H(T) J/mol	Q_T	Qr	$\frac{\Delta H(T).100}{\Delta H_u}$
Sample A	172	37.6	1.0020	0.31	0.75
	175	104.4	1.0057	0.89	2.08
	180	162.1	1.0093	1.47	3.23
	183	214.0	1.0129	2.02	4.26
	185	282.0	1.0170	2.69	5.62
	195	490.8	1.0326	5.21	9.78
	202	565.4	1.0400	6.38	11.26
	210	634.1	1.0477	7.61	12.63
	215	623.1	1.0484	7.74	12.41
Sample B	170	34.4	1.0018	0.28	0.69
	174	81.8	1.0044	0.70	1.63
	181	154.4	1.0090	1.42	3.08
	184	192.1	1.0115	1.83	3.83
	192	290.1	1.0187	2.99	5.78
	198	395.9	1.0269	4.30	7.89
	205	440.0	1.0317	5.06	8.77
	210	481.6	1.0360	5.76	9.59

* See Table 2.4

Table 3.9 Percentage fusion for compression moulded samples based on relative increment in Q, Q_r

Sample*											
SO		LO5		L10		L15		L30		L45	
T_B/°C	Q_r	T_B/°C	Q_r	T_B/°C	Q_r	T_B/°C	Q_r	T_B/°C	Q_r	T_B/°C	Q_r
161	0.54	160	0.17	159	0.34	160	0.19	-	-	162	0.29
171	1.18	169	0.91	169	0.84	171	0.78	171	0.74	170	0.65
182	2.88	183	1.83	178	1.61	179	1.31	180	1.30	179	1.04
186	3.20	190	2.28	190	2.13	191	2.05	190	1.88	192	1.93
198	4.86	199	4.29	201	4.00	200	3.63	199	3.30	201	2.84
208	6.66	210	5.63	210	5.14	212	4.77	210	4.35	209	3.35
220	8.18	221	7.57	221	6.77	220	6.10	221	5.76	220	4.56

* See Table 2.4

Table 3.10

Variation of activation energy for particle breakdown for KM samples

Breakdown region	Activation energies in kJ/mol Sample S57	S62	S68	S71
I	1.092	0.844	0.673	0.612
II	1.551	1.719	1.567	1.542

The activation energies obtained in this work, 1.0 to 2.2 kJ/mol, for the two regions of fusion, are much lower than the value, about 100kJ/mol, reported by Collins and Metzger[192] for flow. It must, however, be noted that the values obtained in this study refer to the melting of the particles. This activation energy is thus essentially that required for localized coordinated mobility of the chain molecule or its segment. As a result of the high viscosity of PVC melt, the activation energy for flow would be expected to be much higher than that for fusion as suggested by these results.

3.6.4.2 Evaluation of Fusion Level using the Distribution Model

Percentage fusion is evaluated from the reduced relative increment in Q, Q_r:

$$\% \text{ Fusion} = \frac{Q_T - Q_o}{Q_u - Q_o} \times 100 = Q_r \qquad 3.18$$

where Q_u is the maximum value of freeable units available in the perfect crystal. It is obtained from eqn. 3.17 using the heat of fusion, ΔH_u, of the 'perfectly syndiotactic' PVC crystal reported by Gouinlock[193] and his crystalline melting temperature, T_m° = 538K. Choice of these values is discussed later.

Detailed results of % fusion evaluated from eqn. 3.18 are shown in Tables 3.8 and 3.9 for L- and CM-samples respectively. These results are summarized in Figures 3.23, 3.24, and 3.25 for the L-, CM-, and KM-samples respectively.

It can be concluded that the results of evaluating fusion levels from Q_r provide further support for the model. Maximum fusion levels for all processed samples fall within the range 7-8% in excellent agreement with primary crystallinity values of 9% obtained by Juijn,[48,49] 8% obtained by Manson et al.,[194] and 5-10% generally found in the literature from x-ray diffraction studies.[39] Furthermore, the closeness of the values for all samples irrespective of processing history suggests that the contribution of shear to the maximum fusion level observable for a given processing history is much less than that of temperature. This was found previously (section 3.3.2) and it is in agreement with Allsopp's[107] fusion model.

A comparison of fusion levels evaluated from Q_r with values obtained using the simpler expression $100.\Delta H(T)/\Delta H_u$, columns 4 and 5 Table 3.8, shows that for the purpose of ranking fusion levels, it is sufficient to use the simpler expression. However, for determination of absolute fusion level (crystallinity index) the expression involving Q_r appears to be more representative of the true value.

3.6.5 Heat of Fusion, ΔH_u, of the Perfect PVC Crystal

Clearly the 'fusion level' evaluated by thermal analysis (eqn. 1.29, section 1.5.4) refers to the crystallinity index of the material. The term order factor[129] may be preferred to crystallinity index since the crystallinity of conventional PVC is poor.

To obtain comparable values of the order factor (fusion level) a value of ΔH_u should be generally accepted.

Literature values of ΔH_u are compiled in Table 3.11. The value obtained is influenced by the choice of the material (the syndiotactic fraction, α) as well as the method of measurement.[49,193,198] Gouinlock's[193] values, ΔH_u = 5.02 kJ/mole and T_m° = 265°C, were chosen from Table 3.11 and used in this study. This heat of fusion is based on independently measured crystallinities and heats of fusion for two low molecular weight, highly crystalline, PVC samples. The method used does depend on the accuracy of the crystallinity values but it is not based on any assumptions or problems which arise in accurate measurement of T_m° as do some of the other reported methods. Also Gouinlock's value, although not exactly the arithmetic mean, appears to be representative of the range produced in Table 3.11; particularly if the suitability of the method used is taken into account. The three calculations from collated literature data are included for comparison.

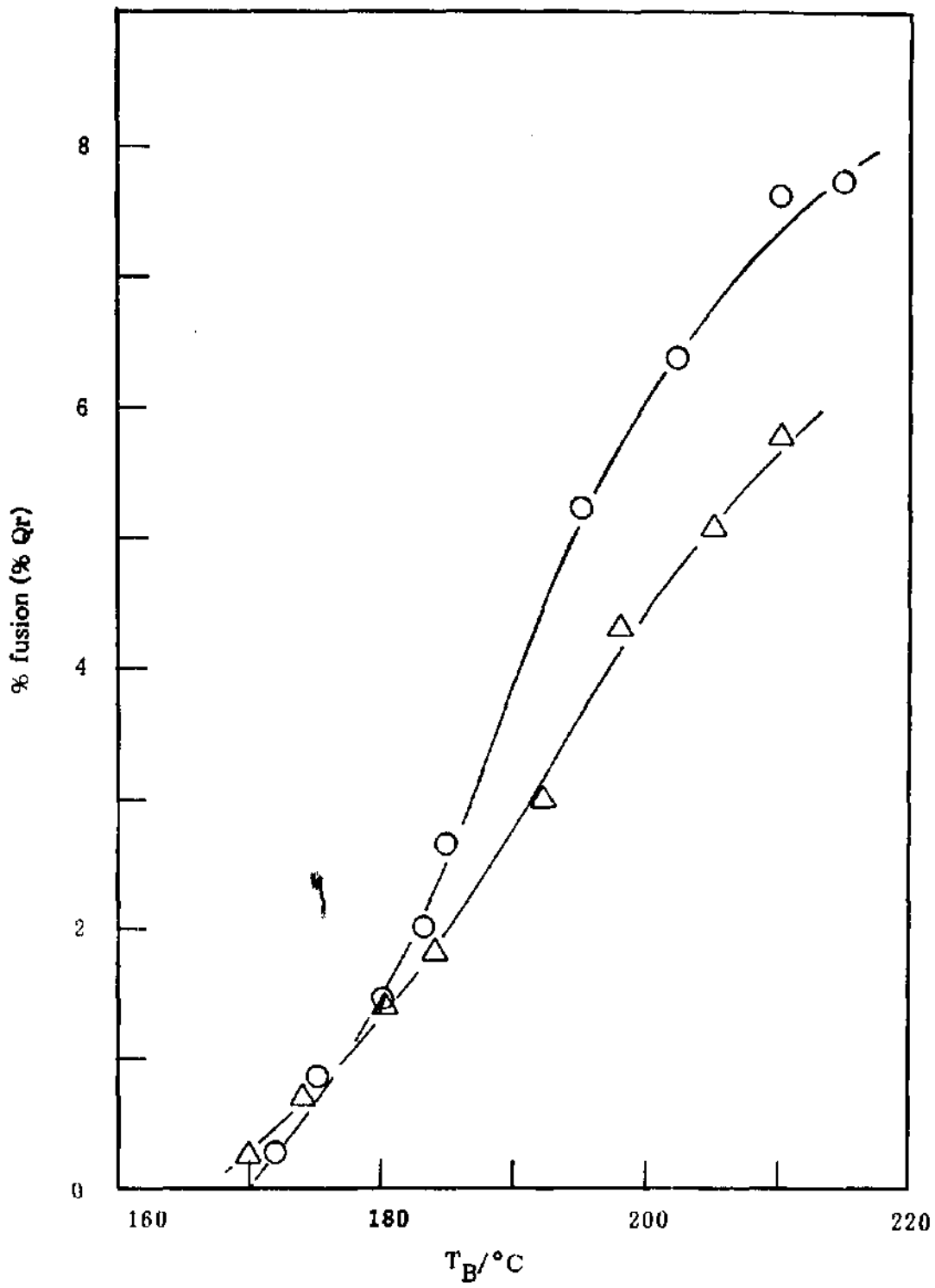


Fig. 3.23
Dependence of fusion level (based on reduced increment in Qr) on processing temperature for L-samples O, A; △, B

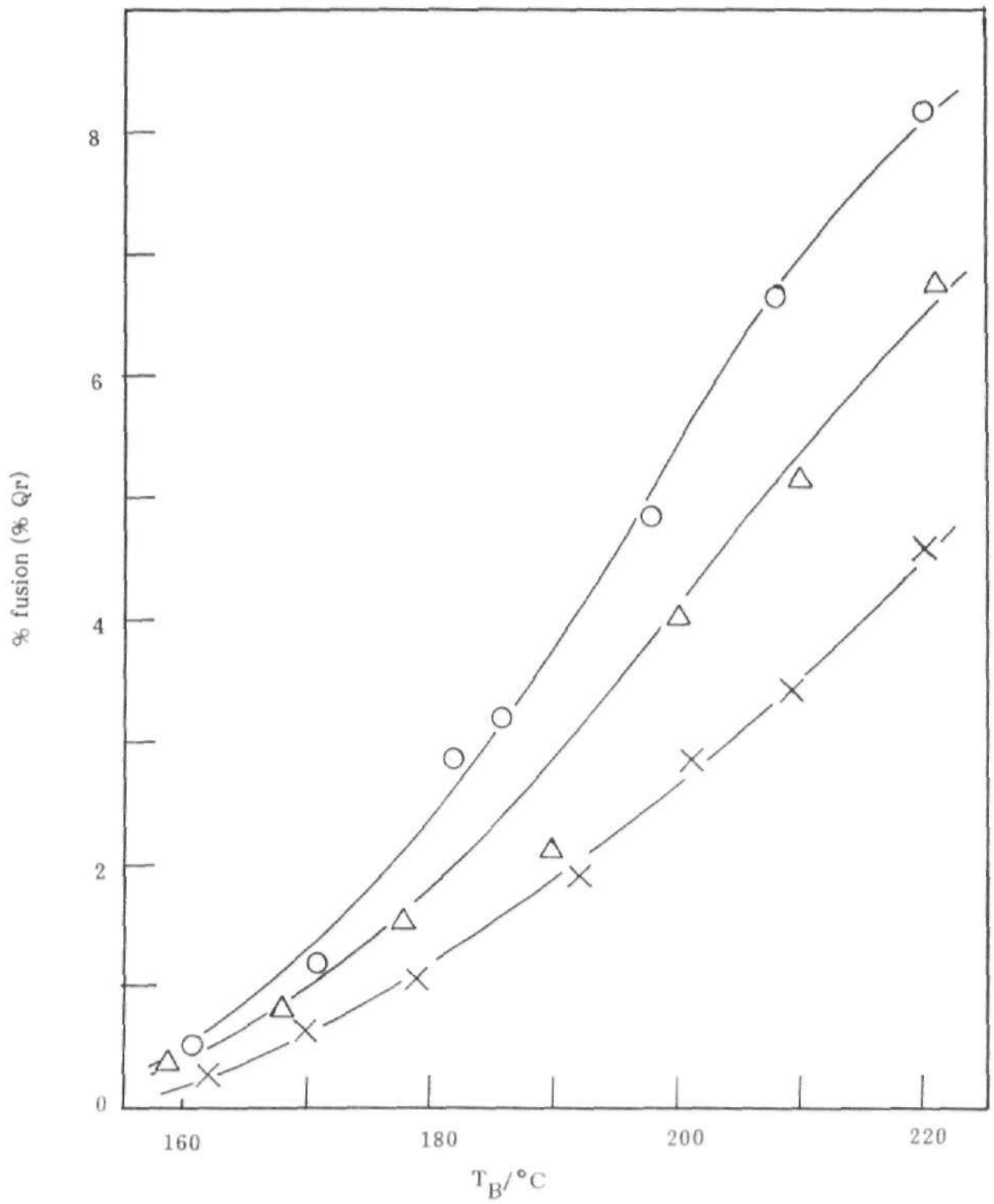


Fig. 3.24
Dependence of fusion level (based on Qr) on processing temperature for CM-samples:
O, SO; △, L10; X, L45

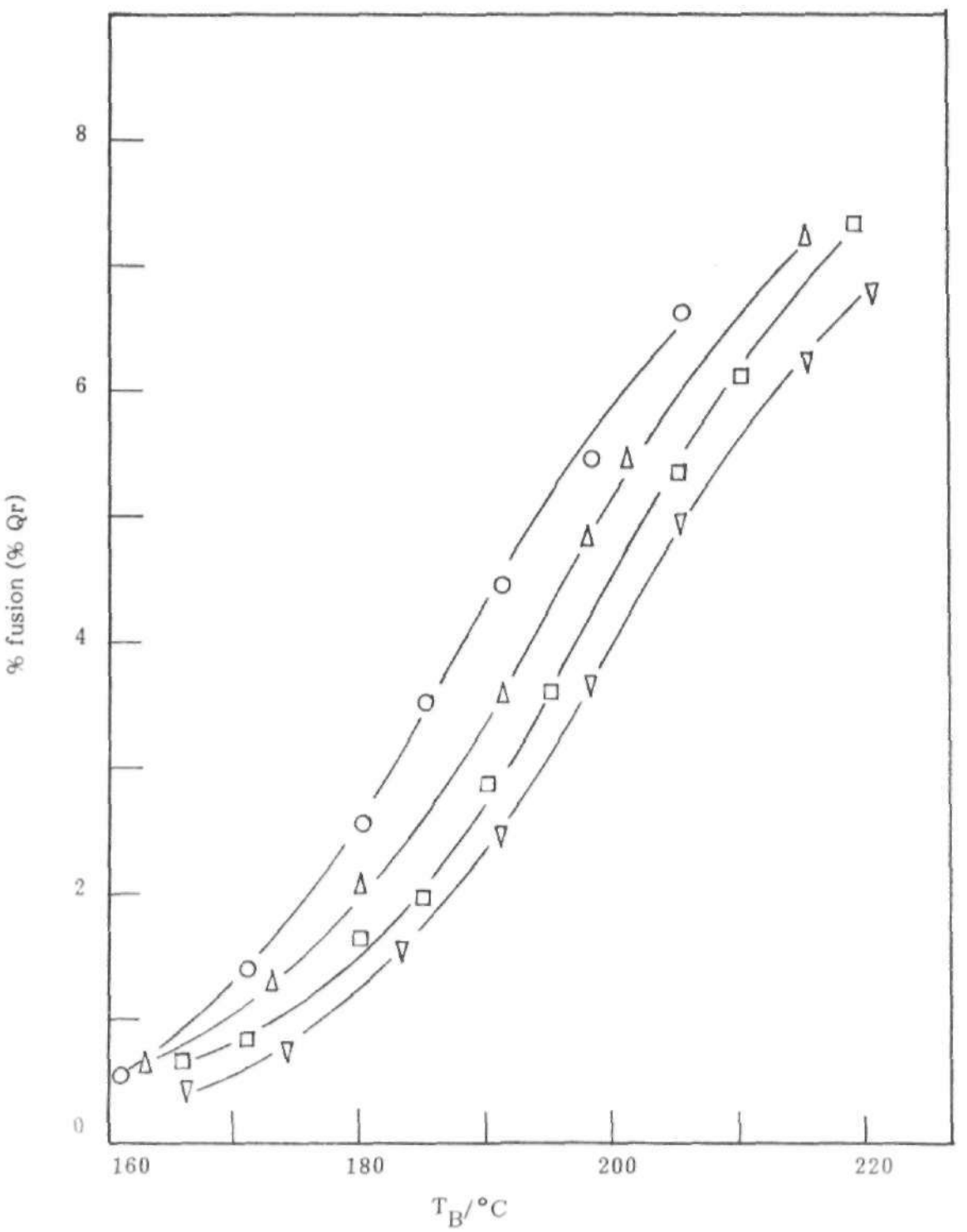


Fig. 3.25

Dependence of fusion level (based on Qr) on processing temperature for KM-samples:
O, S57; Δ , S62; □ , S68; ∇ , S71

Table 3.11 Reported heats of fusion of the fully syndiotactic crystalline PVC, ΔH_u

Heat of fusion kJ/mol ΔH_u	Polymer specification	Measuring method	References
11.3	α = 1.0	X-ray	Kockott[195]
6.69	α = 0.64	X-ray, recalculated	Gouinlock[193]
7.40	-	Calculated by the author from heat capacity, C_p, temperature functions provided in reference[196] using Hess' law	Alford and Dole[196]
5.02	α = 0.64	DSC	Gouinlock[193]
4.23 - 5.08	- -	Calculated by the author from the enthalpy of melting per unit volume given by Harrison et al. using the values of molar volume, v_o, and the hole volume, v_h, reported by Wunderlich	Harrison et al.[53] and Wunderlich[197]
2.51 - 5.02	Commercial	Polymer - diluent, T_ms were determined with the aid of a Kofler bar.	Colborne[198]
3.56	Commercial T_{pol} = -30°C	DSC	Juijn et al.[48]
3.28	T_{pol} = 75°C	Polymer - diluent	Nakajima et al.[35]
2.76	Commercial	Polymer - diluent	Anagnosto-poulos et al.[199]
3.20	-	Calculated by the author using C_p = 0.068cal./gK reported by Wunderlich	Wunderlich[197]

3.7 Conclusions

The following conclusions can be drawn from the gelation studies:

(1) Similar results can be obtained from capillary rheometry (CR), methylene chloride test (MCT), and thermal analysis (TA).

(2) Although sigmoid curves are widely reported in CR tests, a linear curve is possible. It is shown that sigmoid curvature results from lubricant effects on elastic development. A detailed description of these effects can be given. The negative gelation level can thus be easily explained on the basis of the same lubricant effects. Dependence of entrance pressure loss on formulation and equipment shear level makes ranking of gelation levels with the aid of a standard gelation curve meaningless when wide variations in formulation and/or shear levels are involved.

(3) MCT is simple and fast but it is only capable of passing or failing the sample. Differences in fusion level are not observable once a minimum degree of fusion is reached.

(4) TA provides information about the crystallinity index but this can be regarded as equivalent to the gelation level because of the unique relationship between PVC crystallinity and morphology. Gelation levels obtained by TA prove to be effectively independent of formulation and shear. They depend mainly on the processing temperature. This

technique has the advantage of ability to detect minor differences in the melt temperature across product cross-section and similar variations in gelation level. TA seems very suitable to accurate control of g-level. The g-levels, however, have to be related to the mechanical properties by an independent technique.

(5) Changes in the heat of fusion in TA can be simulated using a distribution model developed in the study. The simulation provides an accurate measure of the temperature at which morphological changes occur during processing. The relative shear levels of different processing equipment can be quantified. Activation energy for the breakdown of the morphological unit can be evaluated. The values 1.0 kJ/mol and 2.2 kJ/mol were obtained for the breakdown of the grain and the primary particle respectively. The fusion level (or order factor) can be more accurately evaluated from the relative amounts of fused chain molecules.

Chapter 4

RESULTS AND DISCUSSION

II. EFFECTS OF PROCESSING ON CRYSTALLINITY

In this chapter the effects of processing on the crystallinity is studied using solvent sorption, density, and wide-angle x-ray techniques. The primary objective was not the development of crystallinity with processing in itself but an understanding of the state of molecular order with increased fusion. Towards this goal solvent sorption was followed by monitoring gravimetric acetone sorption with time at room temperature, i.e. well below the T_g of the sample. To confirm the sorption results the crystallinity of processed samples was measured by density and WAXD techniques.

The study has focused mainly on extrusion, therefore, detailed studies did not include compression moulding. However, equilibrium acetone uptake was measured on CM samples to establish trends observed with extrudates and x-ray analysis was performed on a CM sample to confirm sorption results.

4.1 Acetone Absorption

4.1.1 Sorption Kinetics

Acetone uptake was followed gravimetrically as described in section 2.4(a). Detailed results are included in Tables 4.1A to 4.3A (appendix). These results are quite similar for all extrudates, therefore, only the results using sample A are analysed in detail.

The rate of acetone sorption is largely the same for samples processed above a melt temperature of 180°C (Figure 4.1). It increases only slightly above this temperature. Below a melt temperature, T_B, of 180°C, however, a substantial reduction in the rate is observed

The equilibrium amount of acetone absorbed also increases with increased melt temperature. This amount is moderate below 180°C T_B, but shows a sudden increase at about 190°C T_B. Above 190°C, however, the increase is moderate.

For the basis of the ensuing discussion it is useful to refer to section 1.5.3.

It is now widely agreed that the transport of organic vapours and liquids in glassy polymers involves both a diffusion process controlled by a concentration gradient, and a relaxation process controlled by a time-dependent response of the polymer to a swelling stress. As the relative contributions of these two processes change and interact, a wide range of behaviour can be encountered.[141] Alfrey et al.[133] consider simple Fickean diffusion for which sorption is initially linear with $t^{\frac{1}{2}}$ and Case II sorption where diffusion is initially linear with t as limiting cases representing domination by diffusion and relaxation respectively.

Kwei et al.[139] have shown that the diffusion of acetone in moulded PVC sheets can be described by a generalized model incorporating Fickean and Case II sorption (eqn. 1.23). Gilbert and Mulla[200] have also shown that the sorption of toluene at 25°C by films of low temperature polymerized and annealed PVC can be described by Case II mechanism.

The results of this study can also be described by the generalized model and are in agreement with Case II mechanism (Figure 4.1). A plot of % weight gain vs reduced time (Figure 4.2) shows clearly that different

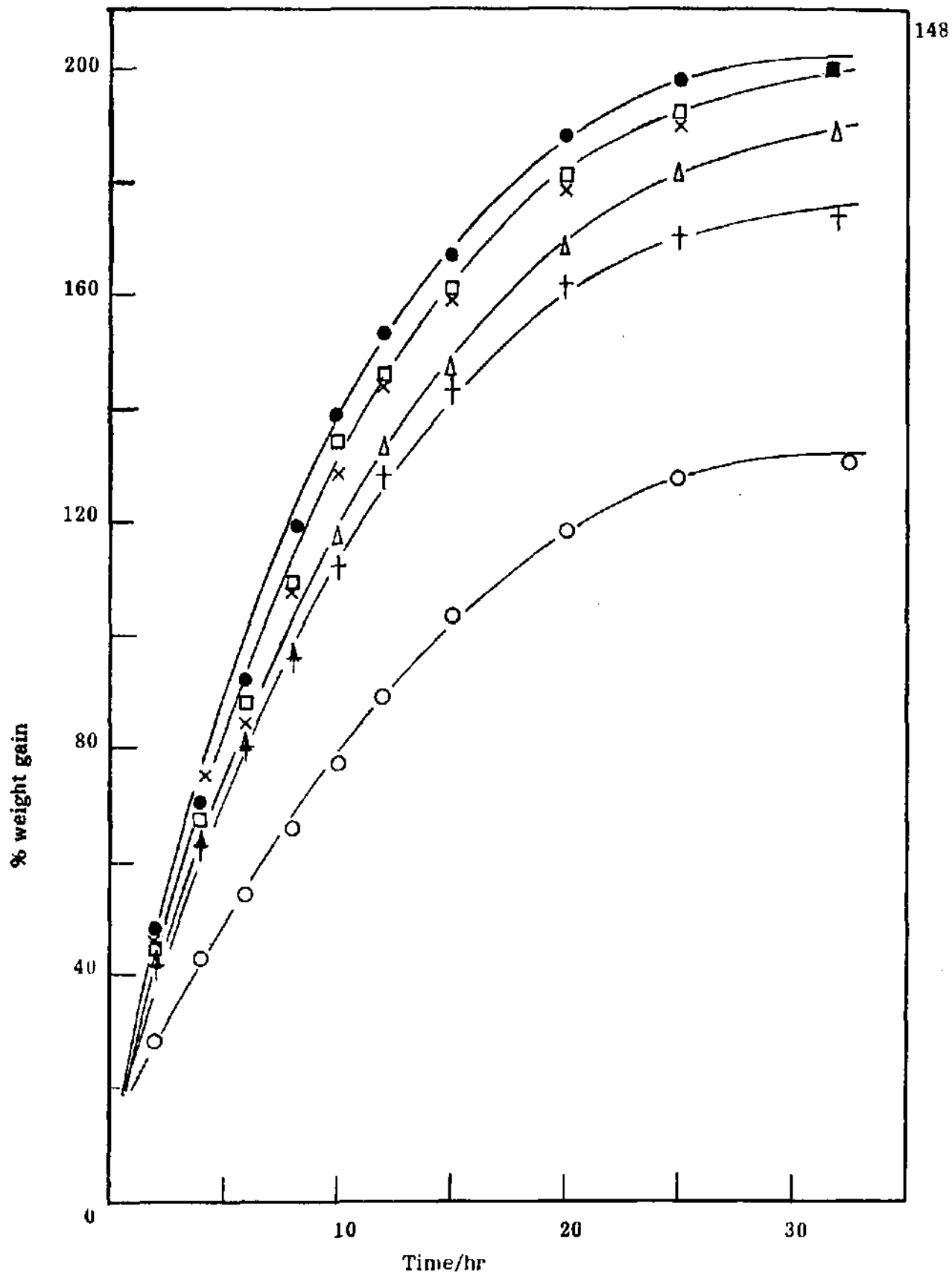


Fig. 4.1

Sorption curves for sample A processed over a range of melt temperatures using the Leistritz: O, 176; +, 184; Δ , 195; X, 200; □ , 208; ●, 220

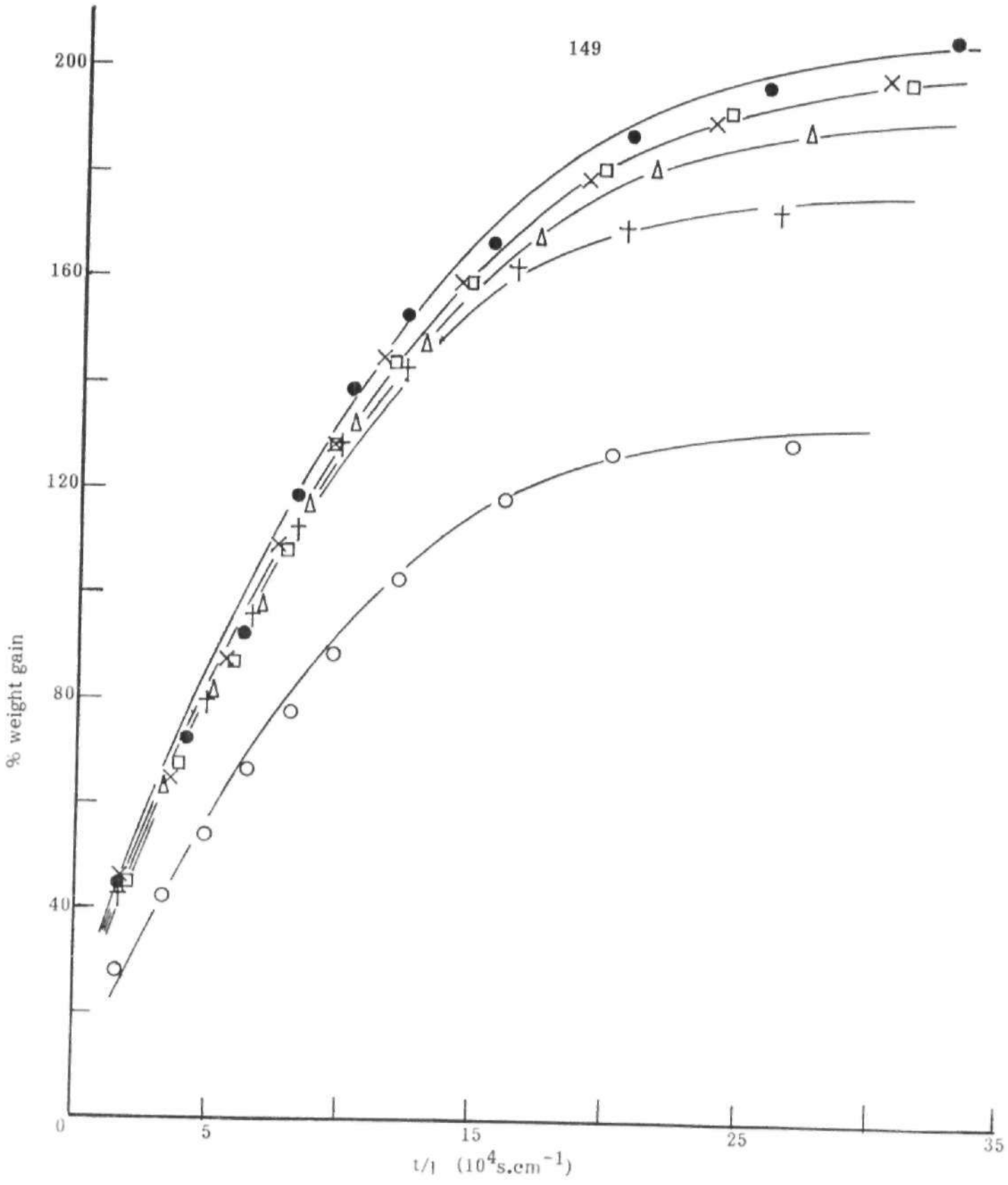


Fig. 4.2

Results of Figure 4.1 replotted as % weight gain vs reduced time (symbols are the same as in Fig. 4.1)

transport behaviour of penetrant molecules exists below and above 190°C melt temperature of the processed sample. This difference is of course accountable on the basis of structural differences below and above this temperature as noted previously[181] (see also Chapter 3). As far as is known Figure 4.2 is the first demonstration of this difference by solvent absorption.

Equilibrium sorption (ES) value (Figure 4.2) increases with g-level and equilibration time shifts to longer periods with "increased" g-level above a melt temperature, T_B, of 200°C (corresponding in this case to a die temperature, T_p, of 213°C (see Table 3.1). The % weight gain is linear with time up to 10 hrs (Figure 4.3) in even better agreement with eqn. 1.23 than the 60 minutes covered by the results of Kwei et al.[139] The shift of equilibration time to higher values above 200°C is particularly interesting in the light of Case II mechanism. It implies that the relaxation time of the molecules under swelling stress increases with increased melt temperature, T_B, above 200°C. This further implies that above this temperature either the sorbing (amorphous) phase contains an increasing amount of higher molecular weight species and/or this phase contains relatively better ordered structures than in the case of the sample processed at 200°C T_B. This observation is discussed in greater detail later.

The diffusion coefficient, D, depends on the frictional coefficient of the penetrant molecule[17] which can be related to a geometric impedance Ψ and a molecular mobilization factor β by eqn. 1.16. Hence knowledge of D can provide useful information about the state of molecular order. It was in recognition of this fact that sorption kinetics was studied. D can be evaluated from the sorption half-time, $t_{0.5}$ (where

$M_t = 0.5M_\infty$, Figure 4.2) using eqn. 1.26, or alternatively it can be evaluated from the intercept of a plot of M_t vs t (Figure 4.3) using eqn. 1.23.

The difference in transport behaviour of penetrant molecules noted previously involves differences in the velocity, v, below and above 190°C T_B. This is clearly evident in Figure 4.2. The observation can easily be verified by calculating v from the slopes of Figure 4.3 following eqn. 1.23.

The parameters M_t and C_o appearing in eqn. 1.23 have been calculated as

$$M_t = (g_t - g_o)/A_o \qquad 4.1$$

and $$C_o = W/A_o \qquad 4.2$$

where g_t is the sample weight at time t after immersion in the liquid, g_o is the weight of the dry sample prior to immersion, A_o is its total initial surface area and W is the weight of the liquid (kept constant through the run). Definition of these parameters yields D and v with the correct units. The point is noted because the definition is often not obvious in the literature especially where the parameters are defined differently in the same text for various purposes. The correct units of D are often quoted, however, even when M_t or C_o is not, or is differently, defined.

Values of D evaluated from Figure 4.2 using eqn. 1.26 are compared with corresponding values obtained from Figure 4.3 using eqn. 1.23 in Table 4.1; this table also includes values of v.

Large differences in D are found for the values obtained from the two figures. These difference arise from the fact that equilibration time was not truly reached within the duration of the experiment.

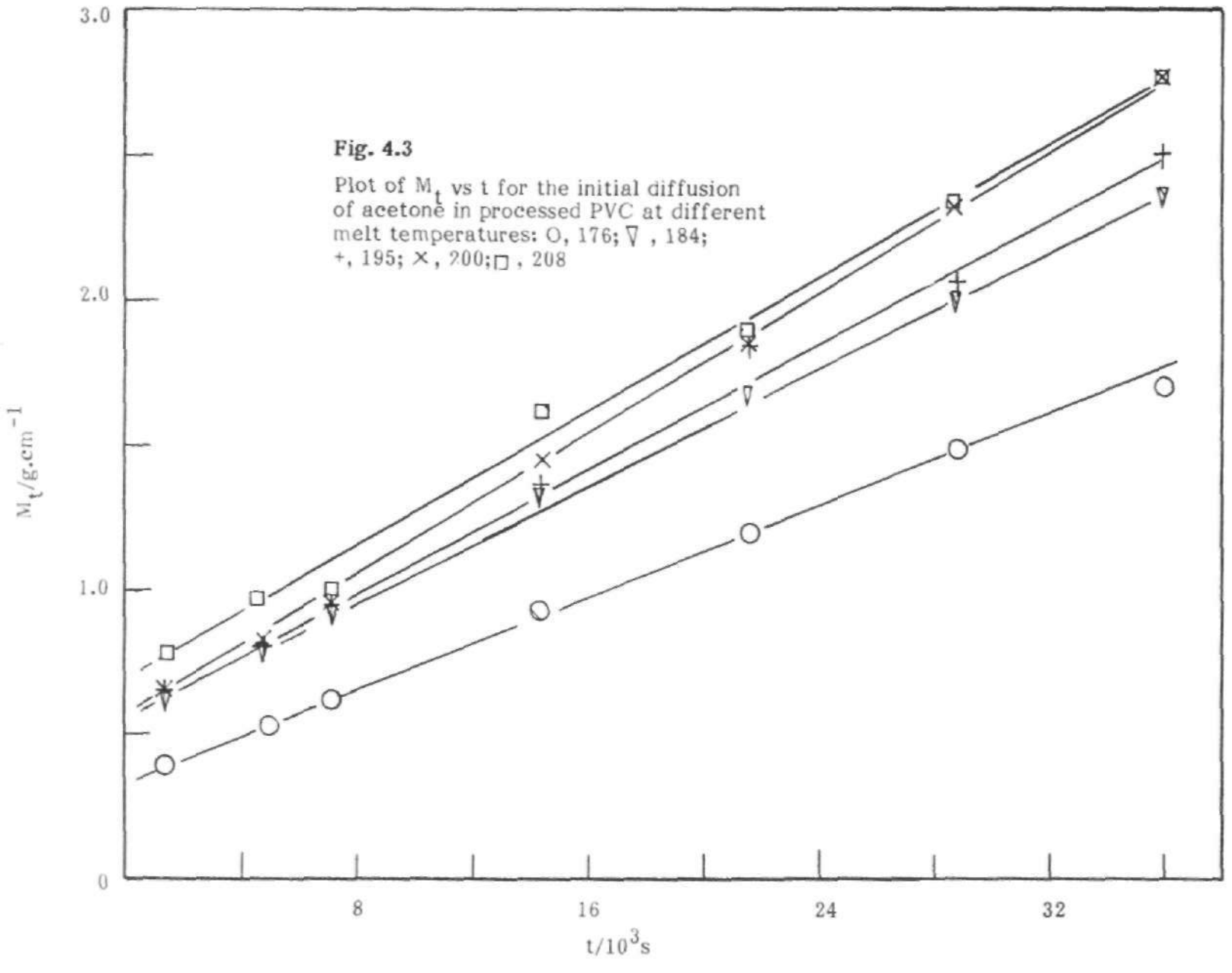


Fig. 4.3

Plot of M_t vs t for the initial diffusion of acetone in processed PVC at different melt temperatures: O, 176; ∇ , 184; +, 195; ×, 200; □ , 208

Inconveniently long equilibration times for films or sheets of any reasonable thickness has been discussed at length by Berens.[141] Unattainment of equilibrium is not very obvious in Figures 4.1 and 4.2; if, however, the results are plotted as reduced weight gain vs $t^{\frac{1}{2}}$ or t (Figure 4.4) it becomes evident that the study had been conducted only to the approach of equilibrium. For this reason values of $t_{0.5}$ from Figure 4.2 are approximations of the true values, therefore, values of D calculated from Figure 4.3 using eqn. 1.23 are more accurate than those based on Figure 4.2. To illustrate this point further the more accurate D values from Figure 4.3 have been used to recalculate $t_{0.5}$ with eqn. 1.26. The calculated and the estimated values are compared in Table 4.2. Whereas no trend is found in the estimated values, recalculated $t_{0.5}$ show an obvious trend observed also for D, and in subsequent tests. Furthermore, calculated $t_{0.5}$ is of the order of 100 days for the average sample thickness in agreement with theoretical predictions.

Table 4.1

Kinetic parameters for acetone absorption at 23°C

Sample code	melt temp. T_B	$D \cdot 10^{-6}$ ($cm.^2/s$)		$V \cdot 10^{-5}$ (cm/s)
		from eqn. 1.23	from eqn. 1.26	
A2-1	176	0.5	6.8	0.4
A3	184	4.0	7.3	1.9
A4	195	3.9	8.4	2.0
A5	200	4.6	5.4	1.9
A6	208	3.4	5.3	2.0
A7	220	3.1	4.9	2.0

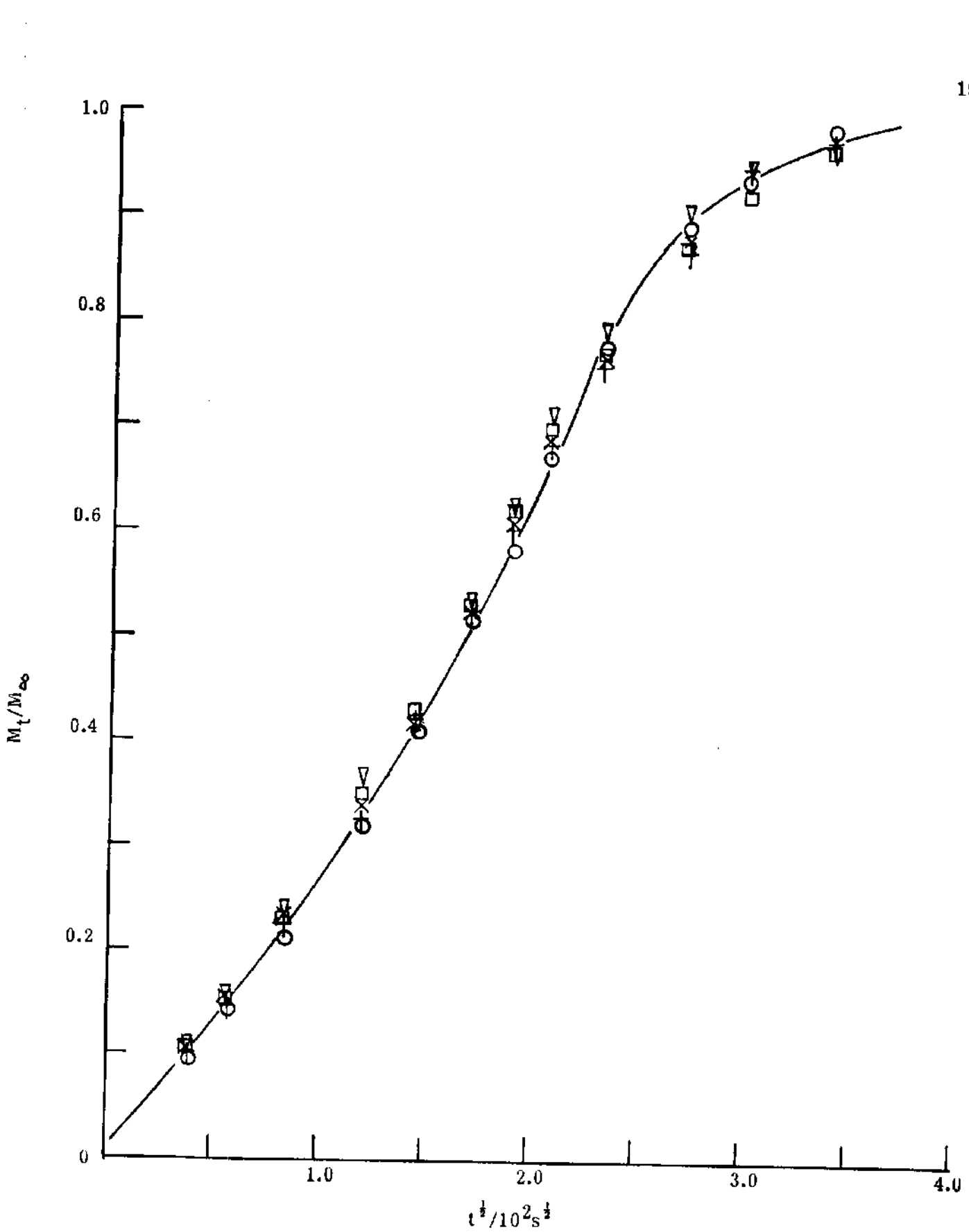


Fig. 4.4

Plot of M_t/M_∞ from data of Figure 4.1 (symbols same as in Figure 4.3)

Table 4.2

Comparison of observed and calculated sorption half time, $t_{0.5}$

Sample	A2-1	A3	A4	A5	A6	A7
$t_{0.5}/10^4$s (estimated)	3.0	2.6	2.1	2.7	2.6	2.5
$t_{0.5}/10^5$s (recalculated)	4.1	4.8	4.5	3.1	4.0	3.9

It is further shown (Table 4.1) that, within the limits of experimental error, the rate of transport of penetrant molecules, v, is much slower for samples processed below 190°C T_B than for those processed at, and above, this temperature. However, v remains substantially constant above 190°C although differences in D still exist. These results confirm the observation previously made from Figure 4.2 that differences exist in the transport behaviour below and above 190°C T_B.

The values of v found in this study beyond 190°C T_B are in excellent agreement with values reported for the diffusion of acetone in PVC reported by Kwei et al.[139] However the values of D in the same region differ generally by two orders of magnitude. These authors reported a value of D on the order of $10^{-8}cm^2/s$ at similar test temperatures, while the value found in this study is on the order of $10^{-6}cm^2/s$. D values found in this work are in the same order of magnitude with values reported by Lapcik et al.[140] for a series of organic liquids over a range of test temperatures. Considering that acetone will show greater activity than vinyl chloride monomer (VCM) the value $10^{-6}cm^2/s$ compares well with the value $10^{-8}cm^2/s$ obtained by Berens[141] for VCM. Kwei's order of magnitude of D for acetone cannot be recalculated from their data for confirmation.

4.1.2 Estimation of Relative Crystallinity from Sorption Kinetics

Eqns. 1.16 and 1.17 can be combined to give

$$D = D^* \alpha^n / \beta \qquad 4.3$$

Since the chain mobilization factor, β , is characteristic of the chemical structure of the polymer and changes little with small changes in the amorphous fraction, α ,[135] it should be expected that the more crystalline the material the lower the value of the diffusion coefficient, D.

A maximum is observed for changes in D (based on eqn. 1.23) with increased melt temperature (Table 4.1). This maximum occurs at 200°C. An identical trend was also observed for changes in density and the intensity of WAXD as shown later. These results demonstrate clearly that the processed sample is most amorphous at a melt temperature of 200°C. The observation is discussed in greater detail in section 4.3.3.

It is not possible to obtain a quantitative value of the amorphous fraction α without knowledge of n and β. Micheals and Bixler[135] have, however, described a method for obtaining this value. Their procedure is not considered here because density measurement and WAXD can be more readily performed.

4.1.3 Dependence of Equilibrium Sorption on Gelation Level

An attempt was made to relate the equilibrium amount of acetone absorbed to the processing temperature, and, therefore, to the g-level. The results are summarized in Figures 4.5 to 4.7 and discussed below.

(a) L-samples (Figure 4.5)

Equilibrium sorption (ES) increases linearly with melt temperature but levels off above 200°C. Values at equivalent temperatures are higher for the less lubricated sample, A, than for the more lubricated sample, B.

In the light of section 4.1.2, these results demonstrate once again that the crystallinity decreases with increased melt temperature up to 200°C. It is further shown by ES values that at equivalent processing temperatures on the Leistritz the less the lubricant concentration the more amorphous the extrudate. The difference may be due to the effects of relative shear levels as discussed in section 3.2. Increased shear levels (with decreased lubricant level) results in greater destruction of the crystallites as found by Kau and Filisko.[201]

The minimum in crystalline fraction occurring at 200°C revealed in the kinetics treatment is not detectable in Figure 4.5 which suggests that ES is less sensitive to small changes in the crystalline fraction than, say, the diffusion coefficient D.

(b) CM-samples (Figure 4.6)

A clear maximum is observed for the changes of ES with T_B as would be expected from the observed trend of D for the extrudates. The maximum occurs also in the neighbourhood of 200°C for all moulded samples covering a broad range of lubricant concentrations.

The difference between the trends observed in ES values for the extrudates and for the compression moulded samples may be related to differences in shear levels and in relative crystallinities. For example at equivalent melt temperatures the CM samples are shown by WAXD to be much more crystalline than the extrudates.

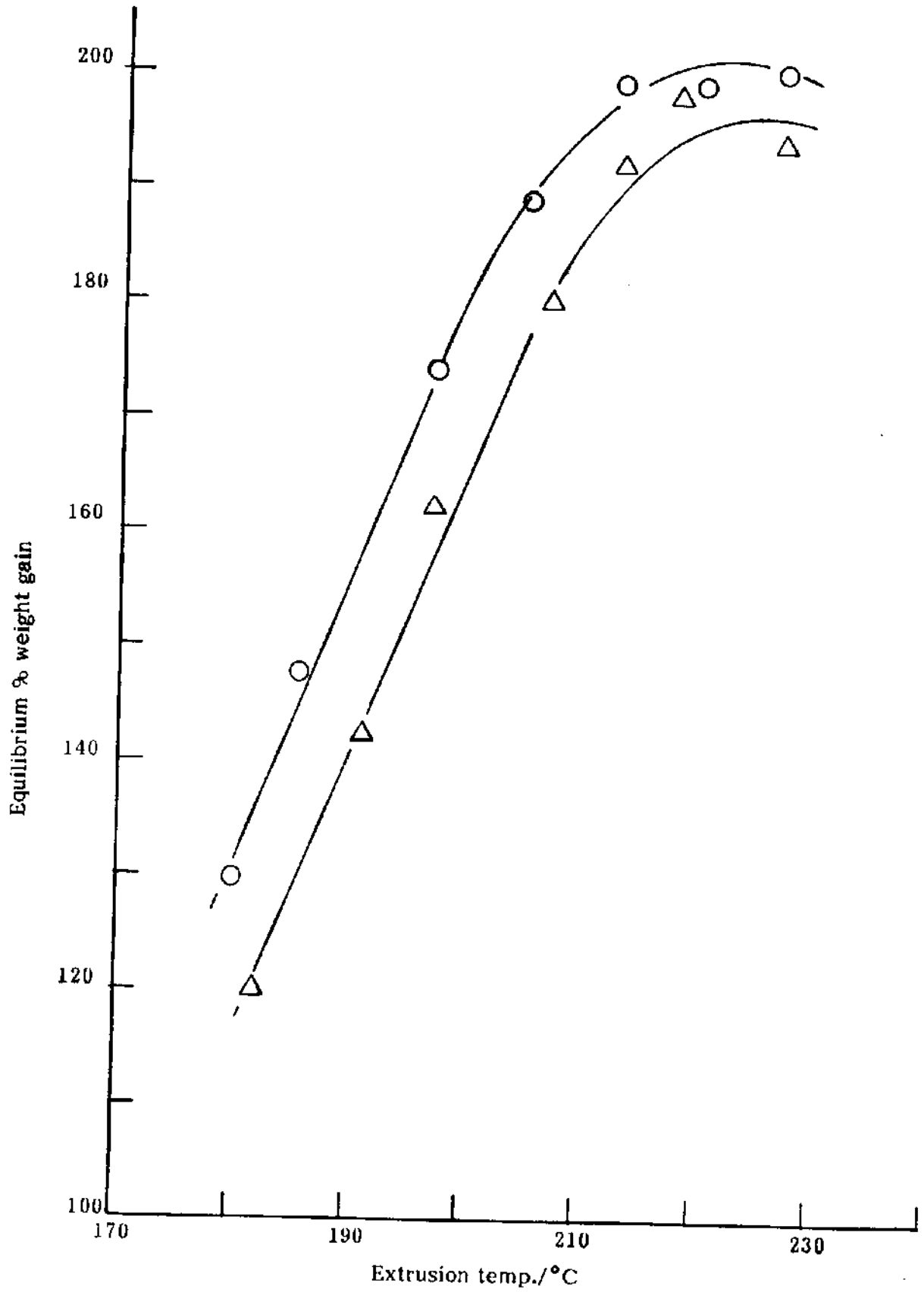


Fig. 4.5

Equilibrium % sorption curves for samples extruded in the Leistritz over a range of temperatures: O, sample A; △, sample B

In contrast with the L-samples, ES values increase with increased lubricant level in compression moulding. It attains a maximum value at 4.0phr total lubricant level for the formulation studied and decreases sharply above this concentration. The reason for this difference in lubricant effects in extrusion and in compression moulding is not obvious. A suggestion can, however, be made.

It was shown in section 3.6 that with increased lubricant level, melt flow is enhanced in compression moulding. An increase in the melt flow would most likely result in greater shear at constant pressure. Increased shear results in greater destruction of the crystallites as discussed previously. The moulded sheet is more amorphous and, therefore, has higher capacity for absorption. ES values increase with lubricant concentration in this way until a concentration is reached where the PVC grains virtually 'float' in a continuous bed of lubricant. Although at a specific temperature, melt flow is still higher, interparticle shear is greatly reduced since contribution from external shear is negligible. The granular structure is largely preserved in the melt. The primary crystallinity is better developed because annealing effects outweigh those of melt recrystallization. The marked improvement in crystallinity results in a sharp reduction in capacity to absorb the liquid. Figure 4.6 shows that the increase in crystallinity resulting in greatly reduced ES values continues up to the limits of lubricant level studied (7.5phr).

(c) KM-samples (Figure 4.7)

Excessive disintegration due to penetrant attack meant that only limited results could be obtained for sample S57. For the same reason, it is not possible to draw meaningful conclusions from the trend observed for this sample.

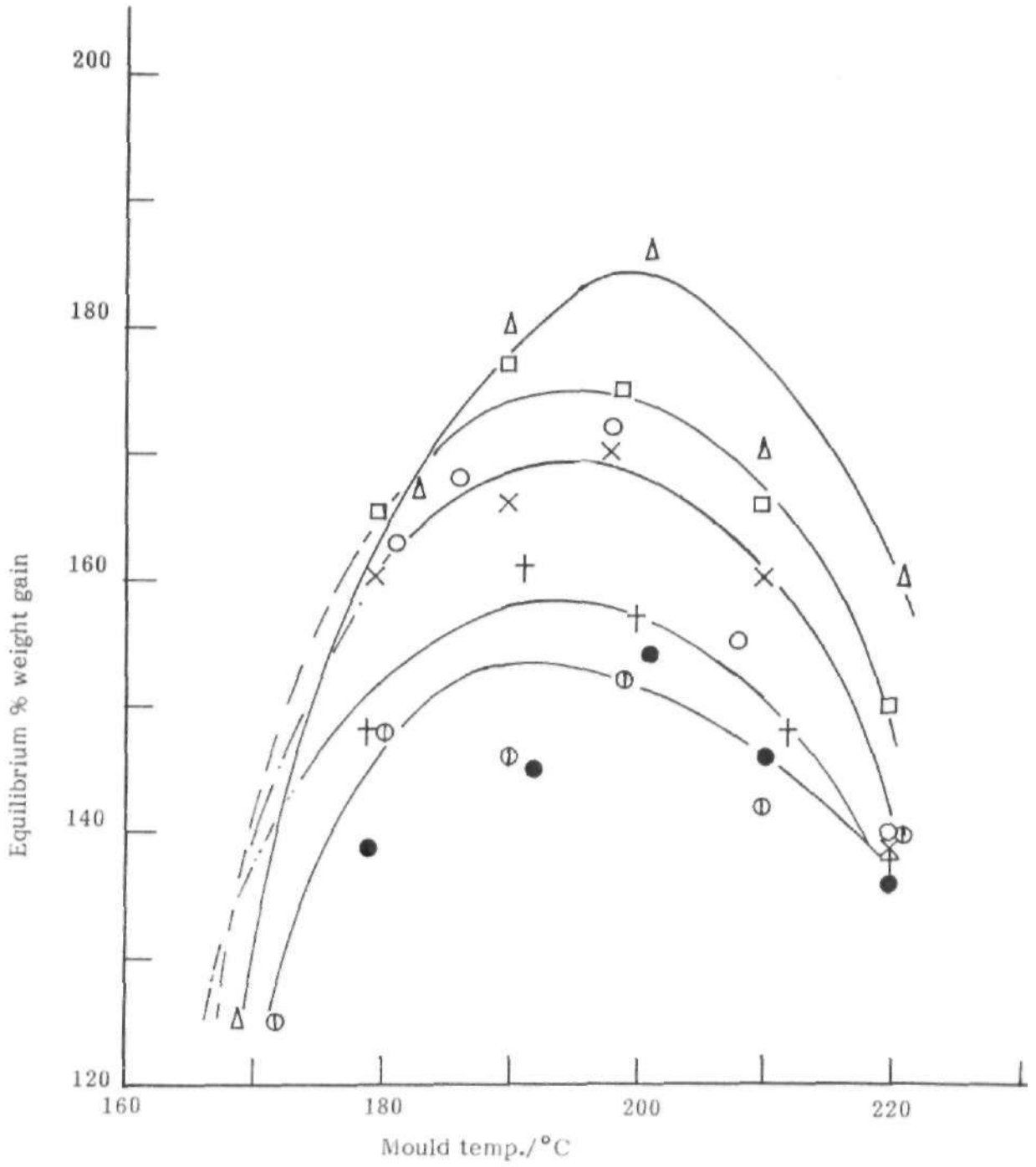


Fig. 4.6

Equilibrium % sorption curves for samples compression moulded over a range of temperatures: O, SO; □ , LO5; X, LO2; Δ, L10; †, L15; Φ , L30; ● , L45

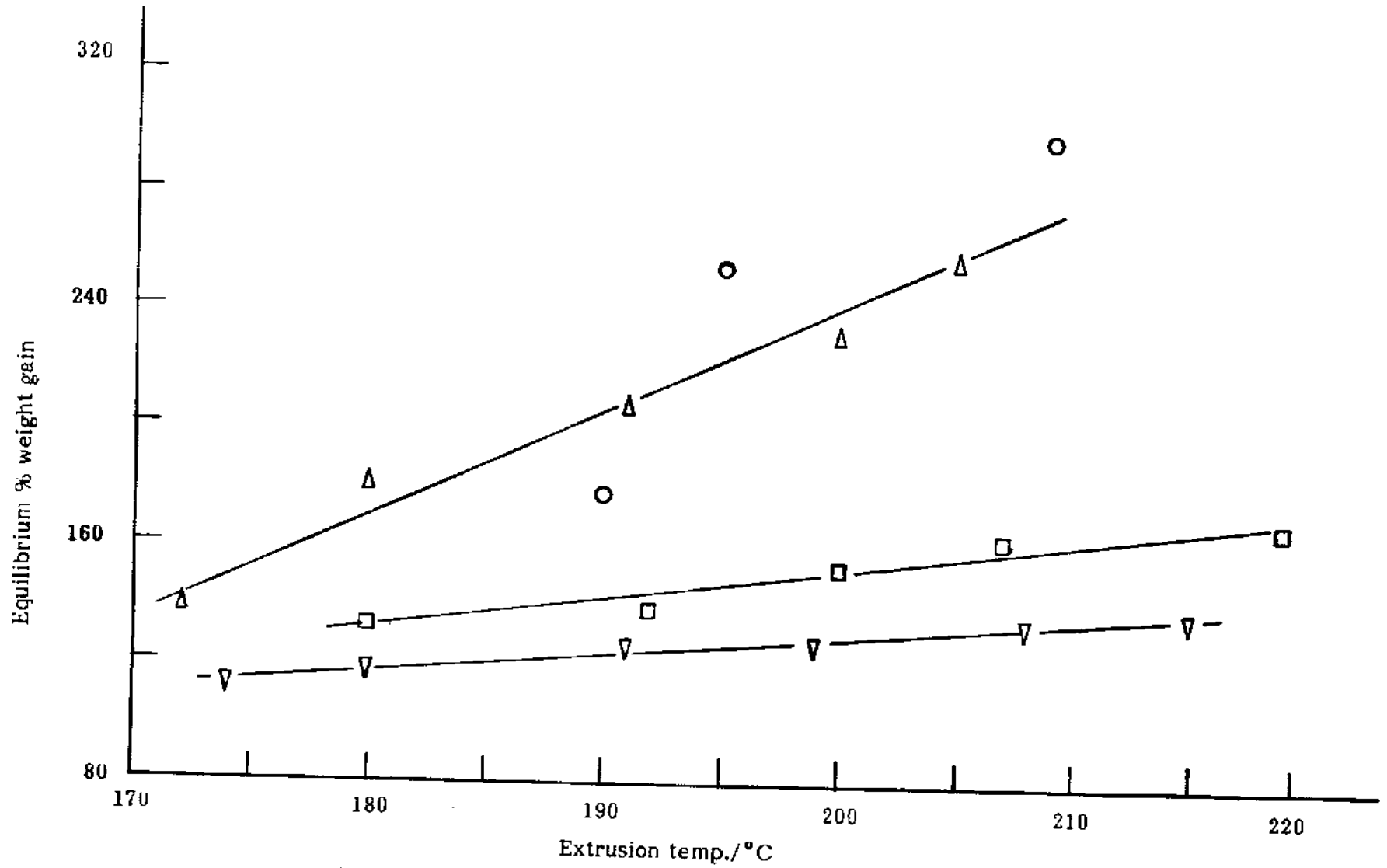


Fig. 4.7

Equilibrium % sorption curves for samples extruded on the **Krauss Maffei** at different temperatures: O, S57; Δ , S62; □ , S68; ∇ , S71

ES values are effectively linear with T_B and much lower slopes are observed than with the L-samples. On the basis of the inverse relationship between the ES value and the crystallinity index, it is shown that the crystallinity of the processed samples vary with molecular weight in the order S71 >S68 > S62 >S57. The decrease in slope compared with the L-samples implies a more gradual change of crystallinity with processing temperature with the Krauss Maffei. The gradual change is not unrelated to the lower shear levels at the processing conditions used as revealed in the theoretical treatment of section 3.6.

At equivalent molecular weights ES values are lower for the KM-samples than for the L-samples, suggesting that the former are more crystalline than the latter in agreement with lesser shear histories with the KM-samples.

It has been shown that true equilibrium was not achieved within the duration of the experiment (Figure 4.4). It is, however, obvious in Figure 4.2 that although absolute ES values may be higher at equilibrium the observed trend can hardly be expected to differ from that found at the experimental time limit. It is likely that differences between the maxima observed for changes in ES values with increased melt temperature in compression moulding and in extrusion are affected by deviations from equilibrium in addition to other effects. These limitations notwithstanding the crystallinity measured by density and by WAXD for the samples agree with observations made from comparative ES values.

4.2 Densities of Processed Samples

The densities of extrudates covering a range of processing temperatures are summarized in Tables 4.3 and 4.5 for the L- and

KM-samples respectively. The densities of samples extruded at constant temperatures over a range of extrusion rates using the Leistritz are included in Table 4.4. Experimental density values have been corrected for total additive concentration using eqn. 2.1 to obtain the values included in the tables.

The effects of processing temperatures are much more pronounced on the density than the effects of extrusion rate (Tables 4.3 and 4.4). The same effect was observed with g-level.

Extrudate density decreases with increased melt temperature reaching a minimum at 200°C which for the Leistritz samples corresponds to a die temperature of 213°C (see Table 3.1). Above 200°C the density increases (Tables 4.3 and 4.5 and Figure 4.8). An identical trend was observed for the diffusion coefficient, D. The results of sample densities confirm that the crystallinity decreases to a minimum value at a melt temperature of 200°C and increases thereafter.

At equivalent melt temperatures the KM-samples have higher densities than the L-samples. A similar result was obtained with ES values where it was shown that ES values are lower for the KM- than for the L-samples. The difference is illustrated in Figure 4.8 which compares the densities of samples A and B with those of sample S68. Higher crystallinities in KM- than in L-samples are implied as discussed previously. The difference can also be observed in Table 4.6 where the crystallinity index has been calculated from the density using eqn. 1.14.

In calculating the crystallinity index from the density, values[33,139] of 1.53 and 1.373 have been assumed corresponding to the densities of the 100% crystalline and the 100% amorphous PVC respectively. As shown by WAXD (section 4.3) it appears that either the

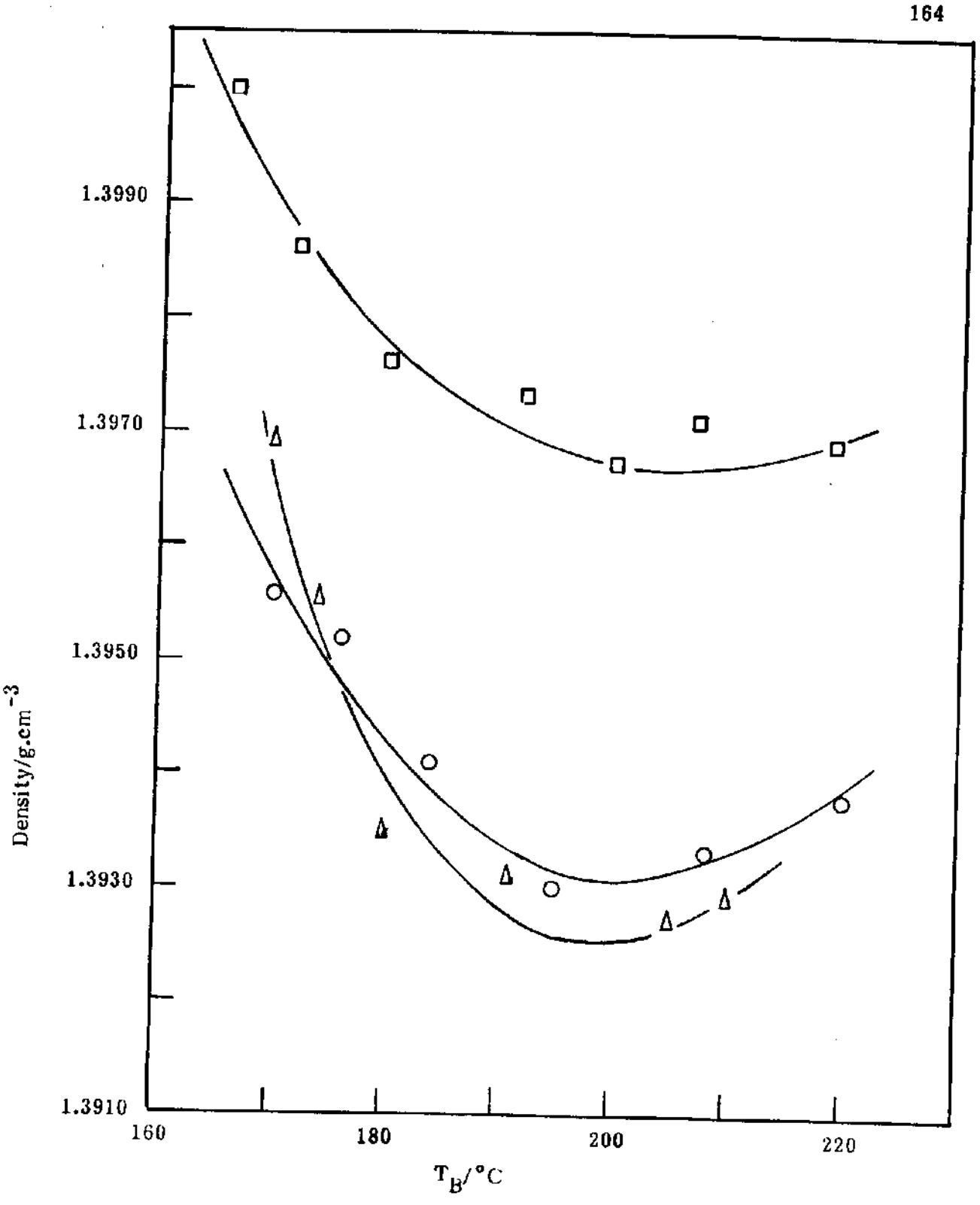


Fig. 4.8

Dependence of density on melt temperature in extrusion: □, S68; O, sample A; Δ, sample B

value 1.53 is lower than expected and/or the value 1.373 is higher than expected. For example when the value 1.70 is used for the 100% crystalline polymer (Tables 4.6(a) and (b)) the crystallinity index obtained agrees reasonably well with values obtained by WAXD.

A disparity in crystallinity indices calculated from densities and values obtained by x-ray analysis has been noted by Chartoff et al.[130] These authors also noted the uncertainties in literature values of densities of the perfectly crystalline and the completely amorphous PVC. Whichever value of ρ_c is chosen in Table 4.6 the results of density measurements agree perfectly well with those of solvent sorption.

Table 4.3

Densities of samples extruded at different temperatures using the Leistritz

(a) Sample A

Code	A1	A2-1	A3	A4	A5	A6	A7
T_B(°C)	170	176	184	195	200	208	220
Density (g/cm^3)	1.3958	1.3952	1.3941	1.3930	1.3917	1.3933	1.3938

(b) Sample B

Code	B1	B2-1	B3	B4	B5	B6	B7
T_B(°C)	170	174	180	191	198	205	210
Density (g/cm^3)	1.3969	1.3955	1.3935	1.3931	1.3914	1.3927	1.3929

Table 4.4

Densities of samples extruded at different speeds using the Leistritz

(a) Sample A

Code	Screw speed (rpm)	Extrusion temp.(°C)	Density (g/cm^2)
A1S	10	199	1.3954
A2S	15	198	1.3962
A3S	20	199	1.3904
A4S	25	201	1.3903
A5S	30	198	1.3906
A6S	35	198	1.3896
A7S	40	198	1.3896
A8S	50	200	1.3901

(b) Sample B

Code	Screw speed (rpm)	Extrusion temp.(°C)	Density (g/cm^2)
B1S	10	202	1.3965
B2S	15	200	1.3961
B3S	20	198	1.3906
B4S	25	201	1.3903
B5S	30	200	1.3903
B6S	35	198	1.3908
B7S	40	198	1.3911
B8S	50	199	1.3911

Table 4.5

Densities of samples extruded at different temperatures using the Krauss Maffei

(a) S57

Code	M11	M12	M13	M14	M15	M16	M17
T_B(°C)	151	161	172	181	190	195	209
Density (g/cm^3)	1.3999	1.3971	1.3959	1.3955	1.3953	1.3953	1.3964

(b) S62

Code	M21	M22	M23	M24	M25	M26	M27
T_B(°C)	151	162	172	180	191	200	205
Density (g/cm^3)	1.4000	1.3974	1.3969	1.3965	1.3965	1.3959	1.3952

(c) S68

Code	M31	M32	M33	M34	M35	M36	M37
T_B(°C)	167	174	180	191	199	208	215
Density (g/cm^3)	1.4000	1.3986	1.3976	1.3973	1.3967	1.3971	1.3969

(d) S71

Code	M41	M42	M43	M44	M45	M46	M47
T_B(°C)	166	172	180	192	200	207	219
Density (g/cm^3)	1.3975	1.3972	1.3961	1.3950	1.3950	1.3944	1.3965

Table 4.6

Crystallinity indices of processed samples calculated from sample densities

(a) Sample A

Code	A1	A2-1	A3	A4	A5	A6	A7
X_d (with ρ_c=1.53)	15.9	15.5	14.7	14.0	13.1	14.2	14.5
X_d (with ρ_c=1.70)	8.5	8.3	7.9	7.5	7.0	7.6	7.8

(b) Sample B

Code	B1	B2-1	B3	B4	B5	B6	B7
X_d (with ρ_c=1.53)	16.7	15.7	14.3	14.1	12.9	13.8	13.9
X_d (with ρ_c=1.70)	8.9	8.4	7.6	7.5	6.9	7.4	7.4

(c) S57

Code	M11	M12	M13	M14	M15	M16	M17
X_d (with ρ_c=1.53)	18.7	16.8	16.0	15.7	15.6	15.6	16.3

(d) S62

Code	M21	M22	M23	M24	M25	M26	M27
X_d (with ρ_c=1.53)	18.8	17.0	16.7	16.4	16.4	16.0	15.5

(e) S68

Code	M31	M32	M33	M34	M35	M36	M37
X_d (with ρ_c=1.53)	18.8	17.8	17.2	16.9	16.5	16.8	16.4

(f) S71

Code	M41	M42	M43	M44	M45	M46	M47
X_d (with ρ_c=1.53)	17.1	16.9	16.1	15.4	15.4	15.0	16.4

4.3 X-ray Analysis

Wide-angle x-ray diffraction traces have been obtained for the processed polymer as described in section 2.7. An illustration of a typical trace is provided in Figure 4.9 using as-polymerized powder of sample A. The double hump amorphous template[39,41,47,130] was fitted by drawing a smooth curve between 12° 2Θ and 21° 2Θ, and between 21° 2Θ and 28° 2Θ. This procedure is necessitated by the well recognized difficulty of obtaining an acceptable amorphous PVC trace.[39,47] For the same reason it was not possible to obtain an amorphous trace between 35° 2Θ and 46° 2Θ. A baseline was drawn between 12° 2Θ and 35° 2Θ and between 35° 2Θ and 46° 2Θ.

The diffraction pattern obtained as described above was analysed by the Hermans-Weidinger (H-W) method as described in section 1.5.1. Normalization was effected by dividing the crystalline and amorphous areas by the total area between 12° 2Θ and 46° 2Θ (Table 4.4A). Plot of normalized crystalline vs normalized amorphous area yields a straight line as expected from eqn. 1.9 (Figure 4.10). The regression line gives a value of C/A = 1.51 which is well within the usual range of 1.34, 1.65, and 1.10 found in the literature.[39,130] Using the regression line the corresponding values of ϕ_a are obtained from the experimental ϕ_c value and the crystalline fraction , X_r, is calculated using eqn. 1.10. The results are shown in Table 4.7.

4.3.1 Advantages of the H-W Method in X-ray Analysis of PVC

Values of the crystallinity index, X_r, obtained by the H-W method are compared to the corresponding values based simply on the relative

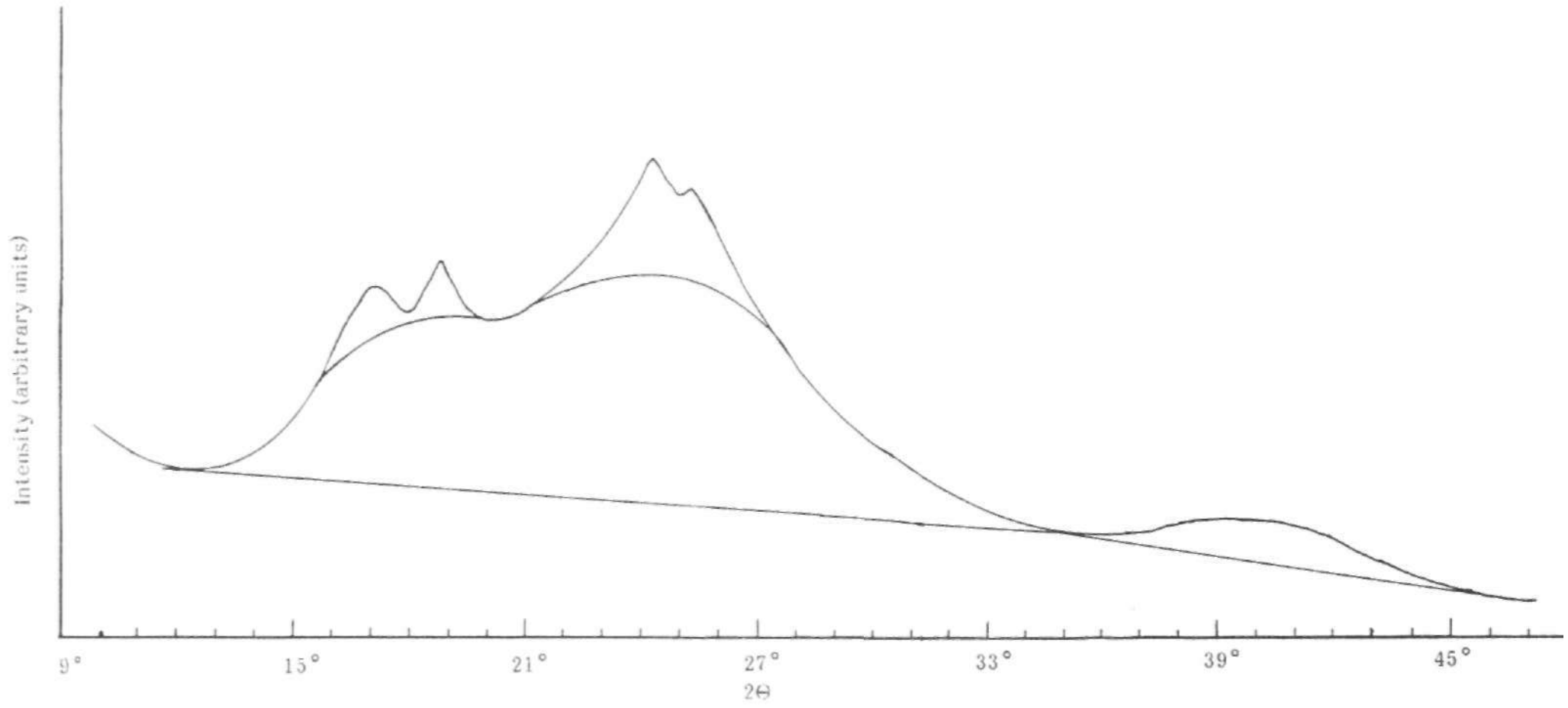


Fig. 4.9

A typical diffraction pattern of powder PVC sample with fitted amorphous template

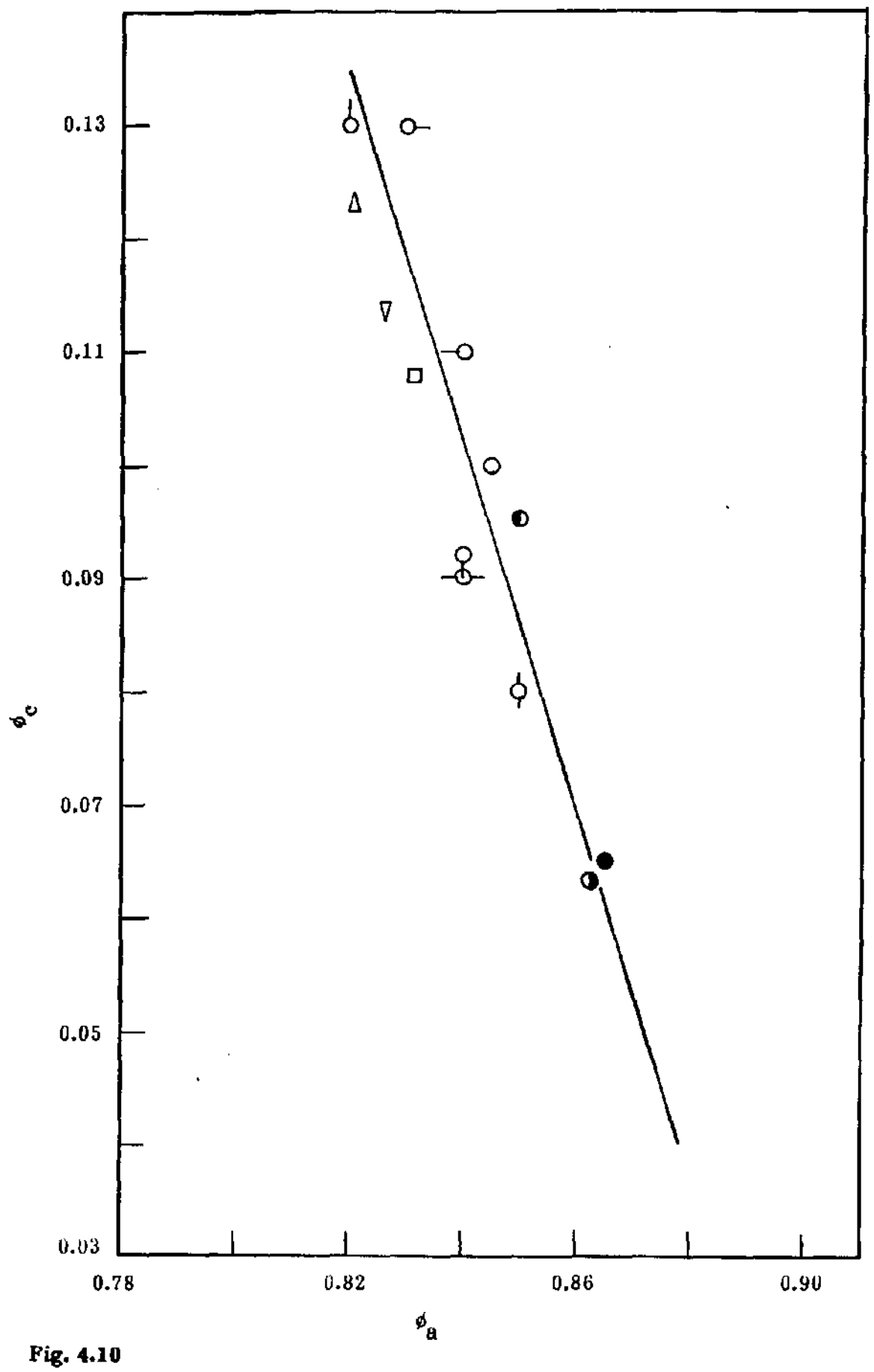


Fig. 4.10

Normalized values of crystalline vs amorphous areas taken from x-ray diffraction curves for some of the samples listed in Table 4.4A : O, P1M; —O, P2M; O–, P5M; O, SO1; Δ , SO2; ∇ , SO3; □ , SO4; Q, SO7, -O-, M11; Q, M12; ◑, M14; ◐, M21, ●, M25

fraction of the crystalline to the total area (eqn. 1.5) in Tables 4.7(b) and (d). It is noted that the H-W method has the advantage of yielding more accurate values of the crystallinity index than the simple division of the crystalline area by the total area. The former values are found, for instance, to be in better agreement with values obtained from thermal analysis than the latter.

For PVC there is the additional advantage of not requiring the true amorphous trace. It is observed that if the amorphous template is fitted as described above by consistently drawing smooth curves between the reflections known to be due only to the amorphous phase, a H-W plot of the results on samples covering a reasonable range of crystallinity would reveal where the crystalline or the amorphous area has been wrongly estimated. These errors are very readily detected since the points would deviate widely from the best-fit line. If the fitting of the amorphous template is carefully performed, very accurate results could be obtained for some samples on which the other samples can be based. Errors in estimates of the crystalline fraction can be easily corrected with reference to the original trace and/or by reference to the results of an independent test. It is not possible to detect these errors otherwise.

However, for the purpose of ranking the crystallinities of a series of samples it may suffice to use eqn. 1.5 but the values so obtained can be far removed from the true values as shown in Tables 4.7(b) and (d).

4.3.2 X-ray Crystallinity Index, X_r, of the Processed and Unprocessed PVC

(a) Unprocessed resin powder (Table 4.7(a))

Considering only the 'Corvic' samples (S57-S71), which belong to

the same grade of commercial resin, a slight increase in crystallinity is observed with increased molecular weight. The exception observed for sample S71 has been noted for all the properties studied. It is shown that the 'Breon' polymer S110/11 is slightly more crystalline than the 'Corvic' polymer of similar molecular weight. This, of course, is related to differences in polymerization. It was not intended in this study to compare the two grades of PVC resin.

It is shown that with the exception of the tin stabilized compression moulded formulations the unprocessed powder is more crystalline than the processed sample. The reason for this decrease in crystallinity has been discussed at length in Chapter 3 and in previous sections of this chapter.

(b) Extrudates (Tables 4.7(b), (c), and (e))

X-ray crystallinity index decreases with increased melt temperatures in exactly the same way as diffusion coefficient, D, and density. With the L-samples the minimum at $T_B = 200°C$ found in solvent test and in density is not obvious because of uncertainties in accurately fitting an amorphous template to the poorly defined diffraction pattern of samples processed above this melt temperature. However, with the KM-samples this minimum is observed. It occurs at a lower temperature with decreased molecular weight and shifts to higher temperatures as the molecular weight increases.

At equivalent melt temperatures the KM-samples are more crystalline than the L-samples. The point has been noted from the results of previous tests, but the difference is especially marked if the decrease in X_r is related to the value of the unprocessed powder. Again as shown in section 3.6, it is shown by these results that shear intensity was much

higher with the Leistritz than observed for the conditions used on the Krauss Maffei.

(c) CM-samples (Table 4.7(d))

Although it was not the intention to study the development of crystallinity with compression moulding conditions, it became pertinent to investigate the effect of compression moulding on crystallinity in order to establish the trend observed in sorption tests. Sample SO (Table 2.4) was chosen for this study. Results of WAXD on more highly lubricated sample LO5 show the same trend as found for SO. Discussion is, therefore, confined to the results from sample SO.

Crystallinity is found to decrease with increased melt temperature in exactly the same way as in extrusion. A minimum is observed for sample SO at 198°C which is close to the value 200°C obtained for the extrudate. It has been noted (Figure 4.6) that ES values are maximum in the region of 200°C for all moulded samples irrespective of lubricant level. The results of x-ray analysis provide further confirmation of the results of previous tests. In addition it is confirmed that the minimum crystallinity at 200°C T_B is independent of the processing technique and of the formulation.

It has been shown [79,80] that a tin stabilizer, being liquid, diffuses into the polymer during processing and increases the crystallinity as does a plasticizer. For this reason much higher crystallinities are found for the compression moulded samples than for the extrudates especially since shear is much less in compression moulding than in extrusion. For the same reason the KM-samples would be even more crystalline but for the effect of shear.

Table 4.7

The crystallinity index, X_r, measured by x-ray analysis of processed PVC samples

(a) Unprocessed powder

Code	S57	S62	S68	S71	S110
$\bar{M}_w .10^{-4}$	6.13	7.24	10.43	10.26	10.00
X_r	7.4	8.0	9.1	8.7	9.5

(b) Sample A (Leistritz, extrudate, less lubricated)

Code	A1	A2-1	A3	A4	A5	A6	A7
T_B(°C)	170	176	184	195	200	208	220
X_r (from eqn.1.5)	10.5	8.7	7.8	7.1	6.4	-	-
X_r (from eqn.1.10)	7.2	5.9	5.2	4.8	4.3	-	-

(c) Sample B (Leistritz, extrudate, more lubricated)

Code	B1	B2-1	B3	B4	B5	B6	B7
T_B(°C)	170	174	180	191	198	205	210
X_r	7.1	6.2	5.5	5.0	4.4	-	-

(d) SO (Compression moulded, unlubricated)

Code	SO1	SO2	SO3	SO4	SO5	SO6	SO7
T_B(°C)	161	171	182	186	198	208	220
X_r (from eqn.1.5)	13.5	12.8	12.1	11.5	9.3	10.4	10.2
X_r (from eqn.1.10)	9.5	9.0	8.3	7.9	6.6	7.2	7.0

(Table 4.7 cont'd)

(e) Krauss Maffei extrudates

				S57			
Code	M11	M12	M13	M14	M15	M16	M17
T_B(°C)	151	161	172	181	190	195	209
X_r	6.6	5.9	5.2	4.6	4.4	4.0	4.4
				S62			
Code	M21	M22	M23	M24	M25	M26	M27
T_B(°C)	151	162	172	180	191	200	205
X_r	6.9	6.1	5.5	5.5	4.8	4.4	5.1
				S68			
Code	M31	M32	M33	M34	M35	M36	M37
T_B(°C)	167	174	180	191	199	208	215
X_r	7.0	6.4	5.9	5.5	5.1	4.8	5.3
				S71			
Code	M41	M42	M43	M44	M45	M46	M47
T_B(°C)	166	172	180	192	200	207	219
X_r	6.7	6.0	5.6	5.2	4.8	4.9	5.1

4.3.3 The Minimum Crystallinity at 200°C Melt Temperature

Results of all the tests show that at 200°C melt temperature the processed sample has the lowest level of crystallinity. That is irrespective of processing technique and formulation, processed PVC is most amorphous at 200°C melt temperature.

Although changes in particle structure and in the flow units have been well recognized as discussed in Chapter 3, the characteristic amorphous content at 200°C has not been noted or reported in the

literature. It must be emphasized that the melt temperature, T_B, particularly in extrusion, is often a few degrees lower than the die temperature (see Tables 3.1 and 3.3). In our case the value corresponds to a die temperature of 213°C on the Leistritz and to a similar value on the Krauss Maffei.

It is well established that 200°C corresponds to the complete fusion of the granular structure. However, it has been shown[84] (section 3.6) that the grains are effectively preserved above 200°C in compression moulding. This 'preservation' does not rule out changes in the crystallinity within the primary particles with increased melt temperature. Indeed it has been shown[11,84] that primary particle fusion occurs within the grain even before the granular structure is fused. Therefore, it is not surprising that irrespective of the technique employed the characteristic structural change at 200°C also results in the highest amorphous fraction. An attempt is made below to account for this observation.

The increase in crystallinity above 200°C cannot be positively accounted for in this study without further evidence on molecular structure. An immediate reason, however, is that this increase results from degradation. Degradation can increase the crystallinity and/or affect the results of the tests as follows:

(1) Unstable structures in PVC[70] happen also to be those that cannot be incorporated into the syndiotactic crystal lattice, in particular chain ends and tertiary chlorine. Degradation starts from these structures and where they form the main amorphous phase (see Figures 1.3(a) and (b)) their loss will result in improved packing of the crystallites. No new crystallites are formed but improved overall perfection would result. If the gaseous products of degradation are able to diffuse out without leaving

'holes', a decrease in solvent sorption, in density, and in x-ray diffraction intensity would result as observed.

(2) It is known that degradation results in conjugated double bond formation. This structure is a more dense atomic packing than the C-C single bond of the undegraded polymer chain. The packing also offers greater average electron density along the chain while increasing the apparent periodicity of these atoms. For purely structural reasons increased conjugated double bond formation would lead to reduced sorption, and increased density, and probably increased x-ray diffraction intensity even when crystallite perfection is largely unaffected.

Despite the above suggestions it is noted that the increase in crystallinity above 200°C may not be connected entirely with degradation. The possibility of other factors cannot be ruled out. For example in studies on the crystallization of PVC at high temperatures, Michel and Guyot[202] found little change in infrared spectra of well stabilized samples up to 240°C. The x-ray patterns, however, show an increase in the size of the crystallites but not in the amount of the crystalline fraction. These authors first suggested 260°C for the melting temperature of the perfectly crystalline material latter confirmed by Gouinlock.[193] The results here may once again confirm another of their observations.

Increase in crystallite size and/or perfection would produce the same results as observed in the three tests even in the absence of degradation. This increase is observed above 200°C because it is only above this temperature that primary particles become the predominant flow units in the melt.[181] And since these particles are essentially aggregates of crystalline microdomains,[28] it can be expected that annealing effects[50,114] become more pronounced when they form the flow units.

It is possible that in practice the increase results from a combination of the above effects.

4.4 A Comparison of the Crystallinity Index Measured by Different Methods

4.4.1 Values of X_r for the Unprocessed Powder and Q_r for the Most Fused Processed Sample

In Chapter 3, sections 3.3 and 3.6, it was shown that the crystallinity increased with increased melt temperature, while in this chapter the tests show that the reverse is the case, and a minimum crystallinity is observed with increased melt temperature.

It was shown in section 3.6 that thermal analysis' A-endotherm measures the secondary crystallinity which results from melt recrystallization of the primary crystallinity during processing. This explanation was first rendered by Gilbert and Vyvoda[114] as has been noted. The primary crystallinity fraction remaining after melt recrystallization is measured by the B-endotherm (Figure 1.9) and the area of this endotherm is found to be inversely related to that of the A-endotherm. The relationship is, however, not exactly proportional.

Thus thermal analysis clearly reveals that at a given melt temperature an inverse relationship exists between the weight fractions of the primary and secondary crystallites. It is recognized[47] that the secondary crystallinity is not detectable by wide-angle x-ray diffraction, the technique is, however, sensitive to the primary crystallinity because of the latter's higher level of perfection. Hence, with increased melt temperature an increase in the level of crystallinity can be observed for methods that show specific response to the secondary crystallinity (such as

TA); while for the same samples a decrease will be found if the method responds specifically to the primary crystallinity (such as WAXD). If the method is sensitive to both types of crystallinity (such as solvent sorption and density) any trend can be observed depending on the relative contributions of the two types of crystallinity to the total crystallinity of the sample.

It follows from the above that if some different ordering processes are not involved, and if the crystallinity of the sample changes solely by the conversion of melted primary crystallites to secondary crystallites during processing, then the value of the crystallinity index obtained in thermal analysis, Q_r, corresponding to the completely fused state, should be equal to the x-ray crystallinity index, X_r, of the unprocessed sample. Values of Q_r and X_r are shown in Table 4.8, this table also includes values of $\Delta H(T)/\ \Delta H_u$ from TA for comparison with X_r.

A noticeable difference exists between Q_r at the limits of processing temperatures and X_r for the unprocessed powder (Table 4.8). The values of Q_r are generally lower than those of corresponding X_r. The difference reflects the difficulty of processing PVC to a state where all the primary crystallinity is converted to secondary crystallinity without an unacceptable level of degradation.

Within the limits of experimental error the difference, X_r-Q_r, increases with increasing molecular weight. This difference is highest for sample S71 indicating that this sample has the highest molecular weight as previously noted for all properties.

If fusion is defined in the thermodynamic sense, that is the melting of crystalline structure, then the greater the difference X_r-Q_r the lower the fusion level at the limits of processing temperature and also at

any processing temperature. Thus from Table 4.8 the maximum level of fusion reached by the samples decreased as

$$S71 < S110 < S68 < S62 < S57$$

These results are in perfect agreement with theory and with the previous observation (section 3.3) that at any processing temperature, the lower the molecular weight the higher the degree of fusion. Also it is clearly shown that at a specific processing temperature sample S71 is the least fused of all the samples studied. This latter observation explains the differences observed with this sample throughout the study.

As noted previously (section 3.6) crystallinity index based on the Q_r value (eqn. 3.18) is more representative of the true value than one based simply on the ratio of the heats of fusion (eqn. 1.29). The respective values can be compared in Table 4.8 to the value X_r obtained by WAXD.

Table 4.8

Values of the crystallinity index of the unprocessed polymer measured by thermal analysis and by x-ray diffraction

Sample	S57	S62	S68	S71	S110
$\Delta H(T)/\ \Delta H_u$	11.5	11.6	11.5	10.6	12.4
Q_r	6.7	7.2	7.4	6.8	7.7
X_r	7.4	8.0	9.1	8.7	9.5
$(X_r - Q_r)$	0.7	0.8	1.7	1.9	1.8

4.4.2 Effects of Processing Temperature

The inverse relationship between the primary and the secondary crystallinity and the specific response shown by WAXD and by TA to the

two types of crystallinity respectively imply that over a range of melt temperatures the sum $Q_r + X_r$ should be constant if changes in crystallinity result solely from the depletion of primary crystallinity and the generation of secondary crystallinity.

Within the limits of experimental error $Q_r + X_r$ is largely constant below a melt temperature of 190°C (Table 4.9), above this temperature a substantial increase is observed. This implies that above 190°C changes in crystallinity do not arise solely from the conversion of primary to secondary crystallinity. The same conclusion had been made previously where it was shown that the minimum crystallinity at 200°C results from a reordering process which involves enhanced annealing of the primary crystallinity when these are freed into the melt as a result of fusion of the granular structure. If significant shear occurs during processing the increase due to reordering may not be detectable by WAXD, this is evident in Table 4.9 and was noted previously. If, however, the shear level is moderate, as observed, for the KM samples in Table 4.9 the increase due to reordering is easily observed by WAXD where the minimum at 200°C is also made evident.

The crystallinity index calculated from the density, X_d, contains the contributions of both the primary and the secondary crystallinities to the total. Therefore, in the absence of a reordering process X_d should be constant over a range of melt temperatures. The minimum observed in X_d and in the diffusion coefficient, D, are thus reflective of the reordering process as noted before. It is observed that the changes in density are actually so small as to make them undetectable by a method less sensitive than the density gradient column.

Table 4.9

Effect of processing temperature on the crystallinity index measured by thermal analysis, x-ray diffraction, and density

(a) Sample A

Code	A1	A2-1	A3	A4	A5	A6	A7
T_B(°C)	170	176	184	195	200	208	220
Q_r	0.3	0.9	2.7	5.2	6.4	7.6	7.7
X_r	7.2	5.9	5.2	4.8	4.3	-	-
(Q_r+X_r)	7.5	6.8	7.9	10.0	10.7	(7.6)	(7.7)
$X_d(\rho_c=1.70)$	8.5	8.3	7.9	7.5	7.0	7.6	7.8

(b) S68

Code	M31	M32	M33	M34	M35	M36	M37
T_B(°C)	167	174	180	191	199	208	215
Q_r	0.7	0.8	1.7	3.6	5.3	6.0	7.4
X_r	7.0	6.4	5.9	5.5	5.1	4.8	5.3
(Q_r+X_r)	7.7	7.2	7.6	9.1	10.4	10.8	12.7
$X_d(\rho_c=1.70)$	10.0	9.5	9.2	9.0	8.8	9.0	9.0

Finally, it should be noted that the discussions have not considered the effects of additives such as liquid stabilizers and plasticizers, known to influence the crystallinity, on the changes in the crystallinity index with increased melt temperature. In practice it may be difficult to show whether such effects are restricted to the primary or the secondary crystallinity or to both types of crystallinity.

4.5 Conclusions

Based on the kinetics of acetone absorption at 23°C it has been shown that a processed PVC sample is least crystalline at 200°C which in our case corresponds to a die temperature of 210°C in extrusion. The minimum crystallinity or maximum amorphous fraction is shown to be independent of the processing technique and of formulation, being substantially the same for samples processed on different extruders and compression moulded with a wide range of lubricant concentrations. It is suggested that 200°C is a characteristic melt temperature, not only where the primary particles become the flow units as is well known, but also where the processed sample is most amorphous as revealed in this study.

The results were confirmed by values of the crystallinity index of the processed samples calculated from the density and measured by wide-angle x-ray diffraction.

In agreement with previous suggestions, it is demonstrated the thermal analysis measures the secondary crystallinity level of the processed sample, and it is also shown that WAXD measures the primary crystallinity level. Both solvent sorption and density respond to the total (i.e. primary and secondary) crystallinity level. These results are expected from theoretical considerations but now a quantitative proof is given using commercial PVC samples processed over a wide range of temperatures which includes the commercial temperature range.

Using the differences between the respective values of the crystallinity index measured by WAXD and that measured by TA, it is shown, in agreement with expectation, that at a specific melt temperature the level of fusion measured by the amorphous weight fraction decreases with increased molecular weight. A sample shown by GPC measurement to

be of a lower molecular weight is shown not only to have the highest molecular weight of the range studied but also to be least fused at a specific melt temperature. The same conclusion can be made from the results of thermal analysis, but here quantitative values are obtained for the differences.

The above conclusions are particularly relevant to the mechanical properties of the processed sample as discussed in the next chapter.

Chapter 5

RESULTS AND DISCUSSION

III. IMPACT PERFORMANCE OF PROCESSED PVC

Extrudates were tested for impact strength using an instrumented tester, the Ceast AFS/MK2 Fractoscope, as described in section 2.8. The results are included in Figures 5.4 and 5.5 and in Tables 5.1 and 5.2. Impact strength (IS) values represent the averages of five tests, and error bars in Figure 5.4 represent deviations from the mean value in relation to the processing history.

5.1 Variation of the Force-displacement Trace with Fracture Toughness

The toughness of a given material is a measure of the energy absorbed before and during the fracture process (section 1.6). The area under the stress-strain curve provides a measure of this energy.

The increase in area with increased toughness is shown by the Ceast force-displacement curves in Figure 5.1. In a typically brittle fracture, where the plastic zone at the crack tip is small just before failure, the overall toughness level of the sample is low, and a single peak is often observed in the force-displacement plot (Figure 5.1(a)). As the sample toughness increases with increased melt temperature, the number of peaks, and, therefore, the area under the curve also increases (Figures 5.1(b) and (c)).

A typical example of a ductile failure trace is provided by Figure 5.1(c) using sample A4 which corresponds to the maximum IS for the

samples used in this study. Three peaks are observed, and in some cases the number can even be higher.

It appears that the first peak is a measure of the impulse at impact of the hammer with the sample. For notched specimens (as used in this study) the impulse leads immediately to the development of a zone of plastically deformed material resulting from stress concentration at the crack tip. If this zone is not well developed, the sample yields and fractures almost simultaneously, and only a single peak is recorded. If, however, the plastic zone is sufficiently developed, the plane stress condition at the crack tip will elevate the applied stress above the level necessary for irreversible plastic deformation,[203-205] and more than one peak will be observed in the force-displacement trace. The number of subsequent peaks after the first would depend on the volume of the crack tip plastic zone, and, therefore, on the ductility as well as toughness of the sample.

It must, however, be noted that a brittle fracture can also produce more than one peak if the yield stress is sufficient to resist the impulse at impact. This effect was observed for most of the low melt temperature Leistritz samples, for which two peaks could often be found though the impact energy was generally lower than at higher melt temperature.

A difference in the pattern of the force-displacement plot may be observed with the Ceast as shown in Figure 5.1(d). This figure corresponds to that which was reported previously.[180] It differs in shape from the other figures in having peaks which appear to be cumulatively superposed. No immediate explanation can be given at present for this difference without better knowledge of the electronics of the equipment. Repeated

measurements showed that the difference in shape did not affect the absolute values of the impact energy measured. It was observed that minor variations in the mode of calibration and/or equipment set up could produce quite a wide range of effects on the results obtained from the Ceast Fractoscope.

5.2 Fracture Surface Macromorphology

Scanning electron micrographs of fracture surfaces of impact test specimens are shown in Figures 5.2 and 5.3 for sample A and sample S68 respectively.

A clear difference exists between the fracture surfaces of the sample formulated with lead stabilizer (sample A) and that formulated with tin stabilizer (sample S68). In the former, morphological units, on the order of the primary particles, are observed at melt temperatures in the region of 180°C (Figure 5.2). These units become less distinct with increased temperature. At 200°C a homogeneous surface, devoid of morphological features, is observed. No morphological units are observed with sample S68 even at the lowest melt temperature (Figure 5.3).

The micrographs are in general made up of two distinguishable regions: the dark regions comprising craze patches and bright regions forming the walls of these patches from which elongated fibrils of craze matter can be seen extending in the direction of crack propagation. In both samples A and S68 the micrograpahs indicate increased craze-initiated failure mode with increased fusion level. With sample A, this failure mode is only made distinct with the disappearance of particulate structure at 200°C. With sample S68 however, where no particulate structure is discernible, the boundary between craze patches becomes sharper with

increased melt temperature. The craze patches also show a tendency towards greater elongation at higher melt temperature. Elongated craze patches have been associated with the failure mode of amorphous polymers.[203-205]

5.3 Effects of Material and Processing Variables on Impact Strength

5.3.1 Effect of Formulation

Increased lubricant concentration results in low impact strength at a specific melt temperature, this is illustrated for samples A and B in Figure 5.4 and Table 5.1. The same observation has been made by Gale.[206]

It is established that an external lubricant delays fusion,[79,206] hence with increased lubricant concentration inter-particle network formation is reduced and particle-matrix failure enhanced. For notched test pieces (as used here) the plastic zone around the crack tip is less developed and failure is generally more brittle at equivalent processing temperatures than observed for samples with lower lubricant concentration.

5.3.2 Effect of Extrusion Rate

For the formulations used in this study, extrusion rate makes only marginal contribution to the impact strength, and this contribution, in general, becomes more pronounced at high (shear) rates (Table 5.1).

It is observed that despite excellent screw geometry (see Figure 2.2) and control devices on the Leistritz, it was difficult to obtain constant melt temperature with increased screw speed. Although profile

temperatures (Table 2.6) were strictly controlled differences can still be observed in the melt temperature at high speeds (Table 5.1). This effect obviously masks individual contributions of shear and temperature to measured impact strength. It is found that melt temperatures are generally more constant with increased screw speed for the more lubricated sample B as would normally be expected. Therefore, from the results of sample B at T_B values of 180° and 190°C it can be concluded that temperature has greater influence on IS than extrusion rate. The same effect was found with g-level in Chapter 3.

However, as noted in section 3.1.1.2, there is a clear indication that changes in the power input during extrusion are reflected in the IS value of the extrudate. Underlined values for samples A and B in the respective second periods of Table 5.1 can be compared to changes in slope of power vs. screw speed in Figure 3.2. It is found that the IS values at the speeds where changes in slope occurred correspond to higher values, and in some cases these values are highest for the series. No explanation can be offered for this observation at present.

5.3.3 Effect of Extrusion Temperature

A maximum IS value can be observed with increased melt temperature as illustrated for sample A in Figure 5.4. It appears, however, that the maximum value may not be obvious if the shear is below some minimum value during processing; particularly in the region 185-195°C where the maximum IS value often occurs. Absence of a clear maximum is indicated by sample B in Figure 5.4, and in general by the KM samples.

As noted in section 1.6, several authors have studied the impact behaviour of processed UPVC. A maximum value with increased melt

temperature has been widely reported, notably by Benjamin,[105,159] Bystedt,[158] Terselius,[160,161] and Menges and Berndsten.[179]

Terselius[161] has performed an extensive study of the mechanical properties of UPVC. His work includes tensile tests, and different modes of impact testing, over a range of test temperatures. He found that the response of different impact tests to variations in the g-level varies considerably and demonstrated that falling weight tests (FWIS) at 50% failure and 0°C is the most sensitive. Long-term embrittlement was shown to be caused by formation of creep cracks, and creep crack tendency shifted to longer times with increased g-level.

Using tensile tests Terselius[161] further showed that elongation at break decreased at higher g-levels at a test temperature of 60°C. A transition from ductile to a 'creep crack' mode of failure was observed which also shifted to 'longer times to break' at higher g-levels. This behaviour was explained on the basis of increased disentanglement resistance due to increased number of entanglement couplings and crystalline junctions at higher g-levels. Based on his results this author proposed tensile testing at 100°C as a potential measure of g-level. FWIS of both 'polished' and 'unpolished' samples was shown to pass through a maximum at a melt temperature of 190°C. It was concluded that significant changes occur at moderate g-levels which are responsible for a marked increase in notched impact strength (NIS). It was suggested that the dominating changes in morphology are the build up of interparticle coherent entanglement network.

A brief review of Terselius' works was considered necessary because of the similarity between his findings and those of the present study, and the relevance of his conclusions to the observations made here.

For example, a clear maximum NIS value is shown for sample A in Figure 5.4, and the same is largely true for all the extrudates. Coherent aggregates are clearly evident in Figures 5.2(a) and (b) which correspond to the maximum IS values shown in Figure 5.4.

5.3.4 Effect of Molecular Weight

The KM-samples have much lower IS values than the L-samples, comparable values of the former being only about half of the latter. A number of reasons can be put forward for this difference.

It has been shown (section 3.6.3, Table 3.7) that shear level was lower at the extrusion conditions used on the Krauss Maffei than those used on the Leistritz. The lower shear values are considered to arise from low die back pressures in addition to other factors related to machine variables. Although, in principle, die back pressure is not expected to have much influence on shear in twin-screw extrusion, this is not exactly the case in practice; and Gale[206] has shown that die back pressure affects the melting rate.

It was shown in Chapter 4 (see Table 4.8) that with respect to primary crystallinity melting (i.e. thermodynamic fusion) the KM samples are more fused than the L-samples even at equivalent molecular weights, disregarding sample S71. As noted earlier in this chapter, SEM micrographs of fracture surfaces of the KM-samples do not show evidence of particulate structures even at quite low melt temperatures; these micrographs also show evidence of more brittle failure, indicated by relative smoothness of the fracture surfaces.

As noted in section 1.2.1 and in Chapter 4, tin stabilizers have been found to diffuse into the resin particles and increase both fusion

rate[79] and the crystallinity of the extrudate.[24,40,79,80] Thus the results obtained in this study are in excellent agreement with established mode of action of tin stabilizers (and, maybe, of liquid stabilizers in general). Increased crystallinity has the effect of raising the modulus, thereby lowering the ductility.[79,80] It is obvious, therefore, that reduced IS values for the KM-samples can be related to a combination of all of the above factors.

At equivalent processing temperatures IS increases only slightly with increased molecular weight. However, questions can be raised about the reliability of the absolute IS values obtained from the Krauss Maffei extrudates for reasons related to non-optimum shear conditions. So there is need for caution in drawing conclusions based on these samples.

5.4 Dependence of Failure Mechanism on Fusion

In the preceding sections the measured IS values and SEM fracture surface micrographs were discussed in the light of the existence or otherwise of morphological units, the volume of craze matter (indicated by dark regions) and brittle/ductile failure indicated by the smoothness or roughness of the fracture surface. In this section an attempt is made to account for these effects in relation to the melting of the morphological units.

5.4.1 Formulation with Solid Additives

Comparison of Figures 5.2(a), (b), and (c) with respective IS values at the same melt temperatures (T_B values) in Figure 5.4 shows that existence of particulate structure at the primary particle level, which

includes coherent aggregates of these particles, is necessary for high IS value. It is relevant to restate previous observations to facilitate comparison with the literature.

At melt temperatures below 200°C there is increased fusion of the primary particles with increased melt temperature; although evidence of primary particles can still be found at 195°C (Figure 5.2(b)) the size cannot be readily quantified. At this level of fusion the fracture surface shows no clear dark or bright zones. Both Figures 5.2(a) and (b), i.e. where the primary particles or their (coherent) aggregates still exist in the melt, correspond to structural states which give rise to the highest impact resistance with increased melt temperature, and, therefore, g-level.

It should be recalled that a melt temperature of 200°C was shown in Chapter 4 to correspond to the maximum amorphous state of the melt. Figure 5.2(c) is a micrograph of the fracture surface for the sample processed at 200°C melt temperature (T_B value). In excellent agreement with the previous observation a 'homogeneous' bed of material is shown with no evidence of particulate structures. The impact resistance of the sample (Figure 5.4) drops with the disappearance of the primary particles and their aggregates.

The above observations are in very good agreement with the literature. As noted previously, Terselius[161] suggests the existence of 'interparticular coherent entanglement network' as giving rise to the maximum IS value. These terms aptly describe the structures shown in Figures 5.2(a) and (b); the melt temperatures (T_B values) of 184°C and 195°C respectively give rise to a maximum IS value at precisely 190°C as found by Terselius.

Menges and Berndsten[179] found that 'only' the material in which the impact modifier surrounded 'globules' proved to have the highest impact strength. At higher melt temperatures where the globular structure is lost IS value was found to drop. This observation is well illustrated by relating the micrographs of Figure 5.2 to the respective IS values in Figure 5.4.

From the above a picture of the failure mechanism can be built up based on the structure which corresponds to the highest IS value.

Available evidence[11,84] shows that intragranular fusion of primary particles begins at the lowest melt temperatures, and Summer's fusion model,[28] illustrated in Figure 1.7, indicates that limited intergranular fusion occurs at ca. 160°C. Allsopp's model[107] does suggest that grain memory can be preserved in the melt up to the critical temperature region where a change in the flow unit is observed.

It is not unreasonable to consider the grain as an elastic body at its static equilibrium. Fusion of the primary particles within this body causes extensive internal stress, and even in the absence of external shear, if intergranular boundaries are not well lubricated, deformation of the grain structure to relieve this stress would result in boundary coalescence. This would result in increased intergranular fusion. Similarly a modulus of elasticity can be considered for the grain structure, it will have an average value characteristic of the average size of the grain. And it is not unlikely that the critical temperature marking the change in flow units is actually one where the internal stress field is such that the average value of the modulus has been exceeded and the grain is deformed irreversibly. The deformation can be described by the classical theories of viscoelasticity; persistence of grain boundaries in the melt up to the stage where they

disappear completely can be well accounted for by viscoelastic models. Once grain coalescence occurs, intergranular fusion can begin.

The processed sample will have an optimum deformation resistance once a minimum level of intergranular fusion (entanglement network[161]) is achieved. Further increase in fusion will make only small contributions to the elastic properties of the processed material but will affect the post yield deformation due to increased resistance to disentanglement as proposed by Terselius.[161]

From the above two main reasons can be given for the role of particulate structures in impact resistance. The first is the well known effect of 'blunting' of an advancing crack tip by increased radius and subsequent reduction in stress concentration. If the particulate structure is sufficiently coherent (i.e. where there exists sufficient entanglement network between the particles), particle surface not only reduces the stress concentration, the impact energy is also dissipated in elastic deformation. Where failure occurs the failure mode is more ductile. For the same reasons coherent particulate structures also suppress craze initiation and microvoid nucleation.

The second role of particulate structure in impact resistance is related to additive distribution. Well dispersed additives can be accommodated in the interstices between adjacent particles (recall the distribution of impact modifiers between globular structures shown by Menges and Berndsten[179]). Distribution of additive particles in gaps between resin particles, or aggregates strongly linked together by entanglement networks, results in the suppression of 'additive-aided' craze initiation and microvoid formation. Reference to Figure 5.2 shows that additives become more evident (as white spots) with the disappearance of

the primary particles, indicating that they are now 'released' into the melt pool (loss of the globules[179]).

In the absence of particulate structures there is freer crack propagation and additive-matrix interface serves as craze initiation and microvoid nucleation sites. A lowering of impact resistance is observed. The situation is worsened by increased crystallinity at higher melt temperatures above 200°C (see Chapter 4) as a result of increased embrittlement at higher crystallinity.[79,80]

These effects account for the maximum or a levelling-off of IS values with increased melt temperature widely reported in the literature.

5.4.2 Formulation with Liquid Additives

It is obvious from the above what the effect of a liquid, miscible with the resin, would have on the rate of fusion and the impact strength of the processed sample.

Wetting of particle surface results in substantial reduction in the modulus of the grain structure, and simultaneous intra- and intergranular fusion obtains at the least melt temperature. The same effect leads to loss of primary particle boundaries and a superficial continuous melt is observed at the onset of fusion. These effects are well illustrated in Figure 5.3 where no evidence of particle boundaries is apparent at the lowest melt temperature.

Loss of particle boundaries is literally superficial fusion since capillary rheometry and thermal analysis show clearly that the characteristic structural change still occurs at the well known temperature region. This indicates that the modulus of the grain structure is not a property of the peripheral skin but of the network structure of the

composite primary particles. Thus despite absence of particle boundaries, memory of the grain structure is retained in the melt up to the critical temperature where the modulus of this structure is exceeded and irreversible deformation results in loss of structure memory. Exactly the same situation exists for the loss of the primary particle structure.

Although compatible - liquid - induced fusion is only superficial the loss of particle boundaries causes a dramatic loss of impact resistance due to free crack propagation, and increased craze initiation and void nucleation as discussed above. The material fails by a more brittle mode, embrittlement being enhanced by increased crystallinity.

Increased craze initiation is well illustrated by the existence of elongated fibrils from walls of craze patches at much lower temperatures in Figures 5.3(a) and (b). The reduction in fibrils at higher melt temperatures illustrated in Figure 5.3(c) is an indication of increased amorphous fraction (i.e. increased gelation). This is supported by the parabolic dimples formed by microvoid coalescence characteristic of failure modes of amorphous polymers.[203-205]

An attempt is made in Table 5.2 to compare IS values with 'fusion levels' measured by thermal analysis and by WAXD crystallinity indices. If IS values are plotted against TA crystallinity indices (TA fusion levels) curves similar to Figures 5.4 and 5.5 are obtained as would be expected.

5.5 Conclusions

It has been shown that particulate stretture in processed PVC is a prerequisite for high impact performance. The round outlines suppress craze initiation and microvoid nucleation by increasing the crack tip radius and reducing stress concentration through an established mechanism.

Formulation with liquid additives leads to loss of particle boundaries at the onset of fusion. In the absence of particulate structures, craze initiation and microvoid formation are accelerated. These effects result in relative embrittlement ('creep crack' failure[161]) even at higher g-levels, especially where there is an increase in the crystallinity of the sample, and impact resistance is drastically reduced.

In the absence of a liquid additive the particulate structure is preserved up to a melt temperature below 200°C. If the solid additives are well dispersed, they can be accommodated in interstices between neighbouring particles. Craze initiation and void nucleation are suppressed, propagating cracks terminate at particle boundaries and impact energy is dissipated by resistance to disentanglement of the interparticle networks.

Maximum impact strength was observed in the region 185-195°C, i.e. just before the loss of particulate structures. A levelling-off can be observed if particle memory is preserved, particularly where the shear level is below a minimum level for obliterating the memory. The maximum value corresponds precisely to a melt temperature where there is sufficient entanglement network between coherent particulate structures. These structure can be (unfused) individual primary particles or their aggregates.

These results confirm observations made in the literature and provide some proof for features that have long been recognized in the technology of PVC processing.

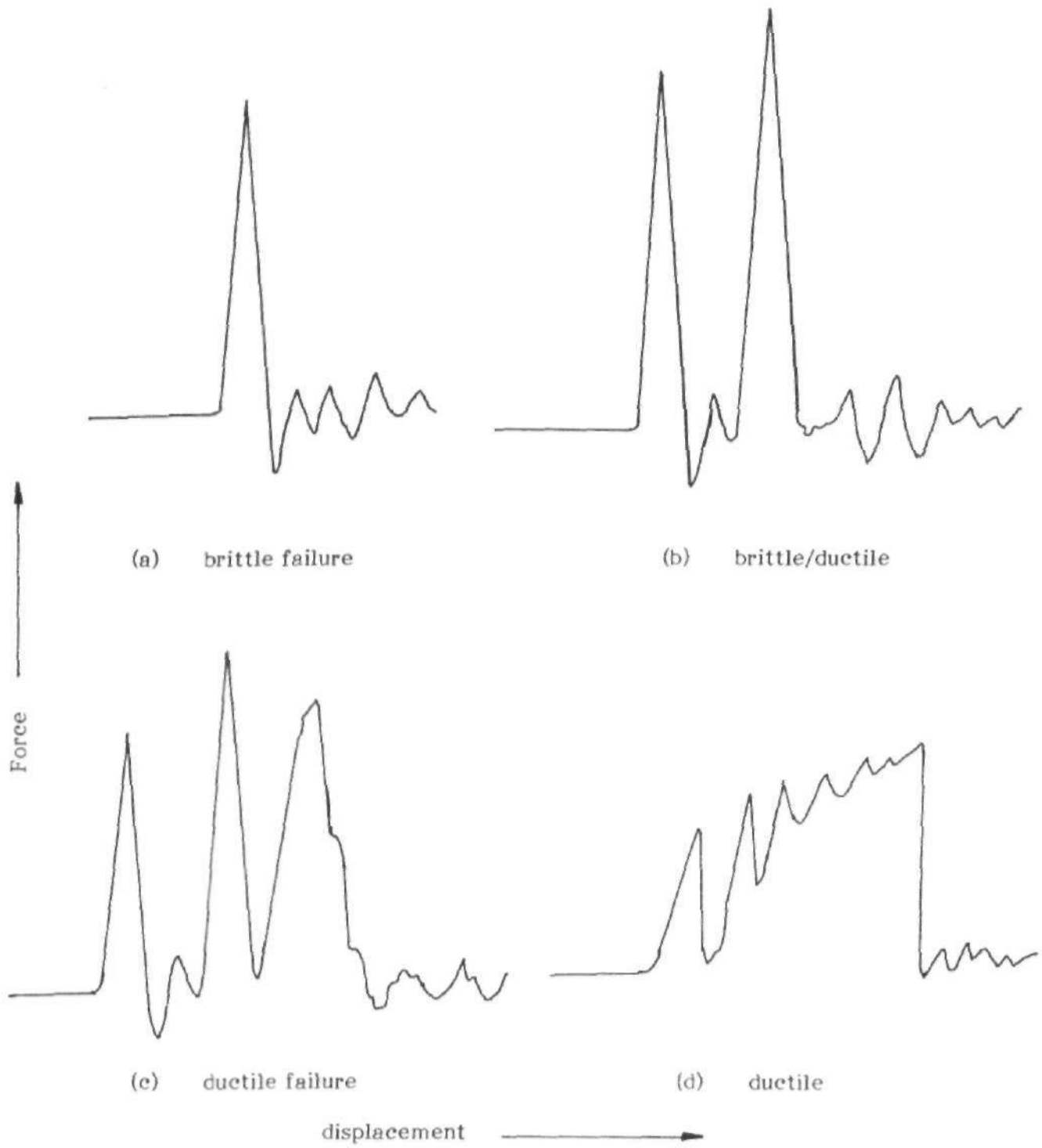
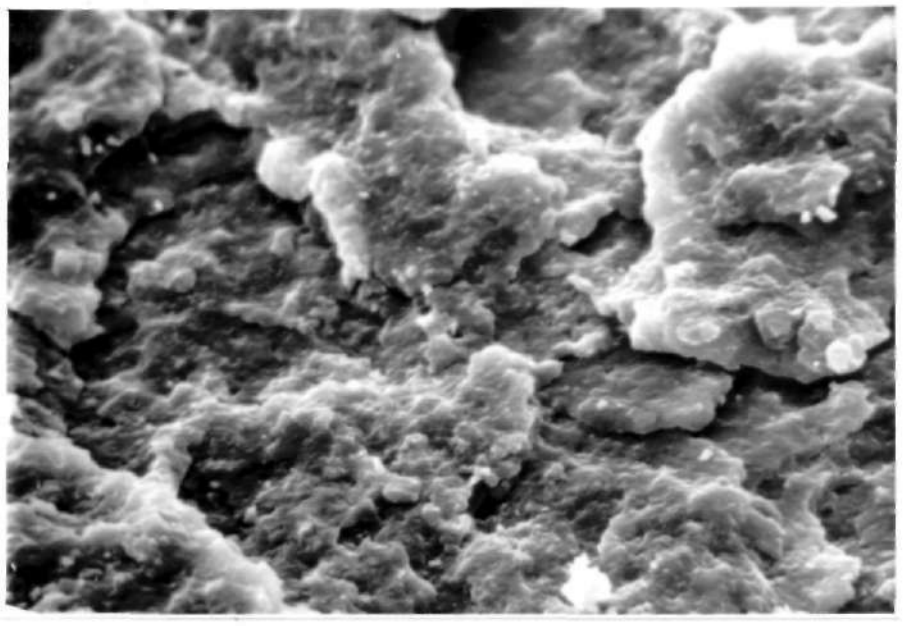


Fig. 5.1

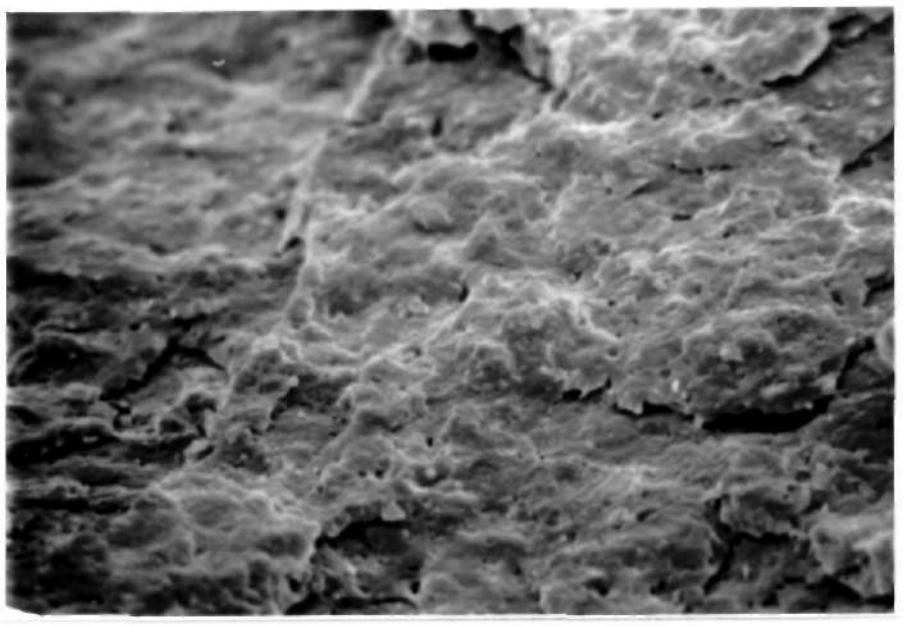
Force-displacement plots from the Ceast Fractoscope for different failure modes



(a)

(x 1600)

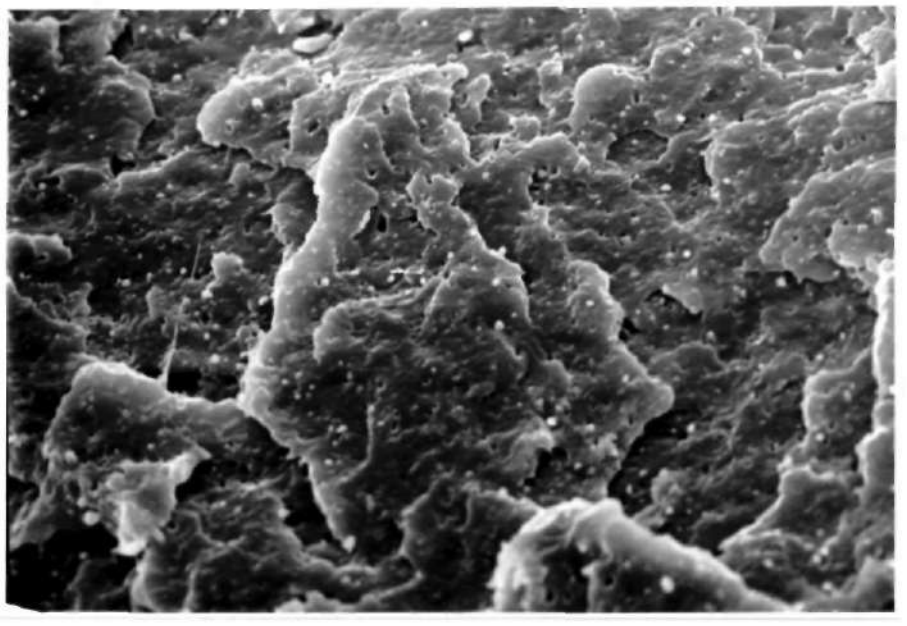
184°C



(b)

(x 1600)

195°C

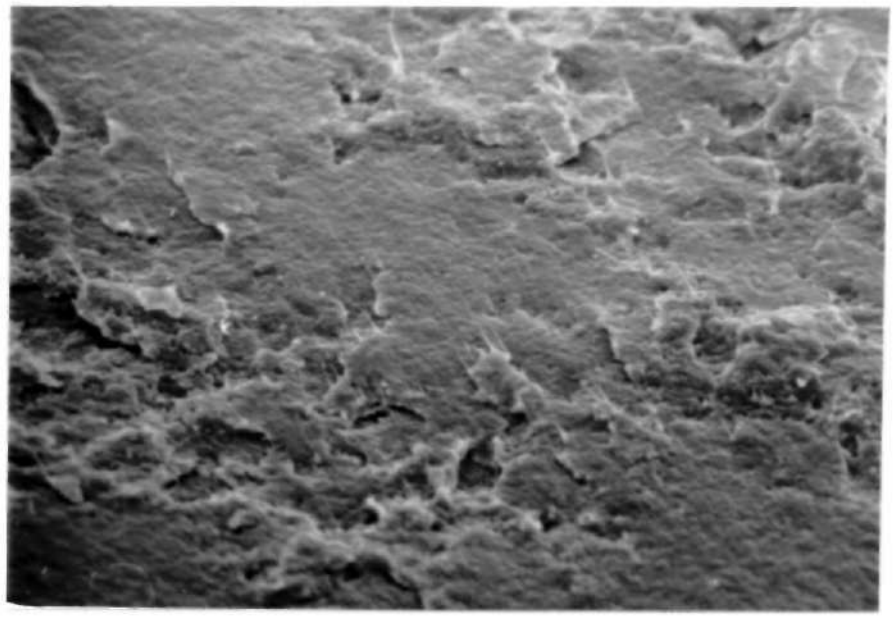


(c)

(x 1500)

200°C

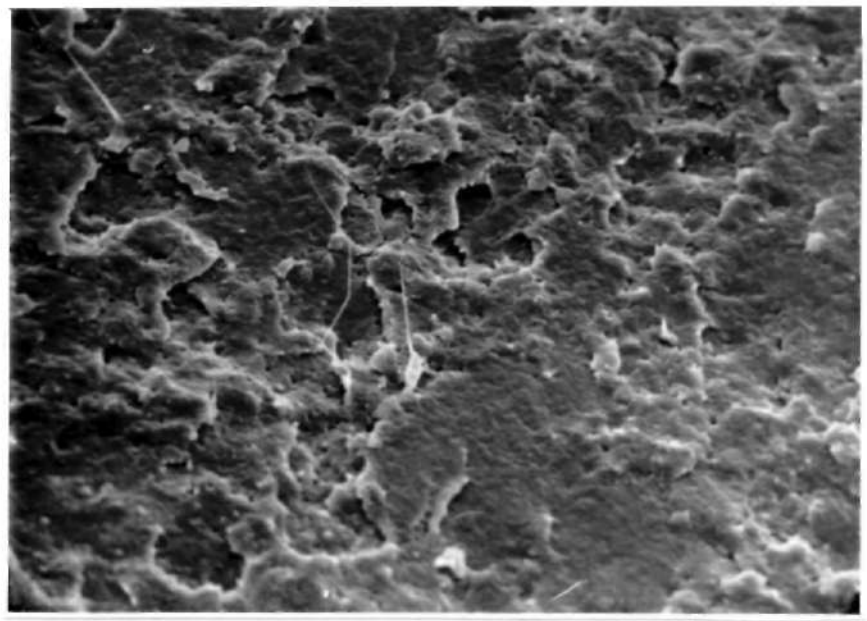
Fig. 5.2 Fracture surface SEM micrographs of sample A at indicated melt temperatures



(a)

(x 1500)

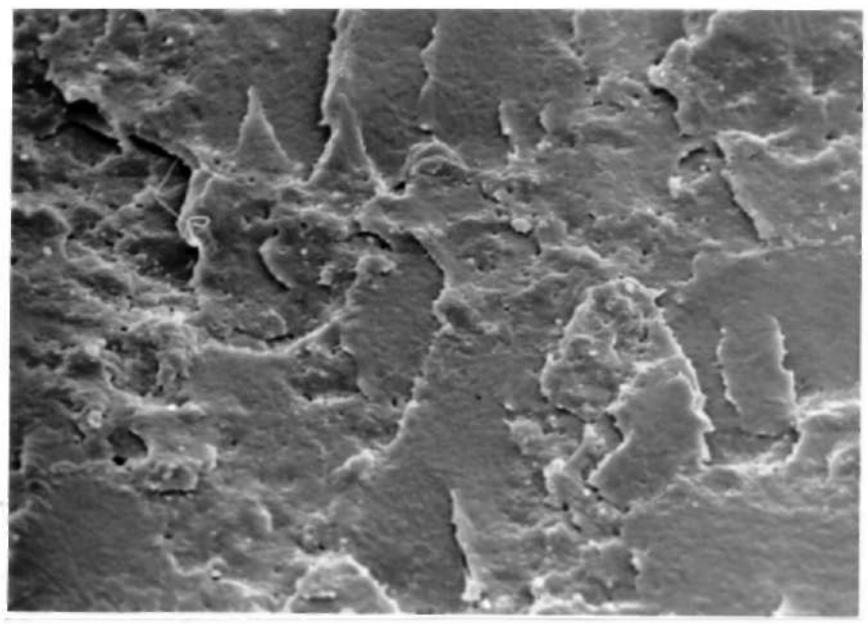
180°C



(b)

(x 1400)

186°C



(c)

(x 1400)

200°C

Fig. 5.3 Fracture surface SEM micrographs of sample S68 at indicated melt temperatures

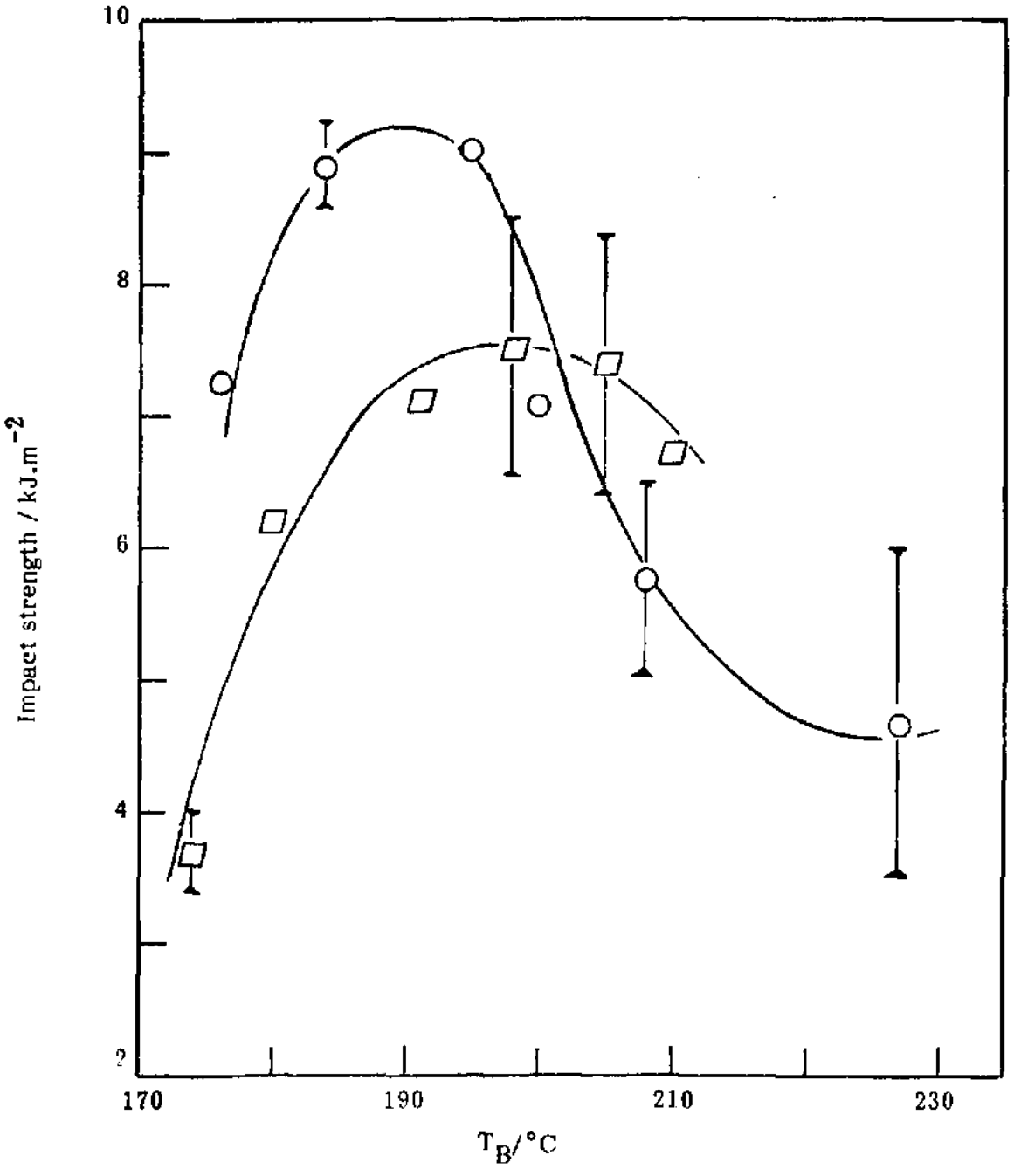


Fig. 5.4

Notched Izod impact strength vs melt temperature for Liestritz extrudates:
O, sample A; △, sample B

Table 5.1

Notched Izod impact strength (NIS/kJ.m^{-2}) of samples A and B extruded at different rates and temperatures (T_B/°C)

	Extrusion rate (rpm)							
	10	15	20	25	30	35	40	50
	Sample A							
T_B	179	180	180	183	180	192	190	-
NIS	6.31	6.10	6.87	7.64	6.04	6.25	6.30	-
T_B	185	186	186	187	186	188	190	196
NIS	-	7.45	7.80	8.01	8.45	9.09	8.36	6.89
T_B	191	193	196	198	200	203	206	210
NIS	4.08	4.06	5.84	6.29	4.95	4.62	4.52	4.08
T_B	205	205	210	213	218	215	215	215
NIS	3.75*	3.69*	4.26	3.86	3.82	3.55	3.82	3.74
	Sample B							
T_B	178	180	180	180	180	181	181	180
NIS	3.73	3.77	3.39	3.72	5.21	4.21	4.42	4.90
T_B	185	186	187	185	186	188	187	186
NIS	5.36	6.21	8.48	6.41	5.39	6.17	4.70	4.56
T_B	192	190	190	190	190	190	190	191
NIS	5.19	4.96	4.29	4.68	4.23	4.48	4.41	4.77
T_B	-	195	195	206	210	198	198	198
NIS	-	4.29*	4.28*	3.76	4.52	3.75	3.79	3.97

* Sample visibly degraded

Table 5.2

Dependence of impact strength on the crystallinity index measured by thermal analysis, x-ray diffraction, and sample density

			Sample A				
T_B/°C	170	176	184	195	200	208	220
IS/kJ.m^{-2}	-	7.25	8.88	8.97	7.05	5.67	4.67
Q_r	0.3	0.9	2.7	5.2	6.4	7.6	7.7
X_r	7.2	5.9	5.2	4.8	4.3	-	-
X_d	8.5	8.3	7.9	7.5	7.0	7.6	7.8
			S68				
T_B/°C	167	174	180	191	199	208	215
IS/kJ.m^{-2}	-	1.49	1.71	1.40	1.96	3.33	4.02
Q_r	0.7	0.8	1.7	3.6	5.3	5.1	4.8
X_r	7.0	6.4	5.9	5.5	5.1	4.8	5.3
X_d	10.0	9.5	9.2	9.0	8.8	9.0	9.0

GENERAL CONCLUSIONS

This study has focused mainly on the existence of a distribution of ordered states as the main structural feature of processed PVC. The distribution has been shown previously, and found in this study, to be composed of two block distributions of order made up of what is generally referred to as primary and secondary crystallinities. The secondary crystallinity is essentially the amorphous phase in which some local order may be found; and the primary crystallinity is formed by more perfect crystalline structure, presumably of the chain folded lamellar type. It is presently an open question whether the secondary crystallinity should be regarded as a crystalline structure in the usual context. There is little doubt that this structure is an intermediate order (paracrystalline). Quite a lot of attention has been focused on this state of order in the literature among which the contribution by Statton[207] may be cited as representing the general view.

Whatever attitude is shown to the existence of crystallinity in PVC, the fact remains that the state of molecular order is of fundamental importance to the properties of the processed resin in addition to other factors such as the morphology of the bulk phase. And although the total crystallinity of the sample, measured by the primary crystallinity level, is only about 10% by weight fraction, it is observed that small changes in this value have significant effects on processing behaviour and product performance. The following conclusions can be drawn from the results of this study.

* The sigmoidal nature of the changes in capillary rheometer entrance pressure loss with increased fusion level has been shown here to arise from the effect of lubricant on network formation. It has been shown that particle breakdown plays little if any roles in the shape of capillary rheometer fusion curves.

* At a specific processing temperature the primary and secondary crystallinities of the material are inversely, but not proportionally, related. The former can be measured by WAXD and the latter by thermal analysis.

* The processed sample is least crystalline (i.e. most amorphous) if it is processed at a melt temperature of 200°C. There is evidence to suggest that a reordering process is responsible for the minimum in crystallinity. An attempt has been made to account for this observation.

* Measured heats of fusion arising from the melting of secondary crystallinity in thermal analysis can be simulated. The simulation yields a precise measure of the temperature at which a change in the melt flow units occurred during processing. The results also yield values of activation energies of 1.0 kJ/mol and 2.2 kJ/mol for the breakdown of the grain and primary particle structures respectively. Fusion levels of 7-8% were found for the maximum fused state within the limits of processing temperatures. These values are in good agreement with % (primary) crystallinity measured for the same samples by x-ray diffraction and values found in the literature for commercial PVC. It was further shown

that a quantitative estimate of the relative shear level during processing can be obtained from thermal analysis using the ratio of the observed to the calculated heat of fusion. This ratio is found to increase at higher shear levels.

* It was found that notched Izod impact strength at room temperature peaks at a melt temperature of about 190°C in agreement with the literature. In this work, however, an attempt has been made to account for changes in impact strength by relating failure mechanism to molecular structure. Scanning electron micrographs of fracture surfaces showed that the maximum impact strength occurs just before the minimum crystallinity at 200°C. A dominant structural feature, characterised by a coherent aggregate of primary particles, is shown to give rise to the highest impact strength.

* The study has highlighted several aspects of structure-property relationships in processed PVC. An improved understanding of this complex relationship has been gained and avenues opened up for further research.

SUGGESTIONS FOR FURTHER STUDY

(1) A large amount of data has been generated by the PVC research group at IPT to suggest that thermal analysis, if exploited, could be a much more useful tool for monitoring PVC fusion than existing techniques. This is expected in principle. A theoretical support has been attempted in this study by the development of a model. The scope of the work could be increased by performing tests on industrial samples of known formulations.

(2) Two techniques, by no means new, have been used to follow changes in molecular structure with increased fusion level: these are solvent absorption and wide-angle x-ray diffraction analysis. More work is required to establish the results.

(3) It seems that over the years, attention has focused more on structure than on properties. This is understandable since knowledge of the former is necessary for an understanding of the latter. Both the literature and results at IPT would suggest that an indepth knowledge of the structure has been gained. Attention should now be directed at mechanical properties of the processed material with emphasis on failure mechanisms as related to molecular structure.

(4) This study has been based on very simple formulations which served the purpose of academic interest, bearing little relationship to technological formulations. Future studies should be more related to practical formulations. It will be useful to establish the effects of various additive types and loadings on thermal analysis, in particular, inorganic additives such as fillers, and others such as pigments and impact modifiers.

REFERENCES

1 Rochow, T.G., and F.G. Rowe, Anal. Chem., 21, 461 (1949)

2 Rochow, T.G. J. Appl. Polym. Sci., 9, 569 (1965)

3 Bort, D.N., Y.Y. Rylov, N.A. Okladov, B.P. Shtarkman, and Y.A. Kargin, Polym. Sci., USSR, 7(1), 50 (1965)

4 Berens, A.R. and V.L. Folt, Trans. Soc. Rheol., 11(1), 95 (1967)

5 Berens, A.R. and V.L. Folt, Polym. Eng. Sci., 8, 5 (1968)

6 Berens, A.R. and V.L. Folt, Polym. Eng. Sci., 9, 27 (1969)

7 Singleton, C., J. Isner, D.M. Gezovich, P.K.C. Tsou, P.H. Geil, and E.A. Collins, Polym. Eng. Sci., 14(5), 371 (1974)

8 Barclay, L.M., Angew Chem., 52, 1 (1976)

9 Palma, G., G. Talamini, M. Tavan, and M. Carenza, J. Polym. Sci.: Phys. Ed., 15, 1537 (1977)

10 Geil, P.H., J. Macromol. Sci.- Phys., B14(1), 171 (1977)

11 Sieglaff, C.L., and P.H. Geil, Polym. Eng. Sci., 18, 1174 (1978)

12 Davidson, I.A., and D.E. Witenhafer, J. Polym. Sci.: Phys. Ed., 18, 51 (1980)

13 Chang, J.T., J. Macromol. Sci.- Phys., B20(3), 365 (1981)

14 Cogswell, F.N., Pure and Appl. Chem., 52(8), 2033 (1981)

15 Soni, P.L., P.H. Geil, and E.A. Collins, J. Macromol. Sci.- Phys., B20(4), 479 (1981)

16 Allsopp. M.W., Pure and Appl. Chem., 53, 449 (1981)

17 Flory, P.J., 'Principles of Polymer Chemistry', Cornell University Press, Ithaca, 1971

18 Renninger, A.L., G.G. Wicks, and D.R. Uhlmann, J. Polym. Sci.: Phys. Ed., 13, 1247 (1975)

19 Renninger, A.L., and D.R. Uhlmann, J. Polym. Sci.: Phys. Ed., 13, 1481 (1975)

20 Straff, R.S. and D.R. Uhlmann, J. Polym. Sci.: Phys. Ed., 14, 353 (1976)

21 Meyer, M., J.V. Sande, and D.R. Uhlmann, J. Polym. Sci.: Phys. Ed., 16, 2005 (1978)

22 Hattori, T., T. Tanaka, and M. Matsuo, Polym. Eng. Sci., 12, 199 (1972)

23 Neilson, G.F., and S.A. Jabarin, J. Appl. Phys., 46(3), 1175 (1975)

24 Wenig, W., J. Polym. Sci.: Phys. Ed., 16, 1635 (1978)

25 Gezovich, D.M., and P.H. Geil, Int. J. Polym. Mater., 1, 3 (1971)

26 Tsou, P.K.C., and P.H. Geil, Int. J. Polym. Mater., 1, 223 (1972)

27 Singleton, C.J., T. Stepheson, J. Isner, P.H. Geil, and E.A. Collins, J. Macromol. Sci.- Phys., B14(1), 29 (1977)

28 Summers, J.W., J. Vinyl Tech., 3(2), 107 (1981)

29 Stein, R.S., and A.V. Tobolsky, Textile Res. J., 18, 302 (1948)

30 Alfrey, 5., W. Wiederhorn, R.S. Stein, and A. Tobolsky, Ind Eng. Chem., 41. 701 (1949)

31 Natta, G., and P. Corradini, J. Polym. Sci., 20, 251 (1956)

32 Smith, R.W., and C.E. Wilkes, J. Polym. Sci., B5, 433 (1967)

33 Wilkes, C.E., V.L. Folt, and S. Krimm, Macromolecules, 6(2), 235 (1973)

34 Keller, A., and P.J. Lemstra, J. Polym. Sci.: Phys. Ed., 16, 1507 (1978)

35 Nakajima, A., H. Hamada, and S. Hayashi, Makromol. Chem., 95, 40 (1966)

36 Ceccoruli, G., M Pizzoli, and G. Pezzin, J. Macromol. Sci.- Phys., B14(4), 499 (1977)

37 Warrier, A.V.R., and S. Krimm, Macromolecules, 3, 709 (1970)

38 Rehage, G., and H. Halboth, Makromol Chem., 119, 235 (1968)

39 D'Amato, R.J., and S.J. Strella, Appl. Polym. Symp., 8, 275 (1969)

40 Ohta, S., T. Kajiyama, and M. Takayanagi. Polym. Eng. Sci., 16, 465 (1976)

41 Gouinlock, E.V., J. Polym. Sci.: Phys. Ed., 13, 961 (1975)

42 Baker, C., W.F. Maddams, and J.E. Preedy, J. Polym. Sci.: Phys. Ed., 15, 1041 (1977)

43 Gilbert, M., and J.C. Vyvoda, Polymer, 19, 863 (1978)

44 Mammi, M., and V. Nardi, Nature (London), 199, 247 (1963)

45 Lebedev, V.P., N.A. Okladov, and M.N. Shlykova, Polym. Sci. USSR, 9, 553 (1967)

46 Brady, T.E., and S.A. Jabarin, Polym. Eng. Sci., 17, 686 (1977)

47 Guerrero, S.J., D. Meader, and A. Keller, J. Macromol. Sci.- Phys., B20(2), 185 (1981)

48 Juijn, J.A., J.H. Gisolf, and W.A. de Jong, Kolloid-Z. Z-Polym., 235, 1157 (1969)

49 Juijn, J.A., Ph.D. Thesis, Technical University, Delft, (1972)

50 Juijn, J.A., J.H. Gisolf, and W.A. de Jong, Kolloid-Z. Z-Polym., 251, 456 (1973)

51 Guerrero, S.J., A. Keller, P.L. Soni, and P.H. Geil, J. Polym. Sci.: Phys. Ed., 18, 1533 (1980)

52 Guerrero, S.J., and A. Keller, J. Macromol. Sci.- Phys., B20(2), 167 (1981)

53 Harrison, M.A., P.H. Morgan, and G.S. Park, Eur. Polym. J., 8, 1361 (1972)

54 Mandelkern, L., Polymer Preprints, 23(1), 25 (1982)

55 Illers, K.H., Makromol Chem., 127, 1 (1969)

56 Illers, K.H., J. Macromol. Sci.- Phys., B14, 471 (1977)

57 Manson, J.A., S.A. Iobst, and R. Acosta, J. Macromol. Sci.- Phys., B9(2), 301 (1974)

58 Munstedt, H., J. Macromol. Sci.- Phys., B14(2), 195 (1977)

59 Davis, D.D., and W.P. Shihter, Macromolecules, 6, 728 (1973)

60 Tobb, D.L., and J.L. Koenig, Macromolecules, 8, 929 (1975)

61 Gleissner, A., Kunststoffe, 62, 678 (1972)

62 Lebedev, V.P., N.A. Okladov, K.S. Minsker, and B.P. Shtarkman, Polym. Sci. USSR, 7, 724 (1965)

63 Sieglaff, C.L., Pure and Appl. Chem., 53, 509 (1981)

64 Utracki, L.A., Polym. Eng. Sci., 14(4), 308 (1974)

65 Deanin, R.D., and R.E. Somers, J. Polym. Sci., A1,8, 1949 (1970)

66 Salovey, R., and H.E. Baier, Polymer Reprints, 11, 230 (1970)

67 Mathews, G., 'Vinyl and Allied Polymers', Vol. 2, The Plastics Institute (London), 1972

68 Braun, D., and R.F. Bender, Eur. Polym. J. Supplement, 5, 269 (1969)

69 Schwenk, U., F. Cavagna, F. Lamker, I. Koenig, and H. Streitberger, J. Appl. Polym. Sci., 23, 1589 (1979)

70 Berens, A.R., Polym. Eng. Sci., 14(5), 318 (1974)

71 Bersch, C.F., M.R. Harvey, and B.G. Acchammer, J. Res. Nat. Bur. Std., 60, 481 (1958)

72 Ouchi, I., J. Polym. Sci., A3, 2685 (1965)

73 Penn, W.S., 'PVC Technology', 2nd edn., Maclaren, London, (1962)

74 Brydson, J.A., 'Plastics Materials', 4th edn., Butterworths, London (1982) Chapt. 7

75 Sarvetnick, H.A., 'Polyvinyl Chloride', Van Nostrand Reinhold, (1969) Chapt. 8

76 Nass, L.I., (ed.) 'Encyclopedia of PVC', Vols 2 and 3, Marcell Dekker, New York, (1977)

77 Logan, M.S., and C.I. Chung, Polym. Eng. Sci., 19(15), 1110 (1979)

78 Kulas, F.K., and N.P. Thorshaug, Polym. Eng. Sci., 14(5), 366 (1974)

79 Younan, M.Y.A., M.A. El-Rijai, R. Moshen, and I.M. El-Hennawi, J. Appl. Polym. Sci., 28, 3247 (1983)

80 Aboul-Gheit, A.K., I.M. El-Hennawi, R. Moshen, and M.Y.A. Younan, J. Appl. Polym. Sci., 28, 3349 (1983)

81 Hartitz, J.E., Polym. Eng. Sci., 14, 392 (1974)

82 Krzewki, R.J., and E.A. Collins, J. Macromol. Sci.- Phys., B20(4), 465 (1981)

83 Mathews, G., 'Polymer Mixing Technology', Appl. Sci. Publ., London, (1982)

84 Miadonye, A., Ph.D. Thesis, Loughborough University, U.K., (1983)

85 Berry, J.P., Plastics and Rubber Int., 9(2), 16 (1984)

86 Tester, D.A., in 'Manufacture and Processing of PVC', R.H. Burgess, ed., Appl. Sci. Publ., London, 1982

87 Wunderlich, B., and G. Czonyj, Macromolecules, 10(5), 906 (1977)

88 Lyngaae-Jorgensen, Polym. Eng. Sci., 14(5), 342 (1974)

89 Kulas, F.R., and N.P. Thorshaug, J. Appl. Polym. Sci., 23, 1781 (1979)

90 Witenhafer, D.E., J. Macromol. Sci.- Phys., B4(4), 915 (1970)

91 Bell, J.P., and J.A. Dumbleton, J. Polym. Sci., A2,7, 1033 (1969)

92 Mandelkern, L., 'Crystallization of Polymers', McGraw-Hill, New York, (1964) Chapt. 2

93 Kashmiri, M.I., and R.P. Sheldon, J. Polym. Sci., B7, 51 (1969)

94 Ali, M.S., and R.P. Sheldon, J. Appl. Polym. Sci., 14, 2619 (1970)

95 Ali, M.S., and R.P. Sheldon, J. Polym. Sci., C38, 97 (1972)

96 Singh, P., and J. Lyngaae-Jorgensen, J. Macromol. Sci.- Phys., B19(2), 237 (1981)

97 Fulcher, K.U., D.S. Brown, and R.E. Wetton, J. Polym. Sci., C38, 315 (1972)

98 Kovacs, A.J., A. Gonthier, and C. Straupe, J. Polym. Sci., C50, 283 (1975)

99 Conte, G., L. D'Ilario, and N.V. Pavel, J. Polym. Sci., A2,17, 693 (1979)

100 Zachmann, H.G., and A. Peterlin, J. Macromol. Sci.- Phys., B3(3), 495 (1969)

101 Uitenham, L.C., and P.H. Geil, J. Macromol. Sci.- Phys., B20(4), 593 (1981)

102 Gonze, A., Plastica, 24(2), 49 (1971)

103 Lamberty. P., Plast. Mod. Elastom., 26, 82 (1974)

104 Faulkner, P.G., J. Macromol. Sci.- Phys., B11, 251 (1975)

105 Benjamin, P., Plast. and Rubber: Mat. & Appl., (Nov., 1980) p. 151

106 Krzewki, R.J., and E.A. Collins, J. Macromol. Sci.- Phys., B20(4), 443 (1981)

107 Allsopp, M.W., Preprints Int. Conf. PVC Processing II, PRI, (1983) paper 4.7. 'Manufacture and Processing of PVC', Burgess, R.H., ed., Appl. Sci. Publ., London, 1982 pp. 212-213

108 Portingell, G.C., in 'Particulate Nature of PVC', G. Butters, ed., Appl. Sci. Publ., London, (1982)

109 Philippoff, W., and F.H. Gaskins, Trans. Soc. Rheol., 2, 263 (1958)

110 Bagley, E.B., Trans. Soc. Rheol., 5, 355 (1961)

111 Han, C.D., 'Rheology in Polymer Processing', Academic, New York, (1976)

112 Han, C.D., AIChE J., 17, 1480 (1971)

113 Matlack, J.D., and A.P. Metzger, J. Polym. Sci., Polym. Letters, 4, 875 (1966)

114 Gilbert, M., and J.C. Vyvoda, Polymer, 22, 1134 (1981)

115 Berens, A.R., and I.M. Hodge, Macromolecules, 15, 756 (1982)

116 Gilbert, M., D.A. Hemsley, and A. Miadonye, Plast. and Rubber, Proc. & Appl., 3(4), 343 (1983)

117 Haward, R.N., ed., 'The Physics of Glassy Polymers', Appl. Sci. Publ., London (1973)

118 Wunderlich, B., 'Macromolecular Physics', Vol. 1, Acad. Press, New York (1973)

119 Alexander, L.E., 'X-ray Diffraction in Polymer Science', Interscience -John Wiley, New York (1969)

120 Ruland, W., Acta Cryst., 14, 1180 (1961)

121 Carrega, M.E., Pure and Appl. Chem., 49, 569 (1977)

122 Lebedev, V.P., N.A. Okladov, K.S. Minsker, and B.P. Shtarkman, Polym. Sci. USSR, 7, 655 (1965)

123 Roldan, L.G., F. Rahl, and A.R. Paterson, J. Polym. Sci., C8, 145 (1965)

124 Kargin, V.A., J. Polym. Sci., 30, 247 (1958)

125 Yeh, C.S.Y., CRC. Rev. J. Macromol. Sci., 1, 173 (1972)

126 Geil, P.H., J. Macromol. Sci.- Phys., B12(2), 173 (1976)

127 Boyer, R.F., J. Macromol. Sci.- Phys., B12(2), 253 (1976)

128 Hermans, P.H., amd A. Weidinger, Makromol Chem., 50, 98 (1961)

129 Gray, A., Ph.D. Thesis, Loughborough University, (1975)

130 Chartoff, R.P., T.S.K. Lo, E.R. Harrell Jr., and R.J. Roe, J. Macromol. Sci.- Phys., B20(3), 287 (1981)

131 Crank, J., and G.S. Park, eds., 'Diffusion in Polymers', Academic Press, London, (1968)

132 Crank, J., 'The Mathematics of Diffusion', 2nd Ed., Clarendon Press, Oxford (1975)

133 Alfrey, T. Jr., E.F. Gurnee, and W.G. Lloyd., J. Polym. Sci., C12, 249 (1966)

134 Micheals, A.S., and R.B. Parker, J. Polym. Sci., 41, 53 (1949)

135 Micheals, A.S., and H.J. Bixler, J. Polym. Sci., 50, 413 (1961)

136 Hopfenberg, H.B., and H.L. Frisch, J. Polym. Sci., B7, 403 (1969)

137 Wang, T.T., T.K. Kwei, and H.L. Frisch, J. Polym. Sci., A2,7, 2019 (1969)

138 Tshudy, J.A., and C. Frankenberg, J. Polym. Sci.: Phys. Ed., 11, 2027 (1973)

139 Kwei, T.K., T.T. Wang, and H.M. Zupko, Macromolecules, 5(5), 645 (1972)

140 Lapcik, L., J. Panak, V. Kello, and J. Polavka, J. Polym. Sci.: Phys. Ed., 14, 981 (1976)

141 Berens, A.R., Polymer, 18, 697 (1977)

142 Daniels, C.A., and C.D. Longeway, Polym. Eng. Sci., 19(3), 181 (1979)

143 Quy, R.B., J. Macromol. Sci.- Phys., B20(2), 235 (1981)

144 Micheals, A.S., W.R. Vieth, and J.A. Barrie, J. Appl. Phys., 34(1), 13 (1963)

145 Dole, M., J. Polym. Sci., C18, 57 (1968)

146 Weissberger, A., and B.W. Rossiter, eds., 'Physical Methods of Chemistry', Vol. 1, (1971) Pt. 5

147 Richardson, M.J., in 'Development in Polymer Characterization', Vol. 1, J.V. Dawkins, ed., Appl. Sci. Publ., Essex, (1978) Chapt. 7

148 Wunderlich, B., J. Polym. Sci., C1, 41 (1963)

149 Brighton, C.A., in 'Mechanical Properties of Polymers', Encyclopedia Reprints, N.M. Biakales, ed., Wiley-Interscience, New York (1971) pp. 175-222

150 Gotham, K.V., and S. Turner, Polym. Eng. Sci., 13, 113 (1973)

151 Kambur, R.P., J. Polym. Sci., Macromol. Rev., 7, 1 (1973)

152 Kausch, H.H., 'Polymer Fracture', Springer-Verlag, New York, (1978)

153 Kinlock, A.J., and R.J. Young, 'Fracture Behaviour of Polymers', Appl. Sci. Publ., London, (1983)

154 Menges, G., and N. Berndsten, Preprint. Int. Conf. PVC Processing, Plastics Inst., London, (1978) p. B12-1

155 Summers, J.W., E.B. Rabinovitch, and J.F. Quisenberry, SPE Antec, San Francisco, May 1982, p. 501

156 Malac, J., J. Polym. Sci., 13, 1767 (1969)

157 Gross, R.C., A.W.M. Coaker, and J.D. Hinchen, 27th Antec Meeting, Chicago, May (1969)

158 Bystedt, J., J. Vinyl Tech., 2, 209 (1980)

159 Benjamin, P., Int. Conf. PVC Proc., London, April (1978) preprints p. 10-1

160 Terselius, B., J.F. Jansson, and J. Bystedt, J. Macromol. Sci.- Phys., B20, 403 (1981)

161 Terselius, B., Ph.D. Thesis, The Royal Inst. of Tech., Stockholm, (1983)

162 Pezzin, G., G. Ajroldi, T. Casiraghi, C. Garbuglio, G. Vittadini, J. Appl. Polym. Sci., 16 1839 (1972)

163 Gonze, A., and J.C. Chauffoureaux, Pure and Appl. Chem., 35(3), 315 (1973)

164 Oberst, H., and W. Retting, J. Macromol. Sci.- Phys., B5(3), 559 (1971)

165 Randon, T.C., Polym. Eng. Sci., 12, 425 (1972)

166 Brown, H.R., J. Mater. Sci., 8, 941 (1973)

167 Marshall, G.P., J.G. Williams, and C.E. Turner, J. Mater. Sci., 8, 949 (1973)

168 Platti, E., and J.G. Williams, Polym. Eng. Sci., 15, 470 (1970)

169 Ireland, D.R., in 'Instrumented Impact Testing', ASTM, STP563 (1974) p. 3

170 Turner, S., 'Mechanical Testing of Plastics', Illife, London (1979) p. 117

171 Reed, H.E., in 'Development in Polymer Fracture', E.H. Andrews, ed., Appl. Sci. Publ., London (1979) p. 121

172 Technigram B262, Technical data for suspension PVC, Breon S110/11, BP Chemicals Ltd., Devonshire House, Mayfair, London

173 Corvic Technical Information Sheets, ICI Ltd., U.K.

174 Technical Information Sheet, Akzo Chemie, U.K.

175 Technical Information Sheet, Cornelius Produce Co. Ltd., London

176 Hemsley, D.A., E.M. Katchey, R.J. Linford, and D.E. Marshall, Preprints, Int. Conf. PVC Processing, Egham Hill, Surrey, (1978) paper 9

177 Katchey, E.M., J. Appl. Polym. Sci., 28, 1847 (1983)

178 Sachak, M.T., M.Sc. Project, Loughborough University, 1981

179 Menges, G., and N. Berndsten, Pure and Appl. Chem., 49, 597 (1977)

180 Marshall, D.E., R.P. Higgs, and O.P. Obande, Plastics and Rubber: Proc. Appl., 3, 353 (1983)

181 Collins, E.A., and C.A. Krier, Trans. Soc. Rheol., 11, 225 (1967)

182 Patel, S.V., Ph.D. Thesis, Loughborough University, (1983)

183 Hutchinson, J.M., J.J. Aklonis, and A.J. Kovacs, Polymer Preprints, 16(2), 94 (1975)

184 Hutchinson, J.M., and A.J. Kovacs, J. Polym. Sci., Polym. Phys. Ed., 14, 1575 (1976)

185 Kovacs, A.J., and J.M. Hutchinson, J. Polym. Sci.: Phys. Ed., 17, 2031 (1979)

186 Bunn, C.W., 'Fibres from Synthetic Polymers', Hill, R., ed., Elsevier, Amsterdam, 1953, p. 324

187 Beaman, R.G., J. Polym. Sci., 9, 472 (1953)

188 Boyer, R.F., J. Appl. Phys., 25, 825 (1954)

189 Kovacs, A.J., A. Gonthier, and C. Straupe, J. Polym. Sci., C,50, 283 (1975)

190 Hutchinson. J.M., Private Communications

191 Khanna, R.K., Plastics & Polymers, April, (1974) p. 80

192 Collins, E.A., and A.P. Metzger, Polym. Eng. & Sci., 10, 57 (1970)

193 Gouinlock, E.V., J. Polym. Sci.: Phys. Ed., 13, 1533 (1975)

194 Manson, J.A., S.A. Iobst, and R.J. Acosta, J. Polym. Sci., A-1(10), 179 (1972)

195 Kockott, D., Kolloid-Z. Z-Polym., 198, 17 (1964)

196 Alford, S., and M. Dole, J. Am. Chem. Soc., 77, 4774 (1955)

197 Wunderlich, B., J. Phys. Chem., 64, 1052 (1960)

198 Colborne, R.S., J. Appl. Polym. Sci., 14, 127 (1970)

199 Anagnostopoulos, C.E., A.V. Coran, and H.R. Gomrath, J. Appl. Polym. Sci., 4(11), 181 (1960)

200 Gilbert, M., and M.I. Mulla, Polymer Testing, 3, 171 (1983)

201 Kau, H.T., and F.E. Filisko, Macromolecules 12(3), 479 (1979)

202 Michel, A., and A. Guyot, J. Polym. Sci., C33, 75 (1971)

203 Murray, J., and D. Hull, Polymer, 10 451 (1969)

204 Murray, J., and D. Hull, J. Polym. Sci., A-2,8, 583 (1970)

205 Kusy, R.P., and D.T. Turner, Polymer, 18, 391 (1977)

206 Gale, G.M., RAPRA Members J., March (1974) p. 68

207 Statton, W.O., J. Polym. Sci., C,18, 33 (1967)

APPENDIX

```
LLIST
10  REM  : PROGRAMME TO CALCULATE CUMMULATIVE ENTHALPY CHANGE
                    FOR PROCESSED PUC
20  INPUT "SAMPLE ID            ";SN$
30  DIM H(80),B(80),A(80),C(80),Z(80),T(80)
40 R = 8.314:K = T(0)
50  PRINT "INPUT THE TOTAL NUMBER OF DATA POINTS"
60  INPUT N
70 X = 0:Y = 0:Z = 0
80  FOR I = 1 TO N
90  READ H(I)
100 H(I) = H(I) * 62.5
110 T(I) = K + I
120 A(I) = H(I) / (R * T(I))
130 C(I) =  EXP ( - A(I))
140 B(I) = H(I) * C(I)
150 Z(I) = (2 * I) / (I + 1)
160 X = X + B(I)
170 Y = Y + C(I)
180 S1 = X / (62.5 + Y):S2 = S1 + Z(I)
190  PR# 1
200  IF I = 1 THEN  PRINT SN$: PRINT : PRINT "NO        T(K)        S1
                    S2
210  PRINT I;
220  HTAB 11: PRINT K + I;
230  HTAB 19: PRINT S1;
240  HTAB 33: PRINT S2: PRINT
250  NEXT I
260  PR# 0
270  DATA
400  END
```

Table 3.1A

Output and power requirement for samples extruded at different rates using the Leistritz

Sample code	Extrusion rate (rpm)	Output (kg/hr)	Approx power (kW)
Sample A+			
A 1S	10	4.7	0.13
A 2S	15	6.5	0.21
A 3S	20	8.0	0.28
A 4S	25	9.7	0.37
A 5S	30	11.2	0.46
A 6S	35	13.0	0.51
A 7S	40	14.4	0.67
A8S	50	17.2	0.96
Sample B*			
B 1S	10	5.0	0.08
B 2S	15	6.5	0.13
B 3S	20	8.7	0.20
B 4S	25	10.1	0.23
B 5S	30	11.7	0.27
B 6S	35	13.2	0.30
B 7S	40	14.6	0.41
B 8S	50	20.9	0.56

\+ Die set temp. = 199 ± 1°C; melt temp., T_B = 198 ± 1°C

* Die set temp. = 200 ± 2°C; melt temp., T_B = 190 ± 2°C

Table 3.2A Capillary rheometer pressure and per cent gelation for samples extruded at different temperatures using the Leistritz

	Sample A							
Property	A-1	A-2-1	A-3	A-4	A-5	A-6	A-7	Powder
Extrusion temp. (°C)	170	180	197	205	213	220	227	-
mV (average)	28.5	30.8	40.0	41.3	45.8	46.5	46.8	29.0
Extrusion Pressure (MN/m^2)	18.84	20.50	27.97	29.10	32.76	33.15	33.34	19.16
% Fusion	-2.3	9.5	62	70	96	99	100	0

	Sample B							
	B-1	B-2-1	B-3	B-4	B-5	B-6	B-7	Powder
Extrusion temp. (°C)	171	182	197	207	213	218	227	-
mV (average)	25.8	27.5	34.8	39.0	41.5	44.5	45.0	29.5
Extrusion Pressure (MN/m^2)	16.60	18.01	23.93	27.20	29.31	31.47	31.90	19.54
% Fusion	-2.4	-1.2	36	62	79	97	100	0

Table 3.3A

Capillary rheometer pressure at different rates of extrusion for Leistritz extrudates

Temp.(°C)	Extrusion rate (rpm) 10	15	20	25	30	35	40	50
	Pressure/MPa							
	Sample A (Powder = 19.2)							
190	15.7	15.9	17.1	17.9	19.7	21.0	20.7	-
200	24.3	25.1	25.3	25.3	26.2	24.3	29.1	30.3
210	26.0	25.9	26.2	25.3	25.3	25.2	25.5	24.1
220	31.2	30.1	30.8	30.2	30.3	31.7	31.5	30.5
	Sample B (Powder = 19.5)							
190	12.9	12.7	12.8	12.5	12.9	13.8	14.1	14.6
200	19.2	20.3	20.3	20.3	21.0	20.7	21.1	21.3
210	19.5	20.9	20.7	20.9	21.1	21.0	20.9	21.1
220	-	29.3	29.3	29.8	29.7	29.8	29.5	29.1

Table 3.4A

Capillary rheometer pressure for compression moulded samples

Sample	Powder P_o	Mould temperature (°C) 160	170	180	190	200	210	220
		Pressure/MPa						
SO	13.2	29.0	34.5	38.5	39.9	45.3	50.0	-
SCa0	13.1	20.1	14.9	8.3	10.9	28.6	30.4	26.9
LO2	12.7	14.6	13.0	11.1	14.3	20.3	22.4	-
LO5	12.5	-	11.4	12.3	15.0	20.3	28.2	26.7
L10	11.6	10.9	10.4	11.0	15.8	20.6	25.5	-
L15	11.2	10.7	9.5	9.3	15.0	18.1	20.7	-
L30	9.3	7.9	6.7	8.1	14.1	18.3	24.5	-
L45	7.8	5.2	4.3	4.8	11.4	12.3	18.7	-
L60	6.5	3.1	3.1	5.2	7.2	14.1	14.1	16.2

Table 3.5A

Heats of fusion and 'B'-endotherm temperatures for samples extruded on the Leistritz

Sample code	Extrusion temp. (°C)	Endotherm peak area (cm^2)	Sample mass (g)	Heat of fusion ΔH_f(J/g)	$'T'_B$ (°C)	'B'-heat of fusion ΔH_f(J/g)
Sample A						
A-1	170	1.0	10.0	0.6	172	1.74
A-2-1	180	2.5	9.0	1.7	175	1.61
A-3	197	7.5	10.0	4.5	185	1.22
A-4	205	12.5	9.6	7.9	195	0.48
A-5	213	15.0	10.0	9.1	202	0.46
A-6	220	18.0	10.7	10.2	210	0.41
A-7	227	17.5	11.1	10.0	215	-
Sample B						
B-1	171	1.0	11.0	0.6	168	1.06
B-2-1	182	2.5	11.5	1.3	172	1.51
B-3	197	5.0	10.8	2.8	184	1.35
B-4	207	8.0	10.4	4.6	192	0.51
B-5	213	10.5	10.0	6.3	198	0.56
B-6	218	12.5	10.7	7.0	205	0.33
B-7	227	12.0	9.4	7.7	210	-

Table 3.6A Observed heats of fusion for samples compression moulded at different melt temperatures

SAMPLES													
SO		LO2		LO5		L10		L15		L30		L45	
T_B (°C)	$\Delta H(T)$ (J/g)	T_B (°C)	$\Delta H(T)$ (J/g)	T_B (°C)	$\Delta H(T)$ (J/g)	T_B (°C)	$\Delta H(T)$ (J/g)	T_B (°C)	$\Delta H(T)$ (J/g)	T_B (°C)	$\Delta H(T)$ (J/g)	T_B (°C)	$\Delta H(T)$ (J/g)
161	1.16	166	0.56	160	0.35	158	0.73	160	0.39	158	-	162	1.55
171	2.23	176	1.74	169	1.69	169	1.54	171	1.39	172	1.29	170	1.12
182	4.77	183	3.01	183	2.90	178	2.70	179	2.16	180	2.08	179	1.64
186	5.09	190	4.19	190	3.37	190	3.15	191	2.98	190	2.71	192	2.70
198	6.93	198	6.60	199	5.87	201	5.37	200	4.87	199	4.41	201	3.67
208	8.76	210	7.75	210	7.06	210	6.42	212	5.85	210	5.34	209	4.08
220	9.87	220	-	221	8.79	221	7.83	220	7.08	221	6.55	220	5.14

Table 3.7A

Heats of fusion for Krauss Maffei extrudates: ΔH (J/g)

Melt temp. T_B(°C)	Sample S57	S62	S68	S71
161	1.2			
163		1.3		
166			1.4	1.0
171	2.7		1.6	
173		2.5		
174				1.4
180	4.4	3.6	2.9	
183				2.6
185	5.8	3.2		
191	7.3	5.6		3.9
195			5.5	
198	8.0	7.1		5.5
201		7.8		
205	9.2		7.4	6.9
210			8.1	
215		9.3		8.1
219			9.2	
220				8.5

Table 4.1A Acetone absortion with time for sample A extruded at different temperatures (see Fig. 4.1)

Sample	Thick-ness (cm)	Initial weight (g_o)	Weight gain (M_t) at (hr)											
			0.5	1.0	2	4	6	8	10	12	15	20	25	32
A2-1	0.45	0.984	0.140	0.193	1.284	0.423	0.544	0.663	0.773	0.888	1.026	1.180	1.270	1.296
A3	0.44	0.930	0.180	0.266	0.441	0.630	0.795	0.958	1.122	1.277	1.425	1.621	1.698	1.738
A4	0.42	0.906	0.210	0.272	0.430	0.629	0.808	0.974	1.167	1.327	1.473	1.682	1.810	1.889
A5	0.38	0.821	0.152	0.286	0.465	0.745	0.874	1.080	1.281	1.438	1.587	1.785	1.900	1.987
A6	0.37	0.791	0.178	0.266	0.448	0.673	0.875	1.085	1.290	1.443	1.593	1.813	1.920	1.979
A7	0.35	0.704	0.175	0.234	0.466	0.702	0.924	1.192	1.386	1.529	1.674	1.880	1.970	2.006

Table 4.2A

Equilibrium % weight gain in acetone absorption for compression moulded samples (see Fig. 4.6)

SO							
T_B/°C	161	171	182	186	198	208	220
$\%M_\infty$	*	*	163	168	172	155	140
LO2							
T_B/°C	166	176	183	190	198	210	-
$\%M_\infty$	*	*	*	166	170	160	-
LO5							
T_B/°C	160	169	183	190	199	210	221
$\%M_\infty$	*	*	*	177	175	166	150
L10							
T_B/°C	159	169	178	190	201	210	221
$\%M_\infty$	*	125	167	180	186	170	160
L15							
T_B/°C	160	171	179	191	200	212	220
$\%M_\infty$	*	*	148	161	157	148	138
L30							
T_B/°C	158	172	180	190	199	210	221
$\%M_\infty$	*	125	148	146	152	142	140
L45							
T_B/°C	162	170	179	192	201	209	220
$\%M_\infty$							

* Sample disintegrated before equilibration time

Table 4.3A

Equilibrium % weight gain in acetone absorption for KM samples

S57							
T_B/°C	151	161	172	181	190	195	209
$\%M_{\infty}$	*	*	*	*	177	254	299
S62							
T_B/°C	-	162	172	180	191	200	205
$\%M_{\infty}$	-	*	138	180	207	231	256
S68							
T_B/°C	-	172	180	192	200	207	219
$\%M_{\infty}$	-	*	133	138	152	162	167
S71							
T_B/°C	167	174	180	191	199	208	215
$\%M_{\infty}$	*	113	118	127	129	134	137

* Sample disintegrated before equilibration time

Table 4.4A

Experimental and normalized crystalline and amorphous areas of some x-ray diffraction patterns

Sample	Area/cm^2 Total	Experimental ϕ_c	Experimental ϕ_a	Normalized ϕ_c	Normalized ϕ_a
P1M	72.5	7.4	61.2	0.102	0.845
P2M	70.5	7.8	59.2	0.110	0.840
P5M	90.0	11.7	74.8	0.130	0.831
SO1	78.0	10.1	64.0	0.130	0.821
SO2	74.0	9.1	60.8	0.123	0.821
SO3	66.0	7.5	54.5	0.114	0.826
SO4	65.0	7.0	54.0	0.108	0.831
SO5	47.0	4.3	40.1	0.091	0.854
SO6	86.5	8.5	73.0	0.098	0.844
SO7	67.5	6.5	57.0	0.096	0.844
M11	70.0	6.5	59.0	0.090	0.840
M12	65.5	5.2	55.7	0.083	0.850
M14	70.0	4.4	64.9	0.063	0.863
M21	82.0	7.8	69.7	0.095	0.850
M25	70.2	4.6	60.6	0.065	0.865